TARGETING ALTERED CANCER CELL METABOLISM: MITOCHONDRIAL GLUTAMINASE REGULATION AND INHIBITION BY SMALL MOLECULES

A dissertation

Presented to the Faculty of the Graduate School

of Cornell University

In partial Fulfillment of the Requirements for the Degree of

Doctor of Philosophy

by

Clint Andrew Stalnecker

August 2016

TARGETING ALTERED CANCER CELL METABOLISM: MITOCHONDRIAL GLUTAMINASE REGULATION AND INHIBITION BY SMALL MOLECULES

Clint Andrew Stalnecker, Ph. D.

Cornell University 2016

Cancer cells have been historically characterized as having hijacked normal cellular machinery in order to acquire a proliferative advantage, thus posing the fundamental challenge in the treatment of cancer. The conceptual origins and motivation for this thesis lie in my desire to systematically investigate the newly discovered reprogramming of glutamine metabolism that occurs specifically in cancer cells, with the hope that this will lead to the development of new targets and therapeutic strategies for the treatment of cancer. Transformation of normal cells is often accompanied by a dramatic shift in glucose metabolism, most notably an increase in the glycolytic flux. However, in cancer cells, the end product of glycolysis, pyruvate, is diverted from entering the respiratory TCA cycle and instead secreted from the cell as lactate. In order to compensate for the decrease in glucose-derived carbon entering the TCA cycle, glutamine is taken up and converted to glutamate by the mitochondrial enzyme glutaminase C (GAC), where glutamate can then feed an entry point of the TCA cycle upon conversion to α-ketoglutarate.

The first objective of my thesis study is to investigate the activation of GAC *in vitro* using a novel fluorescence resonance energy transfer (FRET) assay. Using this assay, I gain insights into the mechanism of action of two recently described classes of

allosteric glutaminase inhibitors; the benzophenanthridines, and bis-thiadiozoles, the latter being currently developed as a therapeutic for targeting the altered metabolism in cancer cells.

A second objective is designed to complement these *in vitro* results by employing an *in vivo* model cell system engineered to express the Dbl oncogene in an inducible tetracycline-dependent manner. The *in vitro* FRET assay provides important information regarding how the ability of GAC to undergo a dimer-to-tetramer transition is coupled to the activation of its enzymatic activity, as well as the mode of inhibition of GAC by small molecule inhibitors. The inducible cell model allows me to tie these results to the formation of oligomers *in vivo* and extend this study to human cancer cell lines. The results presented herein add to an emerging detailed portrait of metabolic transformation and a deeper understanding of the role GAC plays in supporting cancer cell growth.

BIOGRAPHICAL SKETCH

The author was born June 6th, 1988 in Reading, Pennsylvania, and raised by his parents, Andrew and Marie Stalnecker, alongside his older sibling, Lindsay Stalnecker, in the small town of Oley Valley, Pennsylvania. During his teenage years, he demonstrated a natural curiosity through the learning of trades passed down from his family members, such as carpentry, craftsmanship, and masonry. Taking great pride in his physical work, following graduation from Oley Valley High School in 2006, it took a great deal of convincing from his parents for him to attend college. As a compromise, he matriculated into the nearby liberal arts institution, Albright College, in Reading, Pennsylvania, in order to stay close to his family and work as he had been. He began his undergraduate studies seeking a degree in Biochemistry, for no particular reason other than it sounded the most interesting. Clint graduated *summa cum laude* with departmental distinction in December 2009, finishing his degree requirements a semester early. His final spring semester he spent teaching freshman chemistry laboratory, continuing his undergraduate research project, and interviewing at several chemistry PhD programs, ultimately deciding to pursue his graduate work at Cornell University. Clint joined Rick Cerione's laboratory in December of 2010, where he focused on methods bridging chemistry, drug development, and cancer biology to investigate the targeting of altered cancer cell metabolism, namely glutamine metabolism. The author now looks forward to publishing his thesis work, and continuing his passion for hard work and scientific inquiry.

for my family

ACKNOWLEDGEMENTS

I would like to acknowledge everyone, in reverse-chronological order, who has shaped my personal development, giving me the fortitude for this achievement. First and foremost, I would like to thank Rick Cerione, who has been an excellent mentor, always displaying enthusiasm and support for my project and career development. He truly is an exemplary graduate advisor and scientist; it has been a real privilege to follow his guidance. In the same light, I owe a great debt of gratitude to Jon Erickson, who has mentored me throughout my graduate work, and has left a lasting impression.

To my committee members: Maurine Linder and Frank Schroeder. I thoroughly enjoyed Frank's course, Advanced Analytical Chemistry. He is an excellent Professor and mentor, always offering me sound advice. I would also like to acknowledge Maurine, who is also an exemplary advisor and scientist. I have been very fortunate to have had her serve on my committee.

It has been a real pleasure to learn and grow within the dynamic laboratory that could only be Professor Rick Cerione's. To the Cerione laboratory members, in no particular order: Jared Johnson, Yeyun Zhou, Sungsoo Yoo, Bo Li, Lindsey Boroughs, Joe Druso (Thanks for the mouse parts!), Joy Lin, Yang Gao, Yunxing Li, Laura Deroschers, Kelly Sullivan, Kristin Wilson, Kathy Rojas, Kai Su Greene, Mike Lukey, Shawn Milano, Bill Katt, Chengliang Zhang, Arash Latifkir, Kinsley French, and past Cerione Lab members.

To Sekar Ramachandran and Marc Antonyak. The two of you have always offered me sound advice and guidance, both scientifically and personally, and I am

very grateful to have had the pleasure of working alongside the both of you. Mark, I still look forward to ice fishing with you some day.

There are two significant collaborations that I would be amiss without mentioning. Early into my graduate work, I teamed up with Scott Ulrich, Professor of Chemistry at Ithaca College, who worked diligently to prepare small molecule inhibitors for my studies. Scott is an outstanding Professor and chemist. He has offered me advice on numerous occasions, and is always a joy to be around. The second collaboration that can't go unmentioned was with Professor Ralph DeBerardinis at UT Southwestern. Ralph is a real gem. As a young naïve graduate student, I contacted him out-of-the-blue to ask if I could spend two months in his lab just to learn, and that experience was extremely impactful to my enthusiasm for science. Additionally, I made great friends in his laboratory: Andrew Mullen, Chris Hensley, Katrik Rajagopalan, and Jiyeon Kim.

There are friendships I've formed during graduate school that need acknowledgement: Alli McSorley, Carmella Calabrese, Lauren Wu, and Michael Houghton. Also, Jacqueline Celiberti has been a noteworthy source of encouragement that I can't quite express how much I appreciate. One that requires significant highlight is Brandon Wenning, who I admire for his considerable strength, perseverance, brilliance, and all-around ridiculousness.

In need of significant acknowledgment is my undergraduate professor and mentor, Pamela Artz. Pam has remained a close colleague and dear friend who has acted as a constant source of support. If it weren't for her dedication to mentoring, I would surely not be where I am today. Also, to the brothers I gained at Albright

College, Brian Rowe, Simon Foster, Dan Nester, Tim Boyle, and Josh Schneider, who have given me constant support through undergraduate and graduate school.

Growing up in the Oley Valley, I was fortunate to develop lifelong friendships with a great group of fellas that have always provided encouragement, Ben Cappa, Tom Stinely, JJ Dolak, Dan Bertschman, Marcus Valeriano, Ben Graeff, and Mike Christman. Although distance has separated us, we have remained as close as we were growing up. Additionally, to my second family, The Cappa's, whose source of love, support, and encouragement has not gone unnoticed, and is deeply appreciated.

And last, but surely not least, I dedicate this achievement to my family: Doreen and Andrew Stalnecker Sr (Gram and Pop), Mom, Dad, and Lindsay. There really are no words adequate to describe my gratitude for your love, patience, and unconditional support. It hasn't gone overlooked or unappreciated, and this achievement is truly yours to share. There are many extended family members that also need acknowledgment: Cousin Beth and the Trout's (including the Schifferts), Uncle Mark and the Rissel family, Uncle John and Aunt Lori, all other Stalneckers, Bollingers, and Bingamans. Thank you all.

TABLE OF CONTENTS

LIST OF FIGURES

CHAPTER ONE

INTRODUCTION

1.1.1 Metabolic changes as a hallmark of cancer

Cancer is generally considered to be a disease characterized by uncontrolled cellular growth. This uncontrolled growth, as defined by the current understanding of the molecular and genetic mechanisms that govern cellular physiology, is supported by the increased expression of tumor promoting genes and decreased expression of tumor suppressor genes. The underlying changes leading to the sustained deregulation of these tumor promoters and suppressors is acquired through alterations within particular segments of DNA. A diverse set of genomic alterations have now been characterized that play essential roles to initiate, support, and sustain unregulated cellular proliferation that gives rise to neoplasia and subsequent malignancies. These discoveries have led to the predominant view that cancer cells develop specific adaptations that enable their sustained survival and growth, and are generally referred to as “hallmarks”. Douglas Hannahan and Robert Weinberg (2000) first described these hallmarks and presented them as a simplified list of the quintessential characteristics of cancer cells. These alterations are described as promoting the cell’s ability to stimulate proliferation, enable motility, initiate the growth of new blood vessels, obtain replicative immortality, disable the influence of growth suppressors, and maintain cellular viability [1]. Ten years later, Hannahan and Weinberg revised their originally proposed hallmarks to reflect the rapid advances in cancer research. They added to their original hallmarks the avoidance of immune destruction and the deregulation of cellular metabolism, as well as adding the cancer-enabling

characteristics of genome instability and inflammation [2]. Defining these hallmarks has provided a common language for cancer researchers in considering the great diversity of altered cellular events that give rise to and support the oncogenic state. The multiple pathologies that encompass the range of human cancers, reflected in a variety of cell types that can give rise to neoplasms, appear heterogeneous, but in fact are generally supported by highly similar and often redundant mechanisms.

Hannahan and Weinbergs' recognition of the importance of cellular metabolism in cancer is not a new discovery, and in fact it was observed in one of the first published studies of tumor growth [3]. This seminal work was carried out by the Nobel laureate Otto Warburg in the 1920's using the then newly developed animal models of tumor formation, such as Flexner-Jobling's rat carcinoma or Jensen's rat sarcoma [3], [4]. Using these contemporary models of cancer, Warburg described the glucose and oxygen consumption of arterial and venous blood of growing tumors, which led him to propose that neoplastic disease was in fact caused by metabolic abnormalities arising in normal cells. When comparing tumor to normal tissue he found that tumors ferment glucose at aberrantly high rates to produce lactate, while normal tissues primarily rely on respiration, whereby glucose is fully oxidized to produce carbon dioxide [4]. These observations led to his landmark discovery; that tumors harbor a significantly altered metabolism from normal cells that relies on the fermentation of glucose to form lactate, even in the presence or absence of oxygen (Figure 1.1A). More specifically, his work lead him to postulate that cancer cells undergo aerobic fermentation as a result of respiratory dysfunction [5].

FIGURE 1.1– The Warburg effect observed in tumors and cells. (**A**) Arterial blood, abundant in glucose and oxygen, supplies the growing tumor. Venous blood is found to have consumed virtually all of the glucose, except instead of fully oxidizing it to carbon dioxide, the primary waste product is lactate. (**B**) Depiction of the Warburg effect in cells, where glucose is imported at high rates and converted to pyruvate, where the bulk of pyruvate is secreted from the cell as lactate as opposed to being imported into the mitochondria as acetyl-CoA. To compensate, cells resort to other metabolic pathways, principally glutamine catabolism, where intracellular glutamine serves as an anaplerotic source.

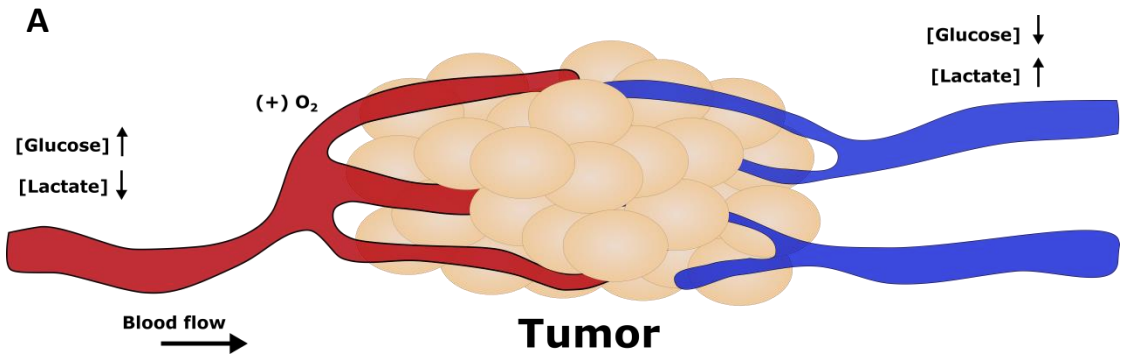
A
[Glucose]
[Lactate]
(+) O_2
[Glucose]
[Lactate]
Blood flow
Tumor

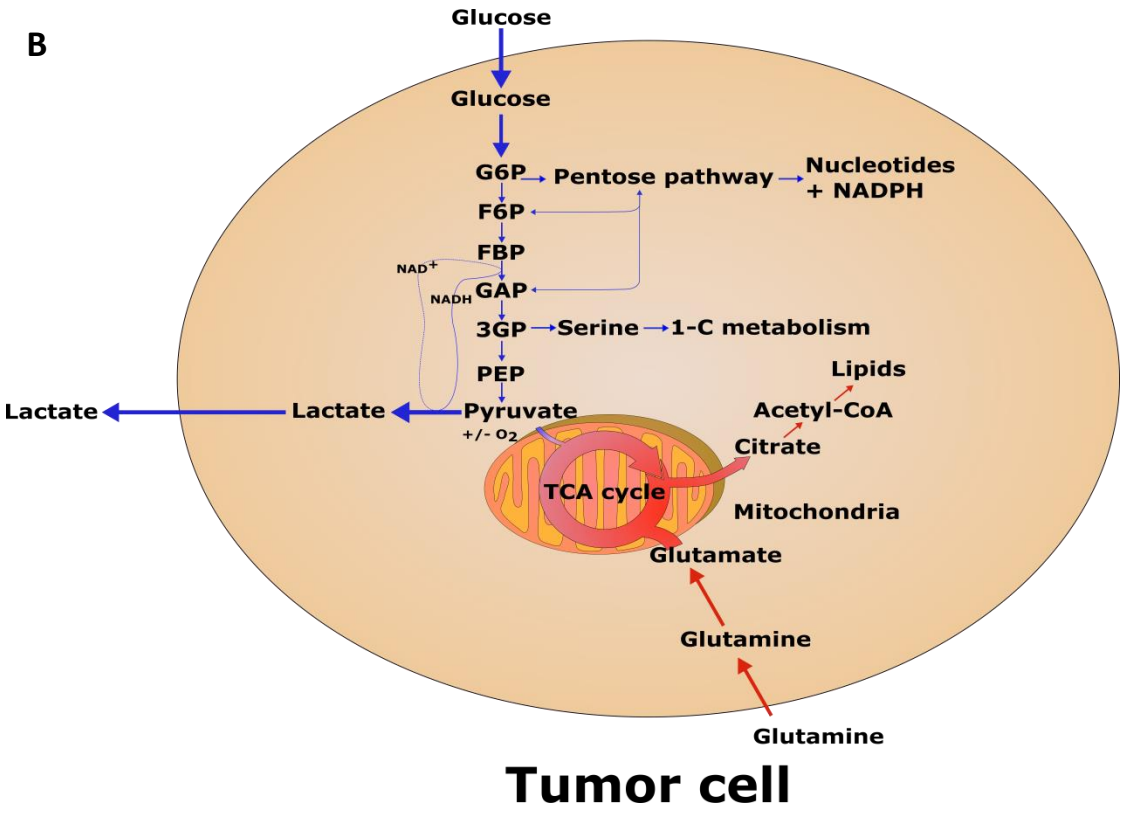
B
Glucose
Glucose
G6P
Pentose pathway
Nucleotides
+ NADPH
F6P
FBP
NAD^+
NADH
GAP
3GP
Serine
1-C metabolism
PEP
Lipids
Lactate
Lactate
Pyruvate
Acetyl-CoA
+/- O_2
Citrate
TCA cycle
Mitochondria
Glutamate
Glutamine
Glutamine
Tumor cell

Today, this metabolic reprogramming is termed the “Warburg effect”, and is a fundamental characteristic of cancer cells altered metabolism. This metabolic phenotype in proliferating cells results in the bulk of glucose carbon being secreted from the cell as lactate, leaving the mitochondria depleted of glucose-derived carbon normally used to fuel the TCA cycle (Figure 1.1B). In order to provide the TCA cycle with an alternative source of catabolic substrates, the amino acid glutamine serves as the primary anaplerotic metabolite in proliferating cells, entering the cycle upon conversion to α-ketoglutarate. The current appreciation of this shift to glutamine dependence represents a new paradigm in cancer research and with it the hope of discovering new opportunities for therapeutic intervention [6].

Although there is a renewed interest in describing the altered metabolism that accompanies oncogenic transformation, this general approach to cancer therapy has a significant historical legacy. There are many cases throughout the past century that have exploited the metabolic alterations of cancer cells to treat patients. Perhaps the most well-known and seminal in the field of chemotherapy was Sydney Farber’s development of anti-folates in 1948 [7]. His initial observation came by supplying doses of folic acid, which at that time was understood to be a dietary factor important for normal bone marrow function, to children with acute leukemia, and found that these supplements exacerbated their cancer [8, pp. 28–29]. This lead him to develop a theory that leukemic cells must rely on folic acid for sustained growth, and therefore antagonists of folic acid might inhibit those cells [9], [10]. Folic acid antagonists, known as antifolates, indeed became one of the first chemotherapies to be developed and shown to be effective, earning Farber the colloquial title of “the father of modern

chemotherapy" [7]. It soon became clear following Farber's investigation into antifolates for the treatment of childhood leukemia, that this vitamin is a crucial cofactor for DNA synthesis, a characteristic thought to be important among the altered metabolic requirements of cancer cells [11], [12]. The discovery of antifolates was made alongside the development of nitrogen mustards by Goodman and Gilman in 1946, the latter initially proving effective in patients with non-Hodgkin's lymphoma, although they subsequently underwent severe relapses and this therapy was discontinued [13]. Farber's contribution to the study of cancer chemotherapies is the first example of intentionally targeting the altered metabolic requirements of cancer cells. Hoping to build on this initial success, scientists interested in developing more effective chemotherapeutics, such as Hitchings and Elion, followed Farber's lead. They began by developing purine antimetabolites, known as thiopurines, just a few years after Farber's antifolates gained appreciation [14]. Thiopurines were subsequently shown to be effective in the clinic and became the first line therapies for hematopoietic cancers, leading to the awarding of the Nobel prize in 1988 for this discovery [7], [15]. Only six years later, following this trend of targeting metabolites that are vital to cancer cells, Heidelberger and colleagues discovered the antimetabolite 5-fluorouracil (5-FU), which is still in use today as a frontline therapy for a many cancers [16]. It is now known that 5-FU, once phosphorylated in the cell by thymidine phosphorylase (TP) to form the active antimetabolite 5-fluorodeoxyuridine monophosphate (FdUMP), acts as a competitive inhibitor of thymidylate synthase (TS) through formation of a ternary complex with 5,10-methylene tetrahydrofolate (CH_2THF) [17]. Taken together, the above examples

provided the first proof of principle that cancer could be effectively targeted with small molecule drugs, and underscored the important role cell metabolism plays in supporting the growth of cancer cells.

It is worth noting that the targeting of the altered metabolism characteristic of cancers was developed at a time when the primary metabolic networks studied today were not very well understood. In fact, Hans Krebs, a former student of Otto Warburg's, first began describing the metabolism of amino acids and the oxidation of carbohydrates through the TCA cycle almost a decade after Warburg's description of tumor metabolism [18]–[22]. The work done by Warburg, Farber, and others preceded the discovery of the DNA double helix by Watson and Crick in 1953 and the chemiosmotic theory of mitochondrial function proposed by Peter Mitchell in 1961 [23], [24]. Despite Warburg's initial discovery that tumors harbor an altered metabolism distinct from normal non-transformed cells, and the subsequent development of effective chemotherapies targeting altered metabolism, the study of cancer metabolism was soon superseded by the rapid advances in molecular genetics and the identification of viral oncogenes that caused cancer in animal models [1].

Until very recently, advances of cancer research have been driven by the characterization of the genetic basis of cancer, namely the consequential lesions occurring in oncogenes and tumor suppressors that give rise to neoplasia and subsequent malignancies. Exhaustive sequencing studies of a great many cancers have revealed that there are dominant genetic events that frequently occur to drive malignant transformation. These dominant genetic events are referred to as 'driver genes', and so far a surprisingly low number (approximately 140 of the more than

20,000 genes in the human genome) have been shown to promote cancer. Furthermore, these genes can be further subdivided into 12 well-characterized signaling pathways to control only three core processes: cell fate, cell survival, and genome maintenance [25]–[27], emphasizing the common features among a variety of cancers. Even with this wealth of information, clinicians are still in need of new approaches for the treatment of cancer. Initial efforts for developing a new generation of chemotherapeutics focused on targeting the common driver genes themselves. While these treatments are effective in many cases, these targeted therapies often give rise to resistance and recurrence [28]–[32]. To further complicate the development of targeted therapies, some of the most potent oncogenes are in fact termed "undruggable". This is due in part to the lack of small molecule binding pockets within proteins. A few principal examples for this would be the small GTPase Ras, the transcription factor Myc, or the tumor suppressor p53 [33]–[36]. Combined, these three proteins are deregulated in some form in virtually all cancer types, representing the fundamental challenge for cancer researchers. Therefore, in the search for new approaches to treat human cancers, strategies that target cellular processes that commonly support transformation, such as altered cellular metabolism, are a promising area of interest.

The study of altered cancer cell metabolism is in the midst of a renaissance. This is due not only to a few recent discoveries in which metabolic enzymes were discovered to be in the "driver's" seat for the first time [37]–[39], such as the case for mutations in the genes encoding the mitochondrial enzymes succinate dehydrogenase (SDH), isocitrate dehydrogenase (IDH), and fumarate hydratase (FH), but also from

new paradigms from the decades of research in primary metabolism and cellular physiology being revisited. One such paradigm has been that the outcome of the Warburg effect leads to a complete rewiring of central metabolic pathways, in order to generate the biosynthetic precursors needed to sustain proliferation and redox control (Figure 1.1B). Now, experimental advances have provided access to the information needed to study the role altered cell metabolism plays in cancer development. In fact, a new field is emerging from recent studies that track intermediates in metabolic pathways, or alternative side products produced from mutated metabolic enzymes, that promote transformation and neoplasia [40]–[44]. Changes in metabolism, stimulated by driver genes, along with genetic events that produce oncometabolites, represent new opportunities for the detection, diagnosis, and treatment of human cancers.

1.1.2 Metabolic enzymes' pleiotropic roles promote more than just the Warburg effect

A discovery that set in motion the recent attention regarding the metabolic changes that accompany oncogenic transformation, was a set of experiments that connected proliferative signaling events, in the form of receptor tyrosine kinase activation, to a key enzyme in glycolysis [45]–[47]. This enzyme, named pyruvate kinase (PK), was shown to directly give rise to and support the Warburg effect [47]. Pyruvate kinase catalyzes the final step in glycolysis, i.e. the transferring of a phosphate group from phosphoenolpyruvate (PEP) to an ADP molecule to form ATP and release pyruvate. Early on, it was shown that the exclusive expression of the embryonic isoform of this metabolic enzyme, pyruvate kinase isoform 2 (PKM2), was present in cancer cells but not normal cells [48]. More recently, it was suggested that

the switch from pyruvate kinase isoform 1 (PKM1) to PKM2 expression directly enables the Warburg effect (i.e. the shift from oxidative phosphorylation to aerobic glycolysis) [47]. In addition to showing PKM2, but not PKM1, is involved in orchestrating the Warburg effect, this study also elucidated two distinct levels of regulation of PKM2. First, that PKM2 is a phospho-tyrosine binding protein, capable of sensing the stimulation by extracellular growth factors through tyrosine kinases (TKs) [46]. Secondly, the direct phosphorylation of PKM2 on tyrosine 105 by the fibroblast growth factor receptor (FGFR1) was demonstrated. The phosphorylation at Y105 disrupts the binding of the allosteric activator fructose-1,6-bisphosphate (FBP) thereby inhibiting its activity [49]. These observations provided evidence that the regulation of metabolic enzymes occurs not only at the genetic level of PK isoform switching, but also as a result of downstream oncogenic proliferative signals (Figure 1.2A).

PKM2 catalyzes the rate limiting step for the entry of carbon derived from glucose into the mitochondria, where the mitochondrial enzyme pyruvate dehydrogenase (PDH) converts pyruvate to acetyl-CoA to be incorporated into the TCA cycle [50]–[52]. Early studies identified two distinct genes that give rise to the two isozymes of pyruvate kinase, which are further classified by two isoforms for each isozyme. The liver form (PKL) and the form found primarily in red blood cells (PKR) are the result of tissue specific promotion of exon splicing of the “L gene”, whereas both the M1 and M2 isoforms are the result of alternate splicing of the “M gene” [53], [54]. Early kinetic studies and crystal structures of pyruvate kinase revealed that the enzyme is a homotetramer when active, and a dimer when inactive [55]–[57].

Furthermore, it was discovered that the metabolic intermediate in glycolysis, fructose-1,6-bisphosphate (FBP), is an important allosteric activator of the pyruvate kinase's R, L, and M2, but not M1, through its binding at the dimer-dimer interface to promote tetramer formation (Figure 1.2A) [58]. It is here where the PKM2 isoform is distinct from the M1 isoform, where PKM2 contains an alternate amino acid sequence that confers the FBP binding pocket that imparts PKM2's activity dependent on FBP binding, whereas PKM1 is a constitutively active pyruvate kinase not regulated by FBP [59], [60]. Together, these observations have led to the current model where increased PKM2 expression in cancer cells is correlated with decreased enzymatic activity. This is due to PKM2 being regulated by the upstream metabolite, FBP, thereby acting as a rheostat for the glycolytic flux. This decreased PK activity, when coupled with the upregulation of lactate dehydrogenase (LDH) activity, promotes the Warburg effect by directing glucose carbons from entering the TCA cycle to secretion as lactate [61], [62].

It is important to note that not long after this model was proposed, small molecule activators were developed that bind to PKM2 and induce tetramer formation, thereby stimulating its activity (Figure 1.2A). Indeed, these molecules were used in mouse tumor models to establish the potential of this discovery in the development of new therapeutics [63]–[65]. Although these small molecule activators are not yet in clinical trials for the treatment of human cancers, they are being developed for the inherited hematological metabolic disorder known as pyruvate kinase deficiency [66]. Perhaps once these activators are validated in Phase I safety trials, researchers will begin investigations into whether these therapies will have a benefit in treating

cancers. In any case, these discoveries demonstrate PKM isoform switching accompanied by oncogenic signaling events provide a molecular mechanism for the Warburg effect.

Along with these new insights regarding the role of PKM2 in the Warburg effect, researchers also identified novel pleiotropic functions of this metabolic enzyme. First, an allosteric regulator was identified that specifically stimulated PKM2 activity, but not the alternative splice isoform PKM1, which differs from PKM2 by only 22 residues. This allosteric activator, known as SAICAR (succinylaminoimidazolecarboxamide ribose-5'-phosphate), is a metabolic intermediate within the de novo nucleotide synthesis pathway. It was shown that the concentration of this small molecule was dependent on glucose metabolism, and more specifically, the pentose phosphate pathway (PPP), where upon glucose starvation SAICAR would accumulate and thus stimulate PKM2 activity [67]. These results suggest that PKM2 is capable of sensing the pool of biosynthetic precursors necessary for nucleotide production in the cell through the binding of this allosteric activator (Figure 1.2B). At the same time that this newly discovered allosteric control of PKM2 activity by SAICAR was being described, an additional mode of allosteric regulation was identified, that provided for a feedback regulation of PKM2 activity by an intermediate in 1-carbon metabolism, L-serine [68]. The *de novo* synthesis of the amino acid serine in proliferating cancer cells was shown to be derived from glucose upon starvation of exogenously supplied serine. The increase in glucose-derived serine was shown to be a direct result of the decrease of PKM2 activity, and hence a buildup of glycolytic intermediates available to be shuttled into anabolic pathways.

FIGURE 1.2 – PKM2 is a central metabolic enzyme directing the Warburg effect. (**A**) X-ray crystal structure of PKM2 in complex with the allosteric activators FBP and the pharmacological small molecule TEPP-46 (4B2D), aligned with a structure of PKM2 with the allosteric activator L-serine bound (3U2Z). The allosteric regulation of PKM2 is modulated by surface contacts at the dimer-dimer interface. (**B**) Cartoon depiction of the pleiotropic roles of PKM2, where PKM2 activity acts as a rheostat for intracellular metabolites through directly binding metabolic intermediates from glycolysis, amino acid, and *de novo* nucleotide pathways. Alternatively, extracellular signals, such as PKM2 binding to phospho-tyrosine residues or direct tyrosine phosphorylation itself, function to abrogate activation signals of PKM2 by antagonizing the action by metabolites. As a dimer, PKM2 is not able to act as a small molecule kinase to produce ATP, but instead is able to translocate to the nucleus where it adopts a protein kinase function to activate gene transcription through direct phospho-transfer from PEP to Tyr residues on transcription factors such as STAT3.

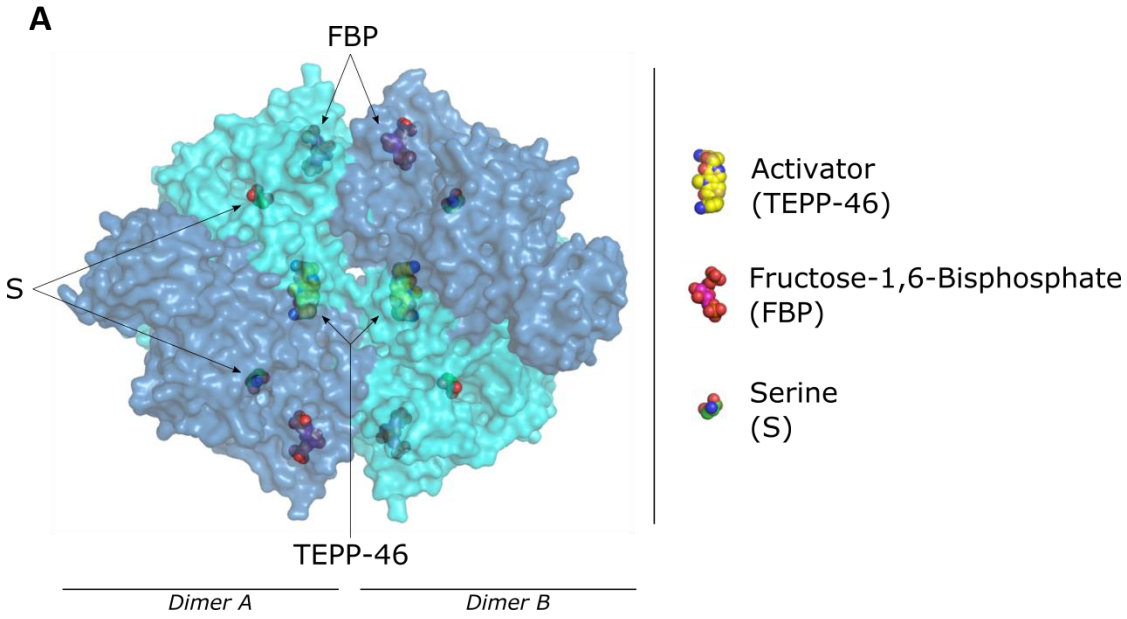
A
FBP
S
TEPP-46
Dimer A
Dimer B
Activator
(TEPP-46)
Fructose-1,6-Bisphosphate
(FBP)
Serine
(S)

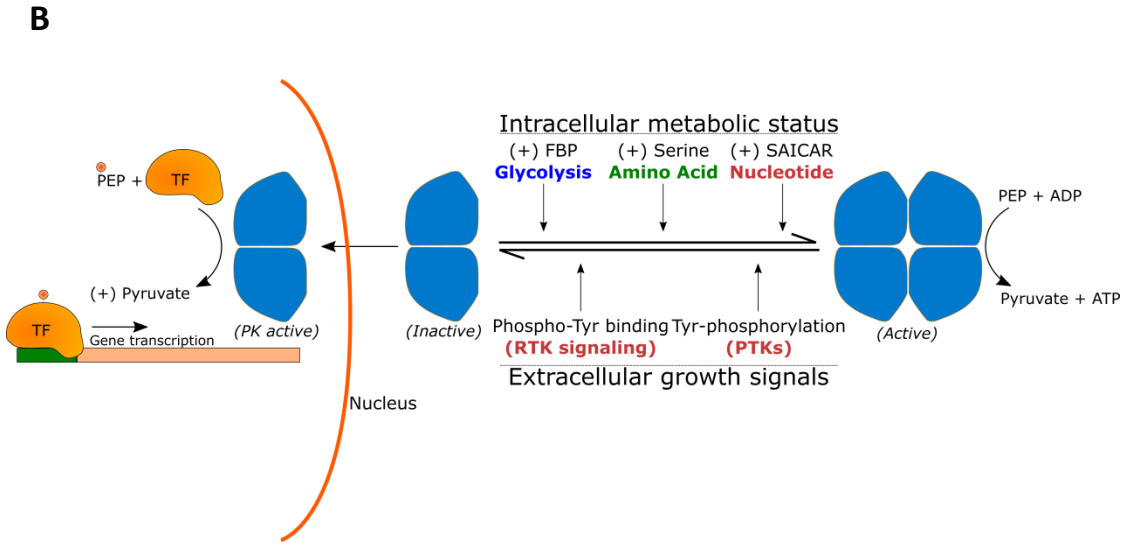
B
PEP +
TF
(+) Pyruvate
TF
Gene transcription
(PK active)
Nucleus
(Inactive)
Intracellular metabolic status
(+) FBP
(+) Serine
(+) SAICAR
Glycolysis
Amino Acid
Nucleotide
Phospho-Tyr binding
(RTK signaling)
Tyr-phosphorylation
(PTKs)
Extracellular growth signals
(Active)
PEP + ADP
Pyruvate + ATP

Together, these results showed that the conversion of PEP to pyruvate, a control step in glycolysis critical for maintaining the altered metabolism in cancer cells exhibiting the Warburg effect, is subject to tight regulation by the *de novo* nucleotide and amino acid synthetic pathways (Figure 1.2B).

Concurrent with this newly discovered metabolite SAICAR being reported, PKM2 was identified as having protein phosphorylating activity, together with being localized within the nucleus to regulate gene expression [69], [70]. Notably, this protein phosphorylation activity, whereby a phosphate group from PKM2's substrate PEP is transferred to both tyrosine and serine/threonine residues of a variety of proteins, is only observed when PKM2 is in the dimeric state. This leads to a model whereby cytosolic PKM2, when in a tetrameric state, functions within glycolysis by acting on PEP to produce ATP and pyruvate, but when in the dimeric state is translocated to the nucleus where it uses PEP to phosphorylate protein substrates (Figure 1.2B). Importantly, the regulation of these pleiotropic activities of PKM2 is dependent on the nutrient status of the cell, where the metabolites SIACAR and FBP act as allosteric regulators of PKM2 activity and thus determine whether the enzyme functions as a pyruvate kinase in the cytoplasm, or a protein kinase in the nucleus [71].

Recent studies have identified other metabolic enzymes that contribute to oncogenesis through unconventional mechanisms, which are distinct from their traditional roles within primary metabolism. One example is hexokinase-2 (HK2), which performs the first irreversible metabolic reaction for glucose utilization in cells. Much like PKM2, HK2 is one of the four isozymes found in human tissues, where it is often highly expressed in aggressive cancers. The HK2 enzyme has the highest

catalytic efficiency of the four HK isozymes, due to two distinct structural characteristics. First, HK2 harbors two duplicated catalytic-active domains within one polypeptide chain, as a result of gene duplication during evolution, whereas the other three isozymes have one [72], [73]. Second, the HK2 isozyme contains an N-terminal hydrophobic domain that promotes its association with the outer mitochondrial membrane [74]. The anchoring of HK2 to the outer mitochondrial membrane allows it to sense the viability of mitochondria through the binding of the integral membrane protein and voltage-dependent anion channel (VDAC). In addition, sequestering HK2 on the mitochondrial membrane promotes its enzymatic activity by giving it access to mitochondrial ATP and shielding it from product inhibition by glucose-6-phosphate (G-6-P) [75], [76]. Together these characteristics make the HK2 isoform a highly efficient glucose kinase, thereby promoting the Warburg effect (Figure 1.3A). The increased HK2 efficiency, compared to other HK isoforms, has been shown to be responsible for supporting aerobic glycolysis (i.e. the Warburg effect) and cancer cell proliferation, and a direct downstream target of the PI3K/Akt signaling cascade [77]–[79]. Importantly, this dramatic increase in a virtually irreversible metabolic step within glucose metabolism enables radiologists to take advantage of this metabolic shift by using an ^{18}F-deoxyglucose (FGD) probe for positron emission tomography (PET), which has become the standard imaging technique for many solid tumors [76], [80] (Figure 1.3B,C).

The targeting of HK2 in cancer has long been a challenge due to the highly accessible and polar surface of the substrate binding site, as well as the inhibitory allosteric site for the product, glucose-6-phosphate (G6P) [81]. However, Lin and

colleagues (2016) have recently identified glucosamine derivatives through high-throughput screening efforts to find HK2 selective inhibitors. These glucosamine derivatives represent a new strategy for the selective inhibition of HK2, but not HK1 isozymes, through the competitive binding of the substrate glucose. The finding of HK2-specific inhibitors through targeting the glucose binding site is an unexpected result. These new small molecules open the door for the development of new therapeutics to target the principal step that initiates the Warburg effect.

Despite HK2's role in promoting the Warburg effect in many cancers, perhaps an equally important function for HK2 in cancer cells is its involvement in apoptosis. Early observations of hexokinase activity within cellular extracts of cancer cells showed a localization of this activity with the mitochondrial fraction. More specifically, this activity was found on the outer mitochondrial membrane [82]. Investigations into this observation found that the prevalent form of hexokinase in cancer cells, HK2, was associated with the outer mitochondrial membrane through the binding of VDAC (Figure 1.3A). This interaction of HK2 with VDAC was shown to act as a sensor for mitochondrial membrane potential, where disruption of the proton gradient within the inner-membrane space would dissociate the adenosine nucleotide transporter (ANT) from VDAC, releasing HK2, and allowing apoptotic proteins with BH3 domains, such as Bax and Bad, to bind to VDAC and facilitate the release of cytochrome C [79], [82]–[84]. Cytochrome-c release results in the initiation of caspase activation, triggering apoptosis throughout the cell. This release of cytochrome c following oxidative stress provides a molecular mechanism for HK2, involved at the first step of glycolysis, to couple nutrient stress with the apoptotic response.

FIGURE 1.3 – HK2 is an efficient glucose kinase that drives the Warburg effect and enables the use of ^{18}F-FDG PET to image cancers. (**A**) X-ray crystal structure of HK2 in complex with the allosteric inhibitor, glucose-6-phosphate (G6P), and a glucosamine derivative in the glucose binding pocket (5HG1). The 15-residue long hydrophobic N-terminus of HK2 is shown associating with the outer mitochondrial membrane, where the N-terminus of HK2 binds to the ion channel VDAC, which couples to the adenosine nucleotide transporter (ANT) on the inner mitochondrial membrane. (**B**) The use of ^{18}F-deoxyglucose as a diagnostic tool depends on the import of glucose through abundant glucose transporters, such as GLUT1, on the plasma membrane. Upon import, FDG is readily phosphorylated in highly proliferative cells, but not normal cells, and becomes trapped within the cell and unable to be metabolized further. (**C**) An example of the utility of FDG-PET in human cancers [79]. Here, a patient with non-small cell lung cancer (NSCLC) is monitored using FDG-PET imaging following treatment with the EGFR kinase inhibitor erlotinib. The solid tumor (left, red arrow) is visualized before, but not after, 14 days of treatment.

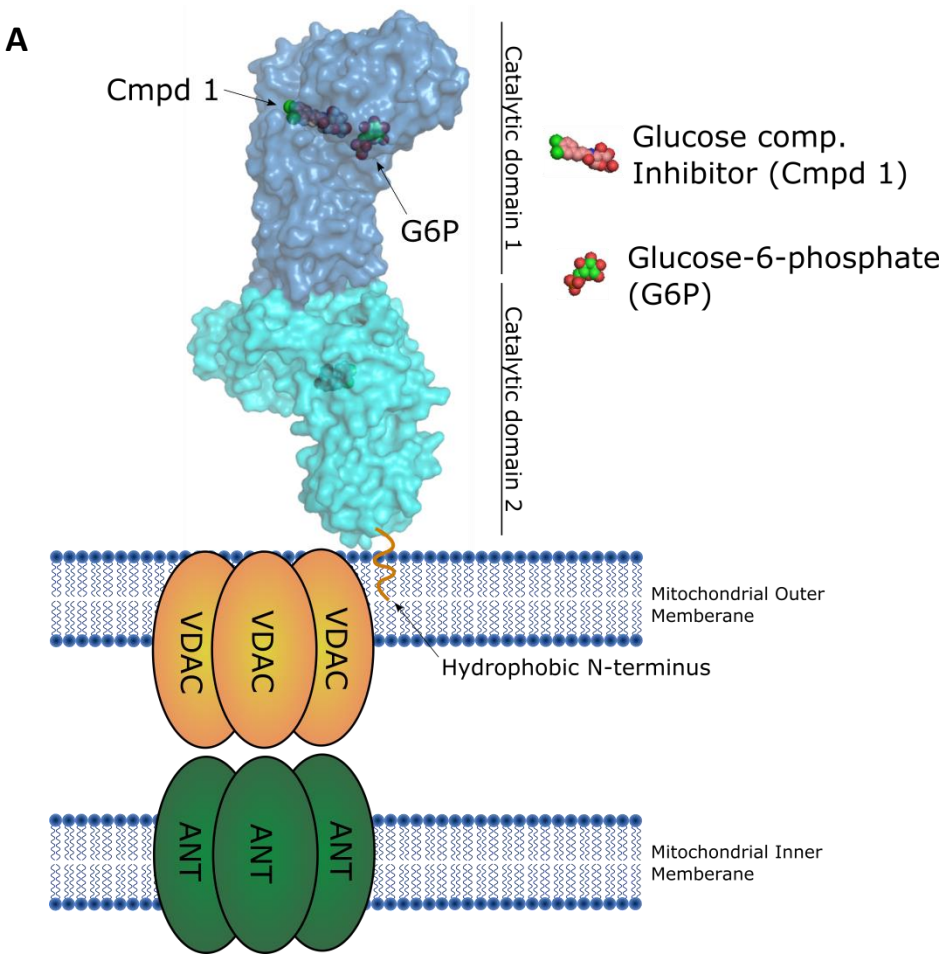
A
Cmpd 1
G6P
Catalytic domain 1
Catalytic domain 2
Glucose comp.
Inhibitor (Cmpd 1)
Glucose-6-phosphate
(G6P)
VDAC
VDAC
VDAC
Mitochondrial Outer
Memberane
Hydrophobic N-terminus
ANT
ANT
ANT
Mitochondrial Inner
Memberane

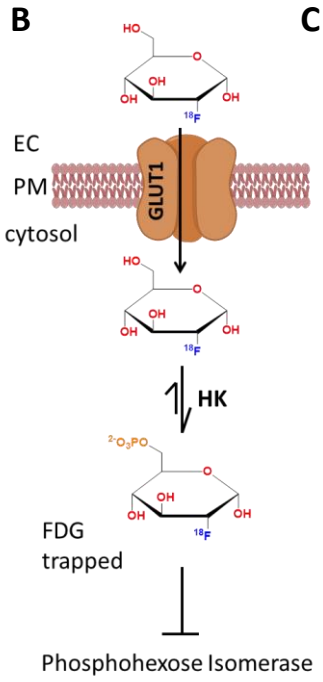
B
EC
PM
cytosol
GLUT1
HK
FDG
trapped
Phosphohexose Isomerase

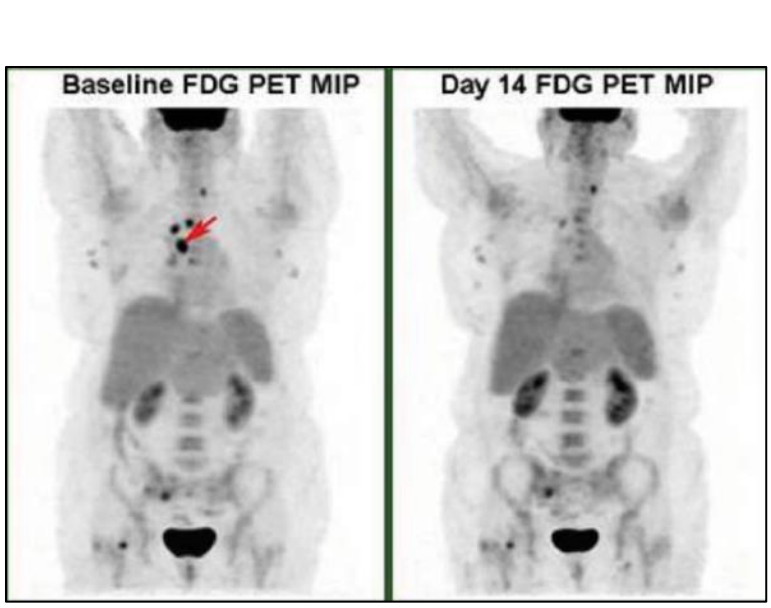
C
Baseline FDG PET MIP
Day 14 FDG PET MIP

1.1.3 Metabolic enzymes as oncogenes and tumor suppressors

Both of these enzymes, HK2 and PKM2, are examples of how metabolic enzymes, and in particular isozyme switching of the enzymes, can play vital roles in orchestrating the Warburg effect. However, neither of these enzymes are sufficient by themselves to drive oncogenesis, and are therefore thought to be essential for supporting the transformed state, but not driving it. In contrast, genetic mutations in a few metabolic enzymes have been shown to drive cells to the transformed state, resulting in the formation of solid tumors. Interestingly, the altered enzymes that have been identified are all localized to the mitochondria and function within the TCA cycle.

The first metabolic enzyme identified to drive tumor formation was the product of inherited genetic variants of the succinate-ubiquinone oxidoreductase complex II, known more commonly as succinate dehydrogenase (SDH). These genetic variants were within the nuclear gene encoding the D subunit, SDHD [39], [85], [86]. Respiratory complex II is a multi-protein complex comprised of four subunits, SDHA, SDHB, SDHC, and SDHD, that act together to oxidize the TCA cycle intermediate succinate to fumarate (Figure 1.4). This is accomplished by an initial hydride transfer from succinate to a bound flavin adenine dinucleotide (FAD^+) molecule in SDHA to produce $FADH_2$ and release fumarate. The reduced $FADH_2$ then transfers the electrons to iron sulfur clusters in SDHB, where the electrons are finally accepted by the ultimate carrier molecule ubiquinone (Q) to form hydroquinone (QH_2) within the mitochondrial transmembrane subunits SDHC and SDHD. Respiratory complex II is an integral membrane protein within the mitochondria, that functions to not only

maintain the TCA cycle turnover, but also to add reducing equivalents of hydroquinone and fuel the proton transport of respiratory complex III, a prerequisite for generating a membrane potential. Therefore, defects in this enzyme that result in ablating its activity have drastic effects on both the metabolite pools throughout the cell, and the membrane potential necessary to maintain healthy mitochondria.

Originally, germline mutations in the SDH subunits D, and later both B and C, were identified in cases of familial head and neck paragangliomas and sporadic pheochromocytomas. Paragangliomas are of neuroendocrine origin derived from the sympathetic nervous system along the cranial nerves and vasculature [39], [87], whereas pheochromocytomas are extra-adrenal tumors derived from the adrenal medulla cells and produce catecholamines, often causing the hypertension that characterizes the condition [85], [86]. These tumors are well studied because they are often driven by germline mutations in well-known proto-oncogenes and tumor suppressors, such as RET, NF1, Myc association factor (Max), VHL, HIF2A, or TMEM127. In the course of searching for the drivers in tumors that do not harbor the known proto-oncogene and tumor suppressor mutations, germline and somatic mutations in the SDH gene products were subsequently discovered [88]. In addition to a variety of mutations identified in the principal components of the heterotetrameric SDH enzyme, occurring in the SDHA, B, C, and D subunits, point mutations have also been identified in the gene that encodes the flavin-transferase for SDH, named SDH5 [89]. SDH5 is a recently characterized mitochondrial protein that associates with SDHA to facilitate the covalent attachment of the flavin adenine dinucleotide (FAD^+) moiety through a poorly understood mechanism.

FIGURE 1.4 – Enzymes of the TCA cycle and glutaminolysis pathways. Each subunit of a mitochondrial complex is colored in blue or cyan, representing oligomeric species of each enzyme along the pathway. Substrates and cofactors are displayed when available as spheres in CPK coloring, highlighting the general trend of binding sites being proximal to oligomer-contacts. Enzymes that function as tumor suppressors, where mutations or deletions give rise to human cancers, are highlighted with red boxes. PDB files used for each enzyme are as follows. Pyruvate dehydrogenase, only the E1 subunit octahedral supercomplex is shown where the E2 and E3 subunits are omitted for simplification (1B5S), citrate synthase (1CTS), aconitase (7ACN), and isocitrate dehydrogenase 2 (3BLW). Alpha-ketoglutarate dehydrogenase was constructed using the E1 dehydrogenase (2JGD). Also included are E2 dehydrogenase (1E2O), and E3 dehydrogenase (2EQ7), succinyl-CoA synthetase (2FP4), succinate dehydrogenase (1NEK) with the newly described flavoprotein transferase SH5 (2LM4), fumarate hydratase (3E04), malate dehydrogenase (4WLU), glutamate dehydrogenase (1HWY), glutamate-pyruvate transaminase (3IHJ), glutamate-oxaloacetate transaminase (5AX8), and glutaminase (3UO9).

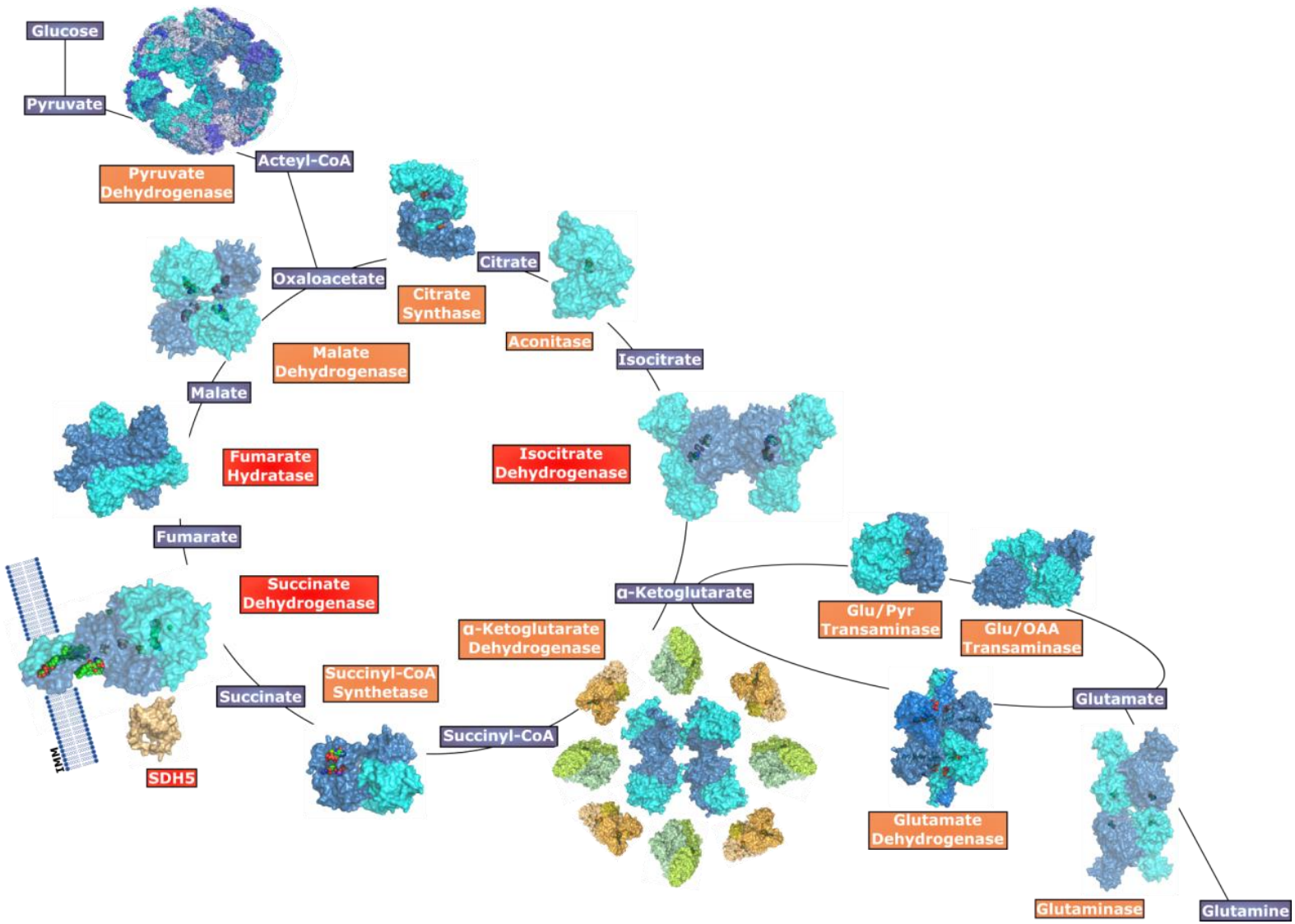
Glucose
Pyruvate
Pyruvate Dehydrogenase
Acteyl-CoA
Oxaloacetate
Citrate Synthase
Citrate
Aconitase
Isocitrate
Isocitrate Dehydrogenase
Malate Dehydrogenase
Malate
Fumarate Hydratase
Fumarate
Succinate Dehydrogenase
IMM
SDH5
Succinate
Succinyl-CoA Synthetase
Succinyl-CoA
α-Ketoglutarate Dehydrogenase
α-Ketoglutarate
Glu/Pyr Transaminase
Glu/OAA Transaminase
Glutamate
Glutamate Dehydrogenase
Glutaminase
Glutamine

Mutations of SDH5 found in human tumors occur at a highly conserved fold mapped to the binding interface of SDH5 to SDHA, and are associated with an inactive SDH enzyme [89], [90]. These mutations in components of the SDH complex all result in an inactive form of the enzyme, thereby increasing the metabolite pool of succinate. The excess succinate acts to competitively inhibit critical enzymes that use the TCA cycle intermediate α-ketoglutarate (αKG) as a substrate. The enzymes that have been shown to be most impacted by increased levels of succinate in SDH deficient cells are the αKG-dependent prolyl hydroxylases (PHDs) that function to regulate the tumor suppressor HIF, as well as the nuclear Jumonji demethylases and TET hydroxylases, by impairing DNA and histone methylation levels [91]–[94]. The accumulation of the intracellular pool of succinate, that is a result of deficiencies in SDH activity, has severe impacts on oxidative stress and epigenetic regulation of gene expression. This has provided important insights as to the role primary metabolism plays in growth, differentiation, and cancer. As is the case with SDH, mutations in other TCA cycle enzymes, namely fumarate hydratase (FH) and isocitrate dehydrogenase (IDH), also give rise to oxidative stress, induction of hypoxia-related genes, and epigenetic changes [95].

The identification of cancer causing mutations within the gene encoding fumarate hydratase, also known as fumarase, followed a similar path to discovery as that of SDH. Initially, genetic alterations in the chromosome 1q42.3-q43 region were found to be associated with familial inheritance of cutaneous and uterine leiomyomatomas, which are benign smooth muscle tumors, and type II papillary renal cell carcinoma [96]–[98]. Fumarate hydratase functions to metabolize fumarate in both

the cytoplasm, where fumarate is a byproduct of the urea cycle, and the mitochondria, where fumarate is a key TCA cycle intermediate [99]. Currently, it is thought that FH requires the formation of homotetramers in order to be catalytically active, although structural studies of the human enzyme are lacking [100]. However, there seem to be a variety of truncations, point mutations, and missense mutations that have been identified and associated with tumorigenesis. Again, as is the case for SDH, FH mutants are associated with a loss of enzyme activity and therefore an increase of intracellular levels of the TCA cycle intermediate fumarate and the upstream substrate succinate. Indeed, the increased level of fumarate in cells has been shown to promote the Warburg effect through activation of HIF genes by inhibiting the prolyl hydroxylase enzymes that act to keep HIF levels regulated in oxygen-abundant environments [41]. In addition to the activation of HIF driven transcription, fumarate has been shown to be involved in the post-translational modification of free thiol groups of both glutathione and cysteine residues within proteins in FH-deficient cells, promoting oxidative damage by ROS [42], [101], [102]. These observations further support the view that disabling mutations within the TCA cycle can promote neoplasia, by causing the accumulation of tumor promoting oncometabolites.

Perhaps one of the most significant breakthroughs in the field of oncometabolites was the discovery that mutations within the active site of the TCA cycle enzyme isocitrate dehydrogenase (IDH) are found in a large percentage (~12%) of tumors of glioblastoma multiforme (GBM), with an even greater occurrence in higher grades of glioblastoma [103]–[105]. Moreover, the mutations in the active site confer a neomorphic enzyme activity, producing the unnatural byproduct D-2-

hydroxyglutarate (2-HG) from αKG [106]. There are three isoforms of IDH, a cytosolic form (IDH1) and two mitochondrial forms (IDH2/3), which function in their respective cellular compartments to catalyze the decarboxylation of isocitrate to produce αKG and release CO_2 upon concomitant reduction of $NADP^+$ to NADPH for IDH1/2, or NAD^+ to NADH for IDH3. The mutations that have since been identified in not just GBM, but also other cancers such as renal cell carcinoma (RCC) or acute myelogenous leukemia (AML), all have the same specific point mutation of a critical arginine residue within the active site (R134 in IDH1, either R172 or R140 in IDH2) [105], [107], [108]. Interestingly, the IDH3 isozyme possesses not only a different substrate specificity for NAD^+ (as opposed to $NADP^+$), but also a distinct quaternary structure. Specifically, IDH1 and IDH2 exists as homo-dimers, whereas IDH3 forms a hetero-trimer of subunits alpha, beta, and gamma [109]. To date, no mutations in the IDH3 isozyme have been associated with tumorigenesis or cancer progression, highlighting the unique property of IDH1/2 mutants to promote cancer [110]. The accumulation of the oncometabolite 2-HG appears to act through a similar mechanism as that observed for accumulations of intracellular succinate, where both act as competitive inhibitors of αKG-dependent enzymes. The result is an activation of the transcriptional program that results from HIF1α stabilization as well as changes in DNA methylation that act together to promote oncogenesis [37], [40], [43].

Taken together, these observations highlight the role that core metabolic enzymes can play in supporting the transformed state and directly driving tumorigenesis. The dysregulation of the metabolic enzymes IDH, SDH, and FH, through either hereditary or somatic mutations has shifted the paradigm and

underscored the important role metabolic pathways play in cellular transformation.

1.1.4 Glutaminolysis as an anaplerotic source for cells under metabolic stress

As mentioned earlier, the shift of cancer cells under metabolic stress from oxidative phosphorylation to aerobic glycolysis leaves the mitochondrial TCA cycle without glucose-derived carbon sources such as acetyl-CoA. Therefore, cells exhibiting the Warburg effect require an alternative carbon source to replenish the TCA cycle intermediates. It has been shown in a variety of cell culture and tumor models that the increase in aerobic glycolysis is often accompanied by an increase in glutamine metabolism [111]–[116]. In this way, glutamine, being the most abundant amino acid in the blood, is deamidated by mitochondrial glutaminase (GLS) to produce stoichiometric amounts of glutamate and ammonia. The glutamate produced from the glutaminase reaction is then deamidated by the mitochondrial enzyme glutamate dehydrogenase (GDH), or by one of the two mitochondrial transaminases, pyruvate transaminase (GPT) or oxaloacetate transaminase (GOT), to result in production of α-ketoglutarate that can directly enter the TCA cycle (Figure 1.4).

The metabolite α-ketoglutarate plays an essential role in the proliferating cell, where it is a common substrate for many metabolic pathways. In addition, it has recently been shown in many cancers that α-ketoglutarate can be carboxylated to produce citrate by the TCA cycle enzyme IDH1/2 (discussed above) in a process termed reductive carboxylation [117]–[119]. Reductive carboxylation is emerging as a process critical for the production of lipids within the cytoplasm/endoplasmic reticulum. It is here where mitochondrial citrate is exported to the cytoplasm and converted to acetyl-CoA, the building block for lipid synthesis, by the enzyme ATP-

citrate lyase (ACL) [120]. Efforts to develop small molecule inhibitors of ACL hold promise for the treatment of human cancers that are driven by Akt/mTORC1 metabolic phenotypes [121]–[123]. However, to date only one clinical trial is active, and that is for the targeting of hyperlipidemia (Esperion Therapuetics©). Perhaps, as is the case with the targeting of PKM2 (discussed above), these small molecules that target metabolic enzymes will prove useful in metabolic disorders first, where clinical trials for specific cancer groups or treatment regimens will follow.

As mentioned above, glutamine fueled reductive carboxylation is an adaptive mechanism for highly proliferative cells using high aerobic glycolytic flux, by providing the biosynthetic precursors for the additional lipids required for continual cell division and growth. In this way, targeting the first committed step of glutaminolysis, namely the mitochondrial glutaminase, provides a way of targeting transformed cells that rely on glutamine metabolism. However, the regulation of glutaminase remains poorly understood despite its apparent upregulation in a variety of oncogenic signaling pathways, such as those involving c-Myc over-expression, HIF1α stabilization, and Rho-GTPase dependent transformation [114], [124]–[127]. Human glutaminase (hGLS) consists of two isozymes, GLS1 and GLS2, where GLS1 has two alternatively spliced isoforms, kidney-type (KGA) and glutaminase C (GAC), with the GAC isoform being the primary isoform expressed in cancer cells (Figure 1.5) [111], [128]–[130].

FIGURE 1.5 – Isozymes and isoforms of glutaminase enzymes. The crystal structures of the liver-type and kidney-type glutaminases are presented, with their domains and corresponding residue assignments depicted above. Both glutaminases crystalize as homotetramers, despite having distinct catalytic properties. The short form, GAC, is primarily upregulated in cancer cells.

Liver type

12q13.3

19 exons

Primarily in liver

Kidney type

2q32-q34

Long isoform (KGA) — Kidney, brain

Short form (GAC) — Muscle, Immune cells, proliferating cells

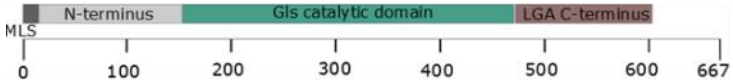

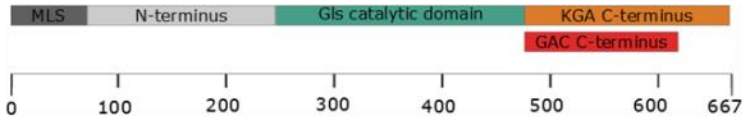

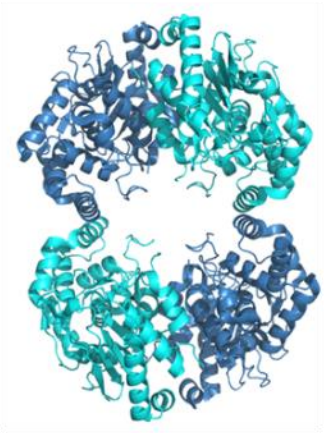

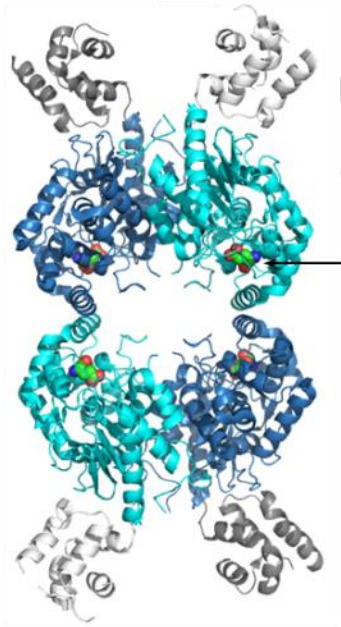

Tetramer

Dimer

N-terminus

Gls domain

Active Site
(Glu bound)

It has previously been shown that the activity of GAC is dependent on the oligomeric state of the enzyme. Increased activation *in vitro* is promoted by the allosteric regulator inorganic phosphate, which causes GAC to undergo a dimer (inactive) to tetramer (active) transition [131], [132]. However, thus far a mechanistic understanding for GAC activation has been lacking, and a detailed picture of this would shed light on how its activation in cancer cells can be blocked by newly characterized small molecule inhibitors, and how one might improve existing platforms [137], [138].

PROPOSED STUDIES

In the initial phase of the this thesis, I will take advantage of a Fluorescence Resonance Energy Transfer (FRET) assay that I have developed to directly monitor the dimer-to-tetramer transition of GAC in combination with real time and single point activity assays in order to probe the dependence of its oligomeric state on activity (Chapter 2). After validating these approaches, I then use them in studies to gain insights into the mechanism of action of the two glutaminase-specific inhibitors, derivatives of the benzophenanthridines (e.g. 968), and BPTES (bis-2-(5 phenylacetamido-1,2,4-thiadiazol-2-yl) ethyl sulfide) (Chapters 3 and 4, respectively).

In order to specifically study the role of GAC up-regulation and activation in oncogenic transformation and its possible role in glutamine addiction, I make use of a model cell system using tetracycline controlled gene expression in mouse embryonic fibroblasts (MEFs) to examine the effects of the induced expression of the oncogenic Rho GTPase GEF (guanine nucleotide exchange factor) Dbl (for Diffuse B-Cell Lymphoma) and subsequent hyper-activation of Rho GTPases (Chapter 5). Our

laboratory and others have reported the activation of glutaminase in mitochondrial extracts from transformed cells in response to mitogenic stimuli and the hyper-activation of Rho GTPases, or upon EGF stimulation in a Raf-Mek-Erk-dependent manner [127], [133]. In addition, using the mechanistic insights gained from Chapters 2-4, I investigate the oligomeric status of the GAC enzyme in Dbl-induced transformed cells and in non-transformed (uninduced) cells, and show that an increase in glutaminolysis in Dbl-induced cells correlates with the shift from a GAC dimer to a GAC tetramer (Chapter 5). Additionally, I use these biophysical approaches to analyze mouse tissues, showing that these oligomeric states are indeed conserved in biological tissues, and present methods to purify and characterize a newly discovered high-molecular weight GAC species (Chapter 5).

1.2 References

[1] D. Hanahan and R. A. Weinberg, “The Hallmarks of Cancer,” *Cell*, vol. 100, no. 1, pp. 57–70, Jan. 2000.

[2] D. Hanahan and R. A. Weinberg, “Hallmarks of Cancer: The Next Generation,” *Cell*, vol. 144, no. 5, pp. 646–674, Mar. 2011.

[3] O. Warburg, “The Metabolism of Carcinoma Cells,” *J. Cancer Res.*, vol. 9, no. 1, pp. 148–163, Mar. 1925.

[4] O. Warburg, F. Wind, and E. Negelein, “THE METABOLISM OF TUMORS IN THE BODY,” *J. Gen. Physiol.*, vol. 8, no. 6, pp. 519–530, Mar. 1927.

[5] O. Warburg, “On the origin of cancer cells,” *Science*, vol. 123, no. 3191, pp. 309–314, Feb. 1956.

[6] M. G. V. Heiden, L. C. Cantley, and C. B. Thompson, “Understanding the Warburg Effect: The Metabolic Requirements of Cell Proliferation,” *Science*, vol. 324, no. 5930, pp. 1029–1033, May 2009.

[7] V. T. DeVita and E. Chu, “A History of Cancer Chemotherapy,” *Cancer Res.*, vol. 68, no. 21, pp. 8643–8653, Nov. 2008.

[8] *The Emperor Of All Maladies [A Biography Of Cancer].pdf (PDFy mirror)*. 2014.

[9] S. Farber and L. K. Diamond, “Temporary remissions in acute leukemia in children produced by folic acid antagonist, 4-aminopteroyl-glutamic acid,” *N. Engl. J. Med.*, vol. 238, no. 23, pp. 787–793, Jun. 1948.

[10] S. Farber, “Some observations on the effect of folic acid antagonists on acute leukemia and other forms of incurable cancer,” *Blood*, vol. 4, no. 2, pp. 160–167, Feb. 1949.

[11] E. L. Stokstad and J. Koch, “Folic acid metabolism.,” *Physiol. Rev.*, vol. 47, no. 1, pp. 83–116, Jan. 1967.

[12] J. Metz, A. Kelly, V. C. Swett, S. Waxman, and V. Herbert, “Deranged DNA Synthesis by Bone Marrow from Vitamin B12-Deficient Humans*,” *Br. J. Haematol.*, vol. 14, no. 6, pp. 575–592, Jun. 1968.

[13] A. Gilman, “The initial clinical trial of nitrogen mustard,” *Am. J. Surg.*, vol. 105, pp. 574–578, May 1963.

[14] G. B. Elion, S. Singer, and G. H. Hitchings, “Antagonists of Nucleic Acid Derivatives Viii. Synergism in Combinations of Biochemically Related Antimetabolites,” *J. Biol. Chem.*, vol. 208, no. 2, pp. 477–488, Jun. 1954.

[15] G. H. Hitchings and G. B. Elion, “The Chemistry and Biochemistry of Purine Analogs,” *Ann. N. Y. Acad. Sci.*, vol. 60, no. 2, pp. 195–199, Dec. 1954.

[16] C. Heidelberger, N. K. Chaudhuri, P. Danneberg, D. Mooren, L. Griesbach, R. Duschinsky, R. J. Schnitzer, E. Pleven, and J. Scheiner, “Fluorinated Pyrimidines, A New Class of Tumour-Inhibitory Compounds,” *Nature*, vol. 179, no. 4561, pp. 663–666, Mar. 1957.

[17] D. B. Longley, D. P. Harkin, and P. G. Johnston, “5-Fluorouracil: mechanisms of action and clinical strategies,” *Nat. Rev. Cancer*, vol. 3, no. 5, pp. 330–338, May 2003.

[18] H. A. Krebs, “Metabolism of amino-acids,” *Biochem. J.*, vol. 29, no. 7, pp. 1620–1644, Jul. 1935.

[19] H. A. Krebs and W. A. Johnson, “Metabolism of ketonic acids in animal tissues,” *Biochem. J.*, vol. 31, no. 4, pp. 645–660, Apr. 1937.
[20] H. A. Krebs, “The role of fumarate in the respiration of Bacterium coli commune,” *Biochem. J.*, vol. 31, no. 11, pp. 2095–2124, Nov. 1937.
[21] H. A. Krebs, E. Salvin, and W. A. Johnson, “The formation of citric and α-ketoglutaric acids in the mammalian body,” *Biochem. J.*, vol. 32, no. 1, pp. 113–117, Jan. 1938.
[22] H. A. Krebs and L. V. Eggleston, “The oxidation of pyruvate in pigeon breast muscle,” *Biochem. J.*, vol. 34, no. 3, pp. 442–459, Mar. 1940.
[23] J. D. Watson and F. H. C. Crick, “Molecular Structure of Nucleic Acids: A Structure for Deoxyribose Nucleic Acid,” *Nature*, vol. 171, no. 4356, pp. 737–738, Apr. 1953.
[24] P. Mitchell, “Coupling of Phosphorylation to Electron and Hydrogen Transfer by a Chemi-Osmotic type of Mechanism,” *Nature*, vol. 191, no. 4784, pp. 144–148, Jul. 1961.
[25] B. Vogelstein, N. Papadopoulos, V. E. Velculescu, S. Zhou, L. A. Diaz, and K. W. Kinzler, “Cancer Genome Landscapes,” *Science*, vol. 339, no. 6127, pp. 1546–1558, Mar. 2013.
[26] I. R. Watson, K. Takahashi, P. A. Futreal, and L. Chin, “Emerging patterns of somatic mutations in cancer,” *Nat. Rev. Genet.*, vol. 14, no. 10, pp. 703–718, Oct. 2013.
[27] The Cancer Genome Atlas Research Network, J. N. Weinstein, E. A. Collisson, G. B. Mills, K. R. M. Shaw, B. A. Ozenberger, K. Ellrott, I. Shmulevich, C. Sander, and J. M. Stuart, “The Cancer Genome Atlas Pan-Cancer analysis project,” *Nat. Genet.*, vol. 45, no. 10, pp. 1113–1120, Oct. 2013.
[28] J. F. Gainor and A. T. Shaw, “Emerging Paradigms in the Development of Resistance to Tyrosine Kinase Inhibitors in Lung Cancer,” *J. Clin. Oncol.*, vol. 31, no. 31, pp. 3987–3996, Nov. 2013.
[29] J. R. Sierra, V. Cepero, and S. Giordano, “Molecular mechanisms of acquired resistance to tyrosine kinase targeted therapy,” *Mol. Cancer*, vol. 9, p. 75, Apr. 2010.
[30] B. O. Van Emburgh, A. Sartore-Bianchi, F. Di Nicolantonio, S. Siena, and A. Bardelli, “Acquired resistance to EGFR-targeted therapies in colorectal cancer,” *Mol. Oncol.*, vol. 8, no. 6, pp. 1084–1094, Sep. 2014.
[31] D. R. Camidge, W. Pao, and L. V. Sequist, “Acquired resistance to TKIs in solid tumours: learning from lung cancer,” *Nat. Rev. Clin. Oncol.*, vol. 11, no. 8, pp. 473–481, Aug. 2014.
[32] B. N. Rexer and C. L. Arteaga, “Intrinsic and Acquired Resistance to HER2-Targeted Therapies in HER2 Gene-Amplified Breast Cancer: Mechanisms and Clinical Implications,” *Crit. Rev. Oncog.*, vol. 17, no. 1, pp. 1–16, 2012.
[33] C. J. Brown, S. Lain, C. S. Verma, A. R. Fersht, and D. P. Lane, “Awakening guardian angels: drugging the p53 pathway,” *Nat. Rev. Cancer*, vol. 9, no. 12, pp. 862–873, Dec. 2009.

[34] M. J. Duffy, N. C. Synnott, P. M. McGowan, J. Crown, D. O'Connor, and W. M. Gallagher, "p53 as a target for the treatment of cancer," *Cancer Treat. Rev.*, vol. 40, no. 10, pp. 1153–1160, Dec. 2014.
[35] A. D. Cox, S. W. Fesik, A. C. Kimmelman, J. Luo, and C. J. Der, "Drugging the undruggable RAS: Mission Possible?," *Nat. Rev. Drug Discov.*, vol. 13, no. 11, pp. 828–851, Nov. 2014.
[36] A. T. Baines, D. Xu, and C. J. Der, "Inhibition of Ras for cancer treatment: the search continues," *Future Med. Chem.*, vol. 3, no. 14, pp. 1787–1808, Oct. 2011.
[37] G. Zadeh and K. Aldape, "Bringing IDH into the Fold," *Cancer Cell*, vol. 29, no. 2, pp. 139–140, Feb. 2016.
[38] I. P. M. Tomlinson, N. A. Alam, A. J. Rowan, E. Barclay, E. E. M. Jaeger, D. Kelsell, I. Leigh, P. Gorman, H. Lamlum, S. Rahman, R. R. Roylance, S. Olpin, S. Bevan, K. Barker, N. Hearle, R. S. Houlston, M. Kiuru, R. Lehtonen, A. Karhu, S. Vilkki, P. Laiho, C. Eklund, O. Vierimaa, K. Aittomäki, M. Hietala, P. Sistonen, A. Paetau, R. Salovaara, R. Herva, V. Launonen, and L. A. Aaltonen, "Germline mutations in FH predispose to dominantly inherited uterine fibroids, skin leiomyomata and papillary renal cell cancer," *Nat. Genet.*, vol. 30, no. 4, pp. 406–410, Apr. 2002.
[39] B. E. Baysal, R. E. Ferrell, J. E. Willett-Brozick, E. C. Lawrence, D. Myssiorek, A. Bosch, A. van der Mey, P. E. M. Taschner, W. S. Rubinstein, E. N. Myers, C. W. Richard, C. J. Cornelisse, P. Devilee, and B. Devlin, "Mutations in SDHD, a Mitochondrial Complex II Gene, in Hereditary Paraganglioma," *Science*, vol. 287, no. 5454, pp. 848–851, Feb. 2000.
[40] W. Xu, H. Yang, Y. Liu, Y. Yang, P. Wang, S.-H. Kim, S. Ito, C. Yang, P. Wang, M.-T. Xiao, L. Liu, W. Jiang, J. Liu, J. Zhang, B. Wang, S. Frye, Y. Zhang, Y. Xu, Q. Lei, K.-L. Guan, S. Zhao, and Y. Xiong, "Oncometabolite 2-Hydroxyglutarate Is a Competitive Inhibitor of α-Ketoglutarate-Dependent Dioxygenases," *Cancer Cell*, vol. 19, no. 1, pp. 17–30, Jan. 2011.
[41] M. Xiao, H. Yang, W. Xu, S. Ma, H. Lin, H. Zhu, L. Liu, Y. Liu, C. Yang, Y. Xu, S. Zhao, D. Ye, Y. Xiong, and K.-L. Guan, "Inhibition of α-KG-dependent histone and DNA demethylases by fumarate and succinate that are accumulated in mutations of FH and SDH tumor suppressors," *Genes Dev.*, vol. 26, no. 12, pp. 1326–1338, Jun. 2012.
[42] L. B. Sullivan, E. Martinez-Garcia, H. Nguyen, A. R. Mullen, E. Dufour, S. Sudarshan, J. D. Licht, R. J. Deberardinis, and N. S. Chandel, "The Proto-oncometabolite Fumarate Binds Glutathione to Amplify ROS-Dependent Signaling," *Mol. Cell*, vol. 51, no. 2, pp. 236–248, Jul. 2013.
[43] E.-H. Shim, C. B. Livi, D. Rakheja, J. Tan, D. Benson, V. Parekh, E.-Y. Kho, A. P. Ghosh, R. Kirkman, S. Velu, S. Dutta, B. Chenna, S. L. Rea, R. J. Mishur, Q. Li, T. L. Johnson-Pais, L. Guo, S. Bae, S. Wei, K. Block, and S. Sudarshan, "l-2-Hydroxyglutarate: An Epigenetic Modifier and Putative Oncometabolite in Renal Cancer," *Cancer Discov.*, vol. 4, no. 11, pp. 1290–1298, Nov. 2014.
[44] J. Fan, X. Teng, L. Liu, K. R. Mattaini, R. E. Looper, M. G. Vander Heiden, and J. D. Rabinowitz, "Human Phosphoglycerate Dehydrogenase Produces the

Oncometabolite d-2-Hydroxyglutarate," *ACS Chem. Biol.*, vol. 10, no. 2, pp. 510–516, Feb. 2015.

[45] T. Hitosugi, S. Kang, M. G. Vander Heiden, T.-W. Chung, S. Elf, K. Lythgoe, S. Dong, S. Lonial, X. Wang, G. Z. Chen, J. Xie, T.-L. Gu, R. D. Polakiewicz, J. L. Roesel, T. J. Boggon, F. R. Khuri, D. G. Gilliland, L. C. Cantley, J. Kaufman, and J. Chen, "Tyrosine Phosphorylation Inhibits PKM2 to Promote the Warburg Effect and Tumor Growth," *Sci. Signal.*, vol. 2, no. 97, p. ra73, Nov. 2009.

[46] H. R. Christofk, M. G. Vander Heiden, N. Wu, J. M. Asara, and L. C. Cantley, "Pyruvate kinase M2 is a phosphotyrosine-binding protein," *Nature*, vol. 452, no. 7184, pp. 181–186, Mar. 2008.

[47] H. R. Christofk, M. G. Vander Heiden, M. H. Harris, A. Ramanathan, R. E. Gerszten, R. Wei, M. D. Fleming, S. L. Schreiber, and L. C. Cantley, "The M2 splice isoform of pyruvate kinase is important for cancer metabolism and tumour growth," *Nature*, vol. 452, no. 7184, pp. 230–233, Mar. 2008.

[48] K. H. Ibsen, "Interrelationships and Functions of the Pyruvate Kinase Isozymes and Their Variant Forms: A Review," *Cancer Res.*, vol. 37, no. 2, pp. 341–353, Feb. 1977.

[49] T. Hitosugi, S. Kang, M. G. Vander Heiden, T.-W. Chung, S. Elf, K. Lythgoe, S. Dong, S. Lonial, X. Wang, G. Z. Chen, J. Xie, T.-L. Gu, R. D. Polakiewicz, J. L. Roesel, T. J. Boggon, F. R. Khuri, D. G. Gilliland, L. C. Cantley, J. Kaufman, and J. Chen, "Tyrosine Phosphorylation Inhibits PKM2 to Promote the Warburg Effect and Tumor Growth," *Sci. Signal.*, vol. 2, no. 97, p. ra73, Nov. 2009.

[50] R. J. DeBerardinis, J. J. Lum, G. Hatzivassiliou, and C. B. Thompson, "The Biology of Cancer: Metabolic Reprogramming Fuels Cell Growth and Proliferation," *Cell Metab.*, vol. 7, no. 1, pp. 11–20, Jan. 2008.

[51] S. Y. Lunt and M. G. V. Heiden, "Aerobic Glycolysis: Meeting the Metabolic Requirements of Cell Proliferation," *Annu. Rev. Cell Dev. Biol.*, vol. 27, no. 1, pp. 441–464, 2011.

[52] M C Scrutton and M. F. Utter, "The Regulation of Glycolysis and Gluconeogenesis in Animal Tissues," *Annu. Rev. Biochem.*, vol. 37, no. 1, pp. 249–302, 1968.

[53] F. A. Farina, J. B. Shatton, H. P. Morris, and S. Weinhouse, "Isozymes of Pyruvate Kinase in Liver and Hepatomas of the Rat," *Cancer Res.*, vol. 34, no. 6, pp. 1439–1446, Jun. 1974.

[54] T. Noguchi, H. Inoue, and T. Tanaka, "The M1- and M2-type isozymes of rat pyruvate kinase are produced from the same gene by alternative RNA splicing.," *J. Biol. Chem.*, vol. 261, no. 29, pp. 13807–13812, Oct. 1986.

[55] G. L. Cottam, P. F. Hollenberg, and M. J. Coon, "Subunit Structure of Rabbit Muscle Pyruvate Kinase," *J. Biol. Chem.*, vol. 244, no. 6, pp. 1481–1486, Mar. 1969.

[56] D. I. Stuart, M. Levine, H. Muirhead, and D. K. Stammers, "Crystal structure of cat muscle pyruvate kinase at a resolution of 2.6 Å," *J. Mol. Biol.*, vol. 134, no. 1, pp. 109–142, Oct. 1979.

[57] T. M. Larsen, M. M. Benning, I. Rayment, and G. H. Reed, "Structure of the Bis(Mg^{2+})−ATP−Oxalate Complex of the Rabbit Muscle Pyruvate Kinase at 2.1

Å Resolution: ATP Binding over a Barrel" *Biochemistry (Mosc.)*, vol. 37, no. 18, pp. 6247–6255, May 1998.
[58] M. S. Jurica, A. Mesecar, P. J. Heath, W. Shi, T. Nowak, and B. L. Stoddard, "The allosteric regulation of pyruvate kinase by fructose-1,6-bisphosphate," *Structure*, vol. 6, no. 2, pp. 195–210, Feb. 1998.
[59] H. P. Morgan, W. Zhong, I. W. McNae, P. A. M. Michels, L. A. Fothergill-Gilmore, and M. D. Walkinshaw, "Structures of pyruvate kinases display evolutionarily divergent allosteric strategies," *R. Soc. Open Sci.*, vol. 1, no. 1, p. 140120, Sep. 2014.
[60] J. D. Dombrauckas, B. D. Santarsiero, and A. D. Mesecar, "Structural Basis for Tumor Pyruvate Kinase M2 Allosteric Regulation and Catalysis," *Biochemistry (Mosc.)*, vol. 44, no. 27, pp. 9417–9429, Jul. 2005.
[61] S. Mazurek, "Pyruvate kinase type M2: A key regulator of the metabolic budget system in tumor cells," *Int. J. Biochem. Cell Biol.*, vol. 43, no. 7, pp. 969–980, Jul. 2011.
[62] H. R. Christofk, M. G. Vander Heiden, M. H. Harris, A. Ramanathan, R. E. Gerszten, R. Wei, M. D. Fleming, S. L. Schreiber, and L. C. Cantley, "The M2 splice isoform of pyruvate kinase is important for cancer metabolism and tumour growth," *Nature*, vol. 452, no. 7184, pp. 230–233, Mar. 2008.
[63] D. Anastasiou, Y. Yu, W. J. Israelsen, J.-K. Jiang, M. B. Boxer, B. S. Hong, W. Tempel, S. Dimov, M. Shen, A. Jha, H. Yang, K. R. Mattaini, C. M. Metallo, B. P. Fiske, K. D. Courtney, S. Malstrom, T. M. Khan, C. Kung, A. P. Skoumbourdis, H. Veith, N. Southall, M. J. Walsh, K. R. Brimacombe, W. Leister, S. Y. Lunt, Z. R. Johnson, K. E. Yen, K. Kunii, S. M. Davidson, H. R. Christofk, C. P. Austin, J. Inglese, M. H. Harris, J. M. Asara, G. Stephanopoulos, F. G. Salituro, S. Jin, L. Dang, D. S. Auld, H.-W. Park, L. C. Cantley, C. J. Thomas, and M. G. Vander Heiden, "Pyruvate kinase M2 activators promote tetramer formation and suppress tumorigenesis," *Nat. Chem. Biol.*, vol. 8, no. 10, pp. 839–847, Oct. 2012.
[64] K. M. Parnell, J. M. Foulks, R. N. Nix, A. Clifford, J. Bullough, B. Luo, A. Senina, D. Vollmer, J. Liu, V. McCarthy, Y. Xu, M. Saunders, X.-H. Liu, S. Pearce, K. Wright, M. O'Reilly, M. V. McCullar, K.-K. Ho, and S. B. Kanner, "Pharmacologic Activation of PKM2 Slows Lung Tumor Xenograft Growth," *Mol. Cancer Ther.*, vol. 12, no. 8, pp. 1453–1460, Aug. 2013.
[65] D. J. Kim, Y. S. Park, N. D. Kim, S. H. Min, Y.-M. You, Y. Jung, H. Koo, H. Noh, J.-A. Kim, K. C. Park, and Y. I. Yeom, "A Novel Pyruvate Kinase M2 Activator Compound that Suppresses Lung Cancer Cell Viability under Hypoxia," *Mol. Cells*, vol. 38, no. 4, pp. 373–379, Apr. 2015.
[66] A. Zanella and P. Bianchi, "Red cell pyruvate kinase deficiency: from genetics to clinical manifestations," *Best Pract. Res. Clin. Haematol.*, vol. 13, no. 1, pp. 57–81, Mar. 2000.
[67] K. E. Keller, I. S. Tan, and Y.-S. Lee, "SAICAR Stimulates Pyruvate Kinase Isoform M2 and Promotes Cancer Cell Survival in Glucose-Limited Conditions," *Science*, vol. 338, no. 6110, pp. 1069–1072, Nov. 2012.

[68] B. Chaneton, P. Hillmann, L. Zheng, A. C. L. Martin, O. D. K. Maddocks, A. Chokkathukalam, J. E. Coyle, A. Jankevics, F. P. Holding, K. H. Vousden, C. Frezza, M. O'Reilly, and E. Gottlieb, "Serine is a natural ligand and allosteric activator of pyruvate kinase M2," *Nature*, vol. 491, no. 7424, pp. 458–462, Nov. 2012.

[69] X. Gao, H. Wang, J. J. Yang, X. Liu, and Z.-R. Liu, "Pyruvate Kinase M2 Regulates Gene Transcription by Acting as a Protein Kinase," *Mol. Cell*, vol. 45, no. 5, pp. 598–609, Mar. 2012.

[70] W. Yang, Y. Xia, H. Ji, Y. Zheng, J. Liang, W. Huang, X. Gao, K. Aldape, and Z. Lu, "Nuclear PKM2 regulates β-catenin transactivation upon EGFR activation," *Nature*, vol. 480, no. 7375, pp. 118–122, Dec. 2011.

[71] K. E. Keller, Z. M. Doctor, Z. W. Dwyer, and Y.-S. Lee, "SAICAR Induces Protein Kinase Activity of PKM2 that Is Necessary for Sustained Proliferative Signaling of Cancer Cells," *Mol. Cell*, vol. 53, no. 5, pp. 700–709, Mar. 2014.

[72] M. L. Cárdenas, A. Cornish-Bowden, and T. Ureta, "Evolution and regulatory role of the hexokinases," *Biochim. Biophys. Acta BBA - Mol. Cell Res.*, vol. 1401, no. 3, pp. 242–264, Mar. 1998.

[73] J. E. Wilson, "Isozymes of mammalian hexokinase: structure, subcellular localization and metabolic function," *J. Exp. Biol.*, vol. 206, no. 12, pp. 2049–2057, Jun. 2003.

[74] A. E. Aleshin, C. Zeng, G. P. Bourenkov, H. D. Bartunik, H. J. Fromm, and R. B. Honzatko, "The mechanism of regulation of hexokinase: new insights from the crystal structure of recombinant human brain hexokinase complexed with glucose and glucose-6-phosphate," *Structure*, vol. 6, no. 1, pp. 39–50, Jan. 1998.

[75] S. P. Mathupala, Y. H. Ko, and P. L. Pedersen, "Hexokinase II: Cancer's double-edged sword acting as both facilitator and gatekeeper of malignancy when bound to mitochondria," *Oncogene*, vol. 25, no. 34, pp. 4777–4786, 2006.

[76] S. P. Mathupala, Y. H. Ko, and P. L. Pedersen, "Hexokinase-2 bound to mitochondria: Cancer's stygian link to the 'Warburg effect' and a pivotal target for effective therapy," *Semin. Cancer Biol.*, vol. 19, no. 1, pp. 17–24, Feb. 2009.

[77] N. Majewski, V. Nogueira, P. Bhaskar, P. E. Coy, J. E. Skeen, K. Gottlob, N. S. Chandel, C. B. Thompson, R. B. Robey, and N. Hay, "Hexokinase-Mitochondria Interaction Mediated by Akt Is Required to Inhibit Apoptosis in the Presence or Absence of Bax and Bak," *Mol. Cell*, vol. 16, no. 5, pp. 819–830, Dec. 2004.

[78] K. Gottlob, N. Majewski, S. Kennedy, E. Kandel, R. B. Robey, and N. Hay, "Inhibition of early apoptotic events by Akt/PKB is dependent on the first committed step of glycolysis and mitochondrial hexokinase," *Genes Dev.*, vol. 15, no. 11, pp. 1406–1418, Jun. 2001.

[79] R. B. Robey and N. Hay, "Mitochondrial hexokinases, novel mediators of the antiapoptotic effects of growth factors and Akt," *Oncogene*, vol. 25, no. 34, pp. 4683–4696, 2006.

[80] M. H. van Gool, T. S. Aukema, K. J. Hartemink, R. A. Valdés Olmos, H. van Tinteren, and H. M. Klomp, "FDG-PET/CT response evaluation during EGFR-

TKI treatment in patients with NSCLC," *World J. Radiol.*, vol. 6, no. 7, pp. 392–398, Jul. 2014.

[81] H. Lin, J. Zeng, R. Xie, M. J. Schulz, R. Tedesco, J. Qu, K. F. Erhard, J. F. Mack, K. Raha, A. R. Rendina, L. M. Szewczuk, P. M. Kratz, A. J. Jurewicz, T. Cecconie, S. Martens, P. J. McDevitt, J. D. Martin, S. B. Chen, Y. Jiang, L. Nickels, B. J. Schwartz, A. Smallwood, B. Zhao, N. Campobasso, Y. Qian, J. Briand, C. M. Rominger, C. Oleykowski, M. A. Hardwicke, and J. I. Luengo, "Discovery of a Novel 2,6-Disubstituted Glucosamine Series of Potent and Selective Hexokinase 2 Inhibitors," *ACS Med. Chem. Lett.*, vol. 7, no. 3, pp. 217–222, Mar. 2016.

[82] I. A. Rose and J. V. B. Warms, "Mitochondrial Hexokinase RELEASE, REBINDING, AND LOCATION," *J. Biol. Chem.*, vol. 242, no. 7, pp. 1635–1645, Apr. 1967.

[83] J. G. Pastorino, N. Shulga, and J. B. Hoek, "Mitochondrial Binding of Hexokinase II Inhibits Bax-induced Cytochrome c Release and Apoptosis," *J. Biol. Chem.*, vol. 277, no. 9, pp. 7610–7618, Mar. 2002.

[84] N. N. Danial, C. F. Gramm, L. Scorrano, C.-Y. Zhang, S. Krauss, A. M. Ranger, S. Robert Datta, M. E. Greenberg, L. J. Licklider, B. B. Lowell, S. P. Gygi, and S. J. Korsmeyer, "BAD and glucokinase reside in a mitochondrial complex that integrates glycolysis and apoptosis," *Nature*, vol. 424, no. 6951, pp. 952–956, Aug. 2003.

[85] O. Gimm, M. Armanios, H. Dziema, H. P. H. Neumann, and C. Eng, "Somatic and Occult Germ-line Mutations in SDHD, a Mitochondrial Complex II Gene, in Nonfamilial Pheochromocytoma," *Cancer Res.*, vol. 60, no. 24, pp. 6822–6825, Dec. 2000.

[86] D. Astuti, F. Latif, A. Dallol, P. L. M. Dahia, F. Douglas, E. George, F. Sköldberg, E. S. Husebye, C. Eng, and E. R. Maher, "Gene Mutations in the Succinate Dehydrogenase Subunit SDHB Cause Susceptibility to Familial Pheochromocytoma and to Familial Paraganglioma," *Am. J. Hum. Genet.*, vol. 69, no. 1, pp. 49–54, Jul. 2001.

[87] B. Baysal, J. Willett-Brozick, E. Lawrence, C. Drovdlic, S. Savul, D. McLeod, H. Yee, D. Brackmann, W. Slattery, E. Myers, R. Ferrell, and W. Rubinstein, "Prevalence of SDHB, SDHC, and SDHD germline mutations in clinic patients with head and neck paragangliomas," *J. Med. Genet.*, vol. 39, no. 3, pp. 178–183, Mar. 2002.

[88] P. L. M. Dahia, "Pheochromocytoma and paraganglioma pathogenesis: learning from genetic heterogeneity," *Nat. Rev. Cancer*, vol. 14, no. 2, pp. 108–119, Feb. 2014.

[89] H.-X. Hao, O. Khalimonchuk, M. Schraders, N. Dephoure, J.-P. Bayley, H. Kunst, P. Devilee, C. W. R. J. Cremers, J. D. Schiffman, B. G. Bentz, S. P. Gygi, D. R. Winge, H. Kremer, and J. Rutter, "SDH5, a Gene Required for Flavination of Succinate Dehydrogenase, Is Mutated in Paraganglioma," *Science*, vol. 325, no. 5944, pp. 1139–1142, Aug. 2009.

[90] H. P. M. Kunst, M. H. Rutten, J.-P. de Mönnink, L. H. Hoefsloot, H. J. L. M. Timmers, H. A. M. Marres, J. C. Jansen, H. Kremer, J.-P. Bayley, and C. W. R. J.

Cremers, “SDHAF2 (PGL2-SDH5) and Hereditary Head and Neck Paraganglioma,” *Clin. Cancer Res.*, vol. 17, no. 2, pp. 247–254, Jan. 2011.
[91] E. H. Smith, R. Janknecht, and L. J. Maher, “Succinate inhibition of α-ketoglutarate-dependent enzymes in a yeast model of paraganglioma,” *Hum. Mol. Genet.*, vol. 16, no. 24, pp. 3136–3148, Dec. 2007.
[92] E. Letouzé, C. Martinelli, C. Loriot, N. Burnichon, N. Abermil, C. Ottolenghi, M. Janin, M. Menara, A. T. Nguyen, P. Benit, A. Buffet, C. Marcaillou, J. Bertherat, L. Amar, P. Rustin, A. De Reyniès, A.-P. Gimenez-Roqueplo, and J. Favier, “SDH Mutations Establish a Hypermethylator Phenotype in Paraganglioma,” *Cancer Cell*, vol. 23, no. 6, pp. 739–752, Jun. 2013.
[93] A. Imperiale, F.-M. Moussallieh, F. Sebag, L. Brunaud, A. Barlier, K. Elbayed, P. Bachellier, B. Goichot, K. Pacak, I.-J. Namer, and D. Taïeb, “A New Specific Succinate-Glutamate Metabolomic Hallmark in Sdhx-Related Paragangliomas,” *PLOS ONE*, vol. 8, no. 11, p. e80539, Nov. 2013.
[94] M. Yang and P. J. Pollard, “Succinate: A New Epigenetic Hacker,” *Cancer Cell*, vol. 23, no. 6, pp. 709–711, Jun. 2013.
[95] C. B. Thompson, “Metabolic Enzymes as Oncogenes or Tumor Suppressors,” *N. Engl. J. Med.*, vol. 360, no. 8, pp. 813–815, Feb. 2009.
[96] N. A. Alam, S. Bevan, M. Churchman, E. Barclay, K. Barker, E. E. M. Jaeger, H. M. Nelson, E. Healy, A. C. Pembroke, P. S. Friedmann, K. Dalziel, E. Calonje, J. Anderson, P. J. August, M. G. Davies, R. Felix, C. S. Munro, M. Murdoch, J. Rendall, S. Kennedy, I. M. Leigh, D. P. Kelsell, I. P. M. Tomlinson, and R. S. Houlston, “Localization of a Gene (MCUL1) for Multiple Cutaneous Leiomyomata and Uterine Fibroids to Chromosome 1q42.3-q43,” *Am. J. Hum. Genet.*, vol. 68, no. 5, pp. 1264–1269, May 2001.
[97] V. Launonen, O. Vierimaa, M. Kiuru, J. Isola, S. Roth, E. Pukkala, P. Sistonen, R. Herva, and L. A. Aaltonen, “Inherited susceptibility to uterine leiomyomas and renal cell cancer,” *Proc. Natl. Acad. Sci.*, vol. 98, no. 6, pp. 3387–3392, Mar. 2001.
[98] M. Kiuru, V. Launonen, M. Hietala, K. Aittomäki, O. Vierimaa, R. Salovaara, J. Arola, E. Pukkala, P. Sistonen, R. Herva, and L. A. Aaltonen, “Familial Cutaneous Leiomyomatosis Is a Two-Hit Condition Associated with Renal Cell Cancer of Characteristic Histopathology,” *Am. J. Pathol.*, vol. 159, no. 3, pp. 825–829, Sep. 2001.
[99] E. Tolley and I. Craig, “Presence of two forms of fumarase (fumarate hydratase E.C. 4.2.1.2) in mammalian cells: Immunological characterization and genetic analysis in somatic cell hybrids. Confirmation of the assignment of a gene necessary for the enzyme expression to human chromosome 1,” *Biochem. Genet.*, vol. 13, no. 11–12, pp. 867–883, Dec. 1975.
[100] T. Weaver and L. Banaszak, “Crystallographic Studies of the Catalytic and a Second Site in Fumarase C from Escherichia coli,” *Biochemistry (Mosc.)*, vol. 35, no. 44, pp. 13955–13965, Jan. 1996.
[101] N. Ternette, M. Yang, M. Laroyia, M. Kitagawa, L. O’Flaherty, K. Wolhulter, K. Igarashi, K. Saito, K. Kato, R. Fischer, A. Berquand, B. M. Kessler, T. Lappin, N. Frizzell, T. Soga, J. Adam, and P. J. Pollard, “Inhibition of Mitochondrial

Aconitase by Succination in Fumarate Hydratase Deficiency," *Cell Rep.*, vol. 3, no. 3, pp. 689–700, Mar. 2013.
[102] M. Yang, T. Soga, P. J. Pollard, and J. Adam, "The emerging role of fumarate as an oncometabolite," *Front. Oncol.*, vol. 2, Jul. 2012.
[103] D. W. Parsons, S. Jones, X. Zhang, J. C.-H. Lin, R. J. Leary, P. Angenendt, P. Mankoo, H. Carter, I.-M. Siu, G. L. Gallia, A. Olivi, R. McLendon, B. A. Rasheed, S. Keir, T. Nikolskaya, Y. Nikolsky, D. A. Busam, H. Tekleab, L. A. Diaz, J. Hartigan, D. R. Smith, R. L. Strausberg, S. K. N. Marie, S. M. O. Shinjo, H. Yan, G. J. Riggins, D. D. Bigner, R. Karchin, N. Papadopoulos, G. Parmigiani, B. Vogelstein, V. E. Velculescu, and K. W. Kinzler, "An Integrated Genomic Analysis of Human Glioblastoma Multiforme," *Science*, vol. 321, no. 5897, pp. 1807–1812, Sep. 2008.
[104] M. Sanson, Y. Marie, S. Paris, A. Idbaih, J. Laffaire, F. Ducray, S. E. Hallani, B. Boisselier, K. Mokhtari, K. Hoang-Xuan, and J.-Y. Delattre, "Isocitrate Dehydrogenase 1 Codon 132 Mutation Is an Important Prognostic Biomarker in Gliomas," *J. Clin. Oncol.*, vol. 27, no. 25, pp. 4150–4154, Sep. 2009.
[105] H. Yan, D. W. Parsons, G. Jin, R. McLendon, B. A. Rasheed, W. Yuan, I. Kos, I. Batinic-Haberle, S. Jones, G. J. Riggins, H. Friedman, A. Friedman, D. Reardon, J. Herndon, K. W. Kinzler, V. E. Velculescu, B. Vogelstein, and D. D. Bigner, "IDH1 and IDH2 Mutations in Gliomas," *N. Engl. J. Med.*, vol. 360, no. 8, pp. 765–773, Feb. 2009.
[106] L. Dang, D. W. White, S. Gross, B. D. Bennett, M. A. Bittinger, E. M. Driggers, V. R. Fantin, H. G. Jang, S. Jin, M. C. Keenan, K. M. Marks, R. M. Prins, P. S. Ward, K. E. Yen, L. M. Liau, J. D. Rabinowitz, L. C. Cantley, C. B. Thompson, M. G. Vander Heiden, and S. M. Su, "Cancer-associated IDH1 mutations produce 2-hydroxyglutarate," *Nature*, vol. 462, no. 7274, pp. 739–744, Dec. 2009.
[107] P. Wang, Q. Dong, C. Zhang, P.-F. Kuan, Y. Liu, W. R. Jeck, J. B. Andersen, W. Jiang, G. L. Savich, T.-X. Tan, J. T. Auman, J. M. Hoskins, A. D. Misher, C. D. Moser, S. M. Yourstone, J. W. Kim, K. Cibulskis, G. Getz, H. V. Hunt, S. S. Thorgeirsson, L. R. Roberts, D. Ye, K.-L. Guan, Y. Xiong, L.-X. Qin, and D. Y. Chiang, "Mutations in isocitrate dehydrogenase 1 and 2 occur frequently in intrahepatic cholangiocarcinomas and share hypermethylation targets with glioblastomas," *Oncogene*, vol. 32, no. 25, pp. 3091–3100, Jun. 2013.
[108] P. S. Ward, J. Patel, D. R. Wise, O. Abdel-Wahab, B. D. Bennett, H. A. Coller, J. R. Cross, V. R. Fantin, C. V. Hedvat, A. E. Perl, J. D. Rabinowitz, M. Carroll, S. M. Su, K. A. Sharp, R. L. Levine, and C. B. Thompson, "The Common Feature of Leukemia-Associated IDH1 and IDH2 Mutations Is a Neomorphic Enzyme Activity Converting α-Ketoglutarate to 2-Hydroxyglutarate," *Cancer Cell*, vol. 17, no. 3, pp. 225–234, Mar. 2010.
[109] Y. O. Kim, I. U. Oh, H. S. Park, J. Jeng, B. J. Song, and T. L. Huh, "Characterization of a cDNA clone for human NAD(+)-specific isocitrate dehydrogenase alpha-subunit and structural comparison with its isoenzymes from different species.," *Biochem. J.*, vol. 308, no. Pt 1, pp. 63–68, May 1995.

[110] D. Krell, M. Assoku, M. Galloway, P. Mulholland, I. Tomlinson, and C. Bardella, "Screen for IDH1, IDH2, IDH3, D2HGDH and L2HGDH Mutations in Glioblastoma," *PLoS ONE*, vol. 6, no. 5, May 2011.

[111] A. P. J. van den Heuvel, J. Jing, R. F. Wooster, and K. E. Bachman, "Analysis of glutamine dependency in non-small cell lung cancer," *Cancer Biol. Ther.*, vol. 13, no. 12, pp. 1185–1194, Oct. 2012.

[112] M. R. Reynolds, A. N. Lane, B. Robertson, S. Kemp, Y. Liu, B. G. Hill, D. C. Dean, and B. F. Clem, "Control of Glutamine Metabolism By the Tumor Suppressor Rb," *Oncogene*, vol. 33, no. 5, pp. 556–566, Jan. 2014.

[113] C. Yang, J. Sudderth, T. Dang, R. G. Bachoo, J. G. McDonald, and R. J. DeBerardinis, "Glioblastoma Cells Require Glutamate Dehydrogenase to Survive Impairments of Glucose Metabolism or Akt Signaling," *Cancer Res.*, vol. 69, no. 20, pp. 7986–7993, Oct. 2009.

[114] A. Le, A. N. Lane, M. Hamaker, S. Bose, A. Gouw, J. Barbi, T. Tsukamoto, C. J. Rojas, B. S. Slusher, H. Zhang, L. J. Zimmerman, D. C. Liebler, R. J. C. Slebos, P. K. Lorkiewicz, R. M. Higashi, T. W. M. Fan, and C. V. Dang, "Glucose-Independent Glutamine Metabolism via TCA Cycling for Proliferation and Survival in B Cells," *Cell Metab.*, vol. 15, no. 1, pp. 110–121, Jan. 2012.

[115] C. T. Hensley, A. T. Wasti, and R. J. DeBerardinis, "Glutamine and cancer: cell biology, physiology, and clinical opportunities," *J. Clin. Invest.*, vol. 123, no. 9, pp. 3678–3684, Sep. 2013.

[116] J. Son, C. A. Lyssiotis, H. Ying, X. Wang, S. Hua, M. Ligorio, R. M. Perera, C. R. Ferrone, E. Mullarky, N. Shyh-Chang, Y. Kang, J. B. Fleming, N. Bardeesy, J. M. Asara, M. C. Haigis, R. A. DePinho, L. C. Cantley, and A. C. Kimmelman, "Glutamine supports pancreatic cancer growth through a KRAS-regulated metabolic pathway," *Nature*, vol. 496, no. 7443, pp. 101–105, Apr. 2013.

[117] A. R. Mullen, W. W. Wheaton, E. S. Jin, P.-H. Chen, L. B. Sullivan, T. Cheng, Y. Yang, W. M. Linehan, N. S. Chandel, and R. J. DeBerardinis, "Reductive carboxylation supports growth in tumour cells with defective mitochondria," *Nature*, vol. 481, no. 7381, pp. 385–388, Jan. 2012.

[118] C. M. Metallo, P. A. Gameiro, E. L. Bell, K. R. Mattaini, J. Yang, K. Hiller, C. M. Jewell, Z. R. Johnson, D. J. Irvine, L. Guarente, J. K. Kelleher, M. G. Vander Heiden, O. Iliopoulos, and G. Stephanopoulos, "Reductive glutamine metabolism by IDH1 mediates lipogenesis under hypoxia," *Nature*, vol. 481, no. 7381, pp. 380–384, Jan. 2012.

[119] D. R. Wise, P. S. Ward, J. E. S. Shay, J. R. Cross, J. J. Gruber, U. M. Sachdeva, J. M. Platt, R. G. DeMatteo, M. C. Simon, and C. B. Thompson, "Hypoxia promotes isocitrate dehydrogenase-dependent carboxylation of α-ketoglutarate to citrate to support cell growth and viability," *Proc. Natl. Acad. Sci.*, vol. 108, no. 49, pp. 19611–19616, Dec. 2011.

[120] D. E. Bauer, G. Hatzivassiliou, F. Zhao, C. Andreadis, and C. B. Thompson, "ATP citrate lyase is an important component of cell growth and transformation," *Oncogene*, vol. 24, no. 41, pp. 6314–6322, Jun. 2005.

[121] G. Hatzivassiliou, F. Zhao, D. E. Bauer, C. Andreadis, A. N. Shaw, D. Dhanak, S. R. Hingorani, D. A. Tuveson, and C. B. Thompson, "ATP citrate lyase

inhibition can suppress tumor cell growth," *Cancer Cell*, vol. 8, no. 4, pp. 311–321, Oct. 2005.
[122] D. W. Sborov, B. M. Haverkos, and P. J. Harris, "Investigational cancer drugs targeting cell metabolism in clinical development," *Expert Opin. Investig. Drugs*, vol. 24, no. 1, pp. 79–94, Jan. 2015.
[123] S. Fulda, L. Galluzzi, and G. Kroemer, "Targeting mitochondria for cancer therapy," *Nat. Rev. Drug Discov.*, vol. 9, no. 6, pp. 447–464, Jun. 2010.
[124] P. Gao, I. Tchernyshyov, T.-C. Chang, Y.-S. Lee, K. Kita, T. Ochi, K. I. Zeller, A. M. De Marzo, J. E. Van Eyk, J. T. Mendell, and C. V. Dang, "c-Myc suppression of miR-23a/b enhances mitochondrial glutaminase expression and glutamine metabolism," *Nature*, vol. 458, no. 7239, pp. 762–765, Apr. 2009.
[125] D. R. Wise, R. J. DeBerardinis, A. Mancuso, N. Sayed, X.-Y. Zhang, H. K. Pfeiffer, I. Nissim, E. Daikhin, M. Yudkoff, S. B. McMahon, and C. B. Thompson, "Myc regulates a transcriptional program that stimulates mitochondrial glutaminolysis and leads to glutamine addiction," *Proc. Natl. Acad. Sci.*, vol. 105, no. 48, pp. 18782–18787, Dec. 2008.
[126] R. C. Sun and N. C. Denko, "Hypoxic Regulation of Glutamine Metabolism through HIF1 and SIAH2 Supports Lipid Synthesis that Is Necessary for Tumor Growth," *Cell Metab.*, vol. 19, no. 2, pp. 285–292, Feb. 2014.
[127] J.-B. Wang, J. W. Erickson, R. Fuji, S. Ramachandran, P. Gao, R. Dinavahi, K. F. Wilson, A. L. B. Ambrosio, S. M. G. Dias, C. V. Dang, and R. A. Cerione, "Targeting Mitochondrial Glutaminase Activity Inhibits Oncogenic Transformation," *Cancer Cell*, vol. 18, no. 3, pp. 207–219, Sep. 2010.
[128] M. Szeliga and M. Obara-Michlewska, "Glutamine in neoplastic cells: focus on the expression and roles of glutaminases," *Neurochem. Int.*, vol. 55, no. 1, pp. 71–75, 2009.
[129] N. P. Curthoys, T. Kuhlenschmidt, and S. S. Godfrey, "Regulation of renal ammoniagenesis: Purification and characterization of phosphate-dependent glutaminase from rat kidney," *Arch. Biochem. Biophys.*, vol. 174, no. 1, pp. 82–89, May 1976.
[130] M. Szeliga and J. Albrecht, "Opposing roles of glutaminase isoforms in determining glioblastoma cell phenotype," *Neurochem. Int.*, vol. 88, pp. 6–9, Sep. 2015.
[131] H. Yz and K. We, "A comparative study of glytaminase isozymes in rat tissues.," *Enzyme*, vol. 21, no. 5, pp. 408–426, Dec. 1975.
[132] N. P. Curthoys and M. Watford, "Regulation of Glutaminase Activity and Glutamine Metabolism," *Annu. Rev. Nutr.*, vol. 15, no. 1, pp. 133–159, 1995.
[133] K. Thangavelu, C. Q. Pan, T. Karlberg, G. Balaji, M. Uttamchandani, V. Suresh, H. Schüler, B. C. Low, and J. Sivaraman, "Structural basis for the allosteric inhibitory mechanism of human kidney-type glutaminase (KGA) and its regulation by Raf-Mek-Erk signaling in cancer cell metabolism," *Proc. Natl. Acad. Sci.*, vol. 109, no. 20, pp. 7705–7710, May 2012.

CHAPTER TWO

Fluorescence resonance energy transfer (FRET) assay to read-out GAC tetramer formation and its response to allosteric activators and inhibitors.

2.1 INTRODUCTION

Recent advances in the understanding of cancer onset and progression have helped shed light on the interconnection between signal transduction pathways frequently observed in human tumors, and metabolic remodeling, which often accompanies oncogenic transformation [1], [2]. The relationship between canonical signal transduction pathways often mutated in human cancers, and accompanying changes in cellular metabolism that support neoplastic growth, provides the motivation to understand these altered metabolic pathways more clearly and identify potential targets for therapeutic intervention. The two major metabolic pathways that have been shown to have aberrant regulation in cancer cells, when compared to their non-transformed precursors, are the glycolytic pathway responsible for oxidizing glucose to pyruvate, and glutaminolysis, which converts imported glutamine to glutamate, where glutamate can be metabolized further in a variety of energetic and biosynthetic pathways [2]–[6]. The mitochondrial enzyme glutaminase is responsible for the deamidation of cellular glutamine, producing glutamate and ammonia. Its regulation still remains poorly understood despite its critical role in a variety of oncogenic signaling pathways, such as those involving c-Myc over-expression, HIF1-α stabilization, and Rho-GTPase dependent transformation [2], [7]–[9].

Human glutaminase (hGLS) consists of two isozymes, GLS1 and GLS2, where GLS1 has two alternatively spliced isoforms, kidney-type (KGA) and glutaminase C

(GAC), with GAC being the primary isoform expressed in cancer cells [10]–[15]. It has been shown previously that the activity of GAC is dependent on the oligomeric state of the enzyme, suggested to be a homo-tetramer [16]–[18]. Additionally, GAC activity was notably stimulated *in vitro* by the allosteric regulator inorganic phosphate, suggesting that the binding of phosphate to GAC stabilizes the active form (tetramer) of the enzyme [18]–[20].

Initial studies of glutaminase enzymes (EC 3.5.1.2) identified various oligomeric forms of these proteins from different tissues. The three oligomeric species originally described for the GLS1 proteins were a KGA dimer, tetramer, and high molecular weight oligomer (i.e. greater than a 20-mer) [16], [17], [21]–[23]. The high molecular weight oligomer was shown to be induced by the addition of multivalent anions, such as phosphate, sulfate, and borate. In fact, original methods for the purification of glutaminase enzymes involved protein precipitations of solubilized tissues using these anionic salts, where glutaminase enzymes would be found in the pellet of centrifuged tissue lysates [21]. Once purified, biochemical studies of these native enzymes indeed established that they exhibited high glutaminase activity, following the addition of anionic salts, and in particular, when activated by inorganic phosphate [23], [24]. The activation by phosphate was shown to be dose dependent and highly cooperative in nature. Studies using analytical centrifugation and size-exclusion chromatography showed the presence of different oligomeric enzyme species, including a dimer, tetramer, and higher molecular weight form of the enzyme. How these different states were able to interconvert, which state exhibited maximal activity, and overall mechanistic basis for the regulation of these interconversions, remained elusive.

The most significant clue regarding how these oligomeric forms of glutaminase were assembled came when the X-ray crystal structures of the mouse and human forms of GAC were determined [11], [25], [26]. These structures showed a GAC tetramer in the asymmetric unit, giving a clear picture of the subunit contacts (Figure 2.1). The crystal structures revealed two principal interfaces of the enzyme, namely the dimer-dimer and monomer-monomer interfaces (Figure 2.1, top inset). The monomer-monomer interface included a large surface area, with the major contacts between the two subunits resembling a lock-and-key fit. However, the dimer-dimer interface included significantly less surface area, and seemed to be governed by the association of two anti-parallel α-helices (Figure 2.1, bottom inset).

Thus far, the mechanistic basis for GAC activation has not been elucidated in great detail, and in particular, how its activation in cancer cells can be blocked by newly characterized small molecule inhibitors, despite the great deal of interest in targeting this pathway [7], [11], [13], [18], [26]–[33]. In the initial phase of this study, I take advantage of a fluorescence resonance energy transfer (FRET) assay that I have recently developed to directly monitor the dimer-to-tetramer transition of GAC, together with real time and single point activity assays to probe the dependence of its oligomeric state on activity. These approaches will set the stage for studies that should provide insights into the mechanism of action of the two glutaminase-specific inhibitors, BPTES (bis-2-(5 phenylacetamido-1,2,4-thiadiazol-2-yl) ethyl sulfide), and derivatives of the benzophenanthridines (e.g. 968) reported previously by our laboratory and others [7], [18], [28], [31], [34].

FIGURE 2.1 – X-ray crystal structure of tetrameric GAC. The crystal structure of GAC is depicted with surface representation, where the monomers of a GAC dimer are represented in either blue or cyan (3UO9) [9]. The dimer and tetramer interfaces are highlighted to display critical polar contacts between the two monomers and dimers, respectively. Residue numbering is for mouse GAC.

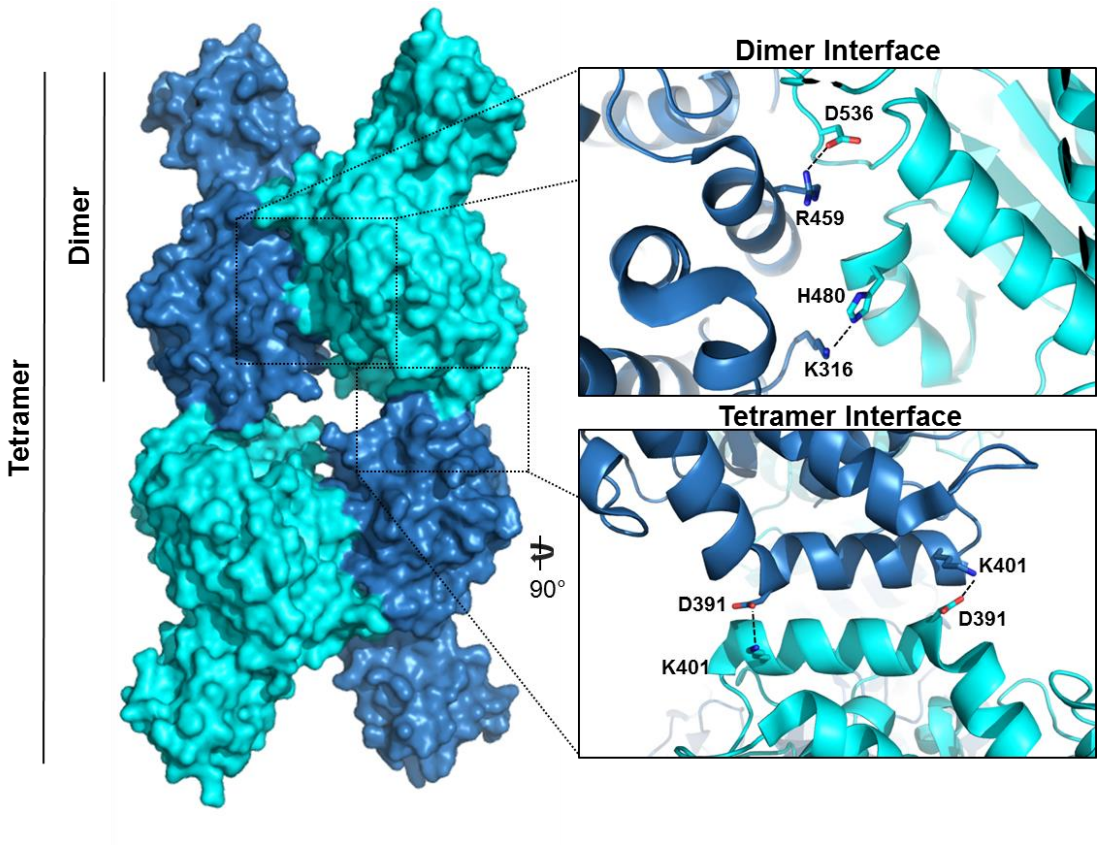
Tetramer
Dimer
90°
Dimer Interface
D536
R459
H480
K316
Tetramer Interface
K401
D391
D391
K401

2.2 METHODS

2.2.1 Recombinant glutaminase preparation and labeling with spectroscopic probes

A plasmid encoding the mouse kidney-type glutaminase isoform 2 (GAC, NP_001106854.1) (residues 72-603) was cloned into a pET23a vector containing an N-terminal histidine (His)-tag and thrombin cleavage site. The expressed protein was purified using Co^{2+} affinity beads (Clontech), followed by His-tag cleavage with human thrombin (Haemetologic Technologies) overnight at 4°C, and subsequently purified by anion exchange (GE healthcare) and gel filtration chromatography. Purified GAC was stored in a high salt-containing buffer (20 mM Tris-HCl pH 8.5, 500 mM NaCl, 1 mM NaN_3) at -80°C, following snap freezing in liquid N_2 for long term use. Labeling recombinant GAC with small molecule probes was performed by exchanging 1.5 mg of enzyme into 50 mM HEPES, pH 7.2, and 100 mM NaCl (labeling buffer), using a PD10 desalting column (GE healthcare). The enzyme was then incubated with 50 μM (5-fold excess of enzyme) of either AlexaFluor 488 succinimidyl ester or QSY9 succinimidyl ester (Molecular Probes) for 1 h at 4°C. After 1 h, the labeling reaction was quenched with 150 mM Tris-HCl, pH 8.5, and unreacted probe was separated from labeled-enzyme using a PD10 desalting column, eluting labeled-GAC back into the high salt-containing buffer. The stoichiometry of labeling was determined using the probe manufacturer's reported molar absorptivity values and instructions. Briefly, the concentration of GAC was determined by first correcting absorbance at 280 nm for the Abs_{280} of each probe, using the reported correction values (0.11 for AlexaFluor 488 and 0.23 for QSY-9) and their absorbance

values at their absorbance maxima (495 nm and 562 nm, respectively). The corrected Abs_{280} was used along with the experimentally determined molar absorptivity of GAC (ε_{280} = 38,850 M^{-1} cm^{-1}). AlexaFluor 488 and QSY-9 probes were quantified using their respective absorbance maxima and the manufacturer's reported molar absorptivity values (ε_{495} = 71,000 M^{-1} cm^{-1} and ε_{562} = 85,000 M^{-1} cm^{-1}). The labeling stoichiometry for 488-labeled and QSY-9 labeled GAC was found to be 0.49 ± 0.09 and 1.00 ± 0.05 respectively, where stoichiometry is defined as moles probe/moles protein.

2.2.2 FRET assays

Fluorescence experiments were performed using a Varian Cary Eclipse Fluorometer in the counting mode. Excitation and emission wavelengths were 490 and 520 nm, respectively. Experiments were all performed using 1-mL samples with continuous stirring at 20°C in 50 mM Tris-Acetate, pH 8.5, 0.1 mM ethylenediamine tetraacetic acid (EDTA). For wild-type (WT) GAC titrations in the absence of inorganic phosphate, 25 nM 488-GAC was equilibrated with 25 μL of QSY9-GAC (at varying concentrations) and allowed to equilibrate for 10 minutes, at which point 75 μL of the appropriate concentration of unlabeled WT GAC was added to provide a 10-fold excess over labeled-GAC. To test whether the purified GAC mutants can form oligomers with WT GAC, 200 nM QSY9-GAC (D391K) or 200 nM QSY9-GAC (D391K, K316E, R459E) was added to an equilibrated sample of 20 nM 488-WT GAC. When assaying the effects of BPTES and 968 on oligomer formation, BPTES or 968 was added following equilibration of a sample of 25 nM QSY9-WT GAC and 25 nM 488-WT GAC. Both BPTES and 968 were prepared in DMSO, and

appropriate dilutions were made so that less than 2% (v/v) DMSO was added to an experimental sample.

2.2.3 Real-time 968 binding and enzyme activity assays

Real-time fluorescence monitoring of 968 binding and GAC activity through production of NADH was performed on a Varian Cary Eclipse Fluorometer, whereas small molecule inhibition and binding titrations were performed in a 96-well format in a Tecan Saphire absorbance and fluorescence plate reader. Samples for monitoring real-time binding of 968 to 488-GAC were prepared by adding 10 μL of varying concentrations of 968 prepared in DMSO to an equilibrated 1 mL sample of 10 nM 488-GAC, while observing 488 fluorescence (490 nm excitation/520 nm emission). Similarly, this method was replicated for monitoring real-time binding of 968 to mutant forms of GAC, namely 488-labeled GAC (GD391K) and 488-GAC (D391K, K316E, R459E). Real-time activity assays monitoring 968 binding and NADH production were prepared in 1 mL samples, where 10 units of glutamate dehydrogenase (Sigma) and 2 mM NAD^+ (Sigma) were prepared in 50 mM Tris-Acetate, pH 8.5, 0.1 mM EDTA and equilibrated at 20°C. WT GAC (10 nM) was added and allowed to equilibrate 2 minutes before monitoring the fluorescence emission of 488-GAC (490 nm excitation, 520 nm emission) and NADH (340 nm excitation, 490 nm emission). Appropriate dilutions of 968 or BPTES prepared in DMSO were introduced after 30s and allowed to equilibrate for 2 minutes before a 180 μL solution of K_2HPO_4 and glutamine was added to make a final concentration of 50 mM K_2HPO_4 and 20 mM glutamine, to initiate GAC activation. The activity of GAC was measured in a coupled assay, by monitoring the NADH produced by

glutamate dehydrogenase, which converts the product of the glutaminase-catalyzed reaction, glutamate, to α-ketoglutarate and ammonia by reducing NAD^+ to NADH. Because solutions containing glutamine undergo non-enzymatic degradation to glutamate, samples were further analyzed by subtracting the NADH produced by glutaminase in the presence of 968, BPTES, or the equivalent volume of DMSO as a control, from the NADH produced in the absence of glutaminase under identical experimental conditions. NADH was quantified using a standard curve of freshly prepared NADH (Sigma) in 50 mM Tris-Acetate, pH 8.5, and 0.1 mM EDTA.

2.2.4 End-point glutaminase activity assays

Activity assays used to compare FRET values and evaluate the activity of GAC mutants followed a two-step protocol adapted from Robinson *et al.* (2007) (2). Briefly, 20 μL of 20 mM glutamine, 50 mM Tris-acetate, pH 8.5, and 0.1 mM EDTA, in either the presence or absence of a K_2HPO_4, was added to a UV-transparent Costar 96-well plate (Corning). To initiate the reaction, 5 μL of a solution of the appropriate concentration of GAC, prepared in 20 mM Tris-HCl, pH 8.5, 100 mM NaCl, and 1 mM NaN_3, was added to the glutamine solution and incubated at 23°C for 2 min before the reaction was quenched using 2.5 μL of 3 M HCl. For reactions that contained more than 250 nM GAC, the first reaction was quenched at 30 seconds instead of 2 min. The second step was initiated by the addition of 200 μL of 12 units/μL GDH, 2 mM NAD^+, 100 mM hydrazine (Sigma), and 100 mM Tris-HCl, pH 9.2, on top of the first quenched reaction and incubated for 45 min at 23°C before reading NADH absorbance. Glutamate produced by the first reaction was determined

from the amount of NADH generated in the second reaction by using the extinction coefficient for NADH (6,220 M^{-1} cm^{-1}).

2.2.5 Multi-angle light scattering (MALS)

Purified GAC and GAC mutants were subjected to multi-angle light scattering (MALS) as previously described by Moller *et al.* (2013) (3). Briefly, 50 μL samples of 5 mg/mL GAC were injected onto a WTC-030S5 size-exclusion column (Wyatt technology), coupled to a static 18-angle light scattering detector (DAWN HELEOS-II) and a refractive index detector (OptiLab T-rEX, Wyatt Technology), at 23°C. The size-exclusion column was equilibrated with 20 mM Tris-HCl, pH 8.5, and 200 mM NaCl with or without 50 mM K_2HPO_4. The flow rate was kept at 1 mL/min. RMS radius and mass distribution (polydispersity) were analyzed using the ASTRA software, with monomeric BSA (Sigma) serving to normalize the light scattering signal.

2.3 RESULTS

2.3.1 Development of a real-time assay to detect tetramer formation of GAC

The dimer-to-tetramer transition of GAC been suggested to be essential for enzyme activity [17], [23]. Additionally, allosteric activators have been proposed to promote activation by inducing the formation of tetramers. However, GAC tetramer formation and its role in enzyme activation have not been well characterized, having only been investigated through bulk enzyme assays and by ultra-centrifugation techniques [16], [21]. Thus, we sought to develop a highly sensitive fluorescence resonance energy transfer (FRET) assay that detects the formation of GAC tetramers from dimers, in order to describe the oligomer dynamics in real-time. Figure 2.2 depicts the proposed FRET assay, where oligomer formation is monitored between two populations of purified recombinant GAC, labeled with either the highly fluorescent AlexaFluor 488 (donor) probe, or with the non-fluorescent QSY9 (acceptor) chromophore (Figure 2.2). These two probes have a Förster distance (R_0) of 64 Å, making them highly useful for monitoring FRET between two GAC dimers within the tetrameric complex, where the largest dimension of the unit cell from solved X-ray crystal structures for tetrameric GAC is ~150 Å. Additionally, a major advantage of using FRET as a direct read-out for GAC tetramer formation is the ability to perform measurements at the relatively low concentrations of GAC commonly used for assaying its enzymatic activity.

The labeling of GAC by the FRET donor, AlexaFluor 488-succinimidyl-ester, resulted in the rapid and stoichiometric covalent modification of GAC, where 488-GAC was easily identified using SDS-PAGE (Figure 2.3A).

FIGURE 2.2 – FRET assay for GAC tetramer formation. A population of highly fluorescent 488-labeled GAC subunits are quenched by the addition of the FRET pair of non-fluorescent QSY9-labeled GAC subunits.

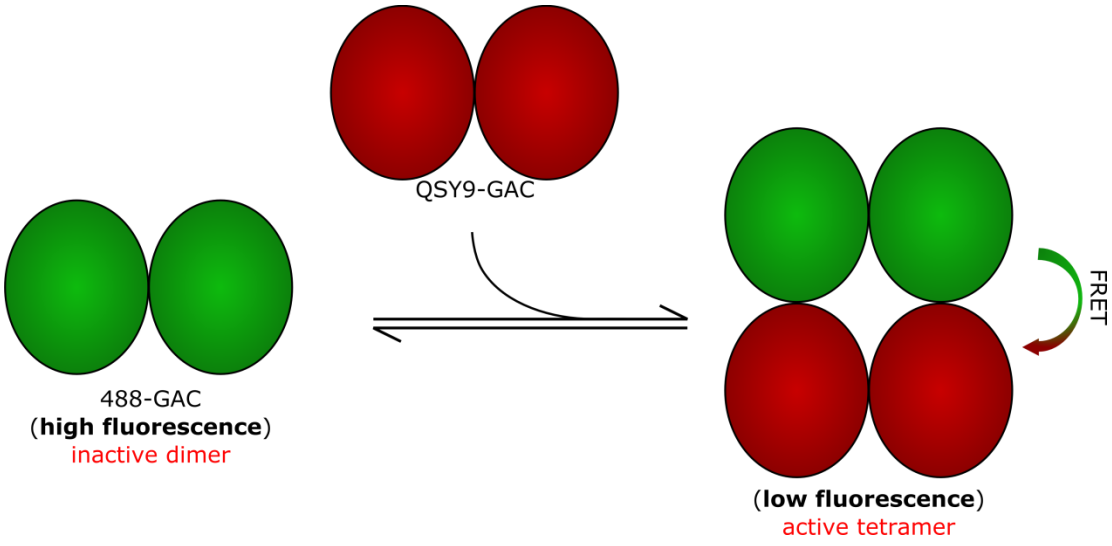
QSY9-GAC
488-GAC
(high fluorescence)
inactive dimer
(low fluorescence)
active tetramer
FRET

Additionally, the labeling of GAC did not alter the oligomeric state of the enzyme, as determined by analytical size exclusion chromatography (SEC) (Figure 2.3B), and the substrate and allosteric activator affinities for labeled GAC were also maintained (Figures 2.3C,D). Labeling GAC with the fluorescence donor and acceptor pair, 488- and QSY9-succinimidyl-ester, under identical conditions, resulted in a moderate inhibition of GAC activity. However, the V_{max} is the only kinetic property that was altered by this covalent modification, where both the K_m value for glutamine and $K_{1/2}$ value for phosphate were in good agreement with the values for WT GAC, suggesting the modification does not significantly alter the affinity for either the substrate or allosteric activators (Figure's 2.3C,D). The site of covalent modification was shown to be within the conserved glutaminase domain, by means of mass spectrometry identification of peptide fragments produced by partial trypsin digestion and separation by SDS-PAGE (Appendix Figures 7.1A-D).

Figure 2.4A depicts the FRET assay, where the addition of increasing concentrations of QSY9-GAC to 20 nM 488-GAC yielded a dose-dependent quenching of the donor 488 emission due to FRET. Additionally, the FRET signal was shown to be reversible upon the addition of excess unlabeled GAC subunits, which act to dilute the FRET pairs (i.e. tetramers), demonstrating that GAC tetramer formation is a dynamic process. Figure 2.4B represents the dose-dependent binding isotherm obtained from the QSY9-GAC titration profile from Figure 2.4A, which yielded an apparent K_D of 164 nM (± 20 nM) for tetramer formation (Figure 2.4B, (○)).

FIGURE 2.3 – Labeling of GAC with FRET probes. (**A**) 10 μM GAC was reacted with 50 μM 488-succinimidyl ester (pH = 7.2) and was monitored using SDS-PAGE and visualized under UV illumination (i.e. fluorescence). The longest time point was analyzed adjacent to MW standards (left panel), and the time dependent labeling shown in the right panel. (**B**) Analytical gel filtration profiles of a 2.5 mg/mL injection of WT GAC (—) and 488-labeled GAC (—), where the elution of the 488 probe (abs 490 nm, (—)) overlaps the A280 curves for both unlabeled and 488-labeled GAC. (**C**),(**D**) Glutamine and phosphate dependent activity curves of 50 nM WT, 488-labeled, and QSY9-labeled GAC, where 488 and QSY9-GAC exhibited a change in the maximum velocity. Labeled GAC was found to have a lower V_{max} (by ~50%), but a highly similar $K_{1/2}$ for phosphate (**D**, 15 mM for 488-GAC and 27.3 mM for QSY9-GAC vs 21.5 mM for WT GAC), while retaining the WT K_m for glutamine (**C**, 4.8 mM for 488-GAC and 3.7 mM for QSY9-GAC vs 4 mM for WT GAC).

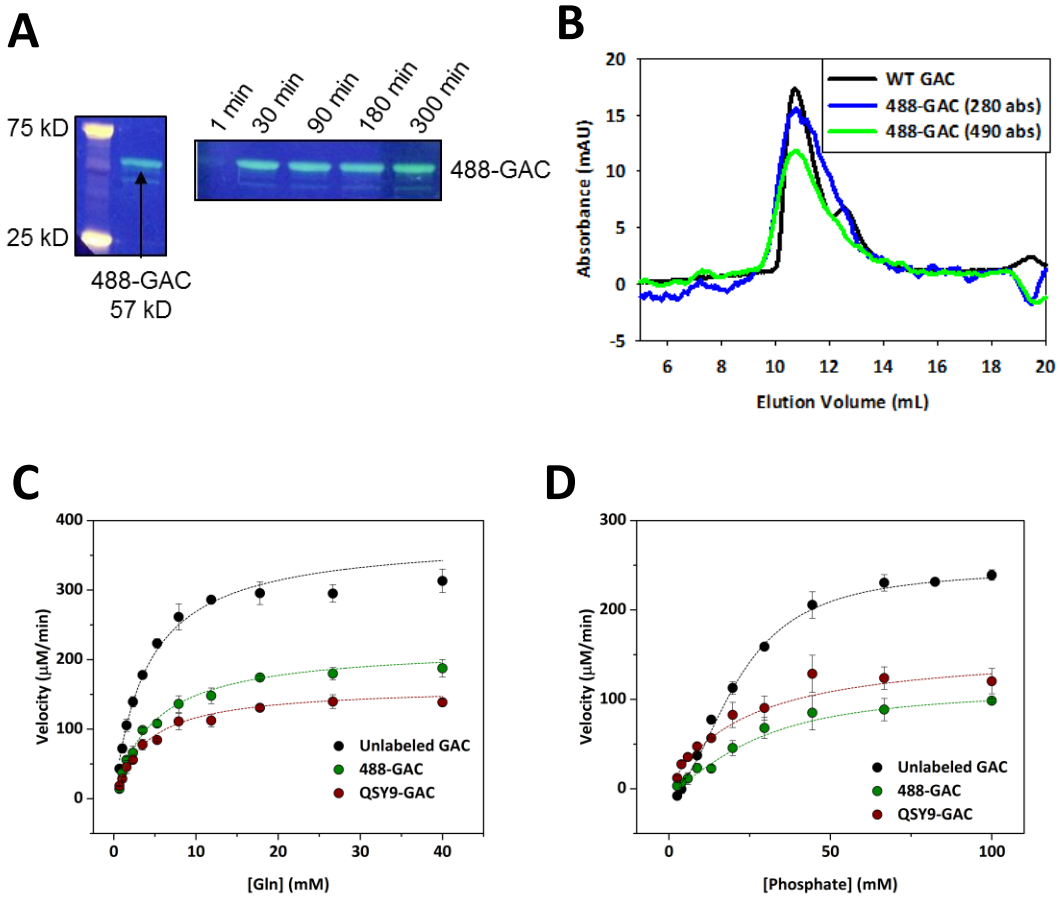
A
75 kD
25 kD
488-GAC
57 kD
1 min
30 min
90 min
180 min
300 min
488-GAC
B
WT GAC
488-GAC (280 abs)
488-GAC (490 abs)
Absorbance (mAU)
Elution Volume (mL)
C
Velocity (μM/min)
[Gln] (mM)
Unlabeled GAC
488-GAC
QSY9-GAC
D
Velocity (μM/min)
[Phosphate] (mM)
Unlabeled GAC
488-GAC
QSY9-GAC

The ability of GAC to form tetramers, as read out by this FRET assay, directly correlated with the basal activation of GAC that occurs at increasing protein concentrations (i.e. due to tetramer formation through mass-action) (Figure 2.4B, (●)). Next, we investigated the effects of the known allosteric activator, inorganic phosphate, using this FRET assay. Inorganic phosphate was added to a population of GAC that consisted of 25 nM 488-GAC and 75 nM QSY9-GAC, so that the FRET signal was not maximal before addition of the allosteric activator. Figure 2.5A represents the real-time FRET measurements with and without the addition of inorganic phosphate, where phosphate was observed to induce a FRET signal upon injection. Indeed, this phosphate-induced FRET was dose-dependent, and was in good agreement with the activation of the WT enzyme (Figure 2.5B, compare (●) to (●)). Together, these results support the contention that the GAC tetramer is the minimal unit for enzymatic activity, and that the potent allosteric activator, inorganic phosphate, promotes tetramer formation to elicit its effects on enzyme activity.

Although these FRET measurements reflect the oligomerization of GAC, and suggest that oligomerization is required for activation, we were interested in developing specific oligomer-deficient mutations that would block both the monomer-monomer interactions necessary for forming dimers, and the dimer-dimer interactions that give rise to tetramers. To accomplish this, we made use of available X-ray crystal structures, where the structure of GAC has been solved as a homo-tetramer in its asymmetric unit. Figure 2.1 illustrates a space filling model of a GAC tetramer, where the dimer and tetramer units are presented (left), along with zoomed in regions of the monomer-monomer and dimer-dimer interfaces (right).

FIGURE 2.4 – Real-time fluorescence assay detecting GAC tetramer formation. (**A**) 25 nM 488-GAC (donor) fluorescence is quenched upon addition of QSY9-GAC (acceptor) in a dose-dependent manner and reversed with the addition of a 10-fold excess of unlabeled GAC. (**B**) FRET resulting from the titration of 25 nM 488-GAC with increasing amounts of QSY9-GAC (○) overlaid with concentration-dependent *in vitro* activation of GAC (●). FRET data was fit to a quadratic binding isotherm.

A

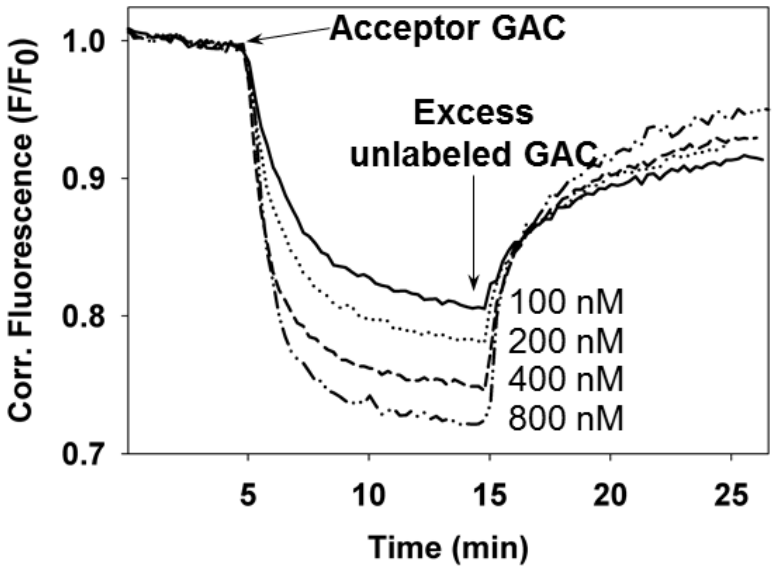
Acceptor GAC
Excess
unlabeled GAC
100 nM
200 nM
400 nM
800 nM
Corr. Fluorescence (F/F0)
1.0
0.9
0.8
0.7
5
10
15
20
25
Time (min)

B

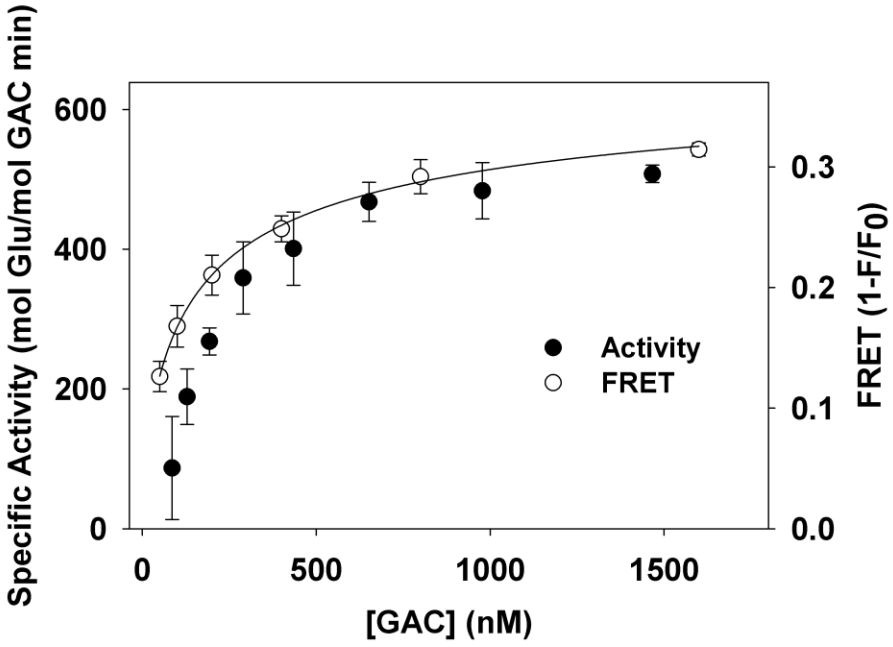
Specific Activity (mol Glu/mol GAC min)
600
400
200
0
0
500
1000
1500
[GAC] (nM)
Activity
FRET
0.3
0.2
0.1
0.0
FRET (1-F/F0)

FIGURE 2.5 – FRET assay as a read out for phosphate-induced GAC tetramers. (**A**) Addition of 100 mM HPO_4^{2-} to an equilibrated population of 25 nM 488-GAC and 75 nM QSY9-GAC quenches 488-fluorescence. (**B**) FRET resulting from the titration of P_i to an equilibrated population of 488:QSY9-labeled GAC (●) overlaid with phosphate activation profile of unlabeled WT GAC (●). Both curves were fit to a Hill equation and found to have a $K_{1/2}$ for phosphate of 20.1 mM determined from FRET and 16.8 mM determined from enzyme activation assays.

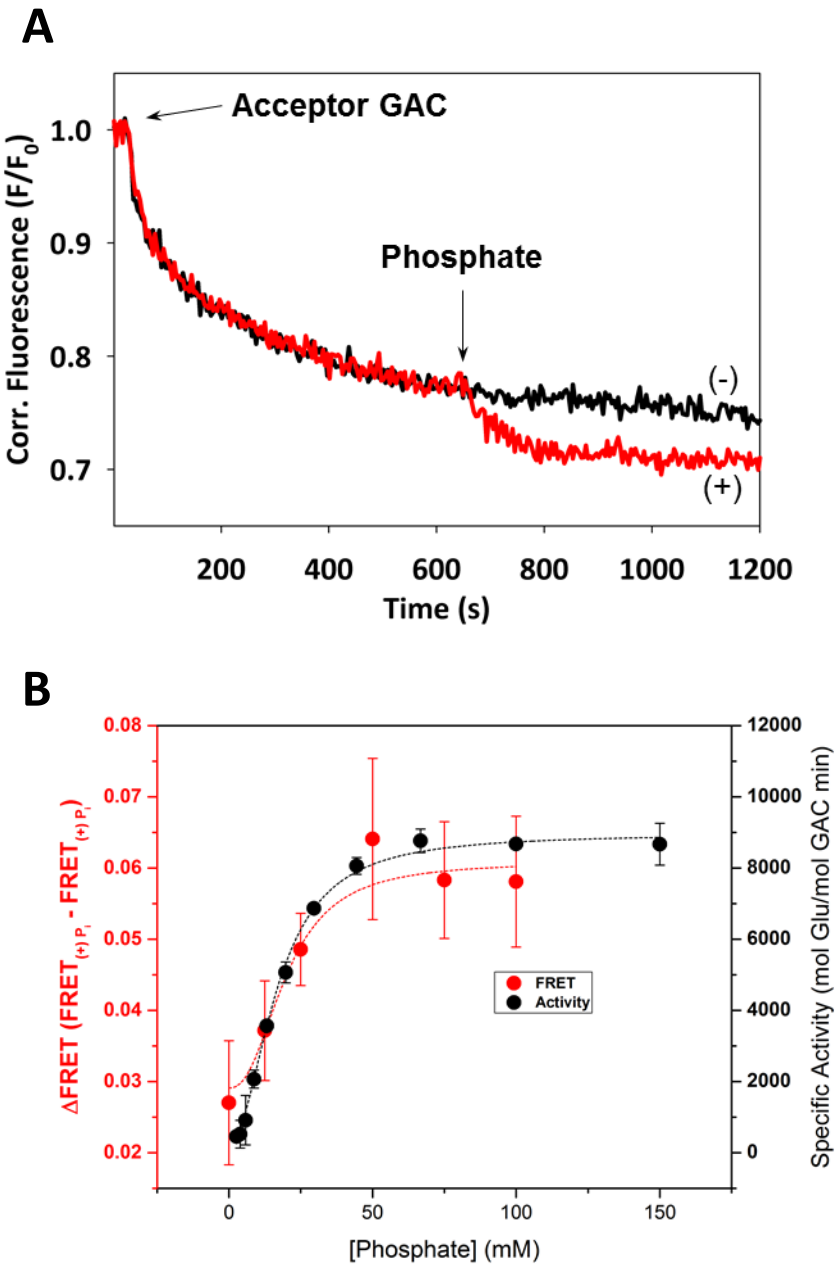
A
Acceptor GAC
Phosphate
(-)
(+)
Corr. Fluorescence (F/F0)
1.0
0.9
0.8
0.7
200
400
600
800
1000
1200
Time (s)
B
ΔFRET (FRET(+) Pi - FRET(+) Pi)
Specific Activity (mol Glu/mol GAC min)
FRET
Activity
0.08
0.07
0.06
0.05
0.04
0.03
0.02
12000
10000
8000
6000
4000
2000
0
0
50
100
150
[Phosphate] (mM)

Residues that were identified to be the principal electrostatic contacts at each interface are highlighted, where mutations that reversed the charge on one of the contacts were made. In particular, introduction of a lysine for the native aspartate at position 391, to create the D391K mutant, was shown by multi-angle light scattering (MALS) to be sufficient for prohibiting the formation of GAC tetramers, and hence to being trapped in the dimeric state (Figure 2.6A, (—)). In addition to this new dimer mutant, mutations were made at the monomer-monomer interface within the D391K mutant background (i.e. by changing both the native lysine at position 316 and arginine at position 459 to glutamate residues), in order to create the K316E-D391K-R459E triple mutant, which yielded a constitutive GAC monomer (Figure 2.6A, (—)).

These oligomeric-deficient GAC mutants, trapped in either the dimeric or monomeric form, were then labeled with the QSY9 FRET acceptor probe and used in FRET assays. Addition of these mutants to 488-labeled WT GAC resulted in the complete ablation of FRET when the constitutive monomer (QSY9-labeled K316E-D391K-R459E) was added, with only a minor amount of FRET being observed for the constitutive dimer (QSY9-labeled D391K), when compared to the addition of QSY9-labelled WT GAC (Figure 2.6B). These results show that the FRET signal resulting from the addition of QSY9-WT GAC to 488-labeled WT GAC is specifically dependent on the ability of GAC dimers to form tetramers. Furthermore, both of these oligomeric-deficient GAC mutants were shown to be inactive over a range of concentrations when assayed in the presence or absence of inorganic phosphate, showing that the ability of GAC to form tetramers is also required for enzyme activation.

FIGURE 2.6 – FRET assay is specific for GAC tetramer formation, but not the inactive dimer or monomer. (**A**) Multi-angle light scattering profiles of 250 μg (each) of WT GAC (—), D391K-GAC (—), and K316E/D391K/R459E-GAC (—), where the solid line represents the elution of each species by monitoring refractive index (R.I.), and the broken line designates the calculated molecular weight for the species eluted at that time. Reference lines for the molecular weights of the monomeric, dimeric, and tetrameric forms of the enzyme are included at 58 kD, 116 kD, and 232 kD respectively. (**B**) FRET assays upon addition of 200 nM WT QSY9-labeled GAC (—), the dimeric QSY9-GAC (D391K) (—), and QSY9-GAC (K316E/ D391K/ R459E) monomer (—) to 20 nM WT 488-labeled GAC. (**C**) Concentration-dependent enzymatic activities of WT GAC, GAC (D391K) dimer, and GAC (K316E/ D391K/ R459E) monomer, without addition of phosphate and (**D**) with the addition of 100 mM phosphate. Activities were measured in a 2-step end-point activity assay where GAC was incubated in the presence of glutamine for 2 m at concentrations under 250 nM GAC, and for 30 s at concentrations above 250 nM GAC.

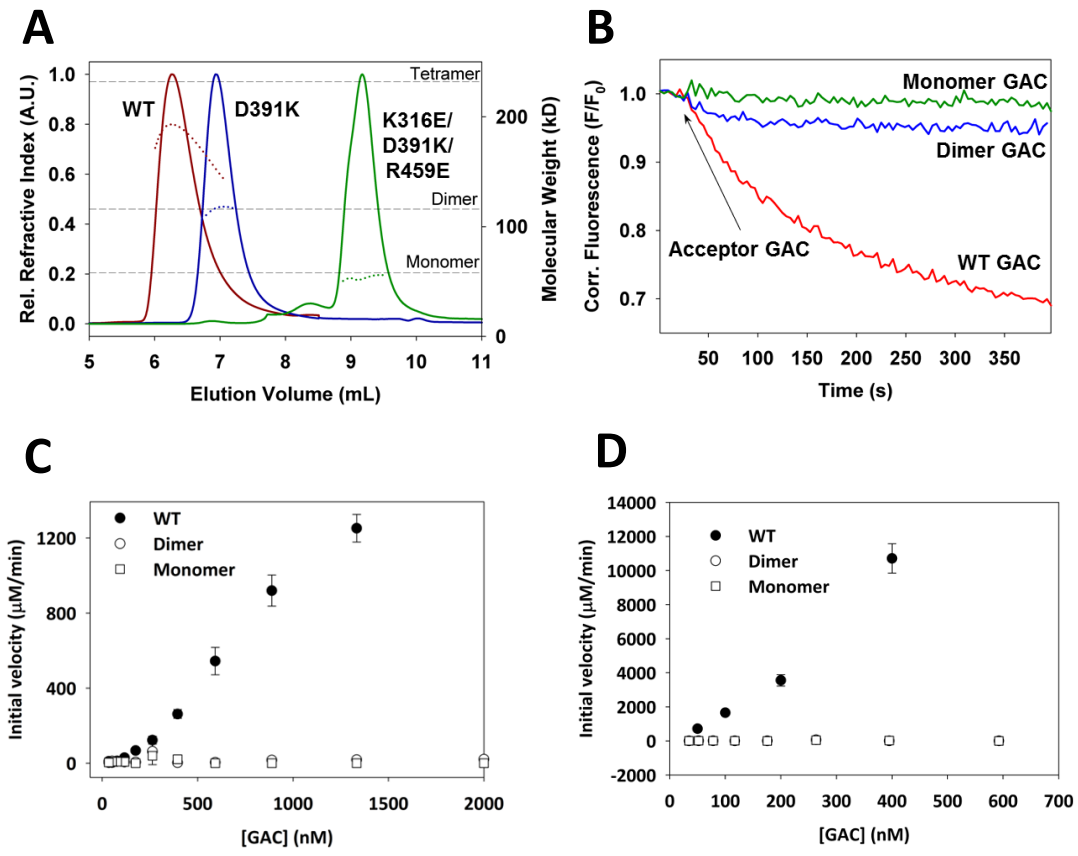
A
Rel. Refractive Index (A.U.)
Molecular Weight (kD)
Elution Volume (mL)
WT
D391K
K316E/
D391K/
R459E
Tetramer
Dimer
Monomer
B
Corr. Fluorescence (F/F0)
Time (s)
Monomer GAC
Dimer GAC
Acceptor GAC
WT GAC
C
Initial velocity (μM/min)
[GAC] (nM)
WT
Dimer
Monomer
D
Initial velocity (μM/min)
[GAC] (nM)
WT
Dimer
Monomer

2.3.2 Examining the effects of 968 and BPTES on the dimer-to-tetramer transition of GAC

Having developed a FRET assay which detects the ability of GAC to form tetramers, we next examined how allosteric inhibitors of GAC affected its ability to form tetramers. There are currently two classes of allosteric inhibitors of GAC (Figure 2.7A). One such class is comprised of derivatives of bis-thiadiazoles, where the small molecule BPTES is the prototype and has been shown by X-ray crystallographic studies to bind at the dimer-dimer interface of the GAC tetramer. The second class of compounds represents derivatives of the benzophenanthridines, with compound 968 being the prototype. Thus far, 968 and its analogues have not been extensively characterized in terms of how they bind to GAC or how they inhibit the enzyme. To investigate the effects of these two classes of inhibitors on the ability of GAC to undergo tetramer formation, they were added to a mixture of WT QSY9-labeled and 488-labeled GAC (Figure 2.7B).

Consistent with previous findings that BPTES stabilizes an inactive, tetrameric form of GAC [18], [28], [35], we found that it caused an immediate quenching of 488-GAC fluorescence emission when added to a mixture of 488-GAC and QSY9-GAC (Figure 7B, (—)), i.e. due to the ability of BPTES to induce the formation of 488-GAC:QSY9-GAC (donor:acceptor) tetramers. The formation of these stable GAC:BPTES tetrameric complexes was dose-dependent, and less susceptible to reversal by the addition of unlabeled GAC (compare the (—) versus (—) traces in Figure 2.8A). Interestingly, 968 elicited a markedly different response, causing a

significant change in the fluorescence emission of 488-GAC, followed by a partial fluorescence recovery upon the addition of excess unlabeled GAC (Figure 2.7B, (—)). The recovery of 488-GAC fluorescence, upon addition of excess unlabeled GAC was due to the elimination of FRET between 488-GAC and QSY9-GAC, i.e. via the formation of mixed tetramers between 488-GAC or QSY9-GAC and unlabeled GAC. The quenching of the fluorescence was dose-dependent, but the fluorescence recovery by the addition of excess unlabeled GAC was not dependent on the concentration of 968 (Figure 2.8B). Thus, 968 does not appear to interfere with GAC tetramer formation. However, the inability to achieve a full recovery of the fluorescence emission suggested that 968 binding was directly affecting 488-GAC donor fluorescence emission. Indeed, we found that 968 caused a dose-dependent quenching of 488-GAC emission (in the absence of the FRET acceptor QSY9-GAC) that matched the 968-mediated inhibition of GAC activity (Figures 2.9A,B). Taken together, these findings show that 968 does not mimic the actions of BPTES by trapping GAC in an inactive tetrameric state, but instead regulates GAC activity through a distinct allosteric mechanism.

FIGURE 2.7 – The FRET assay can distinguish between different allosteric inhibitors. (**A**) Structures of the two distinct allosteric inhibitors of GAC, 968 and BPTES. (**B**) Addition of either BPTES (—) or 968 (—) to an equilibrated mixture of 25 nM 488-GAC and 75 nM QSY9-GAC quenches 488 fluorescence, however, to different extents. For the case of BPTES, the quenching of 488-GAC fluorescence is not reversible by the addition of unlabeled subunits, whereas in the case of 968, some of the 488-GAC fluorescence is recovered, due to FRET pairs being substituted with unlabeled subunits.

A

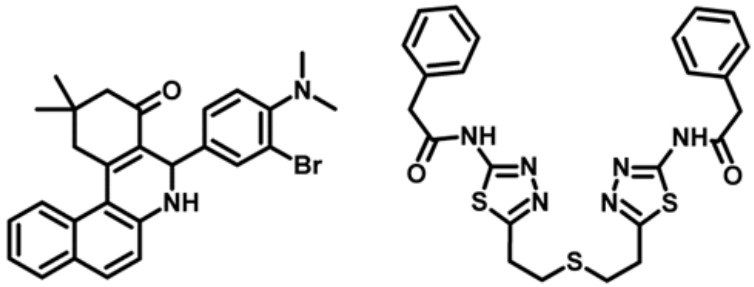
O
N
Br
NH
NH
O
N
S
N
S
N
N
NH
O
S

968 BPTES

B

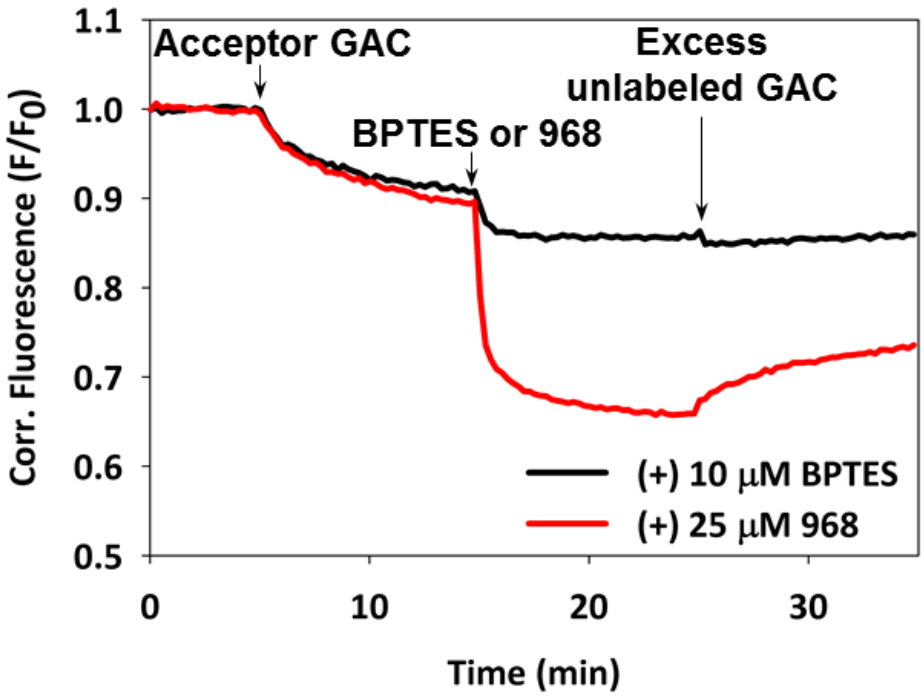
Acceptor GAC
Excess
unlabeled GAC
BPTES or 968
(+) 10 μM BPTES
(+) 25 μM 968
Corr. Fluorescence (F/F0)
1.1
1.0
0.9
0.8
0.7
0.6
0.5
0
10
20
30
Time (min)

FIGURE 2.8 – Quenching of 488-GAC by both BPTES and 968 is dose-dependent. (**A**) Addition of increasing concentrations of BPTES to 25 nM 488-GAC and 25 nM QSY9-GAC induces tetramer formation that is not reversible by addition of 10-fold excess unlabeled GAC; whereas addition of increasing concentrations of 968 (**B**) induces a dose-dependent quenching of 488-GAC fluorescence with partial recovery by addition of 10-fold excess unlabeled GAC.

A

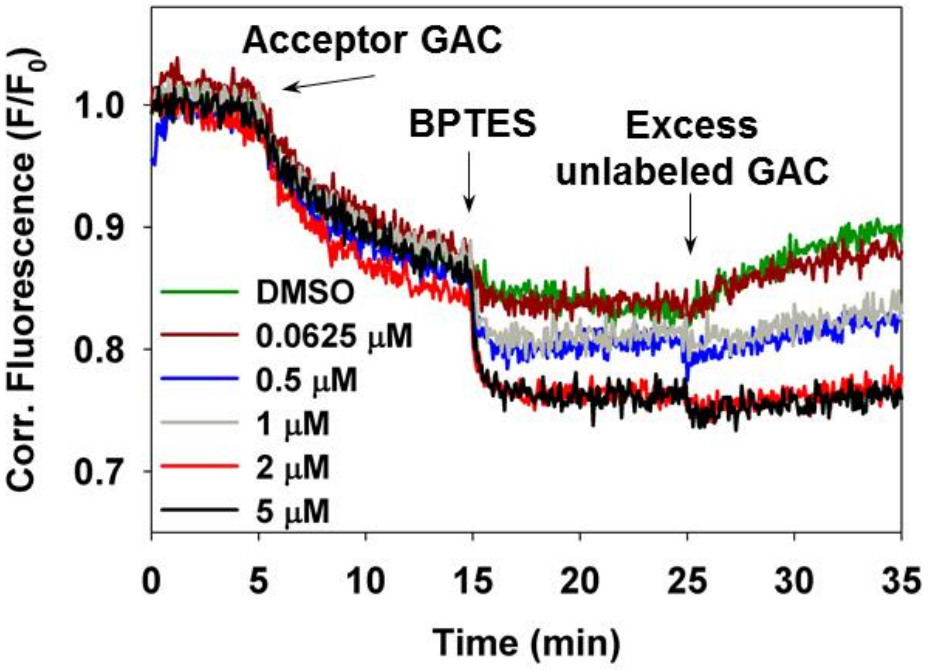
Acceptor GAC
BPTES
Excess unlabeled GAC
DMSO
0.0625 μM
0.5 μM
1 μM
2 μM
5 μM
Corr. Fluorescence (F/F0)
1.0
0.9
0.8
0.7
0
5
10
15
20
25
30
35
Time (min)

B

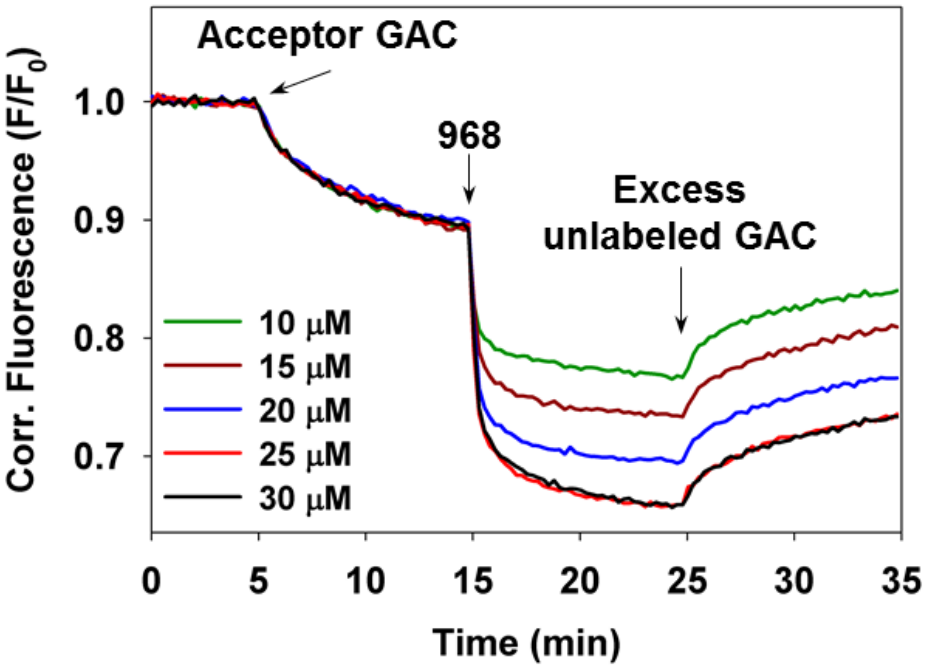
Acceptor GAC
968
Excess unlabeled GAC
10 μM
15 μM
20 μM
25 μM
30 μM
Corr. Fluorescence (F/F0)
1.0
0.9
0.8
0.7
0
5
10
15
20
25
30
35
Time (min)

2.3.3 968 preferentially binds to the monomeric state of GAC

Docking analyses using the x-ray structure of the GAC tetramer, together with mutagenesis studies, suggested that 968 binds in a cove between the monomer-monomer interface [31]. Therefore, we were interested in developing a direct binding assay that would discern whether 968 preferred to bind to a distinct oligomeric state. To address this, we took advantage of the newly developed oligomeric-deficient mutants, along with the novel direct binding assay using 488-labeled GAC, where the constitutive GAC dimer mutant (D391K) and the constitutive GAC monomer mutant (K316-D391K-R459E) were labeled with the AlexaFluor-488 succinimidyl-ester. These 488-labeled mutants were then subjected to fluorescence assays, where the quenching of the 488 probe upon addition of 968 was used as a direct binding read-out.

We found that 968 was capable of binding to WT 488-GAC, as well as to both the dimeric GAC (D391K) and the monomeric GAC (D391K-K316E-R459E), with the monomeric GAC having the highest affinity for 968 (Figure 2.10A). These results suggested that 968 should be most effective at inhibiting WT GAC at relatively low enzyme concentrations, i.e. where equilibrium conditions favor GAC initially existing as a monomer. Figure 2.10B shows that when the concentration of GAC was decreased from 50 nM to 5 nM, 968 was able to inhibit GAC activity with a significantly greater potency. Furthermore, the 968-mediated inhibition of GAC activity at these low enzyme concentrations correlated well with its inhibition of oncogenic transformation.

FIGURE 2.9 – Quenching of 488-GAC fluorescence by 968 as a real-time read out for binding. (**A**) Fluorescence quenching upon addition of different concentrations of 968 to 20 nM 488-GAC in the absence of QSY9-GAC. (**B**) Quenching of 20 nM 488-labeled GAC fluorescence by 968 (●) and inhibition of 20 nM unlabeled WT GAC as measured by real-time NADH fluorescence emission (○), where unlabeled WT GAC (20 nM) was assayed in place of 488-labeled GAC.

A

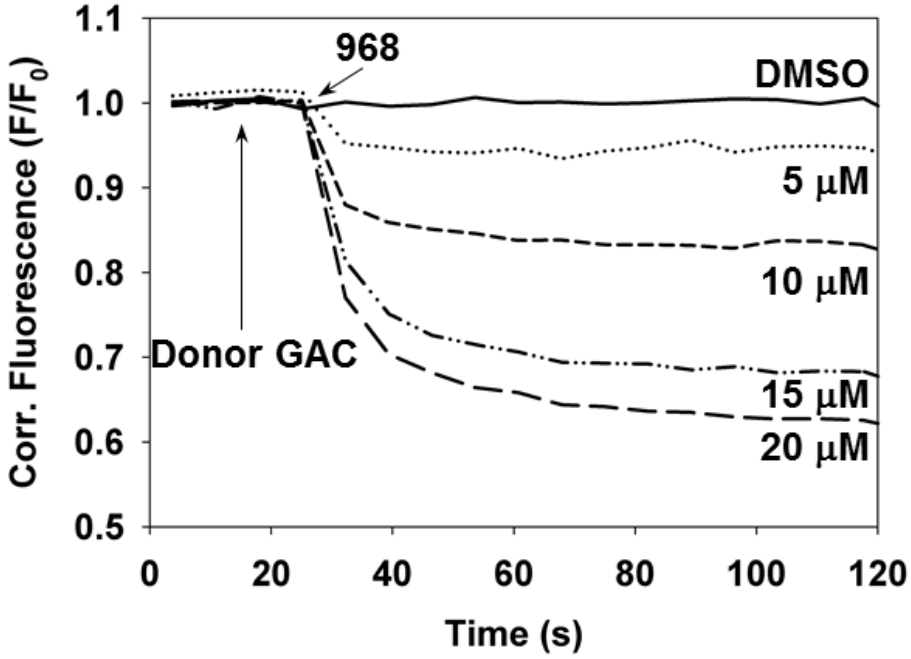
968
DMSO
5 μM
10 μM
15 μM
20 μM
Donor GAC
Corr. Fluorescence (F/F0)
Time (s)
1.1
1.0
0.9
0.8
0.7
0.6
0.5
0
20
40
60
80
100
120

B

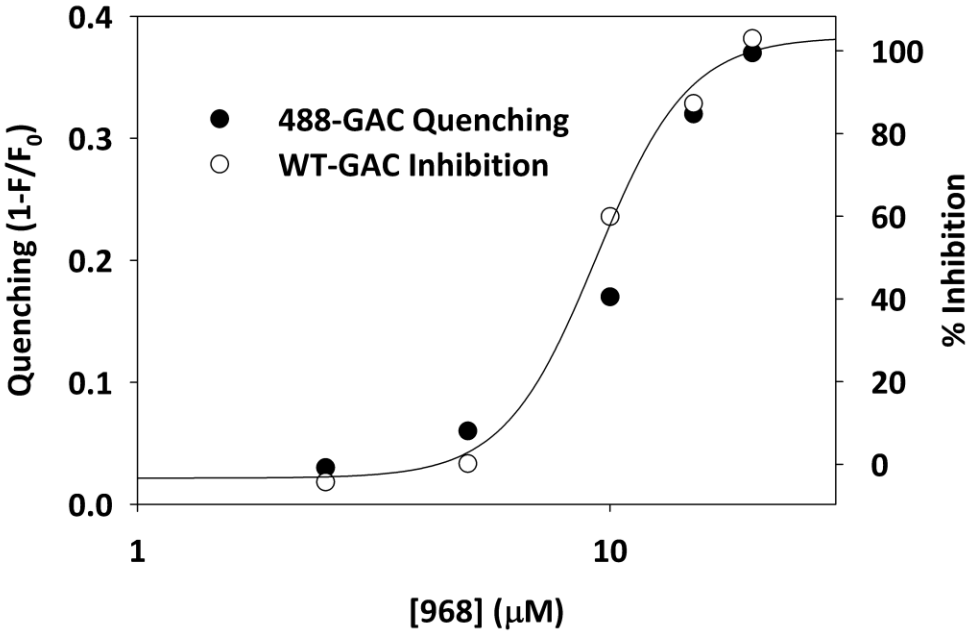
488-GAC Quenching
WT-GAC Inhibition
Quenching (1-F/F0)
% Inhibition
[968] (μM)
0.4
0.3
0.2
0.1
0.0
100
80
60
40
20
0
1
10

These results show that 968 allosterically inhibits GAC activity by binding to the monomeric form, and inducing an inactive state of the enzyme. This is in stark contrast to the mechanism by which BPTES binds to and inhibits GAC activity. Figure 11 illustrates the model of the activation of GAC, where inactive monomers form inactive dimers, which can ultimately form the active tetrameric species. BPTES, a prototype for a distinct class of allosteric inhibitors of glutaminase activity, binds to the tetrameric form of GAC at the dimer-dimer interface to promote inactive stable tetramers. Alternatively, the allosteric inhibitor 968 binds at the monomer-monomer interface of the inactive monomeric form of GAC.

FIGURE 2.10 – Examination of 968 binding to GAC monomeric and dimeric mutants. (**A**) 968 binding monitored by its quenching of the fluorescence of WT 488-labeled GAC, the dimeric 488-GAC (D391K), and the monomeric 488-GAC (K316E/D391K/R459E) (10 nM total monomer in each sample). (**B**) *In vitro* inhibition curves of 50 nM (●) and 5 nM WT GAC (○) pre-incubated with increasing concentrations of 968. Overlaid is the dose-dependent inhibition by 968 of Dbl-induced focus formation (▲).

A

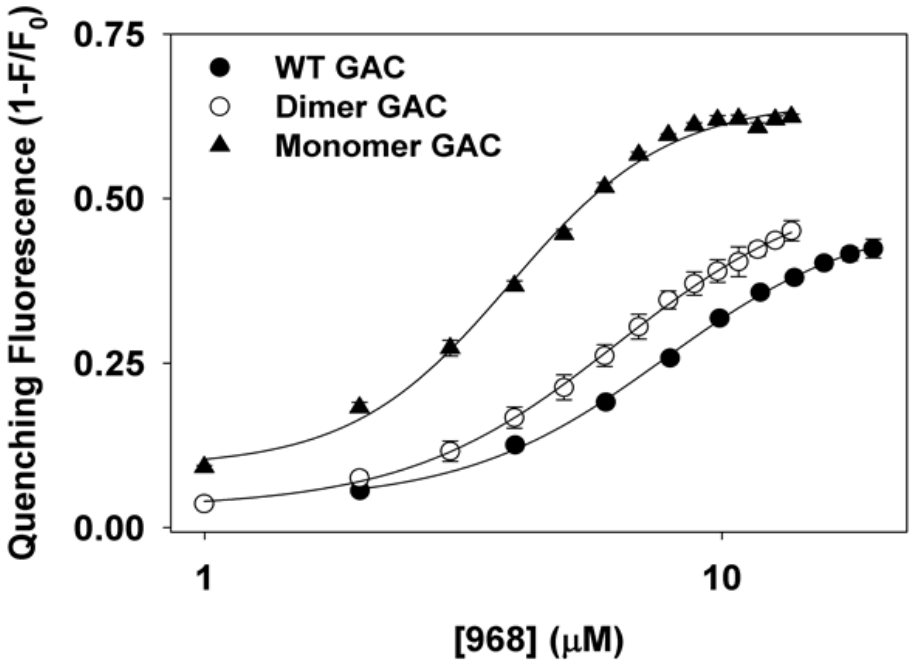
Quenching Fluorescence (1-F/F0)
0.75
0.50
0.25
0.00
WT GAC
Dimer GAC
Monomer GAC
1
10
[968] (μM)

B

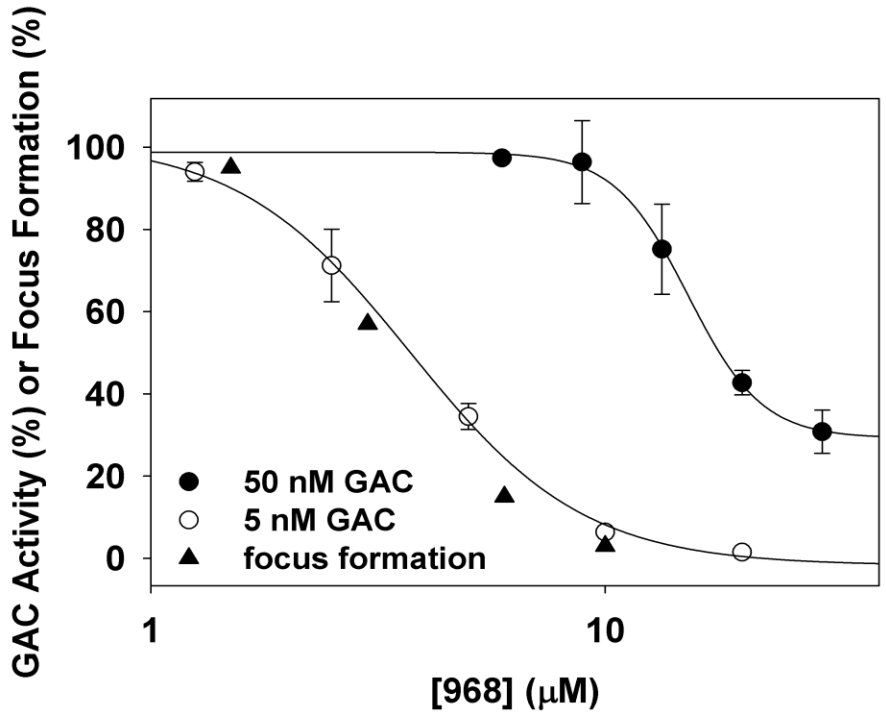
GAC Activity (%) or Focus Formation (%)
100
80
60
40
20
0
50 nM GAC
5 nM GAC
focus formation
1
10
[968] (μM)

FIGURE 2.11 – Model of allosteric regulation of glutaminase activity by small molecules and oligomer formation. Monomeric units of GAC associate to form dimers, where both monomer and dimer GAC species are catalytically inactive. GAC dimers then bind to form tetramers, which represents the active oligomer. BPTES (yellow spheres) binds at the GAC dimer-dimer interface to induce an inactive form of the tetrameric species (PDB 3UO9). Alternatively, 968 (orange spheres) binds to the monomeric form of GAC, presumably at the monomer-monomer interface as suggested by Katt et al. 2013 [29]. These 968 bound monomers can form dimers, and prohibit the activation of the enzyme.

Glutamine
Glutamate
+
NH_3

2.4 DISCUSSION

Previous studies of glutaminase isoforms described the oligomerization of these enzymes as a prerequisite for activation. However, it has remained unclear whether tetramer formation was required for activation, because no direct measurements have been made on the binding affinity of two dimers. Here, we set out to describe the formation of GAC tetramers using a direct binding assay, where one population was labeled with the highly fluorescent probe AlexaFluor488 to act as a FRET donor, and another labeled with the non-fluorescent QSY9 probe as the FRET acceptor. We found that this highly sensitive FRET assay enabled us to directly readout GAC tetramer formation, by monitoring the quenching of 488-labeled WT GAC following the addition of QSY9-labeled GAC. This FRET signal was readily reversible upon the addition of unlabeled GAC subunits, demonstrating the dynamic equilibrium of tetramer formation. Furthermore, we found that the dose dependent GAC tetramer formation directly correlated with enzyme activation, demonstrating that tetramer formation was indeed required for activation.

To show that this FRET assay was a direct read-out for tetramer formation, we made use of novel GAC mutants that were trapped in either the dimeric or monomeric state. The FRET signal was completely ablated when the acceptor-labeled monomeric GAC mutant was added to the donor-labeled WT GAC, and only a minor FRET was observed for the addition of the dimeric mutant, which is most likely due to the FRET resulting from a minor amount of monomer-monomer exchange. Lastly, we tested the activity of these GAC oligomeric-deficient mutants in the presence and absence of the allosteric activator, inorganic phosphate, and found that they were entirely inactive.

Taken together, these results show that the FRET assay developed here is an accurate read-out for the formation of GAC tetramers, and that tetramer formation is absolutely required for activation of the WT enzyme.

We then set out to understand how the allosteric inhibitors BPTES and 968 inhibit the activity of GAC. Because BPTES, a well characterized allosteric inhibitor of GAC, has been shown to bind and stabilize an inactive tetrameric form of the enzyme, one possibility was that 968 had a similar effect. The highly sensitive FRET assay enabled us to directly monitor the effects of 968 and BPTES on the dimer-to-tetramer transition. We found that BPTES induced the formation of stabilized GAC tetramers, which was not reversible, as would be expected by previous studies. However, unlike BPTES, 968 does not influence the tetramer formation of GAC. In fact, we discovered that the binding of 968 to GAC resulted in a quenching of the reporter group fluorescence, thus providing us with a direct spectroscopic read-out for the ability of this inhibitor and various analogs to bind to the enzyme. This direct spectroscopic read-out was found to be dose dependent, with its dose response directly correlated with inhibition of enzymatic activity.

By taking advantage of a direct binding assay for 968, together with the recent development of GAC mutants that exist as monomers or dimers, we discovered that 968 has a marked preference for binding to the monomeric form of the enzyme. While 968 is able to bind, albeit more weakly, to a GAC dimer, as well as to a GAC tetramer that has been activated by the allosteric regulator inorganic phosphate, it is unable to inhibit the activity of the activated enzyme tetramer. Therefore, 968 preferentially binds to an inactive, monomeric state of GAC and prevents it from

undergoing activating conformational changes, whereas, if GAC reaches an activated state prior to 968-binding, then 968 is unable to inhibit enzyme activity.

These findings highlight the distinction between the two classes of allosteric GAC inhibitors for which BPTES and 968 are the prototypes. BPTES is able to bind and inhibit activated GAC, whereas 968 binds preferentially to and stabilizes an inactive state of the enzyme. In addition, we now understand the reason for previous discrepancies when comparing the 968 dose-dependencies for the inhibition of recombinant GAC activity versus oncogenic transformation [10]. Specifically, in those earlier experiments, the concentrations of recombinant GAC routinely being assayed represented a mixture of dimers and tetramers. Consequently, the IC_{50} values for 968 reflected its weaker binding to these oligomeric GAC species. Indeed, when the binding of 968 to GAC, together with its ability to inhibit enzyme activity, is assayed at GAC concentrations where it exists predominantly as a monomer, the dose response profiles for these binding assays match the dose-dependent inhibition of transformation in cell culture.

In conclusion, we show that 968 is capable of directly binding to GAC, the key enzyme responsible for elevated glutamine metabolism in transformed cells and cancer cells, and that 968 preferentially binds to a monomeric, inactive state of the enzyme. While an x-ray crystal structure of 968 bound to GAC has not yet been achieved, these findings shed new light on why this has been so challenging, given that crystallization trials have been routinely performed at GAC concentrations where it exists as a tetramer, i.e. the least favorable species for binding 968. Our ability to generate monomeric GAC mutants now provides new opportunities for achieving such

a structure. Moreover, the availability of a direct binding read-out adapted for plate-reader assays offers exciting possibilities for the identification of 968-like allosteric inhibitors that could yield new therapeutic strategies against cancer.

2.5 REFERENCES

[1] D. Hanahan and R. A. Weinberg, "Hallmarks of Cancer: The Next Generation," *Cell*, vol. 144, no. 5, pp. 646–674, Mar. 2011.

[2] P. S. Ward and C. B. Thompson, "Metabolic Reprogramming: A Cancer Hallmark Even Warburg Did Not Anticipate," *Cancer Cell*, vol. 21, no. 3, pp. 297–308, Mar. 2012.

[3] M. G. V. Heiden, L. C. Cantley, and C. B. Thompson, "Understanding the Warburg Effect: The Metabolic Requirements of Cell Proliferation," *Science*, vol. 324, no. 5930, pp. 1029–1033, May 2009.

[4] W. H. Koppenol, P. L. Bounds, and C. V. Dang, "Otto Warburg's contributions to current concepts of cancer metabolism," *Nat. Rev. Cancer*, vol. 11, no. 5, pp. 325–337, May 2011.

[5] S. Y. Lunt and M. G. V. Heiden, "Aerobic Glycolysis: Meeting the Metabolic Requirements of Cell Proliferation," *Annu. Rev. Cell Dev. Biol.*, vol. 27, no. 1, pp. 441–464, 2011.

[6] R. J. DeBerardinis, J. J. Lum, G. Hatzivassiliou, and C. B. Thompson, "The Biology of Cancer: Metabolic Reprogramming Fuels Cell Growth and Proliferation," *Cell Metab.*, vol. 7, no. 1, pp. 11–20, Jan. 2008.

[7] J.-B. Wang, J. W. Erickson, R. Fuji, S. Ramachandran, P. Gao, R. Dinavahi, K. F. Wilson, A. L. B. Ambrosio, S. M. G. Dias, C. V. Dang, and R. A. Cerione, "Targeting Mitochondrial Glutaminase Activity Inhibits Oncogenic Transformation," *Cancer Cell*, vol. 18, no. 3, pp. 207–219, Sep. 2010.

[8] A. Le, A. N. Lane, M. Hamaker, S. Bose, A. Gouw, J. Barbi, T. Tsukamoto, C. J. Rojas, B. S. Slusher, H. Zhang, L. J. Zimmerman, D. C. Liebler, R. J. C. Slebos, P. K. Lorkiewicz, R. M. Higashi, T. W. M. Fan, and C. V. Dang, "Glucose-Independent Glutamine Metabolism via TCA Cycling for Proliferation and Survival in B Cells," *Cell Metab.*, vol. 15, no. 1, pp. 110–121, Jan. 2012.

[9] D. R. Wise, R. J. DeBerardinis, A. Mancuso, N. Sayed, X.-Y. Zhang, H. K. Pfeiffer, I. Nissim, E. Daikhin, M. Yudkoff, S. B. McMahon, and C. B. Thompson, "Myc regulates a transcriptional program that stimulates mitochondrial glutaminolysis and leads to glutamine addiction," *Proc. Natl. Acad. Sci.*, vol. 105, no. 48, pp. 18782–18787, Dec. 2008.

[10] J.-B. Wang, J. W. Erickson, R. Fuji, S. Ramachandran, P. Gao, R. Dinavahi, K. F. Wilson, A. L. B. Ambrosio, S. M. G. Dias, C. V. Dang, and R. A. Cerione, "Targeting Mitochondrial Glutaminase Activity Inhibits Oncogenic Transformation," *Cancer Cell*, vol. 18, no. 3, pp. 207–219, Sep. 2010.

[11] B. DeLaBarre, S. Gross, C. Fang, Y. Gao, A. Jha, F. Jiang, J. Song J., W. Wei, and J. B. Hurov, "Full-Length Human Glutaminase in Complex with an Allosteric Inhibitor," *Biochemistry (Mosc.)*, vol. 50, no. 50, pp. 10764–10770, Dec. 2011.

[12] M. Szeliga and J. Albrecht, "Opposing roles of glutaminase isoforms in determining glioblastoma cell phenotype," *Neurochem. Int.*, vol. 88, pp. 6–9, Sep. 2015.

[13] M. I. Gross, S. D. Demo, J. B. Dennison, L. Chen, T. Chernov-Rogan, B. Goyal, J. R. Janes, G. J. Laidig, E. R. Lewis, J. Li, A. L. MacKinnon, F. Parlati, M. L. M. Rodriguez, P. J. Shwonek, E. B. Sjogren, T. F. Stanton, T. Wang, J.

Yang, F. Zhao, and M. K. Bennett, “Antitumor Activity of the Glutaminase Inhibitor CB-839 in Triple-Negative Breast Cancer,” *Mol. Cancer Ther.*, vol. 13, no. 4, pp. 890–901, Apr. 2014.

[14] M. Szeliga and M. Obara-Michlewska, “Glutamine in neoplastic cells: focus on the expression and roles of glutaminases,” *Neurochem. Int.*, vol. 55, no. 1, pp. 71–75, 2009.

[15] A. P. J. van den Heuvel, J. Jing, R. F. Wooster, and K. E. Bachman, “Analysis of glutamine dependency in non-small cell lung cancer,” *Cancer Biol. Ther.*, vol. 13, no. 12, pp. 1185–1194, Oct. 2012.

[16] H. Yz and K. We, “A comparative study of glytaminase isozymes in rat tissues.,” *Enzyme*, vol. 21, no. 5, pp. 408–426, Dec. 1975.

[17] N. P. Curthoys, T. Kuhlenschmidt, and S. S. Godfrey, “Regulation of renal ammoniagenesis: Purification and characterization of phosphate-dependent glutaminase from rat kidney,” *Arch. Biochem. Biophys.*, vol. 174, no. 1, pp. 82–89, May 1976.

[18] M. M. Robinson, S. J. Mcbryant, T. Tsukamoto, C. Rojas, D. V. Ferraris, S. K. Hamilton, J. C. Hansen, and N. P. Curthoys, “Novel mechanism of inhibition of rat kidney-type glutaminase by bis-2-(5-phenylacetamido-1,2,4-thiadiazol-2-yl)ethyl sulfide (BPTES),” *Biochem. J.*, vol. 406, no. 3, pp. 407–414, Sep. 2007.

[19] A. Cassago, A. P. S. Ferreira, I. M. Ferreira, C. Fornezari, E. R. M. Gomes, K. S. Greene, H. M. Pereira, R. C. Garratt, S. M. G. Dias, and A. L. B. Ambrosio, “Mitochondrial localization and structure-based phosphate activation mechanism of Glutaminase C with implications for cancer metabolism,” *Proc. Natl. Acad. Sci. U. S. A.*, vol. 109, no. 4, pp. 1092–1097, Jan. 2012.

[20] M. Møller, S. S. Nielsen, S. Ramachandran, Y. Li, G. Tria, W. Streicher, M. V. Petoukhov, R. A. Cerione, R. E. Gillilan, and B. Vestergaard, “Small Angle X-Ray Scattering Studies of Mitochondrial Glutaminase C Reveal Extended Flexible Regions, and Link Oligomeric State with Enzyme Activity,” *PLoS ONE*, vol. 8, no. 9, p. e74783, Sep. 2013.

[21] M. Patel and J. D. McGivan, “Partial purification and properties of rat liver glutaminase.,” *Biochem. J.*, vol. 220, no. 2, pp. 583–590, Jun. 1984.

[22] J. McGIVAN, M. Vadher, J. Lacey, and N. Bradford, “Rat liver glutaminase,” *Eur. J. Biochem.*, vol. 148, no. 2, pp. 323–327, Apr. 1985.

[23] N. P. Curthoys and M. Watford, “Regulation of Glutaminase Activity and Glutamine Metabolism,” *Annu. Rev. Nutr.*, vol. 15, no. 1, pp. 133–159, 1995.

[24] Z. Kovačević, “Importance of the flux of phosphate across the inner membrane of kidney mitochondria for the activation of glutaminase and the transport of glutamine,” *Biochim. Biophys. Acta BBA - Bioenerg.*, vol. 430, no. 3, pp. 399–412, Jun. 1976.

[25] A. Cassago, A. P. S. Ferreira, I. M. Ferreira, C. Fornezari, E. R. M. Gomes, K. S. Greene, H. M. Pereira, R. C. Garratt, S. M. G. Dias, and A. L. B. Ambrosio, “Mitochondrial localization and structure-based phosphate activation mechanism of Glutaminase C with implications for cancer metabolism,” *Proc. Natl. Acad. Sci.*, vol. 109, no. 4, pp. 1092–1097, Jan. 2012.

[26] K. Thangavelu, C. Q. Pan, T. Karlberg, G. Balaji, M. Uttamchandani, V. Suresh, H. Schüler, B. C. Low, and J. Sivaraman, "Structural basis for the allosteric inhibitory mechanism of human kidney-type glutaminase (KGA) and its regulation by Raf-Mek-Erk signaling in cancer cell metabolism," *Proc. Natl. Acad. Sci.*, vol. 109, no. 20, pp. 7705–7710, May 2012.

[27] C. J. McDonald, E. Acheff, R. Kennedy, L. Taylor, and N. P. Curthoys, "Effect of lysine to alanine mutations on the phosphate activation and BPTES inhibition of glutaminase," *Neurochem. Int.*, vol. 88, pp. 10–14, Sep. 2015.

[28] E. W. Hartwick and N. P. Curthoys, "BPTES inhibition of hGA124–551, a truncated form of human kidney-type glutaminase," *J. Enzyme Inhib. Med. Chem.*, vol. 27, no. 6, pp. 861–867, Dec. 2012.

[29] S. C. Zimmermann, E. F. Wolf, A. Luu, A. G. Thomas, M. Stathis, B. Poore, C. Nguyen, A. Le, C. Rojas, B. S. Slusher, and T. Tsukamoto, "Allosteric Glutaminase Inhibitors Based on a 1,4-Di(5-amino-1,3,4-thiadiazol-2-yl)butane Scaffold," *ACS Med. Chem. Lett.*, Mar. 2016.

[30] K. Shukla, D. V. Ferraris, A. G. Thomas, M. Stathis, B. Duvall, G. Delahanty, J. Alt, R. Rais, C. Rojas, P. Gao, Y. Xiang, C. V. Dang, B. S. Slusher, and T. Tsukamoto, "Design, Synthesis, and Pharmacological Evaluation of Bis-2-(5-phenylacetamido-1,2,4-thiadiazol-2-yl)ethyl Sulfide 3 (BPTES) Analogs as Glutaminase Inhibitors," *J. Med. Chem.*, vol. 55, no. 23, pp. 10551–10563, Dec. 2012.

[31] W. P. Katt, S. Ramachandran, J. W. Erickson, and R. A. Cerione, "Dibenzophenanthridines as Inhibitors of Glutaminase C and Cancer Cell Proliferation," *Mol. Cancer Ther.*, vol. 11, no. 6, pp. 1269–1278, Jun. 2012.

[32] A. G. Thomas, C. Rojas, C. Tanega, M. Shen, A. Simeonov, M. B. Boxer, D. S. Auld, D. V. Ferraris, T. Tsukamoto, and B. S. Slusher, "Kinetic characterization of ebselen, chelerythrine and apomorphine as glutaminase inhibitors," *Biochem. Biophys. Res. Commun.*, vol. 438, no. 2, pp. 243–248, Aug. 2013.

[33] A. G. Thomas, C. M. O'Driscoll, J. Bressler, W. E. Kaufmann, C. J. Rojas, and B. S. Slusher, "Small molecule glutaminase inhibitors block glutamate release from stimulated microglia," *Biochem. Biophys. Res. Commun.*, vol. 443, no. 1, pp. 32–36, Jan. 2014.

[34] A. G. Thomas, C. Rojas, C. Tanega, M. Shen, A. Simeonov, M. B. Boxer, D. S. Auld, D. V. Ferraris, T. Tsukamoto, and B. S. Slusher, "Kinetic characterization of ebselen, chelerythrine and apomorphine as glutaminase inhibitors," *Biochem. Biophys. Res. Commun.*, vol. 438, no. 2, pp. 243–248, Aug. 2013.

[35] B. DeLaBarre, S. Gross, C. Fang, Y. Gao, A. Jha, F. Jiang, J. Song J., W. Wei, and J. B. Hurov, "Full-Length Human Glutaminase in Complex with an Allosteric Inhibitor," *Biochemistry (Mosc.)*, vol. 50, no. 50, pp. 10764–10770, Dec. 2011.

CHAPTER THREE

Novel dibenzophenanthridine derivatives as GAC inhibitors: a coupled high throughput binding-inhibition assay leads to the development of tool compounds useful *in vitro* and in transformed cells.

3.1 INTRODUCTION

As discussed in Chapter 1, the mitochondrial enzyme glutaminase (GLS1) has gained significant attention as a therapeutic target for cancer [1]–[3]. GLS1 catalyzes the hydrolysis of glutamine to glutamate, which is used in the TCA cycle of cancer cells undergoing an aberrant glycolytic flux (i.e. the "Warburg effect") as a non-glucose-derived source for anaplerosis. The elevation in glutamine metabolism exhibited by many cancer cells ("glutamine addiction") is critical for sustaining their proliferative capacity as well as for other aspects of their transformed phenotypes [4]–[9]. Work from our laboratory has shown that a specific GLS1 splice variant, GAC, plays an essential role in the transformation of NIH 3T3 fibroblasts by Rho GTPases, as well as in the proliferative and invasive activities of various cancer cells [10]–[12]. Thus, given the importance of GAC expression and activation for oncogenic transformation, the identification of inhibitors that target this metabolic enzyme offers new opportunities for the development of anti-cancer drugs.

As outlined in Chapter 2, our laboratory identified a class of small molecules containing a benzophenanthridine scaffold, that potently inhibited Rho-GTPase dependent transformation [10]. The prototype for this inhibitor scaffold, compound 968, was shown to target the mitochondrial enzyme, GAC. The identification of GAC as the target of 968 was shown through a pull-down assay using an active fragment of

968 (the phenyl bromo-dimethylamine ring, or “hot spot”) immobilized on a solid support. Using mass spectrometry, the short isoform of GLS1 (i.e. GAC), was identified. However, significant questions remained concerning the mechanism by which the 968-class of small molecules inhibited GAC activity, and how these inhibitors might be developed into cancer therapeutics.

Selected derivatives around the central 968 scaffold have been described by our laboratory, and highlight the efficacy of this compound in cell proliferation assays of cancer cells [11]. Ligand-docking studies have suggested 968 binds within a hydrophobic pocket at the monomer-monomer interface of the GAC dimer, which is in good agreement with previous studies presented in Chapter 2 (Section 2.3.3), above. Interestingly, other groups have identified highly similar molecules using high-throughput non-biased screening. Thomas and colleagues (2013) identified a natural product benzophenanthridine, named Chelerythrine, as a potent inhibitor of GAC activity [13]. This natural product alkaloid, derived from a member of the poppy family, has previously been assayed for its biological activity, and was proposed to be an inhibitor of cAMP-dependent kinase (PKC) activity, eliciting anti-proliferative and anti-inflammatory responses [14]–[17]. However, more recent studies have shown that Chelerythrine inhibits cancer cells through a mitochondrial mechanism that is distinct from PKC inhibition [17]–[19]. Perhaps most interestingly is the finding that Chelerythrine treatment of HeLa cells induced apoptotic events that were associated with the activation of the p38 and JNK signaling pathways. Chelerythrine-induced apoptosis could be rescued by the treatment with the antioxidants glutathione and N-acetyl-cysteine, pointing towards a depleted pool of glutathione within Chelerythine-

treated cells, an outcome of the inhibition of glutamine metabolism [4], [18], [20]. Moreover, our laboratory has recently shown a direct relationship between c-Jun expression, JNK activity, and GAC expression in a panel of breast cancer cells, thus connecting glutamine metabolism to JNK signaling [21].

Collectively, these studies suggest that members of the benzophenanthridine class of small molecules are possible lead compounds for a new class of therapeutics. However, these studies have also helped to identify the challenges of developing these small molecules as targets for drug development, as they have poor solubility and pharmacological properties [10], [11], [13], [22]. Therefore, new scaffolds need to be developed to elucidate the specific binding mechanism of these small molecules and increase their chances as potential drug candidates.

In order to profile newly synthesized 968 derivatives, we began by developing a robust screening assay that would be highly specific to this class of inhibitors. Having this high-throughput assay in hand, we then made minor substitutions around the 968 scaffold in search of new 968-analogues to improve the central scaffold. Using the binding and inhibition assays, we went on to show that a new, smaller, 968 derivative could be optimized such that it was as potent an inhibitor as 968 itself. This opens a route for discovering new lead compounds. Additionally, we made use of the 968 structure to install useful physical properties to study the action of 968 both *in vitro* and *in vivo*. We developed a highly fluorescent 968 derivative that could serve as a spectroscopic read-out, followed by the addition of photo cross-linking groups, to covalently modify a target (i.e. the GAC protein) with this new fluorescent 968-molecule. Having developed these novel compounds, together with the robust

screening assay, we were able to generate covalently modified GAC protein for biophysical studies, as well as for use in cellular assays, enabling the subcellular localization of intracellular 968-cross linked targets. These assays provide a strong foundation for the advancement of this unique class of GAC inhibitors, to gain a deeper understanding of how 968 treatment exerts such an effective inhibition of cellular transformation.

3.2 METHODS

3.2.1 Real-time 968 binding and enzyme activity assays

Real-time fluorescence monitoring of 968 binding and GAC activity through production of NADH was performed on a Varian Cary Eclipse Fluorometer, whereas small molecule inhibition and binding titrations were performed in a 96-well format in a Tecan Saphire absorbance and fluorescence plate reader. Samples for monitoring real-time binding of 968 to 488-GAC were prepared by adding 10 μL of varying concentrations of 968 prepared in DMSO to an equilibrated 1 mL sample of 10 nM 488-GAC, while observing 488 fluorescence (490 nm excitation/520 nm emission). Similarly, this method was replicated for monitoring real time binding of 968 to mutant forms of GAC, namely 488-labeled GAC (GD391K) and 488-GAC (D391K, K316E, R459E). Real-time activity assays monitoring 968 binding and NADH production were prepared in 1 mL samples, where 10 units of glutamate dehydrogenase (Sigma) and 2 mM NAD^+ (Sigma) were prepared in 50 mM Tris-Acetate, pH 8.5, 0.1 mM EDTA and equilibrated at 20°C. WT GAC (10 nM) was added and allowed to equilibrate 2 minutes before monitoring the fluorescence emission of 488-GAC (490 nm excitation, 520 nm emission) and NADH (340 nm

excitation, 490 nm emission). Appropriate dilutions of 968 or BPTES prepared in DMSO were introduced after 30s and allowed to equilibrate for 2 minutes before a 180 μL solution of K_2HPO_4 and glutamine was added to make a final concentration of 50 mM K_2HPO_4 and 20 mM glutamine, to initiate GAC activation. The activity of GAC was measured in a coupled assay, by monitoring the NADH produced by glutamate dehydrogenase, which converts the product of the glutaminase-catalyzed reaction, glutamate, to α-ketoglutarate and ammonia by reducing NAD^+ to NADH. Because solutions containing glutamine undergo non-enzymatic degradation to glutamate, samples were further analyzed by subtracting the NADH produced by glutaminase in the presence of 968, BPTES, or the equivalent volume of DMSO as a control, from the NADH produced in the absence of glutaminase under identical experimental conditions. NADH was quantified using a standard curve of freshly prepared NADH (Sigma) in 50 mM Tris-Acetate, pH 8.5, and 0.1 mM EDTA.

Procedures for the real-time binding and inhibition assays were adapted for 96-well microtiter format with minor alterations. Briefly, 2 μL of inhibitor or DMSO was distributed across the 96-well plate, followed by addition of 200 μL 10 nM 488-GAC, unlabeled WT-GAC, or in the absence of added GAC as a negative control, in 50 mM Tris-Acetate, pH 8.5, and 0.1 mM EDTA, followed by immediate monitoring of 488 fluorescence (490 nm/520 nm excitation/emission, 5 nm/20 nm excitation/emission slits). The 488-fluorescence was measured every 2 min with 90s of orbital shaking, followed by 30s resting between each cycle for a total of four cycles (i.e. 6 min). A mixture of GDH and NAD^+ (20 μL) was then added to give 10 units of GDH and 2 mM NAD^+. To activate GAC, 30 μL of a mixture of glutamine and K_2HPO_4 was

added to give a total concentration of 50 mM K_2HPO_4 and 20 mM glutamine in each well. NADH fluorescence was measured (340 nm/460 nm excitation/emission, 10 nm/10 nm excitation/emission slits) every minute with 30s orbital shaking, and a 30s rest between each reading, for 10 cycles (i.e. 9 min). Three wells were prepared for each experimental condition (i.e. each concentration of compound) alongside one well where 2 μL of DMSO was added in place of inhibitor, and one well that contained the small molecule inhibitor but no GAC. To analyze 488-quenching by the added compound, 488-fluorescence (F) was normalized to the DMSO control (F_0). Quenching was quantified as follows: $1-F/F_0$. For compounds that emitted fluorescence within the observed range, fluorescence measured in the well that contained the compound but lacked GAC was used to subtract added fluorescence due to the compound. Similarly, samples were analyzed for NADH fluorescence by subtracting the fluorescence measured for the experimental condition from the NADH fluorescence in the well that contained the added compound but no GAC. Percent inhibition at each drug concentration was calculated using the adjacent DMSO control.

3.2.2 Preparation of 968 analogs

Compounds 742 and 031 were obtained by commercial vendors (ChemBridge and Specs, respectively). Starting materials for chemical synthesis were used without further purification.

3.2.2.1 3-Bromo-4-(dimethylamino)benzaldehyde [23]

4-(Dimethylamino) benzaldehyde (6.7 mmol) was suspended in 1,4 dioxane (13 mL), *N*-bromosuccinimide (7.0 mmol) was added at once and stirred at RT for 3 h. Water (50 mL) and ethyl acetate (50 mL) were added and the organic layer washed with two

more portions of water (50 mL) then removed and dried with magnesium sulfate. The solvent was removed by rotary evaporation and the crude product purified by silica gel chromatography using 2:1 CH_2Cl_2:hexane as the eluent to give 0.84 g of a clear oil (55% yield). ^{1}H NMR (400 MHz, $CDCl_3$): δ = 9.80 (1 H, s), 8.03 (1 H, d, *J* = 1.84 Hz), 7.73 (1 H, dd, *J* = 8.24 Hz, 1.84 Hz), 7.06 (1 H, d, *J* = 8.24 Hz), 2.94 (6 H, s).

3.2.2.2 General procedure for synthesis of 968, SU-1, and SU-14 [24]

The appropriate arylamine, 3-bromo-4- (dimethylamino)benzaldehyde and dimedone (2 mmol each) were heated to reflux in 10 mL ethanol for 1 hour, upon which time a precipitate formed. The precipitate was filtered, washed with ethanol and dried to give the product.

3.2.2.3 General procedure for synthesis of SU-7, SU-8, SU-2

The appropriate arylamine (3.7 mmol) and 3-bromo-4- (dimethylamino) benzaldehyde (3.7 mmol) were dissolved in benzene (5 mL) supplemented with molecular sieves (0.7 g) and stirred at RT for 18 h. The mixture was filtered and the solid material washed with dichloromethane. The combined filtrate was dried with magnesium sulfate, filtered and the solvent removed by rotary evaporation. The crude imine was dissolved in 1-butanol (6 mL), combined with dimedone (2 mmol) and heated to reflux for 2 h. The reaction mixture was cooled and solvent removed by rotary evaporation. The crude product was purified by silica gel chromatography using 1:1 hexanes:ethyl acetate as the eluent.

3.2.2.4 Synthesis of additional compounds

Additional compounds having a compound 968-like scaffold were synthesized as shown below.

General synthetic scheme for inhibitor analogs of the 968 scaffold

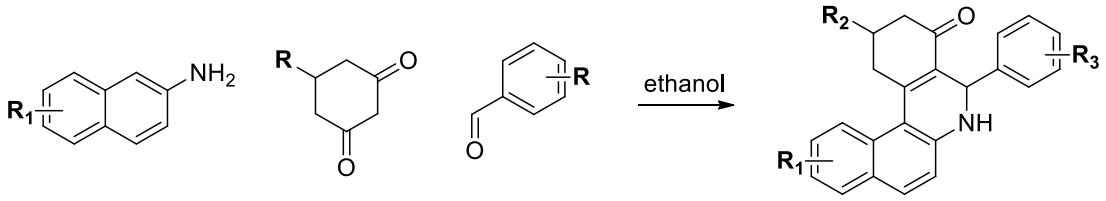

The appropriate aryl amine, 1,3 cyclohexanedione and aryl aldehyde were mixed in equal molar ratios and heated to reflux in ethanol. The resulting product generally precipitates from solution and is recovered by filtration. Representative NMRs are shown in Figures 8A–B.

SU-11 and compounds having a compound SU-11-like scaffold were synthesized as shown below.

General synthetic scheme for inhibitor analogs of the SU-11 scaffold

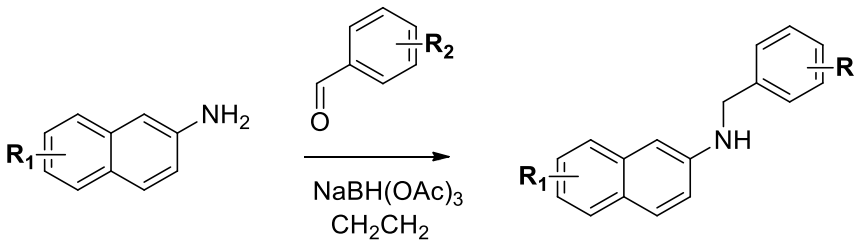

The appropriate aryl amine and aryl aldehyde were mixed in equal molar amounts in dichloromethane, and 1.3 molar equivalents of sodium triacetoxyborohydride was added and the mixture stirred at room temperature overnight. The product was purified by silica gel chromatography.

3.2.3 Covalent cross-linking of photo-reactive compounds *in vitro*

WT GAC, org GAC containing the mutations K316E/D391K/R459E, was purified as detailed 2.4.1. The GAC proteins were incubated with increasing concentrations of the compound SU-22, and excited with a hand-held UV lamp for 120 seconds.

Immediately following UV exposure, samples were loaded onto a 4-20% Tris-Glycine polyacrylamide gel after the addition of SDS-PAGE sample buffer (50 mM Tris-HCl (pH = 6.8), 2% SDS, 10% glycerol, 1% β-mercaptoethanol, 12.5 mM EDTA, 0.02% bromophenol blue), and visualized on a UV light box.

Conditions of *in vitro* cross-linking of WT GAC, and the K316E/D391K/R459E GAC mutant, were adapted for efficient cross-linking and purification of the cross-linked protein product. WT GAC and the K316E/D391K/R459E GAC mutant, both containing the N-terminal His-tag, were diluted to a concentration of 100 nM in 20 mM Tris-HCl (pH = 8.6), 100 mM NaCl, upon which 10 μM SU-22 and 2 mg/mL BSA were added. Following a preincubation time of 5 minutes, samples were exposed to UV light under a hand-held 500W UV lamp to initiate the photo-cross-linking. To isolate the cross-linked product, 2.5 mg cobalt agarose beads (Clontech) were added and the solution was gravity filtered. The beads were first washed with 10 column volumes of 50 mM Tris-HCl (pH = 8.6), 10 mM NaCl, and with 5 column volumes 50 mM Tris-HCl (pH = 8.6), 10 mM NaCl containing 5 mM imidazole, followed by 3 column volumes 50 mM Tris-HCl (pH = 8.6), 10 mM NaCl containing 20 mM imidazole, and finally the cross-linked product was eluted using 4 column volumes of 50 mM Tris-HCl (pH = 8.6), 10 mM NaCl containing 320 mM imidazole. The purified cross-linked protein was then concentrated using spin columns with a 30 kD molecular weight cutoff and quantified using UV-vis spectroscopy, where the protein was quantified by A280 (ε280 = 38,850 M-1 cm-1) and the cross-linked SU-22 by A350 (ε350 = 18,900 M-1 cm-1). Ratios of

cross-linked SU-22 to WT and K316E/D391K/R459E GAC were 0.52 and 0.78, respectively.

To further illustrate specific cross-linking, the cross-linked K316E/D391K/R459E was analyzed using analytical size exclusion chromatography, where 100 μg of cross-linked K316E/D391K/R459E was injected onto a Superdex 200 10/300 GL (GE Healthcare) column equilibrated in 50 mM Tris-HCl (pH = 8.6), 20 mM NaCl, with a flow rate of 0.3 mL/min, by monitoring both the absorbance wavelengths at 280 nm and 350 nm.

The cross-linked WT GAC was subjected to an overnight typsinization by first reacting all purified cross-linked WT GAC (2.5 mg) with 10 mM iodoacetamide, followed by addition of 25 μg sequencing grade trypsin (Roche), and then rotated overnight at 37°C. Following overnight trypsin digestion, the solution was filtered using a 10 kD MW cutoff spin filter and injected onto a SunFire C18 100 Å 5 μm, 4.6 mm x 150 mm (Waters). Peptides were eluted using a binary gradient elution protocol, where mobile phase A (5:95:0.1 acetonitrile:water:trifluoroacetic acid) and mobile phase B (95:5:0.1 acetonitrile:water:trifluoroacetic acid) were varied to produce an increase in acetonitrile up to 80% over 20 minutes at a flow rate of 1 mL/min. The wavelengths 254 nm and 35 nm were monitored.

3.2.4 Covalent cross-linking of photo-reactive compounds in cells.

Cross-linking of SU-22 was also performed in cells transformed by the oncogene, Dbl. For these experiments, Dbl-induced MEFs, as detailed in Example 1 above, were cultured in 150 mm^2 dishes to approximately 80% confluency in DMEM supplemented with 10% FBS. Cells were then washed and DMEM supplemented with

1% FBS and 5 μM SU-22 was added, and cells were cultured overnight. Cells were then exposed to 60 seconds of UV light by a hand-held 50W UV lamp to initiate the in-cell cross-linking, followed by washing with DMEM supplemented with 1% FBS without SU-22. Cells were incubated with DMEM supplemented with 1% FBS following UV exposure for 20 minutes. The cells were then trypsinized, and mitochondria were isolated as outlined in Frezza et al. (2007) [25]. Briefly, suspension of trypsinized cells were spun 600 x g 10 minutes at 4°C and suspended in mitochondrial isolation buffer (10 mM Tris-MOPS (pH = 7.4), 1 mM EGTA/Tris, and 200 mM sucrose). Cells were homogenized in a glass potter with a Teflon pestle using a Dounce homogenizer operated at approximately 1600 rpm for 35 strokes. The homogenate was centrifuged 600 x g 10 minutes at 4°C and the supernatant was isolated. The pellet was lysed in RIPA lysis buffer and used as the P1 fraction containing the nucleus and unbroken cells. The supernatant was centrifuged at 7000 x g 10 minutes at 4°C, where the resultant pellet contained the isolated mitochondria and the supernatant represented the soluble cytosolic and microsomal fractions. The supernatant was isolated and centrifuged at 200,000 x g 1 hour at 4°C, and the resulting pellet was taken to be the S200 fraction containing cytosolic and microsomal components. The mitochondrial pellet was resuspended in mitochondrial isolation buffer and spun again at 7000 x g 10 minutes at 4°C, where the resulting pellet was taken to be the purified isolated mitochondria.

For experiments where cells were visualized using confocal fluorescence microscopy, cells were cultured in the same conditions as stated above in MakTek 50 mm^2 dishes. Cells were treated with 5 μM SU-22 overnight in DMEM supplemented

with 1% FBS. Following 30 seconds of UV exposure, media was replaced with fresh DMEM (1% FBS) and incubated at 37°C for 2 hours. The media was then switched to DMEM (1 FBS) containing 250 nM of the mitochondrial fluorescent probe MitoTracker CMXRos and incubated at 37°C for 30 minutes, at which point the media was changed to DMEM (1% FBS) without the MitoTracker for an additional 30 minutes. Cells were then fixed in 4% para-formaldehyde and 0.1% glutaraldehyde and imaged on an inverted Axio Observer.Z1 microscope using the 405 laser line for excitation of the SU-22 small molecule and 514 laser line to excite the MitoTracker.

3.3 RESULTS

3.3.1 A real-time binding and inhibition assay to distinguish 968 derivatives from BPTES class inhibitors.

The real-time readout of the binding of 968-like inhibitors to the fluorescently labeled 488-GAC provided a useful strategy to simultaneously assay both inhibitor binding and the accompanying effects on enzyme activity. Figure 3.1 illustrates this approach, where the highly fluorescent 488-GAC is used to measure both the binding of 968, coupled with the immediate assaying enzyme activity. First, 968 is added to 488-GAC and the fluorescence quenching of the 488-probe is monitored, reflecting the binding of 968. Immediately after the binding measurement, the substrate glutamine, and the allosteric activator inorganic phosphate, are added to stimulate GAC activity, converting glutamine to the products glutamate and ammonia. Enzyme activity is measured using fluorescence, where a coupled enzymatic reaction catalyzed by glutamate dehydrogenase (GDH) is used to convert the glutamate, the product of the GAC-catalyzed reaction, to α-ketoglutarate, with the concomitant reduction of NAD^+ to NADH. The highly fluorescent NADH is easily monitored. Thus by using highly sensitive fluorescence assays, the binding of small molecule inhibitors of the 968-like scaffold to GAC, and their inhibition of GAC activity, can be monitored simultaneously.

The real-time binding and inhibition assays were developed using a fluorescence cuvette, where the temperature and sample mixing could be readily controlled. Figure 3.2A illustrates the results of this coupled assay using both the inhibitors 968 and BPTES.

FIGURE 3.1 – Coupled real time binding and inhibition assay. The highly fluorescent 488-GAC is first preincubated with a small molecule drug (e.g. 968), where the change in 488-fluorescence is monitored (490 nm excitation, 520 nm emission) as a direct read-out for drug binding. Immediately following drug binding, the substrate glutamine, and the allosteric activator inorganic phosphate, are added to stimulate GAC activity. The product of this reaction, glutamate, is then converted by glutamate dehydrogenase (GDH) to α-ketoglutarate with the concomitant reduction of NAD^+ to NADH, with the latter compound being highly fluorescent (360 nm excitation, 450 nm emission), such that it serves as a read-out for this coupled enzyme reaction.

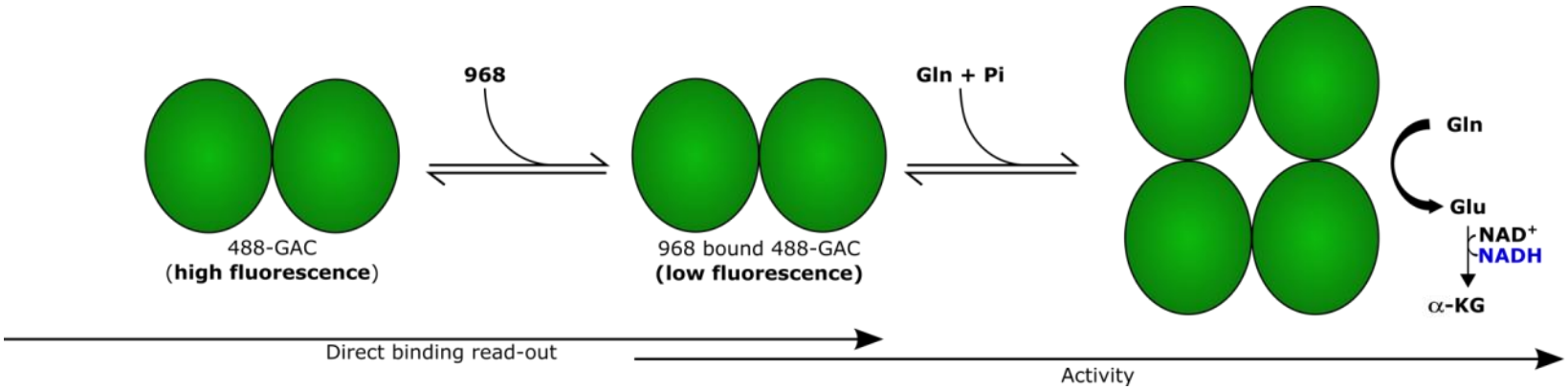
968
Gln + Pi
Gln
Glu
NAD+
NADH
α-KG
488-GAC
(high fluorescence)
968 bound 488-GAC
(low fluorescence)
Direct binding read-out
Activity

It has been shown previously that BPTES does not bind to the same allosteric site as 968. Therefore, BPTES does not cause a quenching of the 488-GAC fluorescence, whereas the addition of 968 to 488-GAC potently quenches the reporter group emission (Figure 3.2A, compare (—) to (···) and (---) (left axis)). Both 968 and BPTES potently inhibit glutaminase activity, as read out by NADH fluorescence, compared to the control experiment where the drug vehicle DMSO was used (Figure 3.2A, compare (—) and (···) to (---) (right axis)). These results demonstrate that the real-time quenching is specific for 968-like inhibitors.

To further validate the assay, we compared the dose-dependent quenching and inhibition of 488-GAC versus unlabeled WT GAC, i.e. to account for any effects arising from the covalent attachment of a fluorescent probe to GAC. Unlabeled WT GAC was assayed using the same protocol, however, without the monitoring of 488-fluorescence. The dose-dependent inhibition of WT GAC by 968 was in good agreement with the quenching and inhibition of 488-GAC (Figure 3.2B). This newly developed assay now provides a convenient method to examine small molecule drug candidates that inhibit GAC activity through the same allosteric mechanism as 968, as opposed to the other allosteric mechanism of BPTES inhibition.

FIGURE 3.2 – Simultaneous binding and inhibition assays of GAC specific for 968. (**A**) Real time binding (green curves, left axis) and activity (blue curves, right axis) of GAC were monitored in the same cuvette. Addition of 10 μM of 968 (—), BPTES (---), or DMSO (···), to 488-GAC yielded a 968-dependent quenching of 488-fluorescence. The activity of GAC was monitored directly upon drug binding, where both 968 (—) and BPTES (---) were found to inhibit GAC activity when compared to the DMSO (···) control. (**B**) Overlay of the dose-dependent drug binding, represented by the quenching of 488 fluorescence (●, left axis), and GAC inhibition, for 488-labeled GAC (●) and WT GAC (○), using this coupled assay.

A

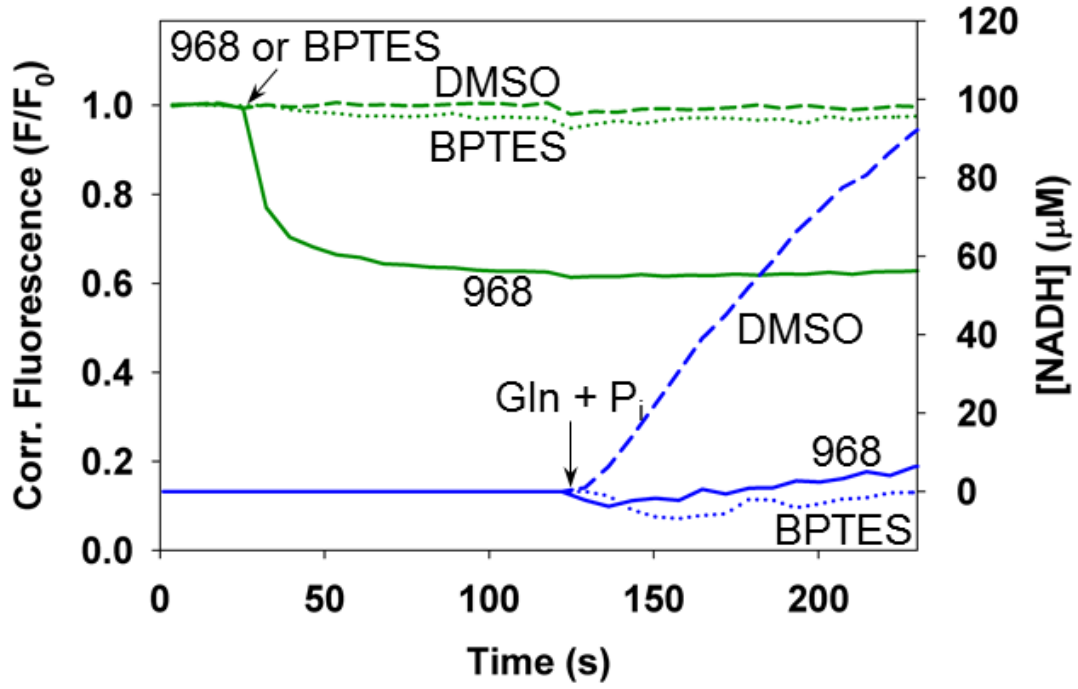
968 or BPTES
DMSO
BPTES
968
DMSO
Gln + Pi
968
BPTES
Corr. Fluorescence (F/F0)
[NADH] (μM)
Time (s)
0.0
0.2
0.4
0.6
0.8
1.0
0
20
40
60
80
100
120
0
50
100
150
200

B

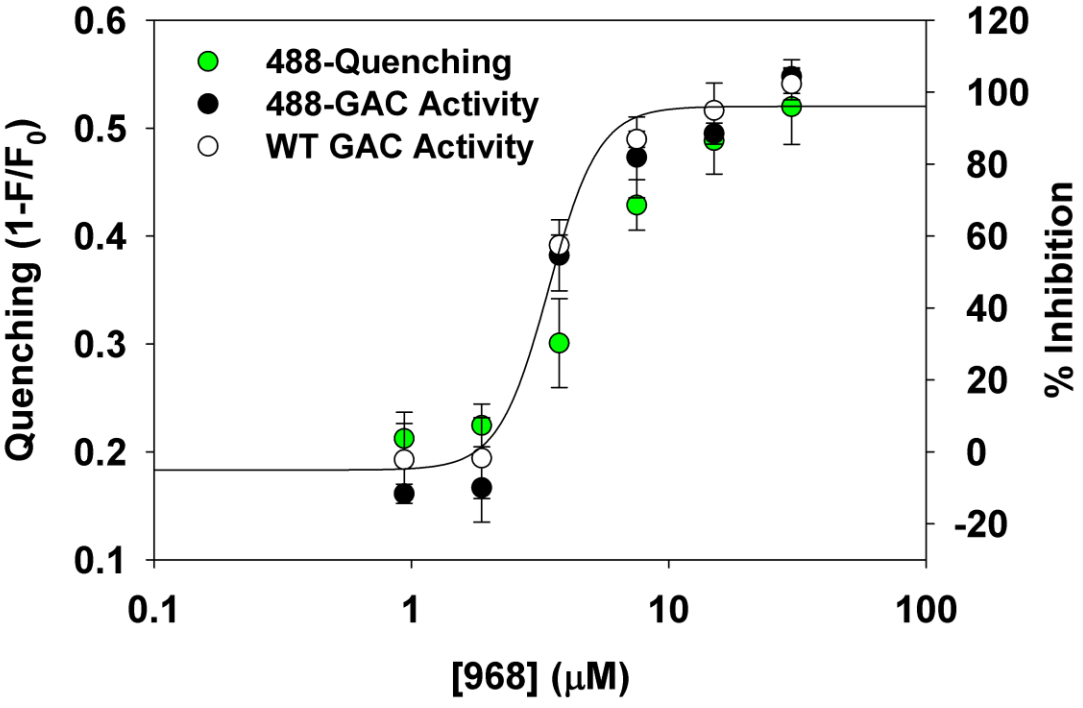
488-Quenching
488-GAC Activity
WT GAC Activity
Quenching (1-F/F0)
% Inhibition
[968] (μM)
0.1
0.2
0.3
0.4
0.5
0.6
-20
0
20
40
60
80
100
120
0.1
1
10
100

3.3.2 A high-throughput binding and inhibition assay for screening 968 analogues.

Although compound 968 has been an effective inhibitor both *in vivo* and *in vitro*, we were interested in modifying the central scaffold in search for new and improved inhibitor molecules. One primary goal was to increase the aqueous solubility of 968, a noticeable drawback for its use as a therapeutic agent. To accomplish this, we took advantage of the facile synthetic route for 968 synthesis (Figure 3.3A). Here, the central 968 scaffold could be easily modified by using alternate reactants (highlighted in blue, green, and orange). Substitutions were made that could be readily synthesized, and were later tested for their efficacy against recombinant GAC. In Figure 3.3B, the compounds are grouped by the modification of the central scaffold, and in decreasing order of their inhibition against recombinant GAC activity.

Having the developed real-time binding and inhibition assays in hand, we were interested in adapting this approach to a more high-throughput assay using 96-well microtiter plates and a fluorescence reader. To accomplish this, we scaled the reactions appropriately to fit within 200 μL, and monitored the fluorescence signal of 488-GAC and NADH in succession, upon the addition of drug, followed by the addition of substrate (Gln) and activator (P_i). This assay proved to be a robust readout for monitoring drug binding and enzyme inhibition, similar to the single-cuvette assay depicted in Figure 3.2A. Here, multiple drug concentrations could be analyzed simultaneously and in triplicates to give statistical validation of inhibitory and binding constants (IC_{50} and K_D values, respectively).

FIGURE 3.3 – 968 derivatives used for binding and inhibition assays. (**A**) General synthetic route for the synthesis of 968 derivatives, where fragments from each starting material are differentiated by the colors blue, green, and orange. (**B**) Synthesized 968 derivatives, with significant changes color coded by the fragment that was altered from the 968 structure. The prototype compound, 968, is highlighted with a red box. Names for the compounds, along with IC_{50} values (± s.d.) from inhibition assays using 488-GAC, are included to the right of each compound.

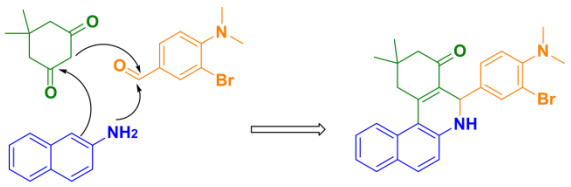

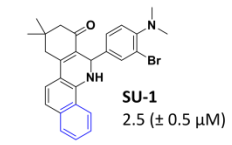

SU-1
2.5 (± 0.5 μM)

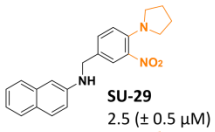

SU-29
2.5 (± 0.5 μM)

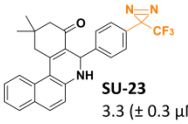

SU-23
3.3 (± 0.3 μM)

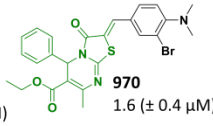

970
1.6 (± 0.4 μM)

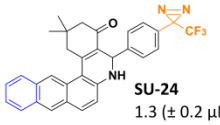

SU-24
1.3 (± 0.2 μM)

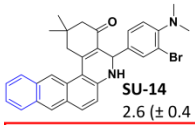

SU-14
2.6 (± 0.4 μM)

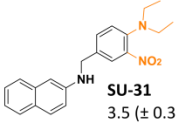

SU-31
3.5 (± 0.3 μM)

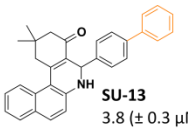

SU-13
3.8 (± 0.3 μM)

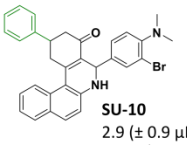

SU-10
2.9 (± 0.9 μM)

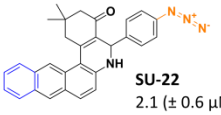

SU-22
2.1 (± 0.6 μM)

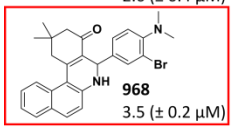

968
3.5 (± 0.2 μM)

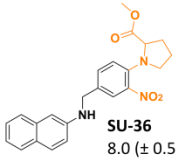

SU-36
8.0 (± 0.5 μM)

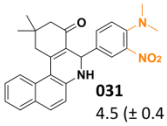

031
4.5 (± 0.4 μM)

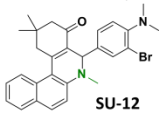

SU-12
2.9 (± 0.9 μM)

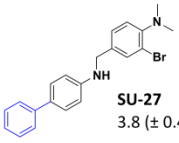

SU-27
3.8 (± 0.4 μM)

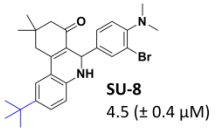

SU-8
4.5 (± 0.4 μM)

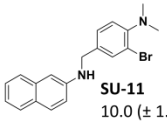

SU-11
10.0 (± 1.6 μM)

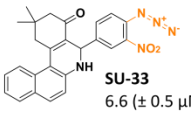

SU-33
6.6 (± 0.5 μM)

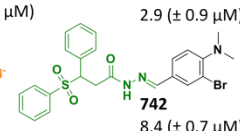

742
8.4 (± 0.7 μM)

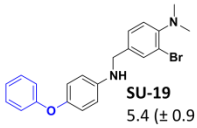

SU-19
5.4 (± 0.9 μM)

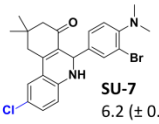

SU-7
6.2 (± 0.7 μM)

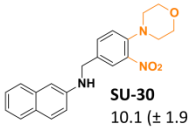

SU-30
10.1 (± 1.9 μM)

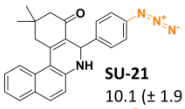

SU-21
10.1 (± 1.9 μM)

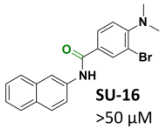

SU-16
>50 μM

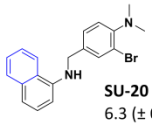

SU-20
6.3 (± 0.8 μM)

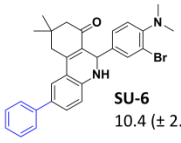

SU-6
10.4 (± 2.0 μM)

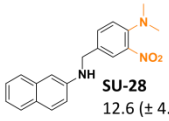

SU-28
12.6 (± 4.6 μM)

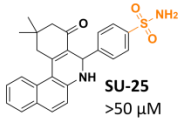

SU-25
>50 μM

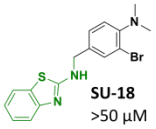

SU-18
>50 μM

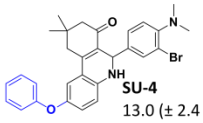

SU-4
13.0 (± 2.4 μM)

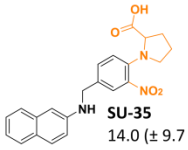

SU-35
14.0 (± 9.7 μM)

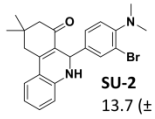

SU-2
13.7 (± 1.5 μM)

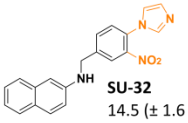

SU-32
14.5 (± 1.6 μM)

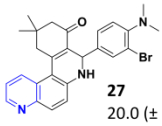

27
20.0 (± 2.6 μM)

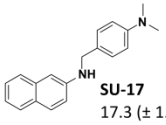

SU-17
17.3 (± 1.7 μM)

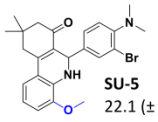

SU-5
22.1 (± 8.3 μM)

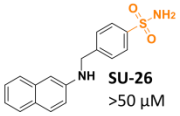

SU-26
>50 μM

FIGURE 3.4 – Inhibition and binding constants for 968 derivatives. (**A**) The IC_{50} values obtained from the real-time binding and inhibition assays against 488-GAC are plotted from most to least potent from left to right. (**B**) IC_{50} values represented in (**A**), plotted against the K_D values obtained from the binding portion of the coupled assay, show good agreement when fit by linear regression (slope = 1.09, Pearson's R = 0.799, n=30). The prototype, compound 968, is highlighted in blue for reference.

A

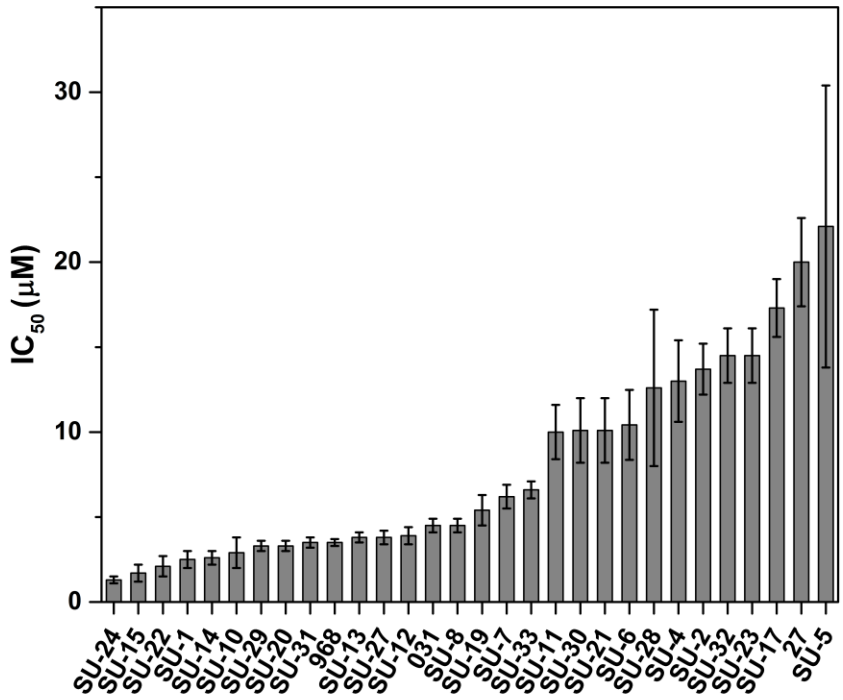
IC50 (μM)
0
10
20
30
SU-24
SU-15
SU-22
SU-1
SU-14
SU-10
SU-29
SU-20
SU-31
968
SU-13
SU-27
SU-12
031
SU-8
SU-19
SU-7
SU-33
SU-11
SU-30
SU-21
SU-6
SU-28
SU-4
SU-2
SU-32
SU-23
SU-17
27
SU-5

B

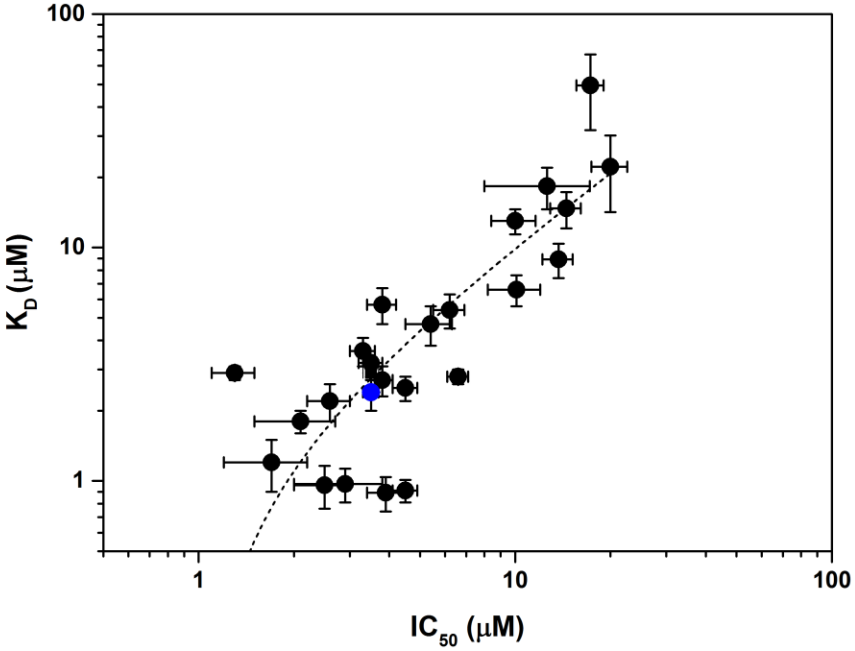
KD (μM)
1
10
100
IC50 (μM)
1
10
100

The screening of the compounds presented in Figure 3.3B against 488-GAC, using the real-time binding and inhibition assays, described above, resulted in a distribution of IC_{50} values (Figure 3.4A), which were then plotted with respect to the measured K_D values (Figure 3.4B). Importantly, the measured IC_{50} values and K_D values were in good agreement with respect to one another, as a plot of IC_{50} versus K_D gave a linear relationship with a high correlation coefficient. This further demonstrates that the inhibitory potency of the compound is directly related to its ability to bind to GAC, and not due to an allosteric mechanism that depends on the placement of specific functional groups within the binding pocket.

Unfortunately, the original 968 scaffold was not significantly improved with the substitutions that were synthesized. The general trend for increasing the potency of inhibition tracked with the addition of hydrophobic groups, such as aromatic rings (compare SU-14, SU-13, and SU-10, from left to right, in Figures 3.3B). However, unexpectedly, we identified a smaller scaffold that did not require the addition of the dimedone reactant (green, Figure 3.3A), but maintained potency when compared with 968 (compare SU-11 in second column to 968 in first column, Figure 3.3B). Furthermore, this smaller scaffold based from SU-11 was optimized to have a similar potency to 968, where the substituents around the phenyl ring were changed from a dimethyl amine to a pyrrolidine, while the bromine was substituted for a nitro group. These optimizations resulted in a new scaffold with a similar potency as that for 968. This new scaffold now represents an even more tractable synthetic route for synthesizing new derivatives, where only the naphthylamine and benzaldehyde are needed. Derivatives can be made simply through the nucleophilic addition of a moiety

containing a primary amine to a benzaldehyde to form the imine intermediate, followed by a reductive workup to give the final product. This simple scaffold optimization, together with the assays developed for the direct read-out of drug binding and inhibition, represents an attractive route for a concerted drug discovery effort to fully optimize the SU-11 molecule for an effective therapeutic reagent.

3.3.3 Functionalized 968 derivatives as useful tool compounds

Although the newly developed binding and inhibition assays helped guide new synthetic routes for making more potent or structurally divergent molecules around the 968 scaffold, some outstanding questions remained regarding 968's specific action against the GAC enzyme both *in vitro* and *in vivo*. These include the specific binding site for 968 on GAC, how 968 binding to the GAC monomer affects oligomerization of the enzyme, and whether GAC was indeed the direct target of 968 *in vivo*. To address these questions, we made simple derivatives of 968 that contain useful moieties, such as a fluorescent moiety and UV-activated covalent cross-linking groups.

First, a fluorescent 968-derivative was made by substituting an additional aromatic ring on the naphthyl group, to give the highly fluorescent anthracene moiety (Figure 3.5A). The fluorescence spectrum of this compound, shown in Figure 3.5B, was found to exhibit a large Stökes shift, with an excitation maximum at 345 nm and an emission maximum at 485 nm. This new fluorescent compound, named SU-14, was found to be a slightly better inhibitor for recombinant GAC than 968, suggesting this modification yielded a valuable 968-analogue for investigating the actions of this class of inhibitors in cells (Figures 3.4A,B).

FIGURE 3.5 – Development of highly fluorescent 968 derivatives as tool compounds. (**A**) Compounds SU-14 (left) and SU-22 (right) both contain the highly fluorescent anthracene ring (highlighted in green). Additionally, SU-22 contains a phenyl-azide, a common photo-activated cross-linking group (**B**) Fluorescence excitation and emission spectrum of compound SU-14, showing a strong fluorescence signal with a Stokes shift of >100 nm, making it useful for fluorescence assays.

A

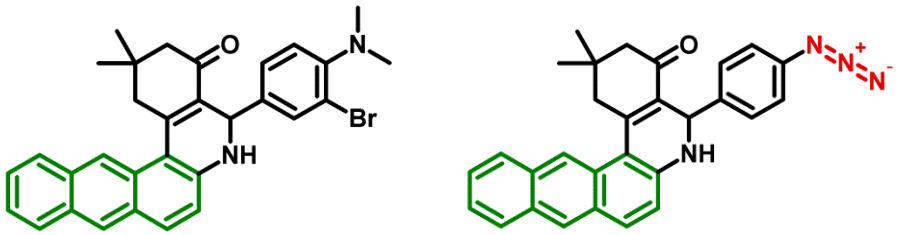
O
N
Br
NH
O
N
N
N
NH

B

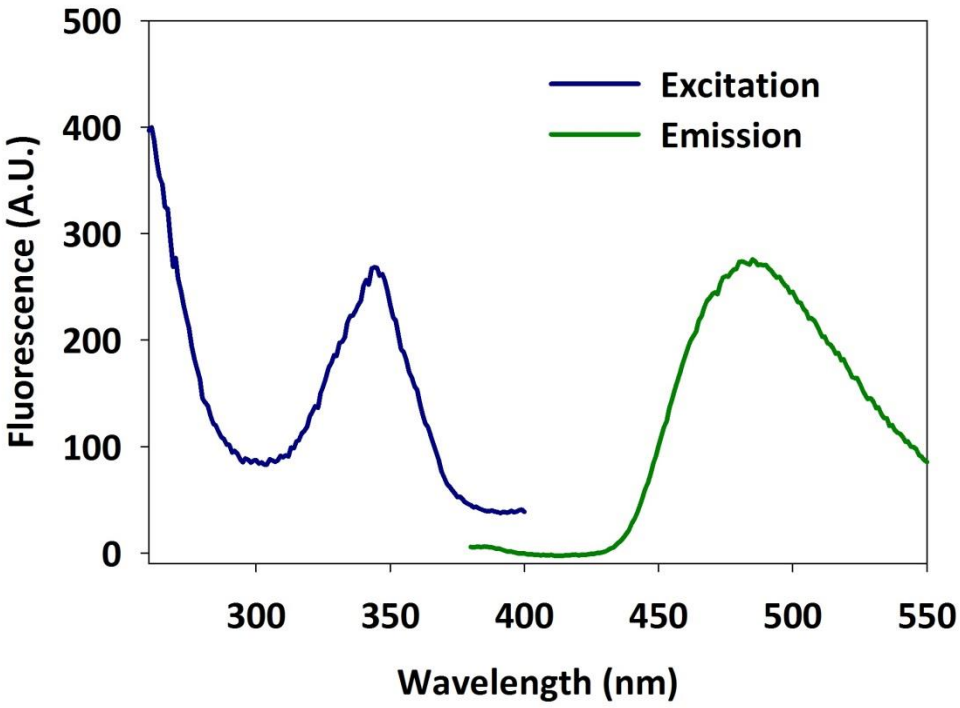
Excitation
Emission
Fluorescence (A.U.)
0
100
200
300
400
500
300
350
400
450
500
550
Wavelength (nm)

Additionally, a derivative of SU-14 containing an UV-activated cross-linking moiety, designated SU-22, also exhibited potent inhibitory and binding properties (Figures 3.4A,B and 3.5A). The added UV-activated cross-linking group was incorporated into SU-14 by replacing the dimethyl amine, previously shown to be critical for 968's action, to give the phenyl azide. Phenyl azides are known to convert to the highly reactive nitrene intermediate upon UV excitation (< 350 nm), which rapidly reacts with any available nucleophile (i.e. primary amines or aliphatic groups) within close proximity. This group is useful for creating proximity-dependent covalent modifications, due to its rapid reaction rates, once the nitrene is formed, and high reactivity towards any available nucleophile within an immediate proximity.

3.3.4 The interactions of the fluorescent photo cross-linking compound SU-22 with GAC *in vitro.*

The new molecule, SU-22, represents an excellent tool compound to investigate 968's mechanism of action. It has potent inhibition and binding properties, and is capable of intrinsic fluorescence and of being covalently cross-linked to GAC, as depicted in Figure 3.6A. The SU-22-conjugated GAC can be visualized by the fluorescence of SU-22, such as under UV illumination following the separation of unreacted SU-22 by SDS-PAGE (Figure 3.6B).

FIGURE 3.6 – Covalent conjugation of a fluorescent 968-analogue prefers the monomeric form of GAC. (**A**) Depiction of the photo-cross-linking of SU-22 to GAC. Upon UV illumination (<350 nm), the phenyl azide reacts with a nucleophile within immediate proximity, resulting in the covalent conjugation of SU-22 to GAC. (**B**) SDS-PAGE of the WT, dimeric (D391K), and monomeric (K316E-D391K-R459E) mutants of GAC, following incubation with increasing concentrations of SU-22 and UV illumination. The labeled enzyme was visualized upon UV illumination.

A

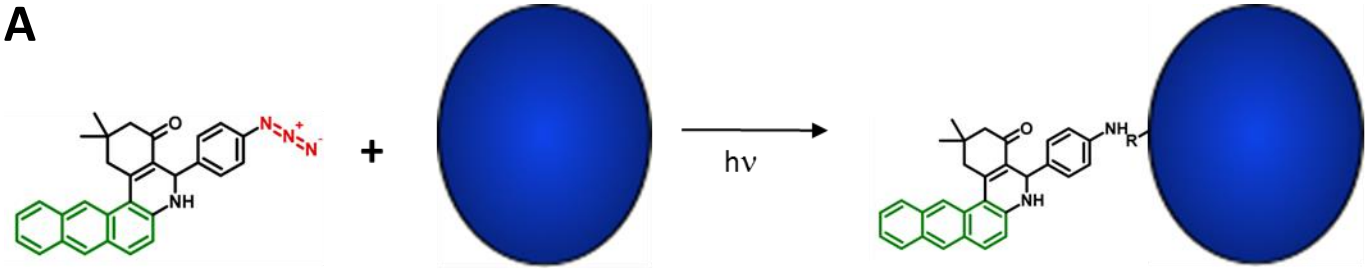
O
NH
+
hν
NH
R
SU-22
GAC subunit
SU-22 conjugated GAC

B

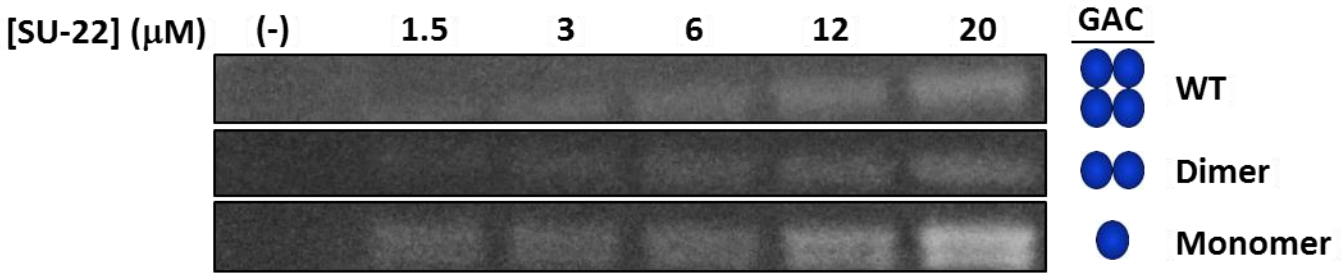
[SU-22] (μM)
(-)
1.5
3
6
12
20
GAC
WT
Dimer
Monomer

To demonstrate the utility of SU-22, we first tested its ability to preferentially bind to the monomeric form of GAC, similar to what was previously observed for the prototype compound 968 (Chapter 2, Section 2.3.3). However, in the previous studies, the real-time binding assay was performed on a fluorescently-labeled GAC (488-GAC) to determine 968's binding affinity for the WT, dimeric, and monomeric forms of GAC, using novel GAC mutants. Here, we used the fluorescence of SU-22, and SDS-PAGE, to perform a similar experiment, monitoring the labeling of WT along with the dimeric and monomeric mutants of GAC with SU-22 (Figure 3.6B). We found that the labeling of WT GAC with SU-22 was indeed dose-dependent and within the concentration range expected by the binding and inhibition assays (1-20 μM). This labeling was slightly improved when the dimeric form of GAC was used. However, the labeling was significantly improved for the monomeric form of GAC. The observation that the monomeric form of GAC exhibited the most robust labeling by SU-22 is consistent with previous results presented in Chapter 2 (section 2.3.3), where 968 was shown to prefer binding the GAC monomer.

The conjugation of GAC with this fluorescent 968-like small molecule, SU-22, offered a new strategy to investigate the effects of 968 binding to GAC; in particular, the purification of a uniformly conjugated GAC species with a 968-like derivative. The motivation for this was to allow further biophysical studies to be performed on a GAC protein with a 968-like molecule covalently bound, such as crystallization trials to obtain an X-ray crystal structure, or mass spectrometry studies to identify the covalently modified residue. We began with the purification of the SU-22 conjugated monomeric GAC mutant (K316E-D391K-R459E), due to its higher affinity for 968

and SU-22. A method was developed whereby the bulk conjugation of SU-22 to an N-terminally $His_{(6x)}$-tagged monomeric GAC and subsequent purification was accomplished using a Co^{2+} affinity column (Figure 3.7A). Here, SU-22 was added to a mixture of purified $His_{(6x)}$-tagged GAC and bovine serum albumin (BSA), which was included to enhance SU-22 solubility and to prevent non-specific binding. Following a preincubation period, the solution was illuminated with UV light and then subjected to a Co^{2+} affinity column to re-purify the $His_{(6x)}$-tagged monomeric GAC from any excess unreacted SU-22 and BSA. As shown in Figure 3.7A, this method resulted in the elution of a highly fluorescent SU-22 GAC adduct (fraction 8, compare top gel visualized under UV excitation to lower gel visualized using total protein stain). The resulting SU-22:monomeric GAC adduct was quantified for labeling stoichiometry using UV absorbance, and found to be 0.7:1 (SU-22:GAC) (Appendix Figure 7.2A). Similarly, this method was then used to purify SU-22 conjugated to WT GAC, and a lower labeling stoichiometry was observed (0.25:1, SU-22:GAC) (Appendix Figure 7.2B). The SU-22:monomeric and SU-22:WT were then assayed for 968 binding and enzyme activity, using methods described in Chapter 2 (Figures 3.7B,C). Both the enzymatic and 968-binding activities were inhibited to the same degree for the SU-22-conjugated GAC when compared to the unconjugated enzyme (Figure 3.7D,E). These results suggest that SU-22 only labels ~50% of the GAC protein. Furthermore, the population of SU-22-labeled GAC is inactive and does not bind 968, as would be expected, presumably due to SU-22 occupying the 968 binding site.

FIGURE 3.7 – Purified SU-22-conjugated GAC both prevents 968 binding and GAC activity. (**A**) SDS-PAGE of selected fractions from the purification protocol of SU-22-conjugated GAC, where SU-22:GAC was identified using UV illumination of the gel (top) and total protein by Coomassie Blue Stain (bottom). The purification of SU-22:GAC was accomplished by first conjugating SU-22 to GAC under UV illumination, followed by His-tag affinity chromatography, where the eluted protein results in robust fluorescence due to the cross-linked SU-22 molecule (fraction 8). (**B**) Purified SU-22:monomeric GAC was labeled with the AlexaFluor-488 probe (as described in Section 2.4.1) and subjected to the real-time 968 binding assay (Section 2.4.3), where a significant inhibition of 968 binding was observed. (**C**) Additionally, SU-22:GAC (WT) was purified by this same method described in (**A**) and assayed for GAC activity, where an inhibition of WT glutaminase activity was observed for SU-22-conjugated GAC when compared to unlabeled GAC. (**D**),(**E**) Inhition of 968 binding to SU-22:monomeric GAC (**D**), and 968 inhibition of glutaminase activity (**E**), was in good agreement with the measured labeling stoichiometry of SU-22 to GAC.

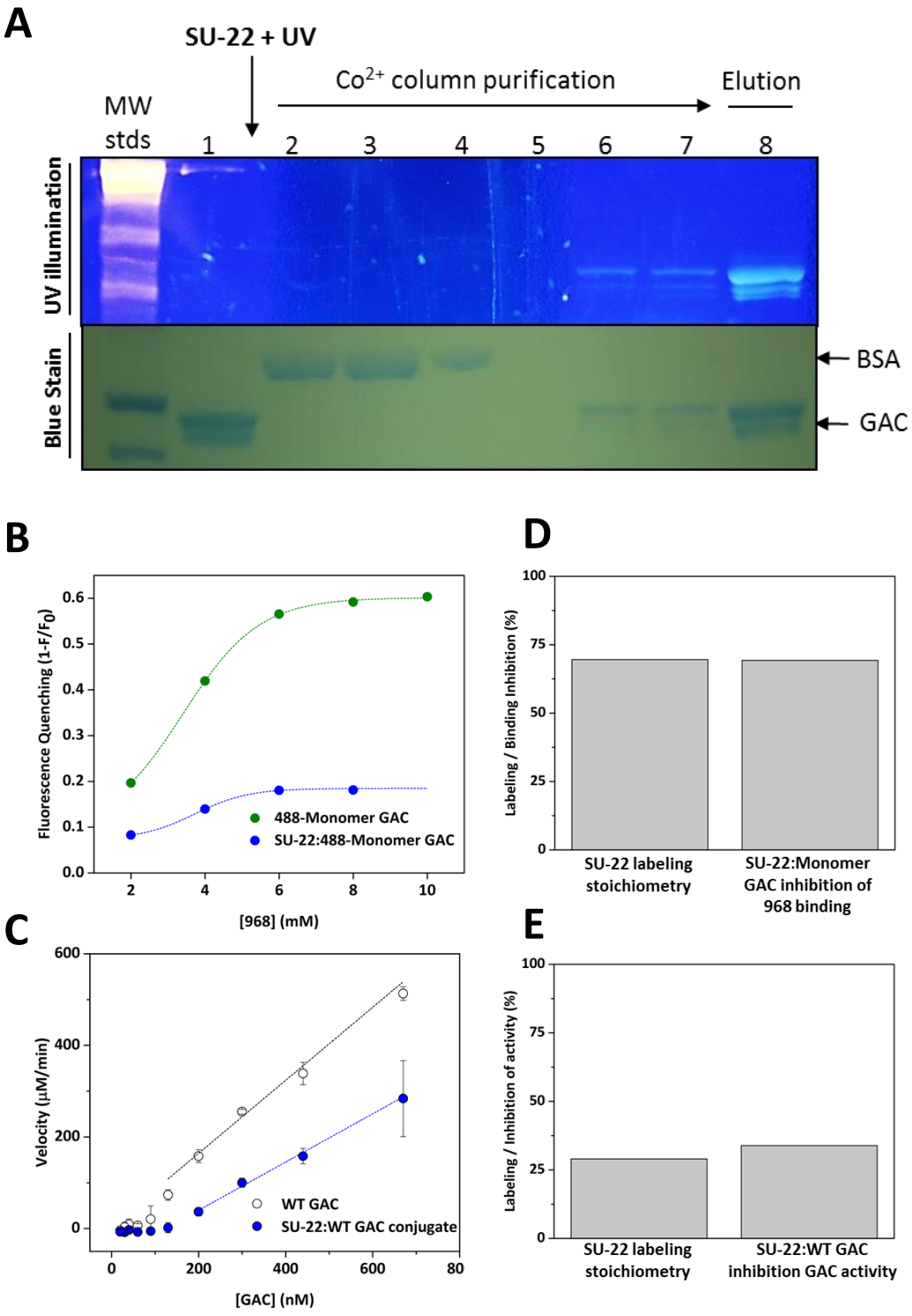
A
SU-22 + UV
Co2+ column purification
Elution
MW stds
1
2
3
4
5
6
7
8
UV illumination
Blue Stain
BSA
GAC
B
Fluorescence Quenching (1-F/F0)
0.0
0.1
0.2
0.3
0.4
0.5
0.6
2
4
6
8
10
[968] (mM)
488-Monomer GAC
SU-22:488-Monomer GAC
C
Velocity (μM/min)
0
200
400
600
0
200
400
600
80
[GAC] (nM)
WT GAC
SU-22:WT GAC conjugate
D
Labeling / Binding Inhibition (%)
0
25
50
75
100
SU-22 labeling stoichiometry
SU-22:Monomer GAC inhibition of 968 binding
E
Labeling / Inhibition of activity (%)
0
25
50
75
100
SU-22 labeling stoichiometry
SU-22:WT GAC inhibition GAC activity

Having the SU-22-conjugated GAC protein in hand, we then sought to study the effects of the conjugation on the oligomerization of GAC. To accomplish this, we used analytical size exclusion chromatography (SEC) to determine the relative size of the SU-22:monomeric GAC adduct and compared it to the unlabeled monomeric and dimeric GAC (Figure 3.8A). The monomeric form of GAC was previously characterized in Chapter 2 above (section 2.3.1), where a uniform monomeric molecular weight species was identified using SEC-MALS; however, the SU-22:monomeric GAC adduct did not follow the same profile. A second peak was eluted before the monomeric peak (i.e. a predicted higher MW species) in the conjugated sample, suggesting that the conjugation of SU-22 to the monomeric form of GAC allowed for another oligomer to form (Figure 3.8A, compare (—) to (···)). When comparing the elution of this second peak to the dimer form of GAC, we found that it had an overlapping elution volume, suggesting this second larger MW species represented a dimeric form of the enzyme (Figure 3.8A, compare (—) to (···)). Both the monomeric and dimeric forms of the conjugated GAC species contained SU-22, as read out by the unique absorbance of the small molecule at 350 nm (Figure 3.8A, compare (—) to (—)). Taking these observations together leads to the model where 968 binds to the monomeric form, perhaps at the interface of two monomers to form a dimer, and then helps to promote dimer formation.

Now, with a purification protocol and efficient labeling strategy, we were poised to try to identify the site of modification. However, as shown in Figure 3.8A, a homogenous solution of monomeric units of GAC becomes a heterogeneous population of monomers and dimers, presenting a significant challenge for

crystallization trials. Of the conditions tested, protein aggregation was a significant problem. We then turned to a proteomics approach, where tryptic peptides were separated on a RP-C18 microbore HPLC column and analyzed using MS/MS at the Mass Spectrometry and Proteomics Resource Core at Harvard University. However, these efforts failed to identify the modification site, most likely due to imperfect parameters for the identification of this novel modification. As an alternative, we analyzed the tryptic fragments of an SU-22:WT GAC adduct on a RP-C18 HPLC column, using UV absorbance as a detector, and identified a single unique peak at 350 nm that was eluted only with high concentrations of acetonitrile in the mobile phase, characteristic of a highly hydrophobic peptide fragment (Figure 3.8B, (—) to (—)). This single peak with 350 nm abosrbance is presumably the SU-22-conjugated peptide fragment, as only SU-22 has an absorbance at that wavelength. Moreover, only one peak was observed with an absorbance of 350 nm, suggesting this modification is site-specific, and not reacting at multiple sites. Furthermore, analysis of partial tryptic peptides of SU-22-conjugated GAC revealed a similar fragmentation pattern as that for 488-labeled GAC (Appendix Figure 3), where the 488-probe was identified within the catalytic domain of GAC (Appendix Figures 1A-E).

FIGURE 3.8 – SU-22 conjugated to a GAC monomer is site-specific and induces the transition to a GAC dimer. (**A**) Analytical size exclusion chromatography profile of a purified sample of SU-22:monomeric GAC contains two distinct peaks for both the absorbance wavelengths of 280 nm (—) and 350 nm (—), where absorbance at 350 nm is unique to the SU-22 molecule. The peak with the later elution volume overlays with the unlabeled GAC monomer (···), whereas the earlier elution volume overlays with the unlabeled GAC dimer (···). (**B**) Peptides obtained from the complete trypsin digestion of purified SU-22:WT GAC were separated by RP-HPLC, using an increasing acetonitrile:H_2O gradient. Both absorbance wavelengths of 254 nm (—) and 350 nm (—) were monitored simultaneously, where the absorbance at 254 nm is characteristic of the eluted peptides, while absorbance at 350 nm is due to the SU-22 molecule (red arrow).

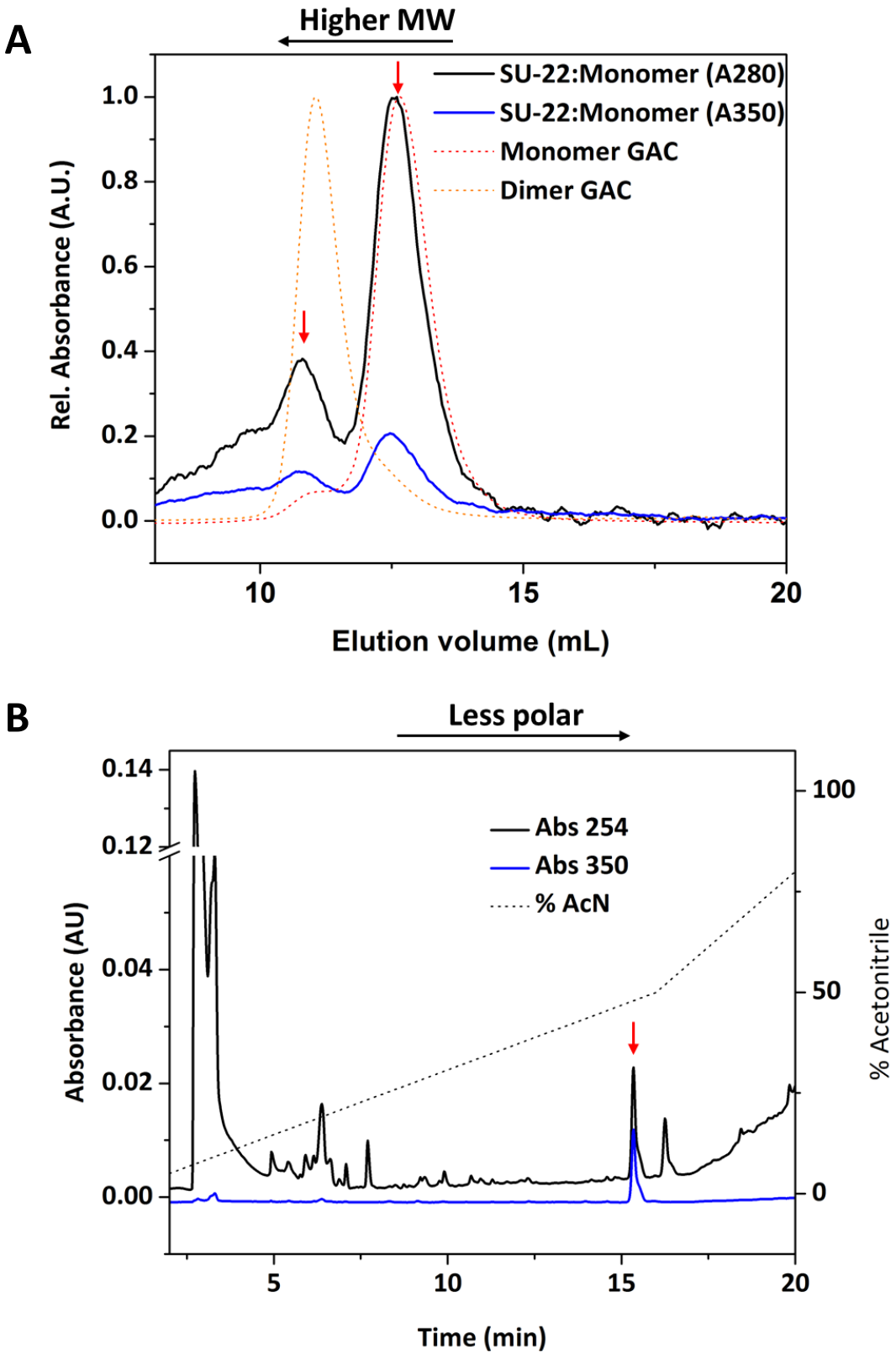
A
Higher MW
SU-22:Monomer (A280)
SU-22:Monomer (A350)
Monomer GAC
Dimer GAC
Rel. Absorbance (A.U.)
1.0
0.8
0.6
0.4
0.2
0.0
10
15
20
Elution volume (mL)
B
Less polar
Abs 254
Abs 350
% AcN
Absorbance (AU)
0.14
0.12
0.04
0.02
0.00
100
50
0
% Acetonitrile
5
10
15
20
Time (min)

3.3.5 Fluorescent photo cross-linking compound SU-22 in transformed cells.

The SU-22 tool compound was found to behave as would be predicted for a 968 analogue; it bound preferentially to the monomeric state of GAC, as well as competitively blocking the binding of 968 and, upon its covalent attachment to GAC, inhibited enzyme activity. We then examined whether SU-22 behaves like 968 in cells. We set out to address this question by first turning to a model cell system, previously used to examine the actions of 968 against oncogenic transformation. The cell system used here was an inducible model, where the oncogenic form of Dbl (for diffuse B-cell lymphoma) is robustly expressed in mouse embryonic fibroblasts (MEFs) upon the removal of the antibiotic doxycycline (Dox), thereby causing normal MEFs to exhibit the transformed characteristics of cancer cells. First, we investigated the effect of SU-22 in a cell saturation density experiment. In this experiment, non-transformed cells grow to confluency and saturate to a uniform monolayer due to cell-cell contact inhibition (Figure 3.9A, left), but cells transformed by onco-Dbl continue to grow through a monolayer due to their oncogene-driven loss of cell-cell contact inhibition. We show that SU-22 behaves like 968 by inhibiting the saturation density of the transformed cells (Figure 3.9A, compare middle to right).

FIGURE 3.9 – Compound SU-22 inhibits Dbl-induced saturation density and labels GAC in cells. (**A**) SU-22 inhibition of cell growth saturation density using mouse embryonic fibroblasts (MEFs) transformed by the induced expression of the oncoprotein Dbl (onco-Dbl). Control cells only grow to a confluent monolayer (left), whereas cells transformed by the induced expression of onco-Dbl overcome cell-cell contact inhibition and grow to a confluent multilayer (middle), which SU-22 potently inhibits (right). (**B**) Cartoon depiction of cell labeling with SU-22. First SU-22 is incubated with cells, and then exposed to UV light, washed, and their mitochondria isolated. (**C**) SDS-PAGE of onco-Dbl-expressing cells labeled with SU-22, following the workflow from (**B**), where 25 μg of protein from the whole-cell lystate (WCL), S200 fraction (cytoplasm and microsomes), and the mitochondrial fraction (mito) was visualized under UV-illumination for fluorescent SU-22:protein adducts (left), followed by immunoblotting for both KGA and GAC (right). GAC/KGA are clearly enriched in mitochondria (right lane), and exhibit an overlapping signal with the fluorescence image (green boxes).

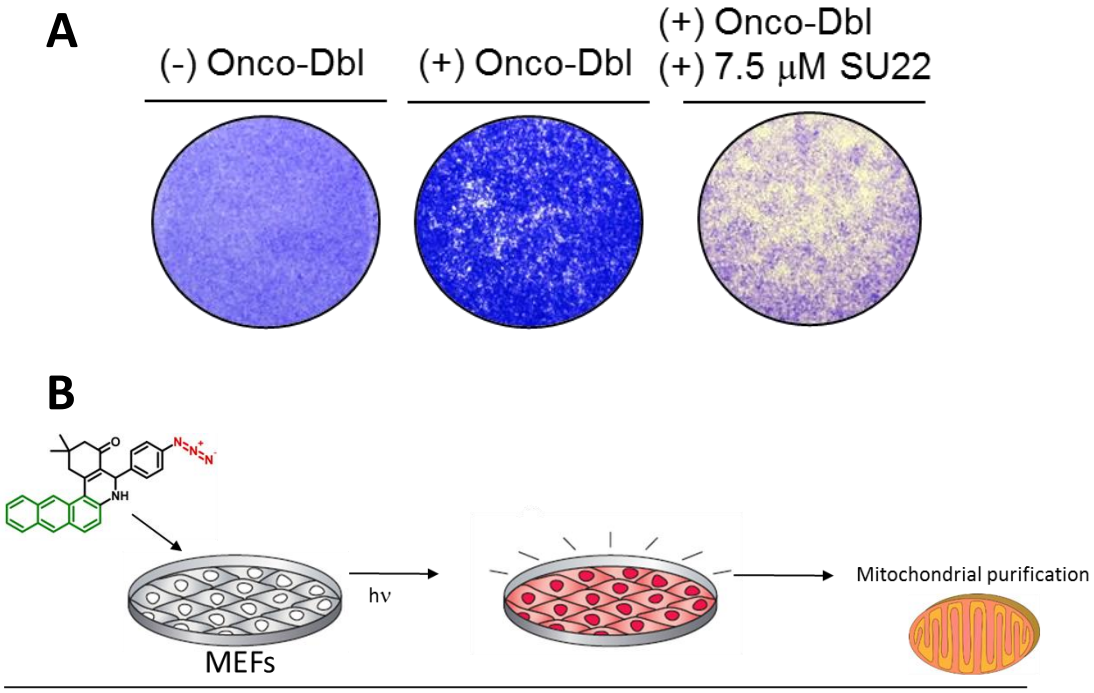

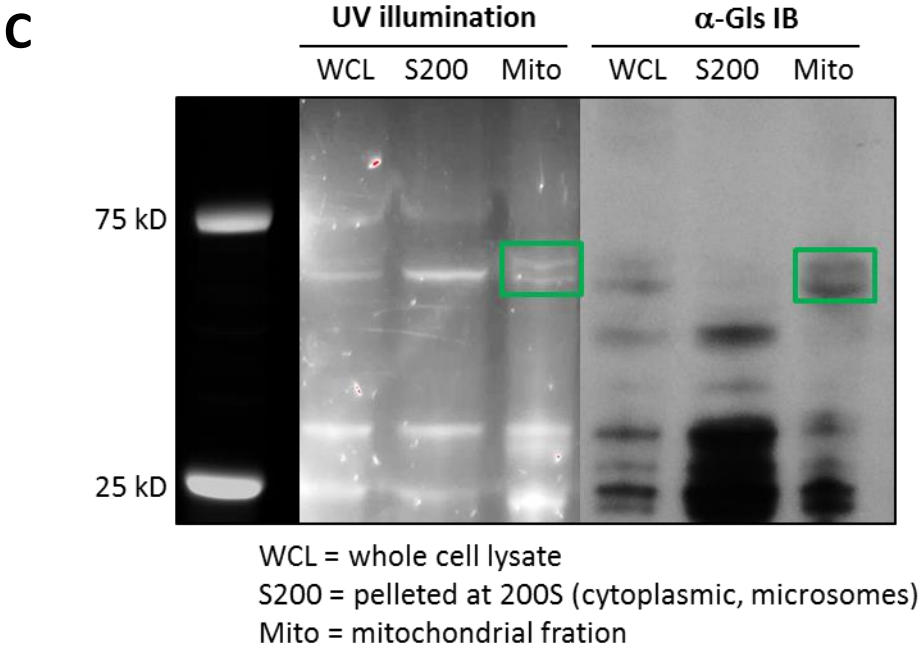

WCL = whole cell lysate
S200 = pelleted at 200S (cytoplasmic, microsomes)
Mito = mitochondrial fration

Having established SU-22 as an inhibitor of the transformed growth phenotype exhibited by Dbl-transformed cells, we sought to develop methods to label these transformed cells to identify SU-22 binding partners *in vivo*. Figure 3.9B depicts this approach, where SU-22 is first incubated with Dbl-induced MEFs to saturate its target in cells, followed by UV illumination to stimulate photo-cross linking, and subcellular purification of mitochondria (i.e. where GAC is localized). Proteins from the whole-cell lysate, cytoplasmic and microsomal, and mitochondrial fractions were separated by SDS-PAGE and analyzed under UV illumination to visualize the fluorescent SU-22:protein adducts, followed by immunoblotting for both KGA and GAC. Interestingly, a relatively small number of proteins were labeled with the photo cross-linking 968 analogue in the whole cell lysate, with a significant labeling in the mitochondrial fraction (Figure 3.9C, compare WCL to Mito). Moreover, the fluorescent bands found within the mitochondrial fraction were also identified using an antibody recognizing GAC/KGA (Figure 3.9C, green box). These data show that the labeling of Dbl-induced cells, which are highly sensitive to treatment with this compound, results in SU-22-labeled protein adducts that are consistent with the mobility of GAC on SDS-PAGE. Furthermore, these results show that the SU-22:protein adducts are indeed localized within the mitochondria, i.e. matching the localization of GAC.

To extend these studies, we analyzed Dbl-transformed cells treated with SU-22, using confocal fluorescence microscopy. As shown in Figure 3.10, Dbl-transformed cells treated with SU-22 and the mitochondrial labeling dye, MitoTracker, demonstrate the subcellular localization of SU-22, with a considerable overlap with

the mitochondrial marker (Figure 3.10, compare top left, middle, and right panels). Additionally, the labeling of SU-22 in cells was shown to be dependent on UV illumination, where cells that were not illuminated to initiate covalent cross-linking showed little detectable fluorescence of the SU-22 compound, when compared to cells that were illuminated (Figure 3.10, compare bottom left two panels to top left two panels). These fluorescence images directly show the SU-22 compound localizing to an intracellular organelle that has an overlapping structure with a mitochondrial marker. These results highlight that this novel 968 analogue indeed localizes to mitochondria, and are consistent with the contention that this small molecule targets the mitochondrial KGA/GAC enzymes.

FIGURE 3.10 – Confocal fluorescence images of cross-linked SU-22 in Dbl-induced cells. Dbl-induced cells were labeled with the fluorescent molecules SU-22 and MitoTracker, by first incubating cells with SU-22, and then cross-linked by UV illumination followed by labeling with MitoTracker to identify mitochondria (top). Cells that were not exposed to UV light to stimulate photo-cross-linking followed the same treatment, however, without exposure to UV light (bottom). Cells were then fixed in 4% para-formaldehyde and 0.1% glutaraldehyde and imaged on an inverted Axio Observer.Z1 microscope using the 405 laser line for excitation of the SU-22 small molecule and 514 laser line to excite the MitoTracker.

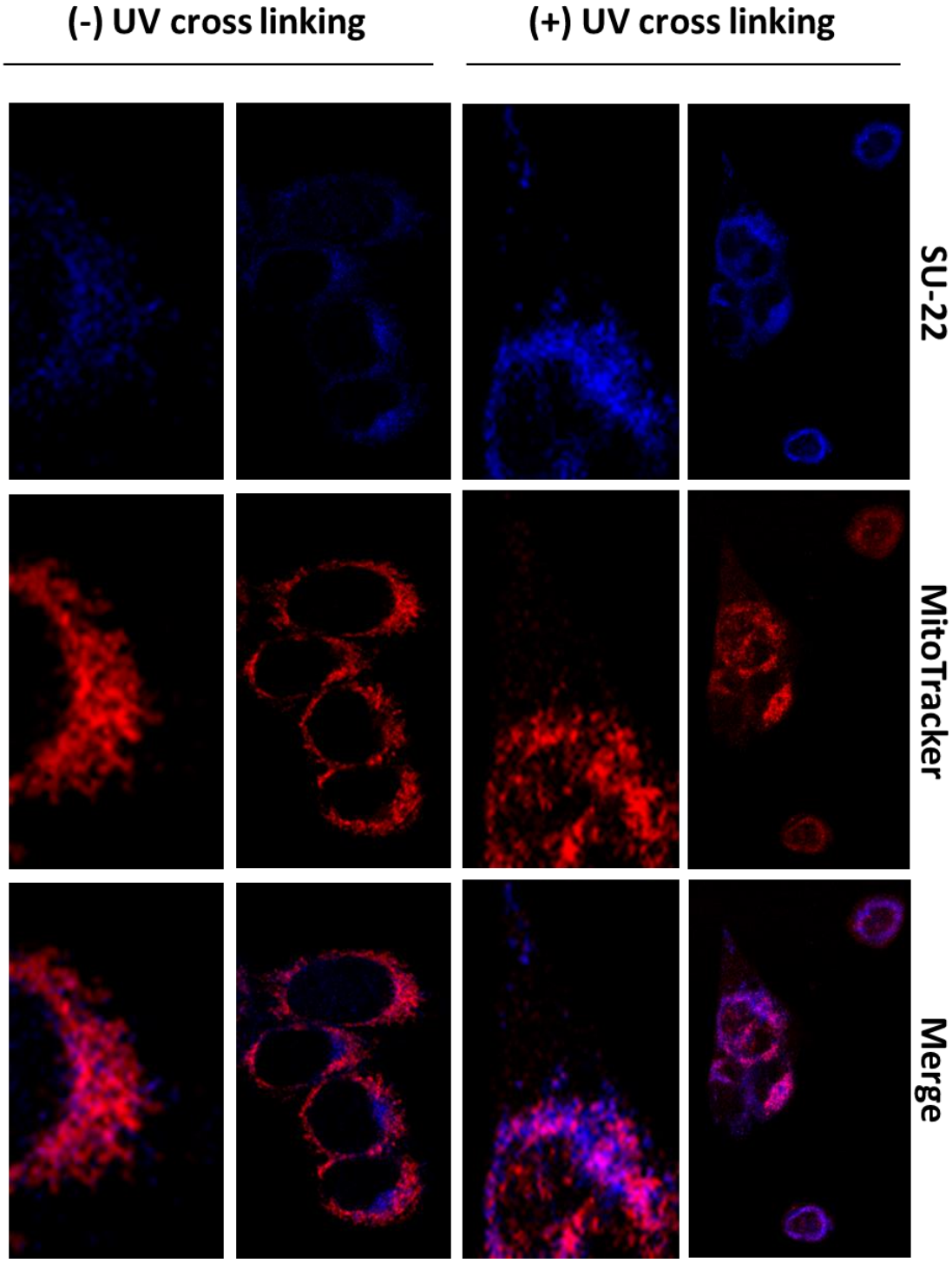
(-) UV cross linking
(+) UV cross linking
SU-22
MitoTracker
Merge

3.4 DISCUSSION

The initial discovery of 968 as a lead compound for the inhibition of the growth and oncogenic properties of cells transformed by hyperactive Rho-GTPases, namely Rho, Rac1, and Cdc42, posed significant questions as to its mechanism of action [10]. The discovery was the result of a high-throughput screen of a Rho-dependent growth phenotype in yeast. The hit compounds found to inhibit the yeast phenotype were then assayed on mammalian cells transformed by hyperactive Rho-GTPases accompanying the expression of the Dbl oncogene. Compounds that were not specific to inhibiting Rho-dependent transformation in mammalian cells were removed from the collection of hit compounds. This top down approach identified the 968 scaffold as a highly potent and specific inhibitor of oncogenic transformation induced by the hyper-activation of the small G-proteins within the Rho family. However, the target of this lead compound, when identified using a mass spectrometry assay of proteins that bound to an immobilized version of the active moiety of 968, surprisingly was not a G-protein, nor any type of conventional signaling protein. The identified target was in fact a metabolic enzyme, GAC, which had no known association with the small G-protein signaling pathways.

The identification of this metabolic enzyme, GAC, as the target of 968 was validated by assaying the glutaminase activity within mitochondria of 968 treated and untreated cells, along with single point enzyme assays of the purified recombinant enzyme. Activity assays of the purified enzyme did not suggest a competitive mode of inhibition, but rather a non-competitive inhibitory mechanism, thus suggesting that 968 was an allosteric inhibitor. Protein docking studies of this small molecule to the

available X-ray crystal structures of GAC revealed a distinct binding pocket within the interface of the GAC dimer (Figure 3.11, orange spheres) [11]. These studies, when combined with a select group of 968 derivatives, demonstrated a viable model for 968 inhibition of GAC activity. However, the lack of a co-crystal X-ray structure of 968 bound to GAC presented significant challenges to further optimize the 968 scaffold, and furthermore, raised the fundamental question as to how binding at such a distal allosteric interface affected GAC activity.

In this study, we were able to first make use of a newly described method of detecting 968-like molecules to directly bind to GAC. These methods, when coupled with read-outs of enzyme activity, allowed a higher through-put effort in optimizing the molecule scaffold. This assay was used to profile new smaller 968-analogues, where SU-29 now represents the lead compound. Furthermore, we successfully designed 968-derivatives to act as tool compounds to investigate the actions of 968 on GAC both *in vitro* and in cells. The prototypic tool compound, SU-22, was found to have properties directly in line with what would be predicted for a 968-derivative. First, we showed that SU-22 interacted preferentially with the monomeric form of GAC, and to a significantly lesser extent to the GAC dimer. Next, we demonstrated the ability of the SU-22, when covalently linked to the GAC monomer, to competitively block the binding of 968. Furthermore, we observed that SU-22 could induce the formation of a GAC dimer. This observation leads to the model presented in Figure 3.11, where 968 binds to the surface of a GAC monomer that interacts with a second monomer to form the dimer.

FIGURE 3.11 – Model of 968 binding to the GAC monomer-monomer interface. Using the previously reported docked structure of 968 to GAC, a model can be proposed whereby a 968 molecule (orange spheres) binds to a hydrophobic pocket of monomeric GAC that enables the binding of another monomer unit to form a dimeric 968-GAC complex.

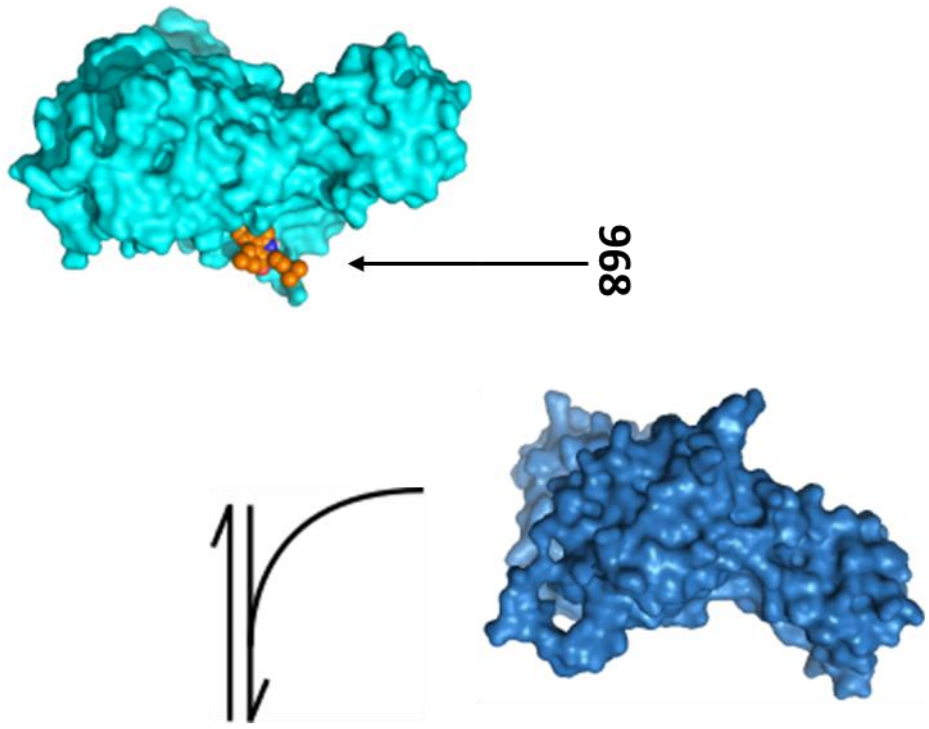
896

When 968 is bound, a second unbound GAC can then favorably interact with the 968-bound GAC monomer to create a 1:2 968:GAC dimer. Finally, we concluded that the purified SU-22 bound to WT GAC was inactive, resulting from SU-22 covalently attached to the 968 binding site. This modification on WT GAC was found to be site specific, through the identification of a unique peptide signal in the HPLC trace of a full trypsin digestion of the SU-22:WT GAC adduct.

Having validated this novel tool compound to behave as would be predicted against the GAC enzyme, we then described its reactivity in cells. Here, we made use of the original cell line that highlighted the inhibitory activity of 968 against transformation. We showed that this new 968 derivative, SU-22, was a potent inhibitor of onco-Dbl induced growth density at saturation, similar to the actions of 968. Importantly, when SU-22 was used to label proteins within live cells, the most significant band identified was within the mitochondrial fraction, a result that establishes this class of molecules as acting specifically within mitochondria. These results were further supported by confocal fluorescence microscopy studies of this SU-22 molecule covalently cross-linked within cells. The fluorescence signal of the SU-22 molecule was localized within subcellular structures that colocalized with mitochondria, consistent with the principle target of the 968-class of compounds being GAC.

These results provide a strong foundation for the building of a more concerted effort to develop 968-like therapeutics. The high-throughput binding and inhibition assay presents a reliable method for the characterization of 968-derivatives. Similarly, the chemical tools presented here have now helped to provide fundamental insights

into how 968 interacts with its target protein, GAC, both *in vitro* and in cells. The use of these 968-derived molecular tools to investigate the binding pocket for 968, and the localization of GAC within a variety of cells, reinforces the view that this small molecule binds to mitochondrial glutaminase *in vivo*.

3.5 REFERENCES

[1] P. S. Ward and C. B. Thompson, "Metabolic Reprogramming: A Cancer Hallmark Even Warburg Did Not Anticipate," *Cancer Cell*, vol. 21, no. 3, pp. 297–308, Mar. 2012.

[2] R. J. DeBerardinis, J. J. Lum, G. Hatzivassiliou, and C. B. Thompson, "The Biology of Cancer: Metabolic Reprogramming Fuels Cell Growth and Proliferation," *Cell Metab.*, vol. 7, no. 1, pp. 11–20, Jan. 2008.

[3] R. J. DeBerardinis and T. Cheng, "Q's next: the diverse functions of glutamine in metabolism, cell biology and cancer," *Oncogene*, vol. 29, no. 3, pp. 313–324, Nov. 2009.

[4] L. Alberghina and D. Gaglio, "Redox control of glutamine utilization in cancer," *Cell Death Dis.*, vol. 5, no. 12, p. e1561, Dec. 2014.

[5] J. Son, C. A. Lyssiotis, H. Ying, X. Wang, S. Hua, M. Ligorio, R. M. Perera, C. R. Ferrone, E. Mullarky, N. Shyh-Chang, Y. Kang, J. B. Fleming, N. Bardeesy, J. M. Asara, M. C. Haigis, R. A. DePinho, L. C. Cantley, and A. C. Kimmelman, "Glutamine supports pancreatic cancer growth through a KRAS-regulated metabolic pathway," *Nature*, vol. 496, no. 7443, pp. 101–105, Apr. 2013.

[6] M. J. Lukey, K. F. Wilson, and R. A. Cerione, "Therapeutic strategies impacting cancer cell glutamine metabolism," *Future Med. Chem.*, vol. 5, no. 14, pp. 1685–1700, Sep. 2013.

[7] A. P. J. van den Heuvel, J. Jing, R. F. Wooster, and K. E. Bachman, "Analysis of glutamine dependency in non-small cell lung cancer," *Cancer Biol. Ther.*, vol. 13, no. 12, pp. 1185–1194, Oct. 2012.

[8] C. Yang, B. Ko, C. T. Hensley, L. Jiang, A. T. Wasti, J. Kim, J. Sudderth, M. A. Calvaruso, L. Lumata, M. Mitsche, J. Rutter, M. E. Merritt, and R. J. DeBerardinis, "Glutamine Oxidation Maintains the TCA Cycle and Cell Survival during Impaired Mitochondrial Pyruvate Transport," *Mol. Cell*, vol. 56, no. 3, pp. 414–424, Nov. 2014.

[9] C. M. Metallo, P. A. Gameiro, E. L. Bell, K. R. Mattaini, J. Yang, K. Hiller, C. M. Jewell, Z. R. Johnson, D. J. Irvine, L. Guarente, J. K. Kelleher, M. G. Vander Heiden, O. Iliopoulos, and G. Stephanopoulos, "Reductive glutamine metabolism by IDH1 mediates lipogenesis under hypoxia," *Nature*, vol. 481, no. 7381, pp. 380–384, Jan. 2012.

[10] J.-B. Wang, J. W. Erickson, R. Fuji, S. Ramachandran, P. Gao, R. Dinavahi, K. F. Wilson, A. L. B. Ambrosio, S. M. G. Dias, C. V. Dang, and R. A. Cerione, "Targeting Mitochondrial Glutaminase Activity Inhibits Oncogenic Transformation," *Cancer Cell*, vol. 18, no. 3, pp. 207–219, Sep. 2010.

[11] W. P. Katt, S. Ramachandran, J. W. Erickson, and R. A. Cerione, "Dibenzophenanthridines as Inhibitors of Glutaminase C and Cancer Cell Proliferation," *Mol. Cancer Ther.*, vol. 11, no. 6, pp. 1269–1278, Jun. 2012.

[12] C. A. Stalnecker, S. M. Ulrich, Y. Li, S. Ramachandran, M. K. McBrayer, R. J. DeBerardinis, R. A. Cerione, and J. W. Erickson, "Mechanism by which a recently discovered allosteric inhibitor blocks glutamine metabolism in transformed cells," *Proc. Natl. Acad. Sci. U. S. A.*, vol. 112, no. 2, pp. 394–399, Jan. 2015.

[13] A. G. Thomas, C. Rojas, C. Tanega, M. Shen, A. Simeonov, M. B. Boxer, D. S. Auld, D. V. Ferraris, T. Tsukamoto, and B. S. Slusher, "Kinetic characterization of ebselen, chelerythrine and apomorphine as glutaminase inhibitors," *Biochem. Biophys. Res. Commun.*, vol. 438, no. 2, pp. 243–248, Aug. 2013.

[14] J. M. Herbert, J. M. Augereau, J. Gleye, and J. P. Maffrand, "Chelerythrine is a potent and specific inhibitor of protein kinase C," *Biochem. Biophys. Res. Commun.*, vol. 172, no. 3, pp. 993–999, Nov. 1990.

[15] T. Tamaoki, H. Nomoto, I. Takahashi, Y. Kato, M. Morimoto, and F. Tomita, "Staurosporine, a potent inhibitor of phospholipidCa++dependent protein kinase," *Biochem. Biophys. Res. Commun.*, vol. 135, no. 2, pp. 397–402, Mar. 1986.

[16] A. E. Eckly-Michel, A. Le Bec, and C. Lugnier, "Chelerythrine, a protein kinase C inhibitor, interacts with cyclic nucleotide phosphodiesterases," *Eur. J. Pharmacol.*, vol. 324, no. 1, pp. 85–88, Apr. 1997.

[17] S. Kumar and A. Acharya, "Chelerythrine induces reactive oxygen species-dependent mitochondrial apoptotic pathway in a murine T cell lymphoma," *Tumor Biol.*, vol. 35, no. 1, pp. 129–140, Jul. 2013.

[18] R. Yu, S. Mandlekar, T.-H. Tan, and A.-N. T. Kong, "Activation of p38 and c-Jun N-terminal Kinase Pathways and Induction of Apoptosis by Chelerythrine Do Not Require Inhibition of Protein Kinase C," *J. Biol. Chem.*, vol. 275, no. 13, pp. 9612–9619, Mar. 2000.

[19] A. Acharya, S. Kumar, P. Deepak, S. Kumar, and P. Gautam, "A benzophenanthridine alkaloid, chelerythrine induces apoptosis in vitro in a Dalton′s lymphoma," *J. Cancer Res. Ther.*, vol. 9, no. 4, p. 693, 2013.

[20] A. Imperiale, F.-M. Moussallieh, F. Sebag, L. Brunaud, A. Barlier, K. Elbayed, P. Bachellier, B. Goichot, K. Pacak, I.-J. Namer, and D. Taïeb, "A New Specific Succinate-Glutamate Metabolomic Hallmark in Sdhx-Related Paragangliomas," *PLOS ONE*, vol. 8, no. 11, p. e80539, Nov. 2013.

[21] M. J. Lukey, K. S. Greene, J. W. Erickson, K. F. Wilson, and R. A. Cerione, "The oncogenic transcription factor c-Jun regulates glutaminase expression and sensitizes cells to glutaminase-targeted therapy," *Nat. Commun.*, vol. 7, p. 11321, Apr. 2016.

[22] A. G. Thomas, C. M. O'Driscoll, J. Bressler, W. E. Kaufmann, C. J. Rojas, and B. S. Slusher, "Small molecule glutaminase inhibitors block glutamate release from stimulated microglia," *Biochem. Biophys. Res. Commun.*, vol. 443, no. 1, pp. 32–36, Jan. 2014.

[23] K. Venkateswarlu, K. Suneel, B. Das, K. N. Reddy, and T. S. Reddy, "Simple Catalyst-Free Regio- and Chemoselective Monobromination of Aromatics Using NBS in Polyethylene Glycol," *Synth. Commun.*, vol. 39, no. 2, pp. 215–219, Dec. 2008.

[24] K. N. Gusak, A. B. Tereshko, and N. G. Kozlov, "Synthesis of Fused Derivatives of 4,7-Phenanthroline by Condensation of 6-Aminoquinoline with Aromatic Aldehydes and Dimedone," *Russ. J. Org. Chem.*, vol. 37, no. 10, pp. 1495–1502, Oct. 2001.

[25] C. Frezza, S. Cipolat, and L. Scorrano, “Organelle isolation: functional mitochondria from mouse liver, muscle and cultured filroblasts,” *Nat. Protoc.*, vol. 2, no. 2, pp. 287–295, Feb. 2007.

CHAPTER FOUR

Conformational changes in the activation loop of mitochondrial glutaminase C: A direct fluorescence read-out that distinguishes the binding of allosteric inhibitors from activators

4.1 INTRODUCTION

As outlined in Chapter 1, the increased reliance of glutamine catabolism by proliferating cancer cells has recently attracted significant attention as a route to developing new therapeutics that target this unique metabolic requirement of transformed cells [1]–[4]. As discussed above, studies of the enzymes that support this aberrant glutamine metabolism have found that the increased expression of a C-terminal splice variant of kidney-type glutaminase (KGA), known as GAC, is the gate-keeper enzyme for this glutamine addiction, making both KGA and GAC attractive therapeutic targets [5], [6]. Recently, clinical investigations have begun that are exploring the impact of therapeutics inhibiting glutamine metabolism, with trials being performed in cancers such as triple-negative breast cancer, multiple myeloma, and acute-lymphoblastic leukemia [7]–[9]. However, the mechanisms by which these best-in-class inhibitors block GAC enzyme activity is still being fully eluciated.

There are three known classes of inhibitors for KGA and GAC. Benzophenanthridines, described in Chapters 2 and 3, act as a non-competitive allosteric inhibitor of GAC, appear to interfere with GAC monomer-monomer interactions [10]–[13]. A second class, analogs of the substrate glutamine, such as diazo-*O*-norleucine (DON), act as competitive inhibitors that bind to the active site of glutaminase to modify the catalytic serine (S291) [14]. The third class, depicted in

Figure 4.1A, consists of a number of bis-thiadiazole derivatives, the prototype being BPTES, recently described to inhibit glutaminase by binding to a flexible loop within the dimer-dimer interface of the GAC tetramer [7], [8], [12], [15], [16]. These compounds are a class of bis-thiadizaole derivatives, with the prototype being BPTES (bis-2-(5 phenylacetamido-1,2,4-thiadiazol-2-yl) ethyl sulfide) (Figure 4.1A). Gross and colleagues (2015) have reported an improved BPTES derivative, CB-839, which is a more potent inhibitor than BPTES, and described its effectiveness against triple negative breast cancer cells [7]. CB-839 efficacy has been examined *in vivo*, and subsequently employed in clinical trials [7]–[9], [17]. Furthermore, medicinal chemistry approaches have identified molecular derivatives that have proven effective *in vitro* and in cancer cells, making this class of GAC inhibitors of great interest [18], [19].

The discovery of BPTES as an inhibitor of glutaminase activity was first reported by Robinson *et al*. (2007) [13]. BPTES was shown not to be a glutamine competitive inhibitor, but rather competed with the allosteric activator, inorganic phosphate, through an ill-defined mechanism. The binding site for BPTES was elucidated through X-ray crystallographic studies of this small molecule bound to the GAC enzyme, and demonstrated its interaction with the flexible loop critical for GAC activation [7], [8], [12], [15], [16]. Indeed, mutations along this loop (^{316}KEPSGLRFNKLF^{327}) can markedly impact enzyme activity. The outcome of these mutations vary from inducing constitutive activation in the absence of phosphate (K325A) [20], to shifting the dose response for phosphate-stimulated activity (F322Y/F327S, K316A) [15], to inhibiting the formation of higher order oligomers

(K316Q) [21]. Therefore, the conformation of this loop, and how small molecules affect its orientation, will provide a more detailed understanding of the fundamental mechanisms underlying the activation of KGA/GAC enzymes.

4.2 METHODS

4.2.1 Protein production

Recombinant GAC was purified as described previously [11]. Briefly, a plasmid encoding the mouse kidney-type glutaminase isoform 2 (GAC, NP_001106854.1) (residues 72-603) was cloned into a pET23a vector containing an N-terminal histidine (His)-tag and thrombin cleavage site. The expressed protein was purified using Co^{2+} affinity beads (Clontech), followed by anion exchange (GE healthcare) and gel filtration chromatography. Purified GAC was stored in a high salt-containing buffer (20 mM Tris-HCl pH 8.5, 500 mM NaCl, 1 mM NaN_3) at -80°C, following snap freezing in liquid N_2 for long term use.

4.2.2 Protein labeling with FRET pairs

Labeling recombinant GAC with small molecule probes was performed by previously described methods [11]. Briefly, 1.5 mg of GAC was first exchanged into 50 mM HEPES, pH 7.2, and 100 mM NaCl (labeling buffer), using a PD10 desalting column (GE healthcare). The enzyme was then incubated with 50 μM (5-fold excess of enzyme) of either AlexaFluor 488 succinimidyl ester or QSY9 succinimidyl ester (Molecular Probes) for 1 h at 4°C. After 1 h, the labeling reaction was quenched with 150 mM Tris-HCl, pH 8.5, and unreacted probe was separated from labeled-enzyme using a PD10 desalting column, eluting labeled-GAC back into the high salt-containing buffer.

4.2.3 Inducible Dbl cell system

Inducible MEFs were generated as described previously [11]. Briefly, the gene encoding oncogenic-Dbl was sub-cloned into the pTRE-HA vector (Clontech). The pTRE-HA-onco-Dbl was then co-transfected with pMET-Puro in a 20:1 ratio into parental MEFs (Clontech), which contained the transcriptional transactivator (tTa), with Lipofectamine (Invitrogen). Cells were placed under puromycin selection at 48 hours post transfection, and colonies were selected after 2-4 weeks for doxycycline-dependent expression of HA-onco-Dbl using HA.11 antibody (Covance). Cells were maintained in DMEM supplemented with 10% (v/v) FBS (clontech) and 100 μg/mL G418 (Gibco). To suppress Dbl expression, 1 μg/mL doxycycline was added to the medium every 2 days. Cells were induced by re-plating in doxycycline-free medium where residual doxycycline was removed by replacing the medium 3 hours after plating.

4.2.4 Inducible MEF saturation density analysis

DMEM medium supplemented with 10% FBS with or without 1 $\mu g\,ml^{-1}$ doxycycline was added to 6-well plates (2 ml per well), and then seeded with 1×10^5 MEFs per dish. Following cell attachment (4 h), growth medium was replaced with DMEM supplemented with 5% FBS. Following an overnight incubation (~16 hrs) medium was replaced again with DMEM supplemented with 5% FBS containing the appropriate drug concentrations where appropriate. Growth medium was subsequently replaced at 48 h intervals. At day 8, growth medium was removed and 1.5 ml 3.7% formaldehyde solution in H_2O was added for 30 min. The formaldehyde solution was removed, and 1.5 ml crystal violet solution was added for 20 min at room temperature.

This was then removed, the dishes washed with H_2O, and allowed to dry before imaging.

4.2.5 SEC-MALS analysis

Purified GAC and GAC mutants were subjected to multi-angle light scattering (MALS) as previously described by Moller et al. (2013) [22]. Briefly, 50 μL samples of 5 mg/mL GAC, with or without 30 min preincubation with 100 μM BPTES, were injected onto a BioSep-SEC-S4000 size-exclusion column (Wyatt technology), coupled to a static 18-angle light scattering detector (DAWN HELEOS-II) and a refractive index detector (OptiLab T-rEX, Wyatt Technology), at 23°C. The size-exclusion column was equilibrated with 20 mM Tris-HCl, pH 8.5, and 200 mM NaCl, and when approprite 50 mM K_2HPO_4 or K_2SO_4. The flow rate was kept at 1 mL/min. RMS radius and mass distribution (polydispersity) were analyzed using the ASTRA software, with monomeric BSA (Sigma) serving to normalize the light scattering signal.

4.2.6 End-point glutaminase assays

Activity assays used to evaluate the activity of GAC mutants and inhibition by BPTES and CB-839 followed a two-step protocol adapted from Robinson et al. (2007) (17). Briefly, for phosphate activity profiles, 20 μL of 20 mM glutamine, 50 mM Tris-acetate, pH 8.5, and 0.1 mM EDTA, containing the appropriate concentration of K_2HPO_4 or K_2SO_4, was added to a UV-transparent Costar 96-well plate (Corning). For inhibition assays, drugs dissolved in DMSO were added to give the appropriate concentration to 20 μL of 20 mM glutamine, 50 mM Tris-acetate, pH 8.5, 0.1 mM EDTA, and 50 mM K_2HPO_4. To initiate the reaction, 5 μL of a solution of the

appropriate concentration of GAC to give 50 or 100 nM, in 20 mM Tris-HCl, pH 8.5, 100 mM NaCl, and 1 mM NaN_3, was added to the glutamine solution and incubated at 23°C for 2 min before the reaction was quenched using 2.5 μL of 3 M HCl. The second step was initiated by the addition of 200 μL of 12 units/μL GDH, 2 mM NAD+, 100 mM hydrazine (Sigma), and 100 mM Tris-HCl, pH 9.2, on top of the first quenched reaction and incubated for 45 min at 23°C before reading NADH absorbance. Glutamate produced by the first reaction was determined from the amount of NADH generated in the second reaction by using the extinction coefficient for NADH (6,220 M-1 cm-1).

4.2.7 Fluorescence experiments

Fluorescence experiments were performed using a Varian Cary Eclipse Fluorometer in the counting mode. Experiments were all performed using 1-mL samples with continuous stirring at 20°C in 50 mM Tris-Acetate, pH 8.5, 0.1 mM ethylenediamine tetraacetic acid (EDTA). For FRET assays, 75 nM QSY9-labeled GAC was added to 25 nM 488-labeled GAC while monitoring fluorescence emission at 520 nm, exciting at 490 nm. After equilibration for 10 min, either 100 mM K_2HPO_4 or K_2SO_4, 500 nM BPTES or CB-839 was added and equilibrated for 5 min. Finally, 1 μM unlabeled WT GAC was added. For tryptophan emission scans, excitation and emission wavelengths were 285 and 310-390 nm, respectively. For kinetics experiments, excitation and emission wavelengths were 285 and 340, respectively. For drug titrations, BPTES and CB-839 at appropriate concentrations were added to 100 nM F327W-GAC to give less than 0.5% DMSO. Points for the dose-dependent quenching were taken from the equilibrated kinetics curve and fit to a bimolecular ligand binding equation after

correcting for fractional saturation, using the relation of free and unbound enzyme/drug complex (i.e. $f_{bound} + f_{free} = 1$, where $f_{bound} = F/F_{max}$). Similarly, 1 μM BPTES was added to 100 nM D391K-F327W. For allosteric activator titrations, 75 mM K_2HPO_4 was injected into increasing concentrations of F327W-GAC. Likewise, 100 mM of K_2HPO_4 or K_2SO_4 was added to 500 nM F327W-GAC. For titrations, the appropriate concentration of K_2HPO_4 or K_2SO_4 was added to 500 nM F327W-GAC. Points for the titration curves were taken from the equilibrated portion of the kinetic curves.

4.3 RESULTS

4.3.1 Comparison of the effects of allosteric activators and BPTES-class inhibitors on GAC.

Previous work by our laboratory and others have demonstrated the requirement for both KGA and GAC to form homo-tetramers in order to become activated [11], [13], [14], [23], [22]. As described in Chapter 2 (section 2.3.2) above, using the developed FRET assay that detects GAC's ability to form tetramers, the effect allosteric activators and inhibitors have on tetramer formation can be monitored in real-time. Using this assay, we observed an increase in the degree of FRET by the addition of the allosteric activators, inorganic phosphate and sulfate (Figure 4.1B). The phosphate/sulfate-bound tetramers were found to be readily reversible upon the addition of excess unlabeled GAC subunits, which competes with the GAC FRET pairs, effectively decreasing the observed FRET signal. Similarly, the addition of the allosteric inhibitors, BPTES and CB-839, to GAC FRET pairs increased the FRET read-out, reflecting the rapid formation of tetramers upon inhibitor binding (Figure 4.1C). However, in the presence of either BPTES or CB-839, tetramers were resistant to dissociation following the addition of excess unlabeled GAC subunits, demonstrating the formation of stable inhibitor-bound GAC tetramers. Under the same conditions, in the absence of BPTES or CB-839, addition of excess unlabeled GAC results in the exchange of dimers and the effective dilution of donor-acceptor FRET pairs (Figure 4.1C; compare DMSO (—) vs. CB-839 (—) and BPTES (—) curves).

FIGURE 4.1 – Both allosteric activators and BPTES-class inhibitors induce GAC tetramer formation. (**A**) The anionic allosteric activators, inorganic phosphate and sulfate, and inhibitors, BPTES and CB-839. (**B**),(**C**) FRET assay where the FRET signal of 25 nM 488-labeled GAC fluorescence (i.e. FRET donor) is stimulated by the addition of 75 nM QSY9-GAC (i.e. FRET acceptor), representing the formation of tetramers. Addition of 100 mM of the anionic activators, inorganic phosphate (—) or sulfate (—) (**B**), or 500 nM of either BPTES (—) or CB-839 (—) (**C**), rapidly increases the FRET signal, characteristic of the formation of GAC tetramers. The increase in FRET is not readily reversible by the addition of a 10-fold excess of unlabeled GAC subunits when compared to DMSO control (—), therefore representing the formation of a stable drug-induced tetramer, but is readily reversible in the presence of activators. (**D**) Scheme illustrating the oligomer transitions from a GAC dimer to tetramer, where the tetramer species is depicted giving rise to the FRET signal and being the active species. Allosteric activators inorganic phosphate and sulfate are depicted at the dimer to tetramer transition to emphasize their ability to activate GAC, whereas inhibitors BPTES and CB-839 bind to the FRET pairs at the dimer-dimer interface forming a stable BPTES-bound inactive tetramer (BPTES shown in green spheres).

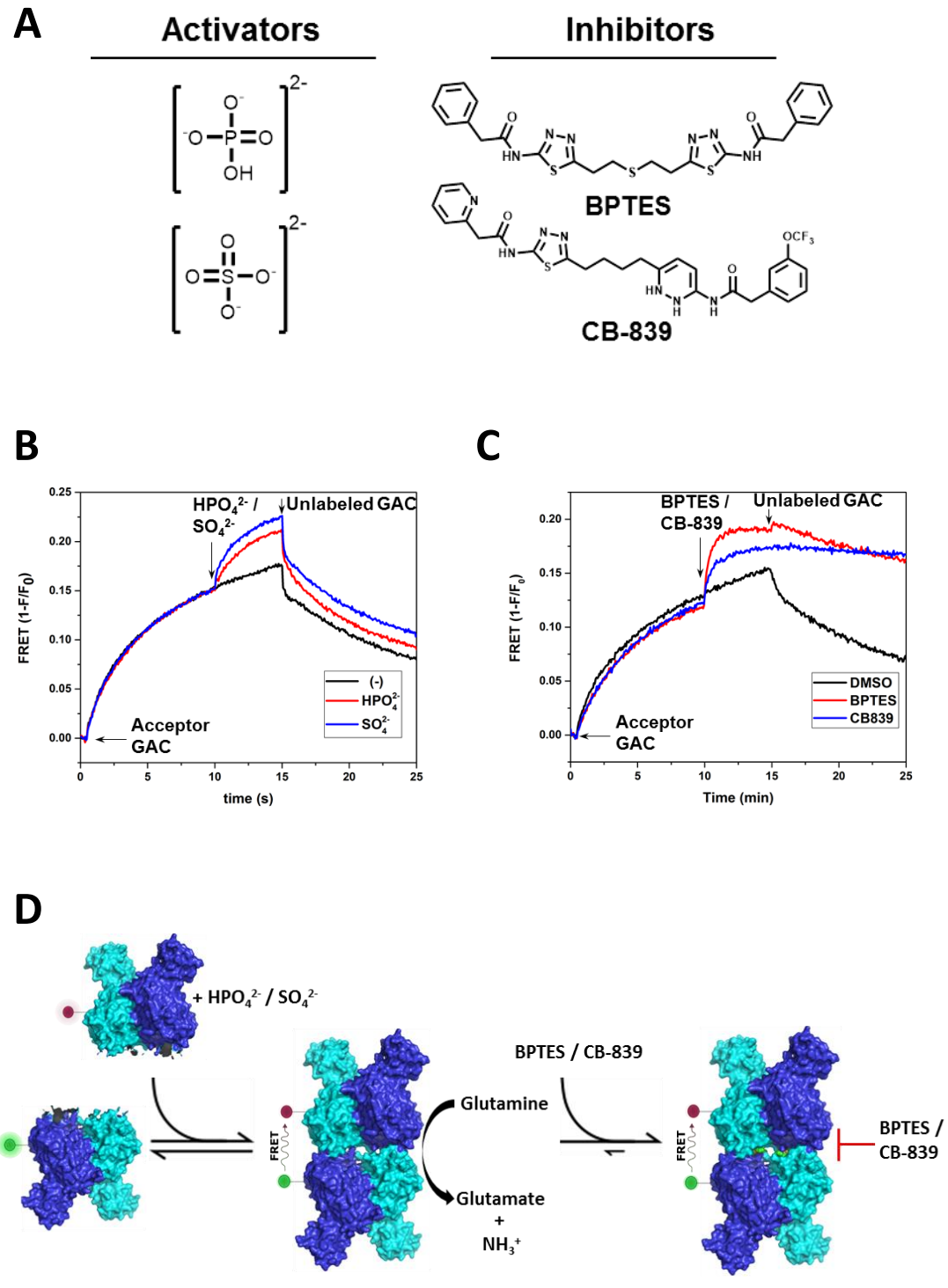
A
Activators
Inhibitors
BPTES
CB-839
B
C
HPO4 2- / SO4 2-
Unlabeled GAC
Acceptor GAC
(-)
HPO4 2-
SO4 2-
FRET (1-F/F0)
time (s)
BPTES / CB-839
DMSO
BPTES
CB839
Time (min)
D
+ HPO4 2- / SO4 2-
FRET
Glutamine
Glutamate + NH3+
BPTES / CB-839

The tetramer formation that underlies the FRET changes and the stabilization provided by anions that potentiate glutaminase activity (i.e. SO_4^{2-} and HPO_4^{2-}) or inhibitors which enhance the formation and stability of tetramers (i.e. BPTES and CB-839) are summarized schematically in Figure 4.1D.

We also compared the ability of BPTES and CB-839 to inhibit recombinant GAC activity, by monitoring the NADH fluorescence that accumulates as a result of a coupled real-time enzyme assay [11]. Figure 4.2A shows a direct comparison of inhibition by BPTES and CB-839 following initiation of the reaction by glutamine, but prior to the addition of the activator HPO_4^{2-} (i.e. basal activity). Consistent with the ability of CB-839 to increase the stability of GAC FRET pairs, when compared to BPTES (Figure 4.1B; compare (—) to (—)), GAC treated with CB-839 was more resistant to phosphate activation (Figure 4.2A; compare BPTES (—) and CB-839 (—) traces). The relative phosphate stimulated activity is shown in Figure 4.2B, where an initial rate analysis reveals a persistent inhibition of CB-839 in the presence of excess phosphate.

Previous studies have established the efficacy of the dibenzophenanthridine-class of glutaminase inhibitors to reverse cell transformation induced by oncogenic Dbl, a guanine nucleotide exchange factor for Rho-GTPases [10], [11]. Activation of the Rho-GTPases, through the tetracycline dependent expression of the oncogenic form of Dbl, has been shown to stimulate glutaminolysis that is required for transformation [10], [11], [24]. Despite the differences between BPTES and CB-839 inhibition *in vitro*, both compounds were found to inhibit the proliferation of MEFs driven by the induced expression of onco-Dbl at similar potencies (Figure 4.3).

FIGURE 4.2 – CB-839, but not BPTES, potently inhibits phosphate stimulated GAC activity. (**A**) Real-time NADH activity assay of GAC activity, where the evolution of NADH that results from the coupled reaction in which GAC catalyzes glutamate production and GDH catalyzes the conversion of glutamate to α-ketoglutarate (and NAD^+ to NADH). Basal activity of 10 nM GAC was first measured upon the addition of 20 mM glutamine, followed by treatment with 1 μM BPTES (—), CB-839 (—), or the vehicle DMSO (—), and finally the addition of 100 mM HPO_4^{2-} (P_i) (**B**) Relative rate analysis was performed on the inhibition of phosphate-stimulated GAC activity from (**A**) and normalized to the DMSO control. Error bars represent the S.D. of three independent experiments.

A

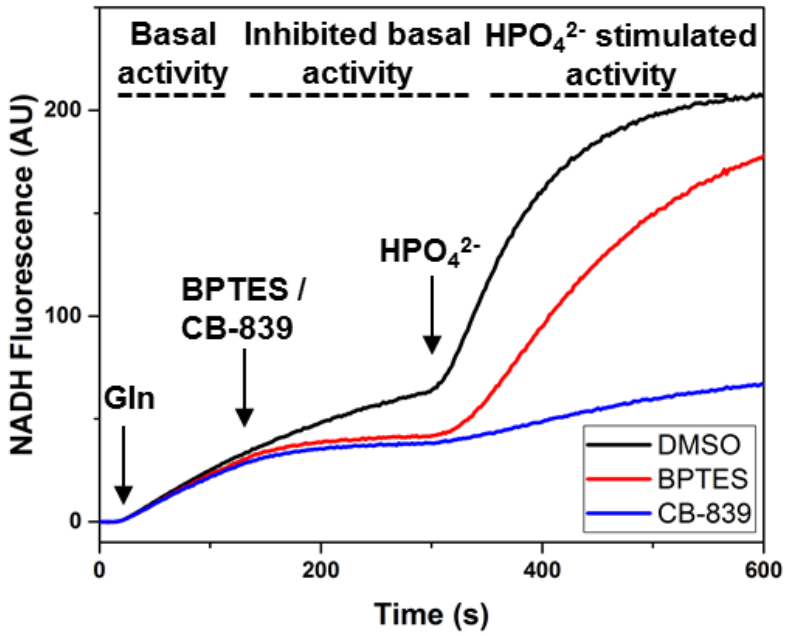
Basal activity
Inhibited basal activity
HPO_4^{2-} stimulated activity
NADH Fluorescence (AU)
200
100
0
Gln
BPTES / CB-839
HPO_4^{2-}
DMSO
BPTES
CB-839
0
200
400
600
Time (s)

B

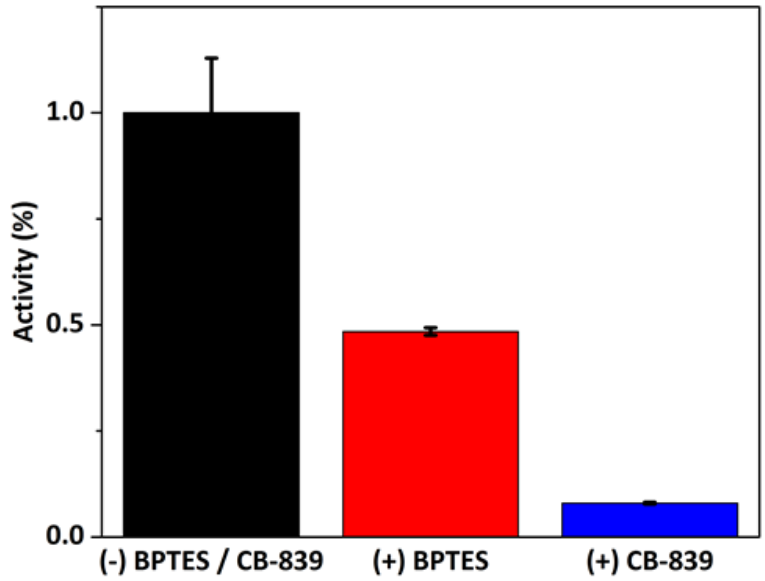
Activity (%)
1.0
0.5
0.0
(-) BPTES / CB-839
(+) BPTES
(+) CB-839

Taking these observations of the inhibitory properties of the BPTES-class of molecules towards glutaminases, as well as an established link between the degree of cellular glutaminase activity and glutamine dependence in cancer cells, the mechanistic detail of how either compound affects the activity of GAC/KGA is still not well defined. Of particular interest is how these small molecules interact with the activation loop within the dimer-dimer interface where BPTES binds. Here, we set out to engineer a fluorescence reporter group within the flexible activation loop in order to monitor its movements in response to allosteric inhibitors and activators.

4.3.2 Examination of the BPTES binding site on GAC.

With respect to their ability to drive tetramer formation, both inhibitors and activators result in similar FRET increases yet result in opposite outcomes for enzyme activity. In order to examine this at a structural level, we compared the available X-ray crystal structures for KGA and GAC in order to better understand the allosteric control of their enzymatic activity. Currently, there are 16 high resolution X-ray crystal structures for either GAC or KGA. It is important to note that KGA and GAC have identical sequences and differ only in their C-termini, which are unresolved in all X-ray crystal structures. Upon analysis of each structure, only six of these provide sufficient electron density of the activation loop (comprising residues ^{320}GLRFNKL^{326}) to resolve atomic positions unambiguously [12], [15], [16]. Of the six structures with a resolved activation loop, four are co-crystal structures with BPTES (3VOZ, 3VP1, 3UO9, 4JKT), one is a co-crystal structure with the active site inhibitor DON (4O7D), and the other is without either BPTES or DON but includes two inorganic anions of sulfate per KGA monomer (3VOY).

FIGURE 4.3 – Both CB-839 and BPTES inhibit Dbl-induced growth at saturation density. Inhibition of cell-cell contact-independent growth assays of Dbl-transformed cells. MEFs were induced to express onco-Dbl upon removal of the antibiotic doxycycline (dox), and then treated with increasing concentrations of BPTES and CB-839. Cells were plated at $1x10^5$ density and grown for 6 days in DMEM supplemented with 5% FBS, with or without dox, fixed and stained with crystal violet.

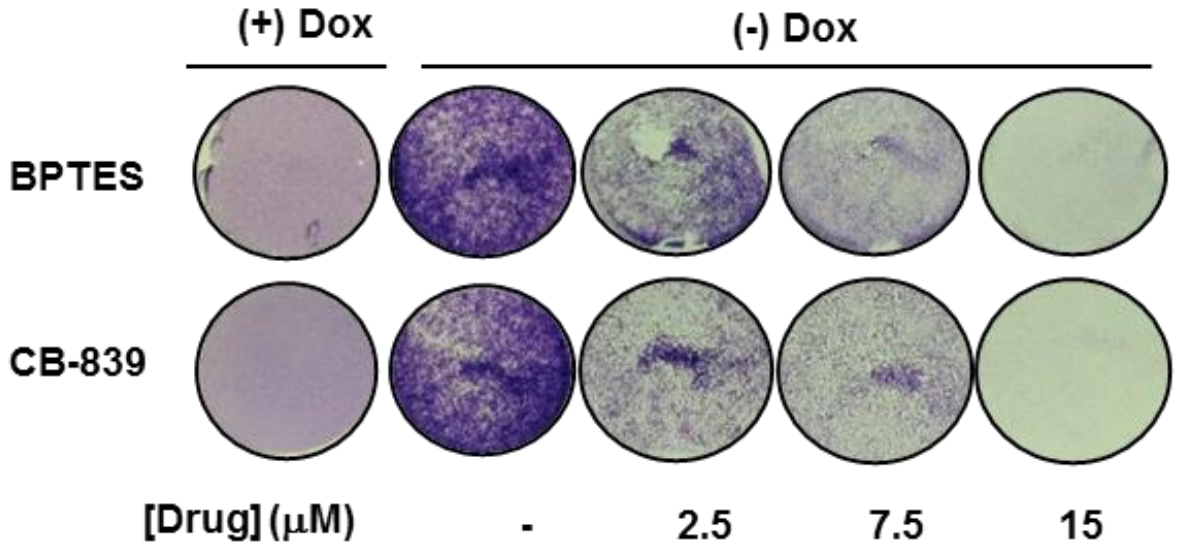
(+) Dox
(-) Dox
BPTES
CB-839
[Drug] (μM)
-
2.5
7.5
15

Interestingly, in the activator/KGA complex, one sulfate is bound proximal to the activation loop resolved in 3VOY through interactions formed directly with tyrosine 399 and lysine 403, and represents the probable binding site for allosteric activators.

We also noted significant differences when comparing the two apo-structures that have sufficient resolution of the activation loop, but without BPTES (4O7D, 3VOY), to all other BPTES-bound glutaminase structures. To illustrate this, Figure 4.4A presents a space filling model of a DON-bound GAC tetramer (4O7D), which has been aligned with the BPTES/SO_4^{2-}-bound GAC structure (3VOZ), to show the BPTES and SO_4^{2-} binding sites. The marked changes in the orientation of the activation loop are illustrated in Figure 4.4B, with the loop in the DON-bound GAC (cyan) being significantly displaced relative to its position in the BPTES-bound GAC structure (magenta). The displacement of the activation loop represents the extremes of the observed conformational states in X-ray crystal structures to date, where the loop assumes a variety of conformations. We reasoned that we might be able to observe this conformational transition in real time by replacing a wild-type residue with the environmentally sensitive amino acid tryptophan. With this in mind, three residues were selected for tryptophan substitution, F323, F327, and Y399. F323 and F327 are significantly displaced in the BPTES-bound structures (Figure 4.4B, the movement of F327 is shown with a red arrow), and Y399 is directly adjacent to the thiadiazole ring of BPTES. These residues have previously been shown to be critical for the activation of the enzyme, as well as for the inhibition of catalytic activity by BPTES [20], [21].

FIGURE 4.4 – Comparison of BPTES-bound and unbound GAC structures. (**A**) Surface representation of the crystal structure of the GAC tetramer bound with ligands DON (4O7D), BPTES, and sulfate (aligned from 3VOZ), where BPTES and sulfate bind proximal to the activation loop and DON binds within the active site. (**B**) Zoomed in region of the aligned DON-bound (cyan) and BPTES/SO_4^{2-} bound (magenta) GAC structures depicting the marked reorientation of the activation loop. The ~180° rotation of the F327 residue with and without BPTES are highlighted (red arrow).

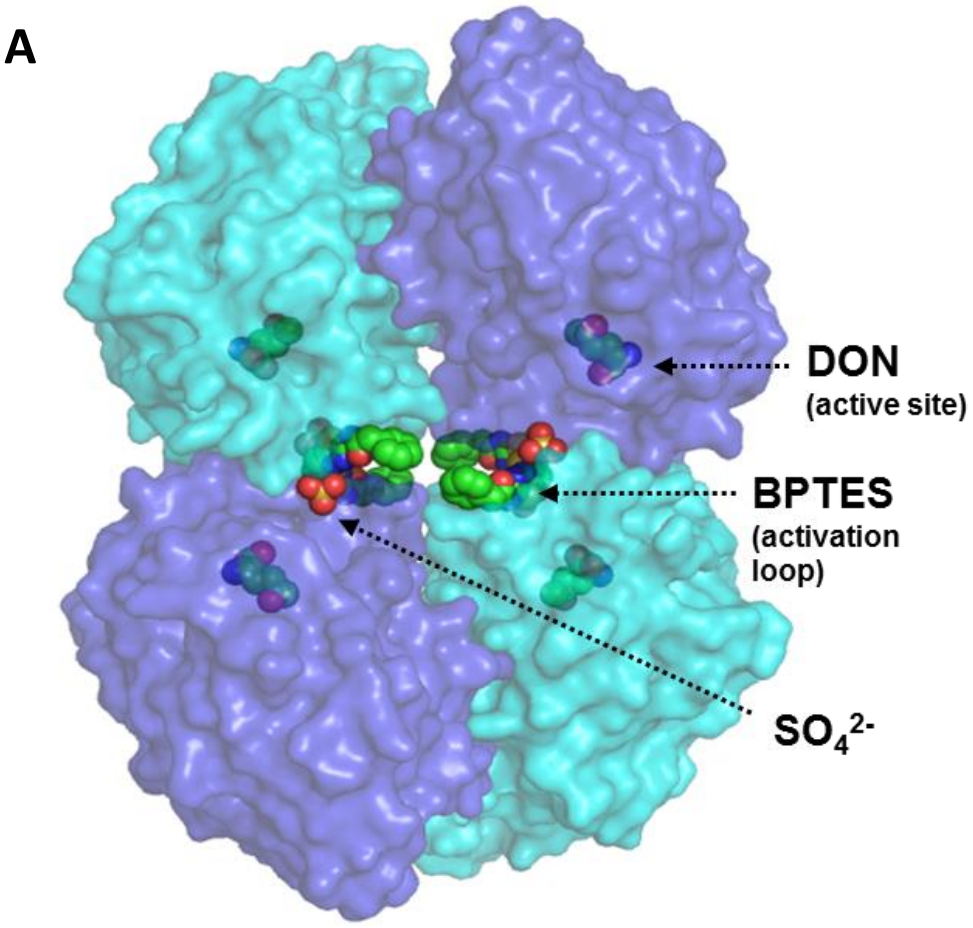
A
DON
(active site)
BPTES
(activation
loop)
SO_4^{2-}

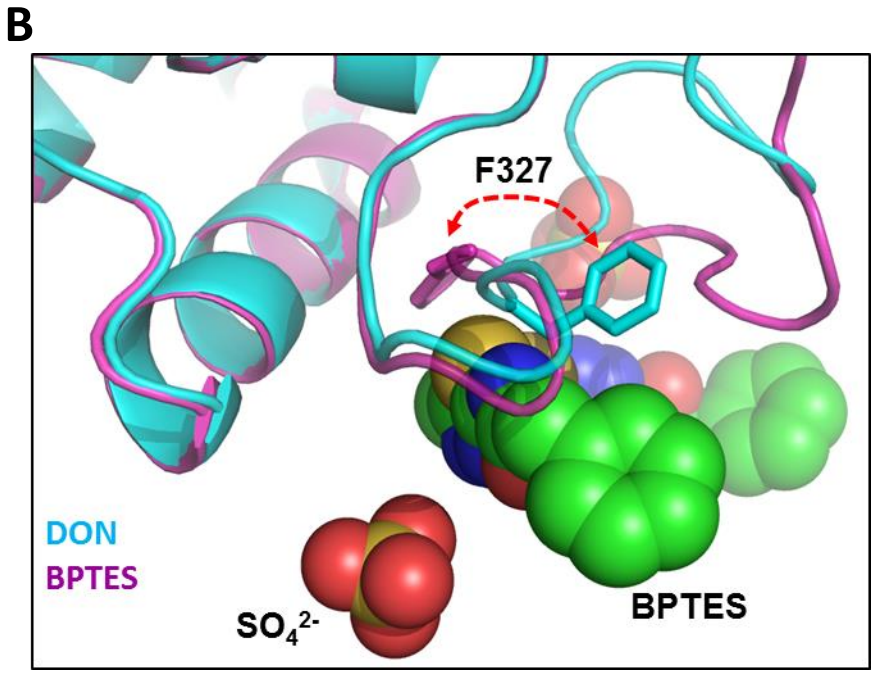
B
F327
DON
BPTES
SO_4^{2-}
BPTES

4.3.3 The F327W mutation is sensitive to inhibitor binding and provides a direct read-out for BPTES and CB-839

Upon substitution of these three residues to tryptophan, we analyzed their fluorescence (excitation = 285 nm, emission = 310-390 nm) before and after the addition of BPTES. Of the positions selected for mutagenesis, we found that substituting tryptophan for phenylalanine at position 327 resulted in a marked quenching of the tryptophan fluorescence upon BPTES addition (Figure 4.5B, compare (—) to (—)). However, no changes in fluorescence emission were observed in wild-type GAC (Figure 4.5B) or the F323W or Y399W mutants in the presence of BPTES (not shown). We then determined the molecular weight profiles of WT GAC, and the individual tryptophan mutants, in both the absence and presence of BPTES, using multi-angle light scattering downstream of size exclusion chromatography (SEC-MALS). A significant shift in the molecular weight distribution for the F327W mutant and WT GAC was observed, but not for F323W or Y399W, following pre-incubation with BPTES (Figures 4.5C-D; solid lines represent elution of GAC, broken lines represent the calculated molecular weight). This trend of an increase in the molecular weight distribution from a GAC dimer to a tetramer, following pre-incubation with BPTES, observed for the F327W mutant, further verifies the ability of the F327W mutant to bind and respond to BPTES. Additionally, the F327W mutant retained a WT activity profile, with a V_{max} and $K_{1/2}$ for phosphate activation closely matching that of WT GAC (Figure 4.5E).

FIGURE 4.5 – F327W detects BPTES binding while retaining WT properties. (**A**) Tryptophan fluorescence spectrum of both WT GAC and (**B**) the F327W mutant, before (—) and after (—) addition of 1 μM BPTES, shows no change for WT GAC but a significant quenching for the F327W mutant. (**C**) SEC-MALS elution profile (solid lines) and molecular weight distribution (broken lines) of a 5 mg/mL sample of WT GAC and F327W (**D**) before ((—), (---)) and after ((—), (···)) pre-incubation with 50 μM BPTES. A significant shift from a heterogeneous population of dimers and tetramers, to a more homogenous population of tetramers, is observed following pre-incubation with BPTES. (**E**) The F327W mutant (●) retains its catalytic properties when compared to WT GAC (○), with an observed $K_{1/2}$ of 15.0 ± 1.7 mMol/L and a V_{max} value of 435 ± 19 μMol/min, versus a $K_{1/2}$ of 16.4 ± 0.4 mMol/L and a V_{max} value of 453 ± 8 μMol/min for WT GAC.

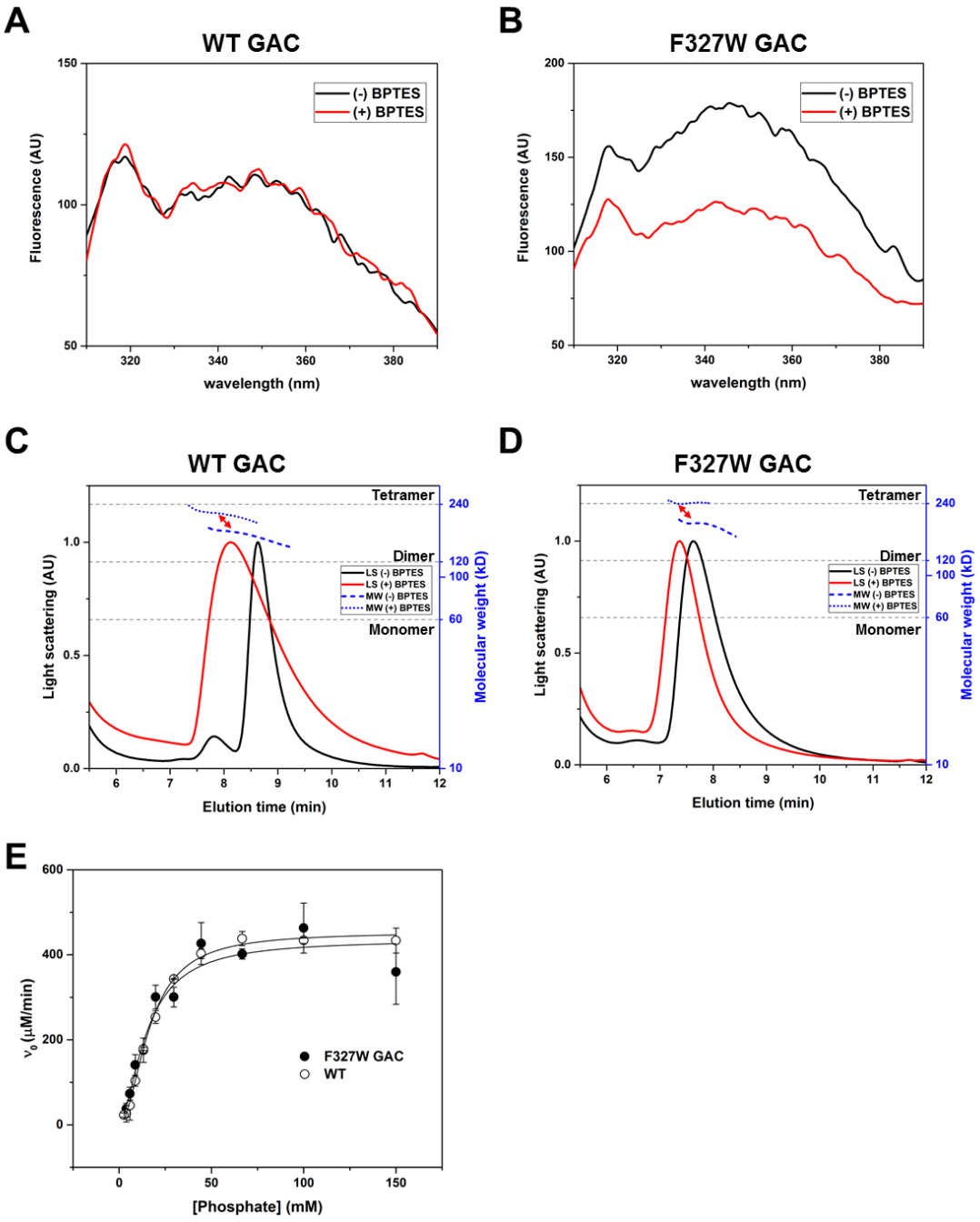
A
WT GAC
(-) BPTES
(+) BPTES
Fluorescence (AU)
wavelength (nm)
B
F327W GAC
(-) BPTES
(+) BPTES
Fluorescence (AU)
wavelength (nm)
C
WT GAC
Tetramer
Dimer
Monomer
LS (-) BPTES
LS (+) BPTES
MW (-) BPTES
MW (+) BPTES
Light scattering (AU)
Molecular weight (kD)
Elution time (min)
D
F327W GAC
Tetramer
Dimer
Monomer
LS (-) BPTES
LS (+) BPTES
MW (-) BPTES
MW (+) BPTES
Light scattering (AU)
Molecular weight (kD)
Elution time (min)
E
F327W GAC
WT
[Phosphate] (mM)

The ability of the F327W mutation to read-out BPTES binding is most likely due to its interactions with BPTES through its peptide bond, and not the outcome of a direct contact with the indole side-chain (Figure 4.6A). The orientation of the native phenylalanine in the BPTES-bound GAC structures shows no interaction of the amino acid side-chain with other residues. However, DeLaBarre and colleagues (2011) described the electrostatic interaction of BPTES with the peptide backbone of residues L326 and F327 [15]. These interactions, which they refer to as a "π-basket", are formed between the peptide backbone and the nitrogen atoms within the thiadiazole ring of BPTES (Figure 4.6A, dotted lines). Interestingly, both Cassago *et al*. (2012) and Thangavelu *et al*. (2012) also reported the electrostatic interaction between BPTES and the peptide backbone of these two residues, but involving the sulfur atom of the thiadiazole ring rather than the nitrogens (Figure 4.6B) [12], [16]. The requirement of BPTES analogues to possess these thiadiazole rings is apparently absolute in order to maintain potency, where bis-thiadiazoles were the original scaffold that characterized the first generation of glutaminase inhibitors [13], [18], [25]. Although tryptophan fluorescence is sensitive to the environment of the indole sidechain, it is also sensitive to the electrostatics of its main chain amino and carboxyl groups, and hence the likely cause of the marked quenching observed here.

Derivatives of BPTES have been proven to be effective inhibitors *in vivo*, with compound CB-839 being the most potent to date with a reported IC_{50} value of ~30 nM.

FIGURE 4.6 – F327 peptide backbone interacts with the thiadiazole ring of BPTES-class inhibitors. (**A**) Close-up of the interaction of BPTES in two different orientations from two separate published structures ((**A**) 3UO9, and (**B**) 4JKT) and the native residues L326 and F327 of GAC [15],[16]. Interactions of the peptide backbone of these residues to the bis-thiadiazole ring of BPTES are highlighted with dashed lines.

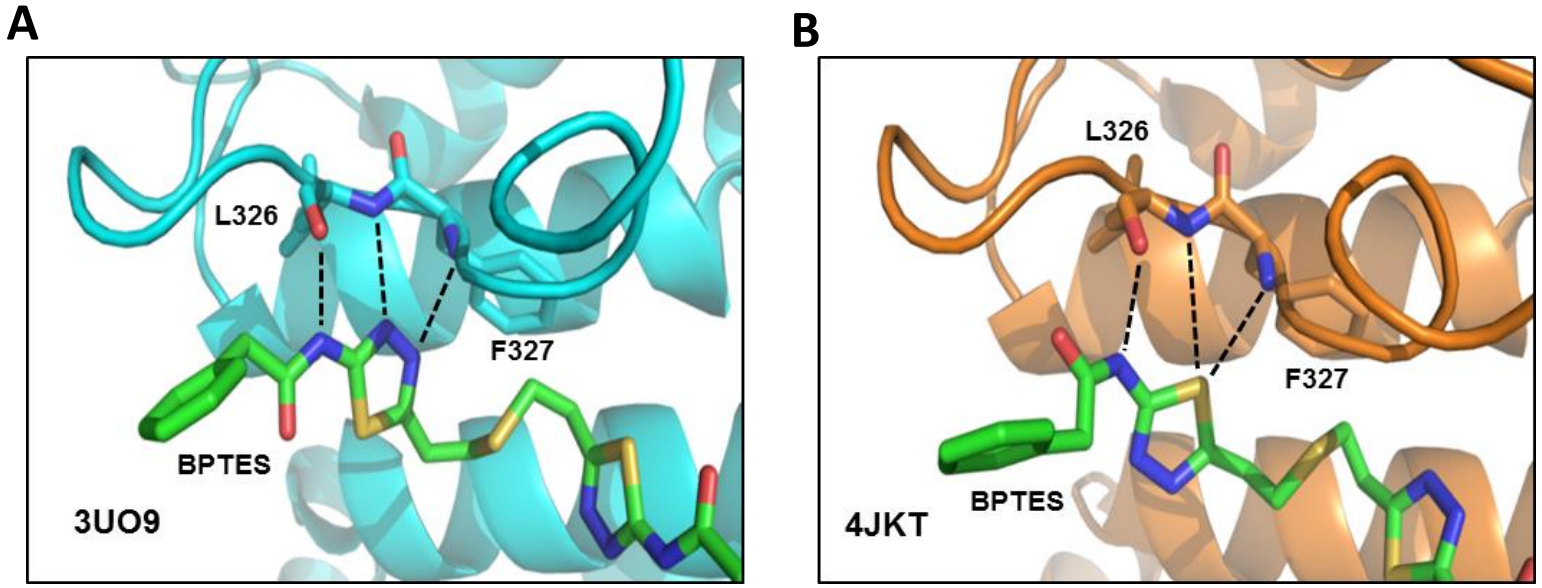
A
L326
F327
BPTES
3UO9
B
L326
F327
BPTES
4JKT

However, the inhibitory properties of CB-839 were shown to be distinct from that of BPTES, where CB-839 increased its potency following pre-incubation with GAC, and retained its inhibitory activity for a longer time period upon removal of excess inhibitor (i.e., suggesting that it has a slower off rate from the enzyme compared to BPTES) [7]. Here, we sought to utilize the quenching of the tryptophan fluorescence of the F327W mutant to compare the kinetics and binding efficiency of both BPTES and CB-839.

Our results show that addition of BPTES or CB-839 to the F327W mutant resulted in a rapid, dose dependent quenching of tryptophan fluorescence (Figures 4.7A,B). We found each inhibitor reached equilibrium within 10 minutes, with CB-839 displaying slightly slower binding kinetics than BPTES. Somewhat unexpectedly, the binding isotherms for each inhibitor gave very similar profiles and K_D values (Figure 4.7C). CB-839 exhibited a slightly shifted binding curve, with a K_D of 34 ± 5 nM, compared to BPTES, with a K_D of 70 ± 5 nM. This shift in binding affinity represents the difference in the apparent ability of these two compounds to bind to the activation loop, and suggests that they have a similar potency. The two-fold difference for the binding affinities as read out by F327W fluorescence quenching was in good agreement with the dose dependent inhibition of WT GAC (Figure 4.7D, CB-839 IC_{50} = 23 ± 1 nM versus BPTES IC_{50} = 108 ± 17 nM).

One aspect of BPTES binding to GAC that has not been investigated is whether BPTES binds to a preformed GAC tetramer, or to the peptide loop of a GAC dimer to promote tetramer formation.

FIGURE 4.7 – F327W fluorescence as a binding assay for BPTES-like molecules. Addition of increasing concentrations of BPTES (**A**) and CB-839 (**B**) quenches the tryptophan fluorescence of 100 nM F327W. (**C**) Fluorescence quenching of F327W mutant by BPTES (—) and CB-839 (—) quantified and fit to a bimolecular interaction equation, giving a K_D value of 70 ± 5 nM and 31 ± 5 nM for BPTES and CB-839, respectively. (**D**) Inhibition of 50 nM WT GAC activity by BPTES (●) and CB-839 (●), giving IC_{50} values of 108 ± 17 nM for and 23 ± 1 nM respectively.

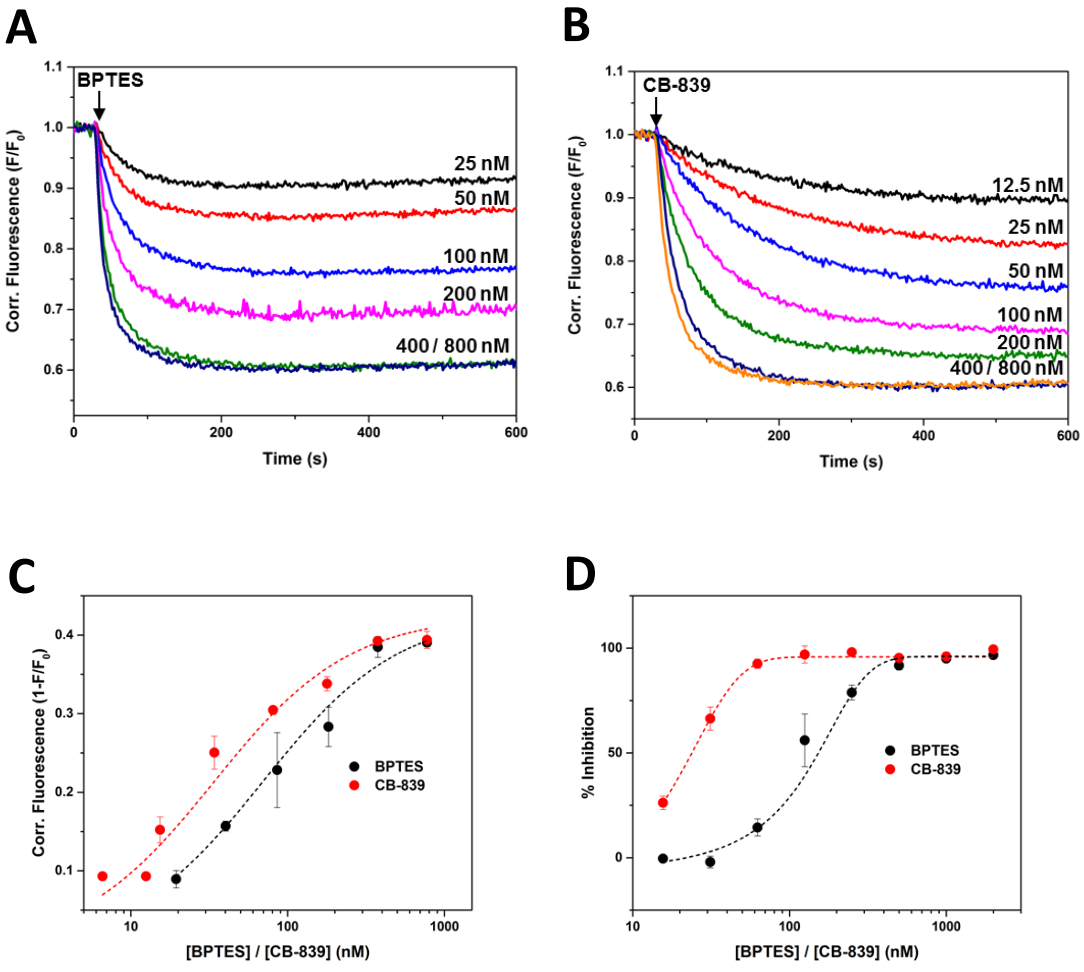
A
BPTES
25 nM
50 nM
100 nM
200 nM
400 / 800 nM
Corr. Fluorescence (F/F0)
Time (s)
B
CB-839
12.5 nM
25 nM
50 nM
100 nM
200 nM
400 / 800 nM
Corr. Fluorescence (F/F0)
Time (s)
C
Corr. Fluorescence (1-F/F0)
BPTES
CB-839
[BPTES] / [CB-839] (nM)
D
% Inhibition
BPTES
CB-839
[BPTES] / [CB-839] (nM)

To demonstrate the requirement of BPTES to bind to the tetrameric form of KGA/GAC, we took advantage of a mutation along the dimer-dimer interface, namely D391K, previously shown in Chapter 2 (section 2.3.1) to block the ability of GAC to form tetramers [11]. Aspartate 391 is critical for tetramer formation, where it forms a salt bridge with K401, both of which reside at the interface between two dimers. Due to the 2-fold axis of symmetry of the GAC tetramer, the single change of aspartate 391 to lysine, and hence the introduction of a charge-charge repulsion, results in four disrupted salt bridges per GAC tetramer that is sufficient to prohibit tetramer formation [11]. To investigate whether BPTES binds to the activation loop of a constitutive GAC dimer, we introduced the D391K mutation into the GAC (F327W) background and found that this single substitution completely ablated the ability of BPTES to induce a change in the tryptophan fluorescence (Figure 4.8A, compare (—) to (—)). We further examined the GAC(F327W, D391K) double mutant using SEC-MALS to confirm that it existed in the constitutive dimeric state, both with and without pre-incubation of BPTES. We found that the double mutant indeed exhibited a molecular weight distribution consistent with a dimeric species, in the presence and absence of BPTES, thus further illustrating the requirement of a GAC tetramer to form in order for BPTES to bind and induce an inhibitory state of the enzyme (Figure 4.8B, solid lines represent elution of GAC and broken lines represent the measured MW).

FIGURE 4.8 – GAC tetramer formation is required for BPTES binding. (**A**) Tryptophan fluorescence of 500 nM of the F327W GAC mutant (—) is rapidly quenched following the addition of 1 μM BPTES, but does not quench the fluorescence of 500 nM of the dimeric mutant GAC (F327W, D391K) (—). (**B**) SEC-MALS analysis of 5 mg/mL GAC (F327W, D391K) mutant shows a constitutive dimer molecular weight distribution, both before (---) and after (•••) pre-incubation with 50 μM BPTES.

A

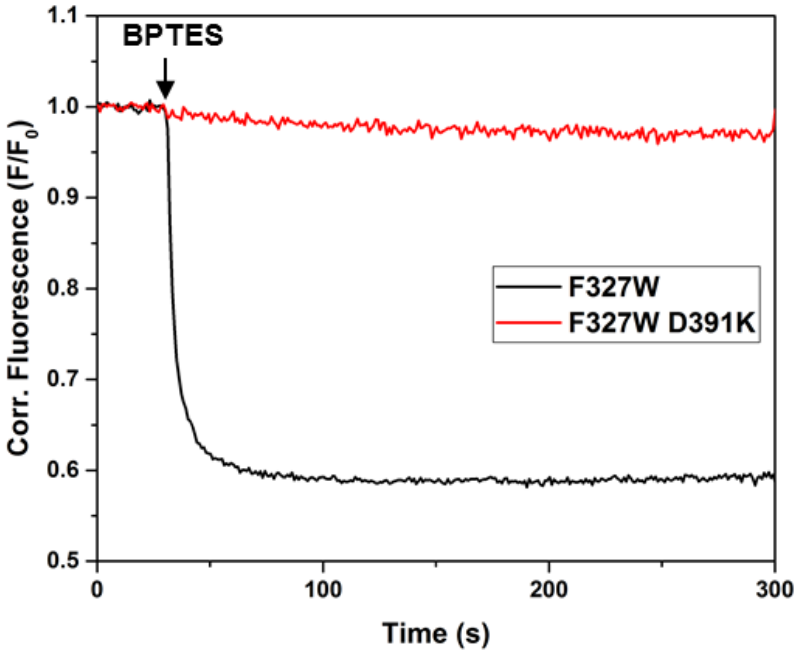
BPTES
Corr. Fluorescence (F/F0)
Time (s)
F327W
F327W D391K
1.1
1.0
0.9
0.8
0.7
0.6
0.5
0
100
200
300

B

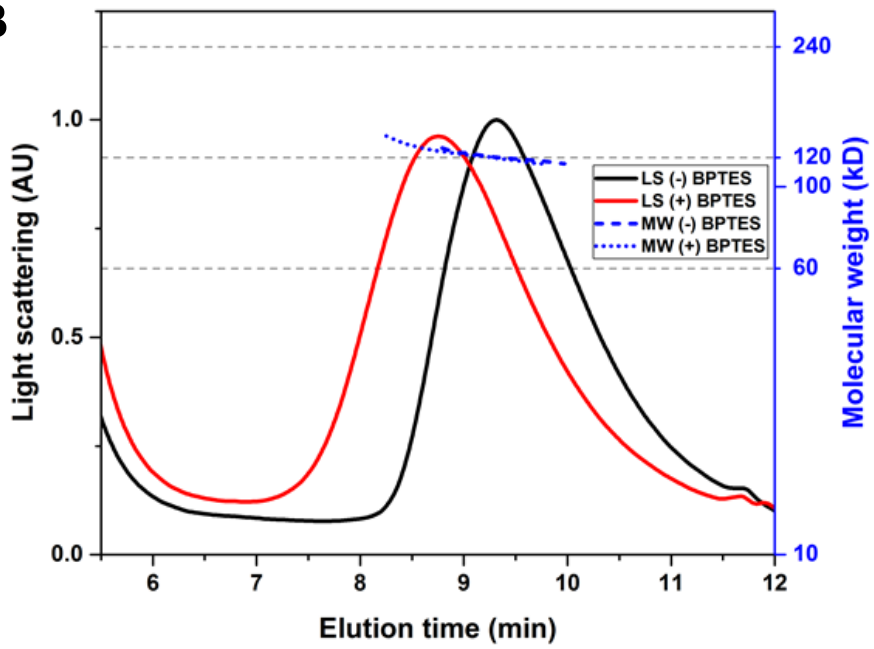
Light scattering (AU)
Molecular weight (kD)
Elution time (min)
LS (-) BPTES
LS (+) BPTES
MW (-) BPTES
MW (+) BPTES
1.0
0.5
0.0
240
120
100
60
10
6
7
8
9
10
11
12

4.3.4 Allosteric activators enhance F327W fluorescence

Previous studies of the activation of the KGA/GAC enzymes revealed that their enzymatic activity was markedly increased upon the addition of various inorganic anionic ions [13], [22], [26], [27]. The most potent of these activators, inorganic phosphate, has been highly studied, having been shown to affect the oligomeric state of both Gls isoforms. Additionally, recent high resolution X-ray crystal structures have revealed potential binding sites for these anions (see Figure 4.4A,B), and suggest that they exert their effects on enzymatic activity by changing the conformation of the activation loop [12].

Here, we examined the effects of these anionic activators on the tryptophan fluorescence of the F327W mutant, in order to further elucidate the mechanism by which they stimulate GAC activity. We first tested those anions that have been reported to lead to the activation of glutaminase enzymes, namely phosphate and sulfate. Unlike the changes observed for BPTES and CB-839, the addition of these anions to GAC (F327W) resulted in the marked enhancement of the tryptophan fluorescence (Figure 4.9A), thus providing evidence that these anions directly affect the conformation of the activation loop. Interestingly, we found that the dose dependent increases of fluorescence enhancement correlated well with the ability of a given anion to activate GAC. More specifically, sulfate was ~50% as effective as phosphate, which correlated well with their abilities to enhance the tryptophan fluorescence of GAC (F327W) (i.e. 15% versus 25%, respectively). Titrations with these anions yielded binding curves that were in good agreement with their ability to activate WT GAC (Figure 4.9B, compare (●) and (●) to (♦) and (▲)), suggesting

they indeed act through a similar mechanism by affecting the conformation of the activation loop.

We next investigated the effects of these ions on the molecular weight distribution of GAC, as read-out by SEC-MALS, and found that sulfate stimulated the formation of a mixture of 16-mer and 8-mer's, but not the larger oligomers that are induced by phosphate (Figure 4.9C, compare (---) and (•••) representing molecular weight for eluted species). This observation is consistent with the overall differences in the ability of sulfate versus inorganic phosphate to stimulate GAC enzymatic activity and to enhance F327W fluorescence.

The mechanism by which inorganic phosphate activates GAC activity is still unclear. In fact, it has been suggested that phosphate binds within the active site following catalysis, where it creates an electrostatic repulsion with the product glutamate to increase its off-rate, thereby effectively increasing the catalytic turnover [16]. The second proposed mechanism, as mentioned above, suggests phosphate interacts with the activation loop at the GAC dimer-dimer interface, much like allosteric inhibitors such as BPTES, and allows the loop to access an active conformation to stimulate catalysis [12]. The sensitization of the tryptophan fluorescence of the F327W mutant observed here is consistent with the latter mechanism. Furthermore, we found that the fluorescence enhancement induced by phosphate addition was dependent on the GAC concentration, and therefore the proportion of tetramers.

FIGURE 4.9 – F327W fluorescence is enhanced by allosteric activators and proportional to their ability to activate GAC activity. (**A**) Addition of inorganic phosphate (HPO_4^{2-}) or sulfate (SO_4^{2-}) to give a 50 mM solution to 400 nM of the F327W mutant resulted in the enhancement of tryptophan fluorescence, where inorganic phosphate stimulated the greatest enhancement (—), followed by sulfate (—). (**B**) Glutaminase activity of 50 nM WT GAC was measured in the presence of increasing concentrations of the anions phosphate (●) and sulfate (●), giving a $K_{1/2}$ of 20.6 ± 0.4 mMol/L and 36.4 ± 3.0 mMol/L respectively. Tryptophan fluorescence enhancement by addition of these anions to 400 nM F327W is overlaid ((♦) and (▲)). (**C**) SEC-MALS of 5 mg/mL WT GAC, where the anions inorganic phosphate (—) and sulfate (—) were included in the running buffer at a concentration of 50 mM, shows the shift from a molecular weight distribution of a heterogeneous population of dimers and tetramers in the absence of either anion (- - -), to an equilibrium of 8 to 16-mers for sulfate (•••) up to greater than 32-mers for phosphate (• • •). (**D**) The increased enhancement of the F327W fluorescence ((●), left axis) upon addition of 50 mM HPO_4^{2-} to increasing concentrations of GAC (F327W) was plotted with previously reported FRET values of 488 and QSY9-labeled WT GAC, and the specific activity of WT GAC measured in the absence of phosphate [11], to give a K_D of 75 ± 28 nM for Tryp fluorescence.

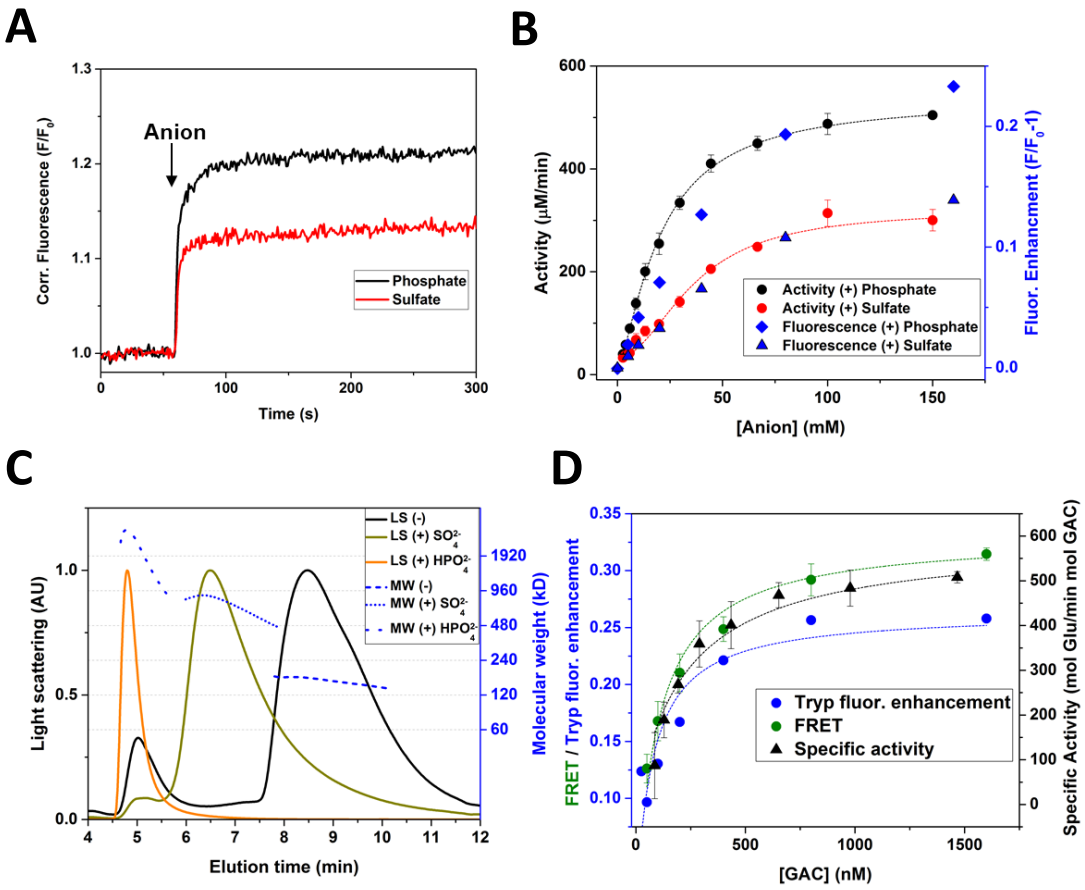
A
Anion
Corr. Fluorescence (F/F0)
Time (s)
Phosphate
Sulfate
B
Activity (μM/min)
Fluor. Enhancment (F/F0-1)
[Anion] (mM)
Activity (+) Phosphate
Activity (+) Sulfate
Fluorescence (+) Phosphate
Fluorescence (+) Sulfate
C
Light scattering (AU)
Molecular weight (kD)
Elution time (min)
LS (-)
LS (+) SO4 2-
LS (+) HPO4 2-
MW (-)
MW (+) SO4 2-
MW (+) HPO4 2-
D
FRET / Tryp fluor. enhancement
Specific Activity (mol Glu/min mol GAC)
[GAC] (nM)
Tryp fluor. enhancement
FRET
Specific activity

When this enhancement was plotted with respect to the concentration of GAC, it was in good agreement with previous FRET measurements that reflect the binding isotherm of GAC dimers to tetramers, and the concentration-dependent activation of the WT enzyme (Figure 4.9D, compare (●) and (●) on left axis to (▲) on right axis). Taken together, these results suggest that phosphate binding affects its catalytic properties by interacting with the GAC tetramer, thereby inducing a conformational change with residues within the activation loop.

4.4 DISCUSSION

Extensive studies of the structure and function relationships of GAC and KGA enzymes have revealed that these metabolic enzymes, which are essential for glutamine metabolism within mammalian cells, are governed by their self-association to form tetramers [23], [27]–[30]. However, the mechanism by which this tetramer formation stimulates enzymatic activity is not fully understood, and represents a challenge for describing the activation of this important enzyme family of drug targets. The fact that a class of small molecule inhibitors, namely the bis-thiadiazole derivatives, binds to the active tetrameric form of the enzyme in order to inhibit activity was a surprising discovery and further highlights the interest in the mechanism governing activation. Here, we set out to develop a spectroscopic read-out for the flexible loop where BPTES binds, to aid in obtaining mechanistic insights into how allosteric activators and inhibitors impact the loop and thereby exert their regulatory functions.

Recently, there has been a concerted effort to find small molecule candidates to inhibit glutaminase enzymes using medicinal chemistry approaches [18], [19], [31].

Here, we first compared the differences between the allosteric activators, inorganic phosphate and sulfate, and the two most commonly used allosteric inhibitors, CB-839 and BPTES, in fluorescence assays that reflect the dynamics of GAC to form tetramers. We showed that both allosteric activators and inhibitors induced the formation of GAC tetramers, however inhibitors were readily distinguished from activators by their ability to form stable irreversible tetramers. We found that compound CB-839 indeed acts similar to BPTES, with the addition of either drug quickly inducing tetramer formation, which is not readily reversible upon the addition of excess unlabeled GAC subunits. These results agree with previous observations that CB-839 acts through a similar mechanism as BPTES, by binding at the dimer-dimer interface and promoting the formation of an inactive tetramer. We also sought to investigate the difference between these two compounds to inhibit a fundamental characteristic of transformed cells, the loss of cell-cell contact inhibition, driven by the potent oncoprotein Dbl, and found that each compound inhibited this property of cellular transformation.

To address how allosteric activators and inhibitors both induce tetramer formation, but exert opposing effects on enzyme activity, we investigated available X-ray crystal structures of GAC/KGA enzymes and noticed differences between the conformations of the activation loop. We reasoned that by comparing the activation loop in the BPTES-bound GAC structure, versus that for free GAC, we might be able to identify potential residues, that when substituted with the fluorescent amino acid tryptophan, would be sensitive to the dynamics of the loop. We show here that the selective substitution of a single amino acid within the activation loop, phenylalanine

327, to a tryptophan, retains the normal catalytic activity of the enzyme, and provides a useful readout for the binding of allosteric inhibitors and activators. This native phenylalanine residue has been shown previously to be an important residue for the activation of the KGA/GAC isoforms. Additionally, F327 is one of the only two residues that differ between Gls2/Gls isozymes along the activation loop, where phenylalanine at position 323 on Gls is a tyrosine in Gls2, and phenylalanine 327 is a serine [12], [15]. Both of these isozymes have been described to have markedly different catalytic properties, and it was of interest here that only the F327W mutant preserved WT GAC activity.

The efficacy of CB-839, when compared to BPTES, has been suggested to be far superior, with reported IC_{50} values of 30 nM for CB-839 and between 80 nM and 3 μM for BPTES [12]–[15], [18], [32]. Here, we used the GAC (F327W) mutant to directly test the binding of these two compounds in real time, and found that they have similar dissociation constants (30 nM and 70 nM for CB-839 and BPTES, respectively). Additionally, when the activity of the WT enzyme was monitored in real time under identical conditions (i.e. at 100 nM GAC concentration), their IC_{50} values were in good agreement with the binding data. Consistent with these molecules binding to the active GAC tetramer, we expected that introducing a mutation which prevents GAC from forming tetramers, i.e. the D391K mutant, would similarly compromise the binding of BPTES. Indeed, we observed that the binding of BPTES was completely ablated using both the fluorescence assay of the F327W mutant and SEC-MALS, further emphasizing the prerequisite of GAC's ability to form tetramers to bind BPTES (Figure 4.10).

Allosteric activators, such as inorganic phosphate, have been shown to promote and or stabilize oligomer transitions of GAC/KGA enzymes. However, although GAC/KGA oligomer formation has been consistently observed, the binding site for these anionic activators, as well as the mechanistic outcome of oligomer formation, is still not well understood. Recent studies have shown that mutations along the activation loop of GAC/KGA result in the hyper-activation of these enzymes, such that anionic activators elicit no additional activation [15], [20], [21]. These observations suggest that the allosteric activators act through the activation loop through an undescribed mechanism. Our findings show that these allosteric activators elicit an enhancement of the tryptophan fluorescence of the F327W mutant, directly correlating with their ability to stimulate GAC activity. These results suggest that the allosteric activators bind at the dimer-dimer interface, changing the conformation and environment of the loop to varying degrees to promote activated GAC tetramers (Figure 4.10).

In conclusion, our results further elucidate the complex role that the critical residues along the activation loop of GAC play in regulating GAC/KGA activity. The results presented here show that BPTES and CB-839 interact with the activation loop in a very similar manner and reveal the utility of this novel F327W mutant for screening the ability of bis-thiadaizoles to bind to the activation loop of KGA/GAC enzymes. Additionally, we show that potent allosteric activators directly impact the conformational dynamics of the activation loop, and the potential usefulness of the F327W mutant in screening for other small molecule activators.

FIGURE 4.10 – Model of oligomeric species of GAC induced by allosteric activators and BPTES-class inhibitors. Inactive dimers associate to form active tetramers in the absence of allosteric activators or inhibitors, stimulating GAC's basal activity. Anionic activators, such as inorganic phosphate (P_i), bind to the GAC tetramer at the activation loop to stimulate an active conformation, inducing "phosphate-stimulated" activity. BPTES-class inhibitors bind to the activation loop in either phosphate-bound or unbound GAC tetramers, locking the activation loop in an inactive state, forming highly stable drug-bound tetramers.

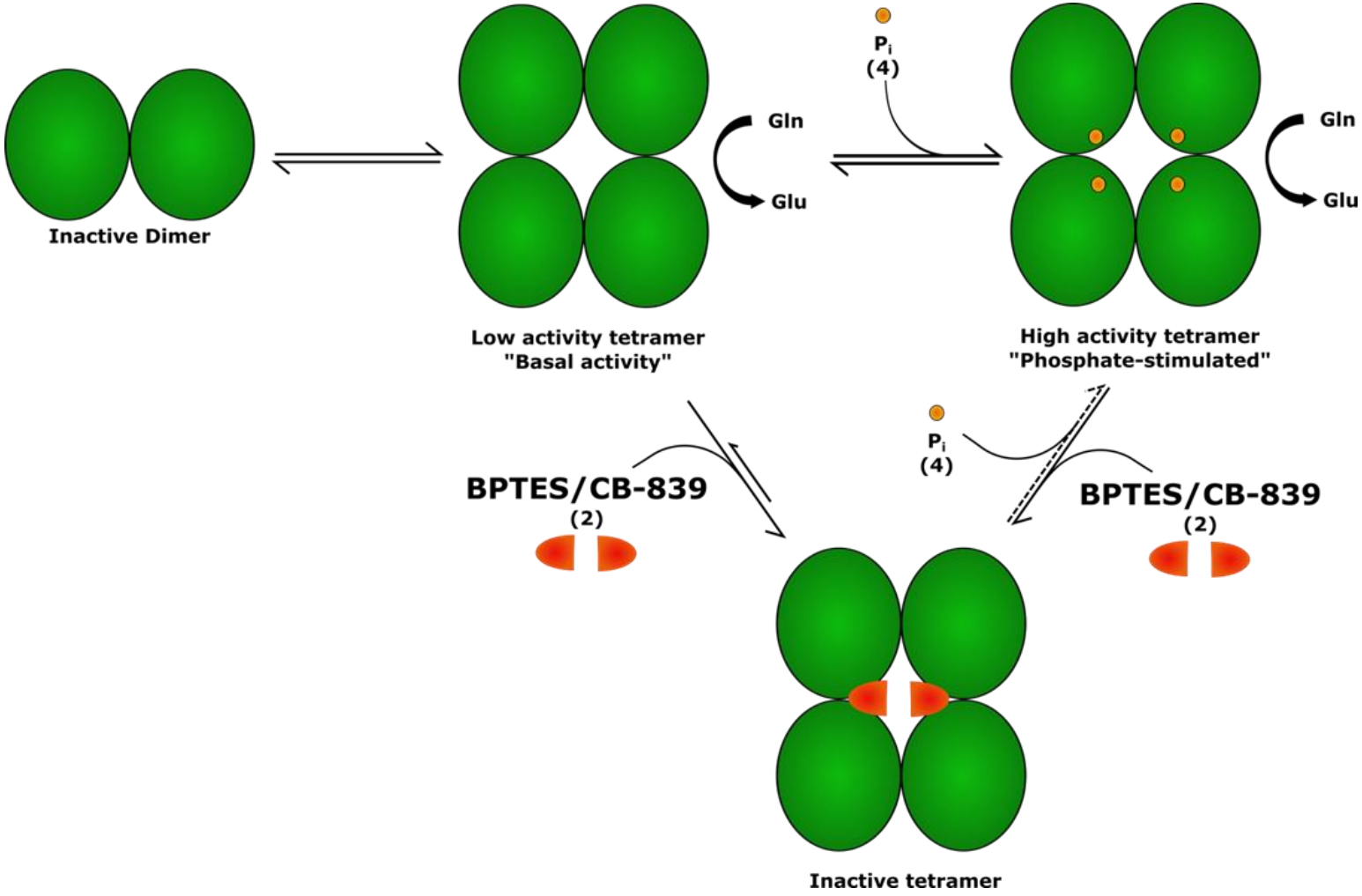
Inactive Dimer
Gln
Glu
Low activity tetramer
"Basal activity"
Pi
(4)
Gln
Glu
High activity tetramer
"Phosphate-stimulated"
BPTES/CB-839
(2)
Pi
(4)
BPTES/CB-839
(2)
Inactive tetramer

4.5 REFERENCES

[1] C. T. Hensley, A. T. Wasti, and R. J. DeBerardinis, "Glutamine and cancer: cell biology, physiology, and clinical opportunities," *J. Clin. Invest.*, vol. 123, no. 9, pp. 3678–3684, Sep. 2013.

[2] R. J. DeBerardinis and T. Cheng, "Q's next: the diverse functions of glutamine in metabolism, cell biology and cancer," *Oncogene*, vol. 29, no. 3, pp. 313–324, Nov. 2009.

[3] A. S. Krall and H. R. Christofk, "Rethinking glutamine addiction," *Nat. Cell Biol.*, vol. 17, no. 12, pp. 1515–1517, Dec. 2015.

[4] R. J. DeBerardinis, J. J. Lum, G. Hatzivassiliou, and C. B. Thompson, "The Biology of Cancer: Metabolic Reprogramming Fuels Cell Growth and Proliferation," *Cell Metab.*, vol. 7, no. 1, pp. 11–20, Jan. 2008.

[5] W. P. Katt, S. Ramachandran, J. W. Erickson, and R. A. Cerione, "Dibenzophenanthridines as Inhibitors of Glutaminase C and Cancer Cell Proliferation," *Mol. Cancer Ther.*, vol. 11, no. 6, pp. 1269–1278, Jun. 2012.

[6] A. G. Thomas, C. Rojas, C. Tanega, M. Shen, A. Simeonov, M. B. Boxer, D. S. Auld, D. V. Ferraris, T. Tsukamoto, and B. S. Slusher, "Kinetic characterization of ebselen, chelerythrine and apomorphine as glutaminase inhibitors," *Biochem. Biophys. Res. Commun.*, vol. 438, no. 2, pp. 243–248, Aug. 2013.

[7] M. I. Gross, S. D. Demo, J. B. Dennison, L. Chen, T. Chernov-Rogan, B. Goyal, J. R. Janes, G. J. Laidig, E. R. Lewis, J. Li, A. L. MacKinnon, F. Parlati, M. L. M. Rodriguez, P. J. Shwonek, E. B. Sjogren, T. F. Stanton, T. Wang, J. Yang, F. Zhao, and M. K. Bennett, "Antitumor Activity of the Glutaminase Inhibitor CB-839 in Triple-Negative Breast Cancer," *Mol. Cancer Ther.*, vol. 13, no. 4, pp. 890–901, Apr. 2014.

[8] P. Matre, M. Shariati, J. Velez, Y. Qi, S. Konoplev, X. Su, C. D. DiNardo, N. Daver, R. Majeti, M. Andreeff, S. M. Chan, and M. Konopleva, "Efficacy of Novel Glutaminase Inhibitor CB-839 in Acute Myeloid Leukemia," *Blood*, vol. 124, no. 21, pp. 3763–3763, Dec. 2014.

[9] N. Jacque, A. M. Ronchetti, C. Larrue, G. Meunier, R. Birsen, L. Willems, E. Saland, J. Decroocq, T. T. Maciel, M. Lambert, L. Poulain, M. A. Hospital, P. Sujobert, L. Joseph, N. Chapuis, C. Lacombe, I. C. Moura, S. Demo, J. E. Sarry, C. Recher, P. Mayeux, J. Tamburini, and D. Bouscary, "Targeting glutaminolysis has antileukemic activity in acute myeloid leukemia and synergizes with BCL-2 inhibition," *Blood*, vol. 126, no. 11, pp. 1346–1356, Sep. 2015.

[10] J.-B. Wang, J. W. Erickson, R. Fuji, S. Ramachandran, P. Gao, R. Dinavahi, K. F. Wilson, A. L. B. Ambrosio, S. M. G. Dias, C. V. Dang, and R. A. Cerione, "Targeting Mitochondrial Glutaminase Activity Inhibits Oncogenic Transformation," *Cancer Cell*, vol. 18, no. 3, pp. 207–219, Sep. 2010.

[11] C. A. Stalnecker, S. M. Ulrich, Y. Li, S. Ramachandran, M. K. McBrayer, R. J. DeBerardinis, R. A. Cerione, and J. W. Erickson, "Mechanism by which a recently discovered allosteric inhibitor blocks glutamine metabolism in transformed cells," *Proc. Natl. Acad. Sci. U. S. A.*, vol. 112, no. 2, pp. 394–399, Jan. 2015.

[12] K. Thangavelu, Q. Y. Chong, B. C. Low, and J. Sivaraman, “Structural Basis for the Active Site Inhibition Mechanism of Human Kidney-Type Glutaminase (KGA),” *Sci. Rep.*, vol. 4, Jan. 2014.
[13] M. M. Robinson, S. J. Mcbryant, T. Tsukamoto, C. Rojas, D. V. Ferraris, S. K. Hamilton, J. C. Hansen, and N. P. Curthoys, “Novel mechanism of inhibition of rat kidney-type glutaminase by bis-2-(5-phenylacetamido-1,2,4-thiadiazol-2-yl)ethyl sulfide (BPTES),” *Biochem. J.*, vol. 406, no. 3, pp. 407–414, Sep. 2007.
[14] E. W. Hartwick and N. P. Curthoys, “BPTES inhibition of hGA124–551, a truncated form of human kidney-type glutaminase,” *J. Enzyme Inhib. Med. Chem.*, vol. 27, no. 6, pp. 861–867, Dec. 2012.
[15] B. DeLaBarre, S. Gross, C. Fang, Y. Gao, A. Jha, F. Jiang, J. Song J., W. Wei, and J. B. Hurov, “Full-Length Human Glutaminase in Complex with an Allosteric Inhibitor,” *Biochemistry (Mosc.)*, vol. 50, no. 50, pp. 10764–10770, Dec. 2011.
[16] A. Cassago, A. P. S. Ferreira, I. M. Ferreira, C. Fornezari, E. R. M. Gomes, K. S. Greene, H. M. Pereira, R. C. Garratt, S. M. G. Dias, and A. L. B. Ambrosio, “Mitochondrial localization and structure-based phosphate activation mechanism of Glutaminase C with implications for cancer metabolism,” *Proc. Natl. Acad. Sci. U. S. A.*, vol. 109, no. 4, pp. 1092–1097, Jan. 2012.
[17] Y. Xiang, Z. E. Stine, J. Xia, Y. Lu, R. S. O’Connor, B. J. Altman, A. L. Hsieh, A. M. Gouw, A. G. Thomas, P. Gao, L. Sun, L. Song, B. Yan, B. S. Slusher, J. Zhuo, L. L. Ooi, C. G. L. Lee, A. Mancuso, A. S. McCallion, A. Le, M. C. Milone, S. Rayport, D. W. Felsher, and C. V. Dang, “Targeted inhibition of tumor-specific glutaminase diminishes cell-autonomous tumorigenesis,” *J. Clin. Invest.*, vol. 125, no. 6, pp. 2293–2306, Jun. 2015.
[18] K. Shukla, D. V. Ferraris, A. G. Thomas, M. Stathis, B. Duvall, G. Delahanty, J. Alt, R. Rais, C. Rojas, P. Gao, Y. Xiang, C. V. Dang, B. S. Slusher, and T. Tsukamoto, “Design, Synthesis, and Pharmacological Evaluation of Bis-2-(5-phenylacetamido-1,2,4-thiadiazol-2-yl)ethyl Sulfide 3 (BPTES) Analogs as Glutaminase Inhibitors,” *J. Med. Chem.*, vol. 55, no. 23, pp. 10551–10563, Dec. 2012.
[19] L. A. McDermott, P. Iyer, L. Vernetti, S. Rimer, J. Sun, M. Boby, T. Yang, M. Fioravanti, J. O’Neill, L. Wang, D. Drakes, W. Katt, Q. Huang, and R. Cerione, “Design and evaluation of novel glutaminase inhibitors,” *Bioorg. Med. Chem.*
[20] C. J. McDonald, E. Acheff, R. Kennedy, L. Taylor, and N. P. Curthoys, “Effect of lysine to alanine mutations on the phosphate activation and BPTES inhibition of glutaminase,” *Neurochem. Int.*, vol. 88, pp. 10–14, Sep. 2015.
[21] A. P. S. Ferreira, A. Cassago, K. de A. Gonçalves, M. M. Dias, D. Adamoski, C. F. R. Ascenção, R. V. Honorato, J. F. de Oliveira, I. M. Ferreira, C. Fornezari, J. Bettini, P. S. L. Oliveira, A. F. P. Leme, R. V. Portugal, A. L. B. Ambrosio, and S. M. G. Dias, “Active Glutaminase C Self-assembles into a Supratetrameric Oligomer That Can Be Disrupted by an Allosteric Inhibitor,” *J. Biol. Chem.*, vol. 288, no. 39, pp. 28009–28020, Sep. 2013.
[22] M. Møller, S. S. Nielsen, S. Ramachandran, Y. Li, G. Tria, W. Streicher, M. V. Petoukhov, R. A. Cerione, R. E. Gillilan, and B. Vestergaard, “Small Angle X-Ray Scattering Studies of Mitochondrial Glutaminase C Reveal Extended Flexible

Regions, and Link Oligomeric State with Enzyme Activity," *PLOS ONE*, vol. 8, no. 9, p. e74783, Sep. 2013.
[23] N. P. Curthoys, T. Kuhlenschmidt, and S. S. Godfrey, "Regulation of renal ammoniagenesis: Purification and characterization of phosphate-dependent glutaminase from rat kidney," *Arch. Biochem. Biophys.*, vol. 174, no. 1, pp. 82–89, May 1976.
[24] M. J. Lukey, K. S. Greene, J. W. Erickson, K. F. Wilson, and R. A. Cerione, "The oncogenic transcription factor c-Jun regulates glutaminase expression and sensitizes cells to glutaminase-targeted therapy," *Nat. Commun.*, vol. 7, p. 11321, Apr. 2016.
[25] R. W. Newcomb, "Selective inhibition of glutaminase by bis-thiadiazoles," US6451828 B1, 17-Sep-2002.
[26] H. Yz and K. We, "A comparative study of glytaminase isozymes in rat tissues.," *Enzyme*, vol. 21, no. 5, pp. 408–426, Dec. 1975.
[27] M. Patel and J. D. McGivan, "Partial purification and properties of rat liver glutaminase.," *Biochem. J.*, vol. 220, no. 2, pp. 583–590, Jun. 1984.
[28] D. Darmaun, D. E. Matthews, and D. M. Bier, "Glutamine and glutamate kinetics in humans," *Am. J. Physiol. - Endocrinol. Metab.*, vol. 251, no. 1, pp. E117–E126, Jul. 1986.
[29] J. H. Laake, Y. Takumi, J. Eidet, I. A. Torgner, B. Roberg, E. Kvamme, and O. P. Ottersen, "Postembedding immunogold labelling reveals subcellular localization and pathway-specific enrichment of phosphate activated glutaminase in rat cerebellum," *Neuroscience*, vol. 88, no. 4, pp. 1137–1151, Feb. 1999.
[30] J. McGIVAN, M. Vadher, J. Lacey, and N. Bradford, "Rat liver glutaminase," *Eur. J. Biochem.*, vol. 148, no. 2, pp. 323–327, Apr. 1985.
[31] B. DeLaBarre, J. Hurov, G. Cianchetta, S. Murray, and L. Dang, "Action at a Distance: Allostery and the Development of Drugs to Target Cancer Cell Metabolism," *Chem. Biol.*, vol. 21, no. 9, pp. 1143–1161, Sep. 2014.
[32] A. G. Thomas, C. M. O'Driscoll, J. Bressler, W. E. Kaufmann, C. J. Rojas, and B. S. Slusher, "Small molecule glutaminase inhibitors block glutamate release from stimulated microglia," *Biochem. Biophys. Res. Commun.*, vol. 443, no. 1, pp. 32–36, Jan. 2014.

CHAPTER FIVE

Glutamine metabolism is directly related to a dimer-to-tetramer shift of GAC in transformed cells and mouse tissues

5.1 INTRODUCTION

Emerging evidence indicates that oncogenes and tumor suppressors, responsible for driving normal cells to the oncogenic state, directly impact cellular metabolism to support the metabolic requirements of uncontrolled growth [1]–[5]. As mentioned earlier, the principal metabolic shift observed in a variety of cultured cancer cell lines is the shift from glucose to glutamine fueled anaplerosis, and causing the cells to exhibit glutamine-dependent growth such that they are deemed to be 'glutamine addicted'. This glutamine addiction has been explored in both mouse models and human tumors and is currently understood as a means for cells to adapt to the nutrient and oxygen stressed environment of the tumor stroma [6], [7]. However, the molecular mechanisms by which these oncogenes and tumor suppressors alter the cells metabolic pathways remain unclear. More specifically, it remains poorly understood how oncogenes exert their influence on metabolic enzymes to affect their enzyme catalysis.

Recent metabolic flux studies take advantage of stable isotope tracing of ^{13}C, ^{2}H, or ^{15}N isotopes in transformed cells, and using these methods have identified the unique metabolic phenotypes associated with individual transformation events [8], [9]. For example, Son *et al*. (2013) have shown K-ras mediated increases in glutamine metabolism in a pancreatic ductal adenocarcinoma (PDAC) model [10]. Similarly, Le and colleagues (2012) characterized the reliance of human Burkitt lymphoma cells on

glutamine dependent anaplerosis resulting from their transformation by the expression of the MYC oncogene [11]. Comparable results have been found in a variety of cancer cells, transformed by a particular lesion within an oncogene or tumor suppressor, such as the loss of the Von Hippel Lindau (VHL) tumor suppressor in renal cell carcinoma [12]–[14] or loss of the phosphatase and tensin homolog (PTEN) in T cell acute lymphoblastic leukemia (T-ALL) [15]. These metabolic flux studies, which utilize stable isotope tracing methods, have served to bring clarity to how the metabolic rewiring is directed by oncogenic transformation.

In most cases, the observed increase in glutaminolysis in cancer cells that are deemed glutamine addicted is attributed to the increased expression of the mitochondrial glutaminase enzyme, GAC. One such case recently discovered by our laboratory was the increased expression of GAC directly downstream of JNK signaling pathways in a panel of breast cancer cell lines, thereby providing a molecular description of GAC up-regulation in breast cancer through increased GAC transcription and translation [16]. Additionally, post-transcriptional regulation mechanisms, such as those through the micro-RNA regulation of RNA transcripts, have also been described. The oncogene MYC and proliferative signaling molecule NF-κB, specifically p65, have been shown to regulate GLS translation through this micro-RNA mechanism by repressing the micro-RNA miR-23a/b, which acts to negatively regulate GLS transcripts [17], [18]. Indeed, increased glutaminolysis, leading to a glutamine dependent phenotype, is consistently reported for MYC transformed cells [11], [19]–[24]. However, it remains uncertain how GAC activity is impacted within mitochondria. As described previously in Chapter 2, KGA/GAC

enzymes depend on the formation of tetramers to become activated, but this has yet to be demonstrated as a direct result of oncogene expression in cells.

In order to study the role of GAC up-regulation and activation in oncogenic transformation, we make use of a model cell system using tetracycline controlled gene expression in mouse embryonic fibroblasts (MEFs) to examine the effects of induced expression of the oncogenic Rho GTPase GEF (guanine nucleotide exchange factor) Dbl (for Diffuse B-Cell Lymphoma) and subsequent hyper-activation of Rho GTPases (Figure 5.1A). Using this model cell system, we show the increased glutaminolysis that results from the induced expression of Dbl, and its inhibition by the small molecule inhibitor described previously in Chapter 3, compound 968. We then extend these studies by directly assaying the oligomeric state of GAC in Dbl induced cells, and show that Dbl induction indeed drives the formation of GAC tetramers. We go on to show the utility of this method in assaying the oligomeric state of GAC in other cancer cells and solid tissues, where it is proven useful for determining the proportion of GAC dimers and tetramers directly that are present in the mitochondria of cells.

FIGURE 5.1 – Oncogenic Dbl gives rise to Rho-GTPase driven transformation. (**A**) Cartoon depiction of GTPase cycle, where a Rho G-protein in the inactive (GDP-bound) state is activated by a guanine nucleotide exchange factor (GEF) to exchange GDP for GTP. The GTP-bound Rho is a signaling-active species (Rho*) that can bind effectors to give rise to actin cytoskeleton remodeling, cell cycle progression, and gene expression of a myriad of targets. To complete the cycle, a GTPase-activating protein (GAP) stimulates the intrinsic GTPase activity of the G-protein, causing the hydrolysis of GTP to GDP, thereby returning the G-protein to the signaling-inactive state. (**B**) Protein domains of the proto-Dbl and onco-Dbl GEFs, where the oncogenic form is an N-terminal truncation of proto-Dbl that lacks the spectrin domain and is no longer susceptible to an auto-inhibitory mechanism, thereby causing Dbl to function as a de-regulated, activated GEF towards the Rho-GTPases Rac, Rho, and Cdc42. (**C**) Onco-Dbl activates the Rho-GTPases Rac, Rho, and Cdc42, which give rise to distinct cellular phenotypes. Aberrant Rac, Rho, and Cdc42 activation is known to stimulate formation of lamellipodia, stress fibers, and filopodia, respectively.

A

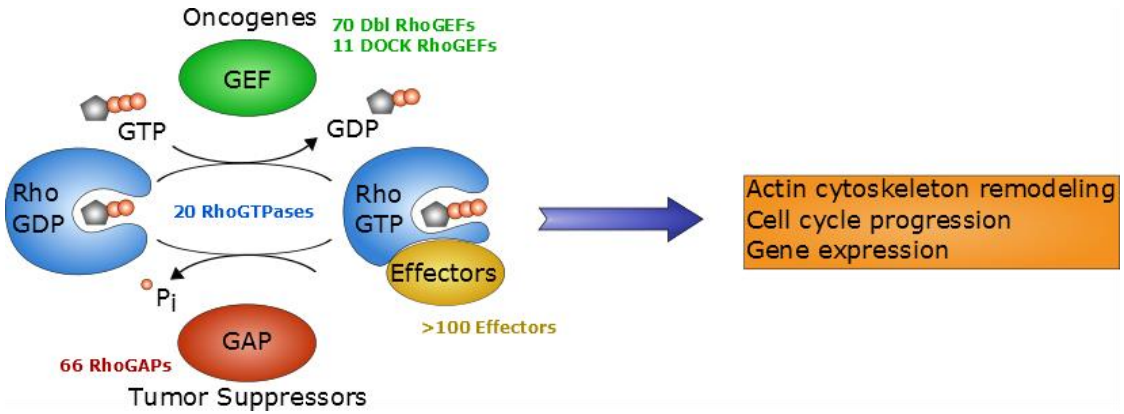
Oncogenes
70 Dbl RhoGEFs
11 DOCK RhoGEFs
GEF
GTP
GDP
Rho
GDP
20 RhoGTPases
Rho
GTP
Effectors
Pi
GAP
66 RhoGAPs
>100 Effectors
Tumor Suppressors
Actin cytoskeleton remodeling
Cell cycle progression
Gene expression

B

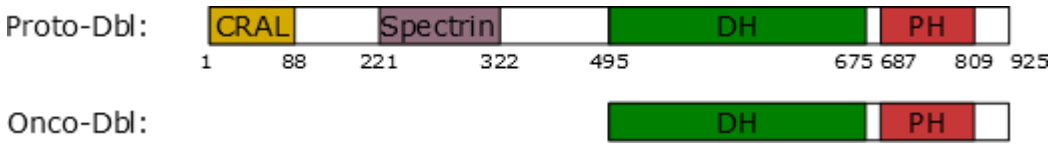
Proto-Dbl:
CRAL
Spectrin
DH
PH
1
88
221
322
495
675
687
809
925
Onco-Dbl:
DH
PH

C

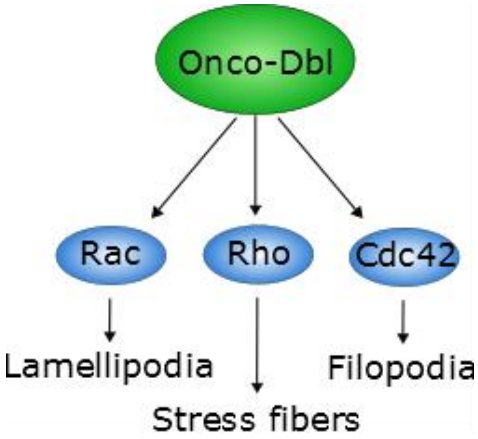
Onco-Dbl
Rac
Rho
Cdc42
Lamellipodia
Filopodia
Stress fibers

5.2 METHODS

5.2.1 Isogenic, Dbl-inducible cell system culture conditions and immunofluorescence staining

Inducible oncogenic Dbl cell lines were created using the TET-OFF system in mouse embryonic fibroblasts (MEFs) following the manufacturer's instructions (Clontech). Briefly, PCR products for onco-Dbl-containing NotI and XbaI restriction endonuclease sites were cloned in the pcr2.1 vector using the TOPO-TA cloning kit (Invitrogen) and subsequently subcloned into the p-TRE-HA vector (Clontech). The pTRE-HA-onco-Dbl was then co-transfected with pMET-Puro in a 20:1 ratio into parental MEFs (Clontech), which contained the transcriptional transactivator (tTa), with Lipofectamine (Invitrogen). Cells were placed under puromycin selection at 48 hours post transfection, and colonies were selected after 2-4 weeks for doxycycline-dependent expression of HA-onco-Dbl using HA.11 antibody (Covance). Cells were maintained in DMEM supplemented with 10% (v/v) Tet system-approved FBS (clontech) and 100 μg/mL G418 (Gibco). To suppress Dbl expression, 1 μg/mL doxycycline was added to the medium every 2 days. Cells were induced by re-plating in doxycycline-free medium where residual doxycycline was removed by replacing the medium 3 hours after plating. Immunofluorescence was conducted on cells grown 48-72 hours on glass cover slips and fixed with 3.7% formaldehyde. Fixed cells were permeabilized with 0.2% Triton-X 100 and co-stained with α-HA (rabbit polyclonal, Covance) and α-actin (mouse monoclonal, Covance) for 1 hour at 37° C, followed by incubation with Oregon green-conjugated α-rabbit IgG (Molecular Probes) and

Rhodamine-conjugated α-mouse IgG (molecular probes). Digital images were collected using a Zeiss fluorescence microscope and AxioVision 3.1 software.

5.2.2 Metabolic tracing and saturation density assays

DMEM medium supplemented with 10% FBS with or without 1 μg ml^{-1} doxycycline was added to 6-well plates (2 ml per well), and then seeded with 1 × 10^5 MEFs per dish. Following cell attachment (4 h), growth medium was replaced with DMEM supplemented with 5% FBS. Following an overnight incubation (~16 h), medium was replaced again with DMEM supplemented with 5% FBS containing the appropriate drug concentrations where appropriate. Growth medium was subsequently replaced at 48 h intervals. At day 8 for Dbl-MEFs, growth medium was removed and 1.5 ml 3.7% formaldehyde solution in H_2O was added for 30 min. The formaldehyde solution was removed, and 1.5 ml crystal violet solution was added for 20 min at room temperature. This was then removed; the dishes washed with H_2O, and allowed to dry before imaging.

Methods for mass isotopologue distribution analyses using [U-^{13}C]glutamine or [U-^{13}C]glucose (Cambridge Isotope Laboratories) were adapted from Cheng et al. (2011) (1). Briefly, induced (16 h in complete media without Dox) or non-induced cells (complete media with 1 μg/mL Dox) were plated into 100 mm^2 dishes at a density such that the cells were approximately 60% confluent when adhered, at which point the cells were washed with PBS and grown to 80% confluence in DMEM supplemented with 1% Tet-approved FBS and 8 μM 968/WPK968 for drug treated samples, or 0.8% DMSO for control samples, with or without 1 μg/mL Dox (i.e. overnight). When 80% confluent, cells were then washed with PBS and ^{13}C-labeling

media containing the appropriate drug, DMSO, and Dox concentrations. Media was prepared from glucose- and glutamine-free DMEM powder (Sigma) and supplemented with 1% Tet-approved FBS, 2 mM L[U-^{13}C]glutamine and 15 mM unlabeled glucose or 15 mM D[U-^{13}C]glucose and 2 mM unlabeled glutamine (Figure S1F-G), together with 1 μg/mL dox for non-induced samples. For samples containing [U-^{13}C]glutamine, cells were incubated for 1 hour before extracting metabolites, whereas samples containing [U-^{13}C]glucose were incubated for 8 hours. Metabolites were extracted by first washing cells twice with ice cold normal saline (0.9% w/v NaCl), followed by addition of 0.5 mL of a 1:1 methanol:water mixture (-20°C). An internal standard (50 nmol of 2-oxobutyrate) was added and samples were subjected to 3 freeze-thaw cycles, after which macromolecules were separated by centrifugation. The supernatant was evaporated completely and remaining metabolites silylated in 100 μL of a trimethylsilyl donor (Tri-Sil, Thermo) for 30 min at 42°C. Metabolites were subjected to GC-MS analysis using an Agilent 6970 gas chromatograph networked to an Agilent 5973 mass selective detector. Metabolites were identified and isotope enrichment calculated as described by Cheng et al. (2011) (1).

Metabolites were quantified from fresh culture medium after 6 h of both non-induced and induced cells in the presence of compound 968 or compound 27 using the GDH assay as described by the manufacturer (Megazyme, Bray Ireland).

5.2.3 Mitochondrial isolation and solubilization by detergents

Mitochondria were isolated from induced and un-induced Dbl-MEFs, TSE cells, HeLa cells, and ruptured mouse kidney and liver tissues as described by Frezza *et al*. (2007) [36]. Briefly, Dbl-MEF's, TSE, and HeLa cells were harvested from four 15 cm^2

dishes following an overnight serum starvation in DMEM or RMPI supplemented with 1% FBS. First, cells were washed with PBS (3x) before being scrapped, added to a 50 mL-conical tube, and centrifuged 600g at 4°C for 10 min. Cells were suspended in 3 mL in isolation buffer (IC, 10 mM Tris-MOPS, 1 mM EGTA/Tris, 200 mM sucrose, pH 7.4), and then homogenized in a glass potter with a Teflon pestle using a Dounce homogenizer operated at approximately 1600 rpm for 35 strokes. The homogenate was centrifuged 600 x g 10 minutes at 4°C and the supernatant was isolated. The supernatant was centrifuged at 7000 x g 10 minutes at 4°C, where the resultant pellet contained the isolated mitochondria and the supernatant represented the soluble cytosolic and microsomal fractions. The mitochondrial pellet was resuspended in mitochondrial isolation buffer and centrifuged again at 7000 x g 10 minutes at 4°C, where the resulting pellet was taken to be the purified isolated mitochondria. Mitochondria were suspended in solubilization buffer (SB, 50 mM NaCl, 50 mM imidazole/HCl, 2 mM 6-aminohexanoic acid, 1 mM EDTA, pH 7.0) then solubilized in 2% dodecylmaltoside and incubated on ice for 20 min. Solubilized proteins were taken from the supernatant following centrifugation at 16,700g 10 minutes at 4°C.

Purification of mouse kidney and liver tissue was performed similarly with minor alterations. First, adult mice were euthanized under CO_2 for 5 minutes followed by cervical dislocation. Organs were harvested and washed thoroughly with ice cold isolation buffer to remove visible amounts of blood. Then, organs were minced using sterile blades and homogenized in a glass potter with a Teflon pestle using a Dounce

homogenizer operated at approximately 1600 rpm for 5 strokes on ice. Mitochondria were purified and solubilized in 2% DDM following the same protocol as above.

5.2.4 1 and 2-Dimensional blue-native/SDS-PAGE assays

Blue native PAGE gels were prepared by methods adapted by Wittig *et al*. (2006) [26]. Briefly, 4-13% acrylamide gels with a 3.5% stacking gel were prepared from a mixture of acrylamide and bis-acrylamide (AB-3, 48g acrylamide and 1.5g bisacrylamide per 100 mL) and 3x gel buffer (75 mL imidazole, 1.5 M 6-aminohexanoic acid, pH 7.0). For 2-D BN/SDS-PAGE assays, 5 μL 50% glycerol and 2.5 μL Coomassie blue G-250 was added to 400 μg DDM solubilized mitochondrial proteins and then added to each lane, whereas for sucrose fractions, 30 μL of each fraction was directly loaded. Proteins were separated using the cathode buffer B (50 mM Tricine, 7.5 mM imidazole, 0.02% Coomassie blue G-250) and anode buffer (25 mM imidazole) at 4°C at 100 V for ~ 1 h. Once proteins entered the resolving gel, the cathode buffer B was removed and cathode buffer B/10 was added (Cathode buffer B with 0.002% coomassie blue G-250) and electrophoresis was continued at 15 mA for 2-4 hours. The gel was then either stained directly using the manufacturer's protocol for Coomassie blue staining (Pierce) or transferred to PVDF for immunoblotting with only one modification from standard procedures. Following transfer to PVDF, the membrane was briefly rinsed in 25% methanol 10 % acetic acid to remove excess blue dye.

For 2-dimensional BN/SDS-PAGE assays, lanes were cut from the BN-PAGE described above and incubated in a 1% SDS solution for 10 mins. Individual lanes were then added on top of a prepared 10% Tricine SDS-PAGE gel described by

Herman Schagger (2006) [37]. Briefly, a 10% Tricine gel was prepared using AB-3 mix described previously and 3x gel buffer (3 M Tris base, 1 M HCl, 0.3% SDS, pH 8.45) with a 4% stacking gel. Samples were electrophoresed using cathode buffer (100 mM Tris, 100 mM Tricine, 0.1% SDS, pH 8.25) and anode buffer (100 mM Tris, 22.5 mM HCl, pH 8.9) at 4°C using 30 V until samples entered the resolving gel, then at 190 V. Gels were then transferred to PVDF as described above.

5.2.5 Continuous sucrose density gradients and activity assays

Continuous sucrose density gradients were prepared in 5 mL thinwall polypropylene ultracentrifugation tubes compatible with the SW 55 Ti rotor. Gradients were prepared using equal volumes of 50 mM Tris/MOPS, 2 mM EDTA, 0.02% DDM, pH 7.4 buffer containing 5%, 10%, 15%, 20%, 25%, 30%, or 50% sucrose (w/v) and equilibrated at either room temperature for 4 hours or 4°C overnight. 2.5 mg of solubilized mitochondria (2.5 mg total protein) were added to the top of the prepared sucrose gradient and centrifuged 32,500 x g for 16 h at 4°C. Equal volume fractions were manually isolated from top to bottom. Fractions were assayed for glutaminase activity as described in Section 2.4.4 above with minor alterations. Reactions were performed in 50 μL, comprised of 40 μL of each isolated sucrose gradient fraction, with the reaction being started with 10 μL of a 100 mM mixture of glutamine and 500 mM K_2HPO_4. Reactions were incubated 30 minutes at 37°C. The glutaminase reaction was quenched by adding 5 μL 3 mM HCl. Then, 200 μL 2 mM NAD^+, 10 U/mL GDH, 130 mM Tris-acetate, 100 mM hydrazine, pH 9.4, was added to the quenched glutaminase reaction to initiate the coupled reaction, reducing NAD^+ to NADH.

5.3 RESULTS

5.3.1 Transformation by onco-Dbl relies on glutamine-fueled anaplerosis

Originally, the classification of a gene product as an "oncogene" could be ascribed if the transfection of the gene into mouse fibroblast cells (i.e. NIH3T3 cells) was sufficient to cause cellular transformation. Cellular transformation is reflected by the ability of cells to overcome a normal growth phenotype, enabling the normal NIH3T3 fibroblasts to no longer exhibit cell-cell contact inhibition and thus form foci, or to exhibit anchorage-independent growth. Both of these cellular characteristics, cell-cell contact inhibition and anchorage-dependent growth, are fundamental properties of normal cells that transformed cancer cells are able to overcome. With this in mind, we sought to investigate the effects of the Dbl oncogene on the metabolic state of mouse embryonic fibroblasts (MEFs). To accomplish this, we developed an inducible TET-OFF model cell system, where the Dbl oncogene is under the tight regulation of a transcriptional regulator that is inhibited by the antibiotic doxycycline (Dox). Removal of Dox allows for the robust expression of the Dbl oncogene, causing the normal MEFs to be a uniformly transformed population of cells.

Given that the Dbl oncogene is a founding member of a major family of Rho GEFs, it is capable of causing dramatic changes in cell morphology through activation of Rho G-proteins and their abilities to trigger actin cytoskeletal rearrangements. These cytoskeletal rearrangements are readily observed in our inducible cell system, where following a 24 hour induction period, the cell morphology shows marked changes as observed by normal phase contrast (Figure 5.2A) and immunofluorescence images probing for filamentous actin (Figure 5.2B, top

panes). Additionally, immunofluorescence images probing for HA-tagged Dbl in cells, before and after induction, show a robust expression of the oncogene, correlating with the observed morphological changes (Figure 5.2B, bottom panes).

We then sought to investigate the sensitivity of these Dbl-inducible MEFs to treatment with 968. In Chapters 2 and 3 above (sections 2.2.3 and 3.1-3.2), we described the binding and inhibition of the glutaminase enzyme, GAC, by 968 and various 968-analogues. These small molecules have been validated to inhibit GAC *in vitro*, however, they have not been examined for their ability to inhibit glutamine metabolism in cells. To describe the action of this small molecule in transformed cells, we used the prototype compound 968 and a less potent derivative, compound 27, both shown to bind to and target GAC in Chapter 3 (section 3.2.1), above, with *in vitro* IC_{50} values of 3.5 μM and 20.0 μM, respectively (Figure 5.3A). Indeed, these compounds followed the same trend for their ability to inhibit Dbl-induced cell growth at saturation density, a principal characteristic of these transformed cells (Figure 5.3B, compare results under (+) Onco-Dbl).

To show the inhibition of GAC in Dbl-transformed cells, we measured the accumulation of the products of the glutaminase reaction, namely glutamate and ammonia, in extracellular media. These metabolites have been shown previously to be a reliable measure of the level of glutamine metabolism within cells [20], [25]. The induction of the Dbl oncogene resulted in an increase in both glutamate and ammonia levels in the extracellular media (Figure 5.4A, compare black to gray). Additionally, Dbl induction promoted the expression of GAC within the mitochondrial fraction (Figure 5.4B).

FIGURE 5.2 – Induction of onco-Dbl gives rise to transformed morphological phenotypes. (**A**) Dbl induction results in a significant alteration in cellular morphology, characteristic of the onco-Dbl-induced activation of Rho-GTPases, as shown by phase contrast images. (**B**) The activated Rho-GTPases induce the formation of actin stress fibers, which are visualized by imaging the actin cytoskeleton using anti-actin antibodies (middle panels). The robust expression of the HA-tagged Dbl oncogene, upon induction, is visualized using immunofluorescence with an anti-HA antibody (bottom panels).

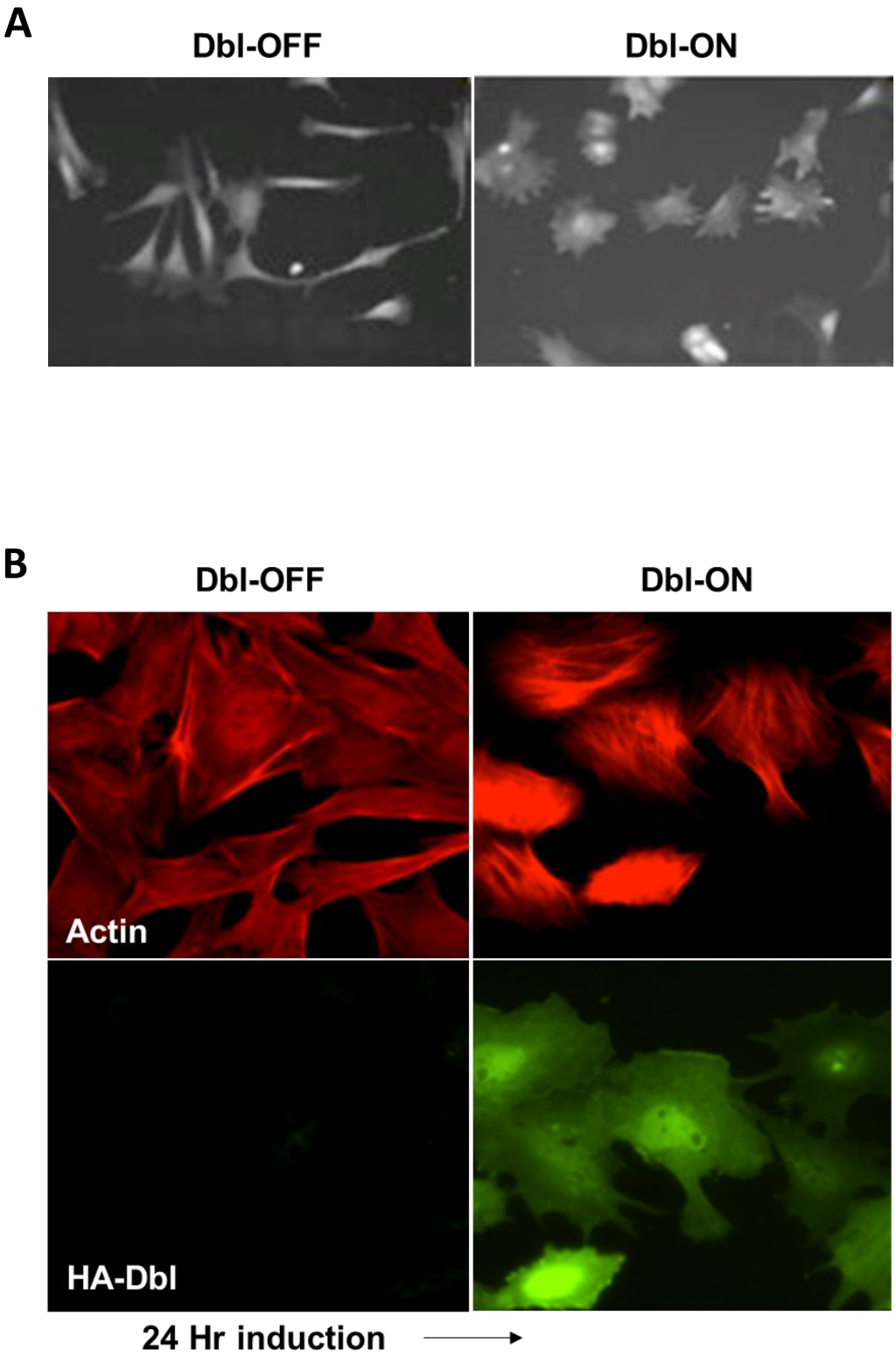
A
Dbl-OFF
Dbl-ON
B
Dbl-OFF
Dbl-ON
Actin
HA-Dbl
24 Hr induction

FIGURE 5.3 – Treatment of Dbl-induced cells with 968 inhibits cell growth at saturation density. (**A**) The reaction catalyzed by mitochondrial glutaminase converts intracellular glutamine to glutamate with the release of ammonia, and is inhibited by the small molecule 968, but not by the inactive 968-analogue, compound 27. (**B**) Dbl-expressing MEFs ($1x10^5$ cells) and control (uninduced) MEFs are grown to saturation density in DMEM supplemented with 5% FBS for 10 days, with the Dbl-expressing cells also being treated with either 968 (7.5 μM), compound 27 (7.5 μM), or left untreated. After 10 days of growth, the cells were fixed with formaldehyde and stained with crystal violet to visualize cell density.

A

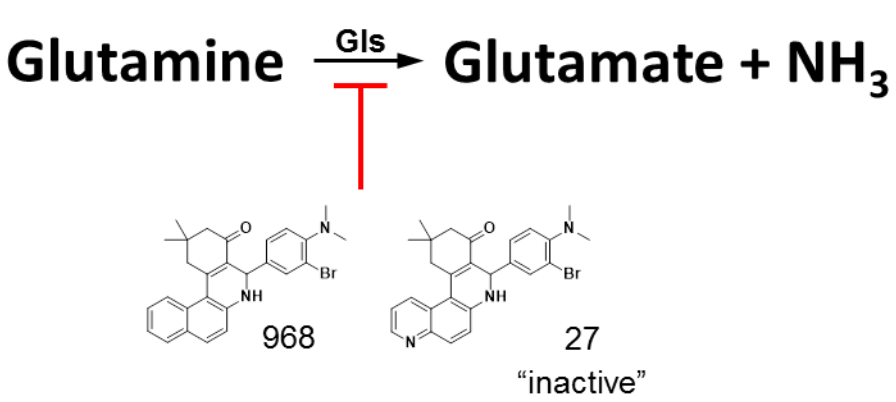
Glutamine
Gls
Glutamate + NH3
968
27
"inactive"

B

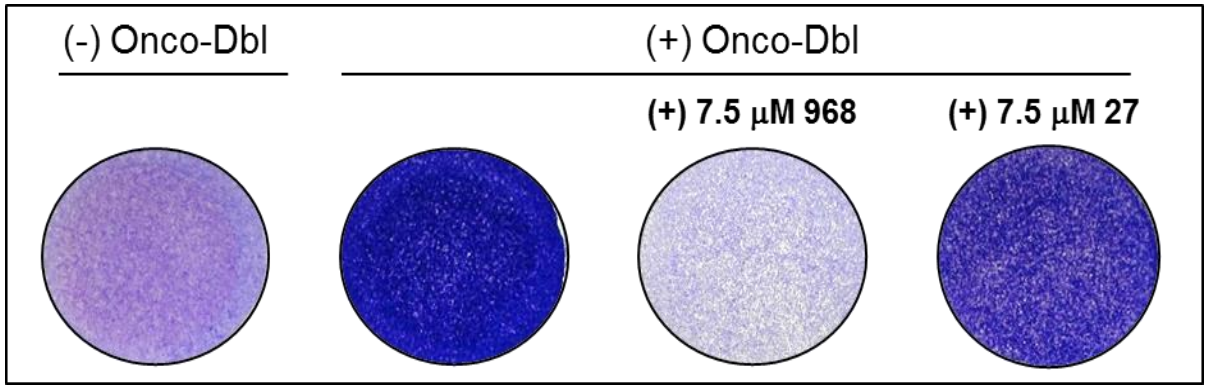
(-) Onco-Dbl
(+) Onco-Dbl
(+) 7.5 μM 968
(+) 7.5 μM 27

FIGURE 5.4 – Dbl induction stimulates increased mitochondrial Gls expression as well as glutamate and ammonia secretion. (**A**) The metabolites glutamate and ammonia were quantified in the extracellular media using an enzyme-coupled spectroscopic assay from uninduced cells, and cells that were induced to express the Dbl-oncogene with and without the treatment of 8 μM 968 or 8 μM compound 27 for 12 h. Bars represent the mean (± SD) of triplicate determinations. P-values were determined by the Students t-test (* $p < 0.05$, ** $p < .005$). (**C**) Mitochondria were isolated from uninduced and induced cells and probed for Gls expression using an antibody that recognizes the KGA and GAC isoforms. The WCL was analyzed for HA-Dbl expression, showing a robust expression of the oncogene in induced cells only. VDAC, a mitochondrial marker, was used to normalize protein for the mitochondrial fraction.

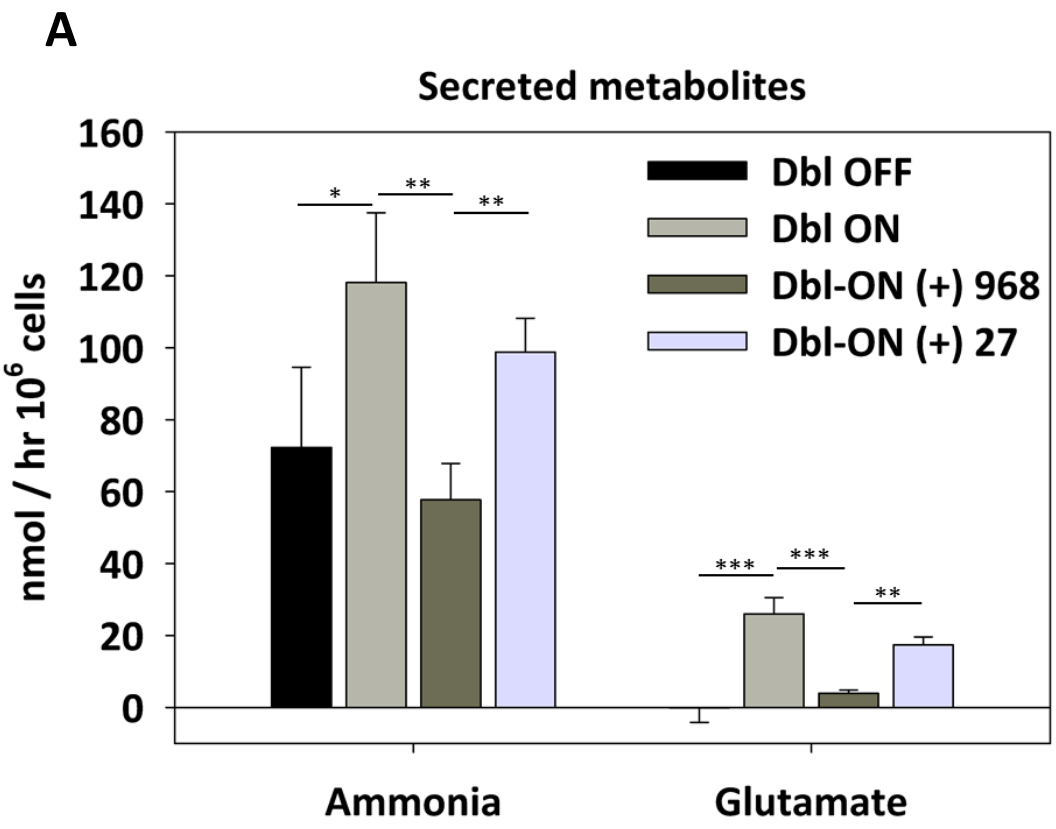
A
Secreted metabolites
160
140
120
100
80
60
40
20
0
nmol / hr 10^6 cells
Dbl OFF
Dbl ON
Dbl-ON (+) 968
Dbl-ON (+) 27
*
**
**
***
***
**
Ammonia
Glutamate

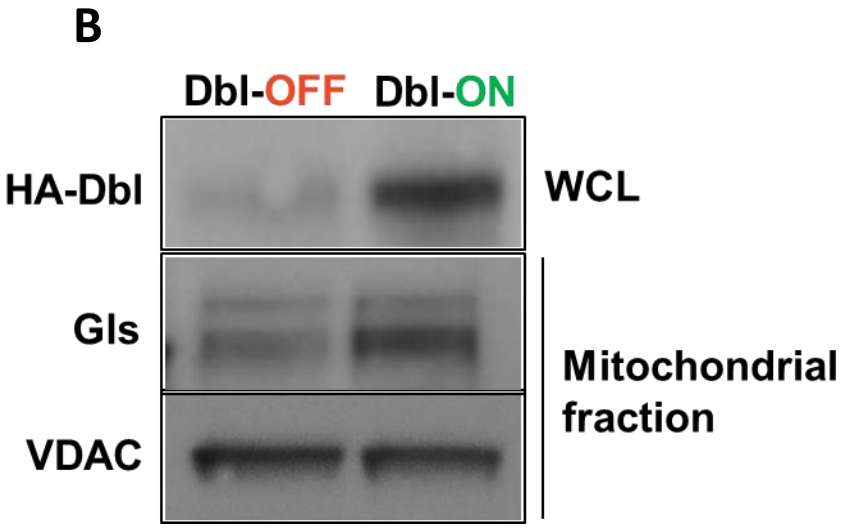
B
Dbl-OFF
Dbl-ON
HA-Dbl
WCL
Gls
VDAC
Mitochondrial fraction

The increased secretion of both glutamate and ammonia was potently inhibited by compound 968, but not by the inactive 968-analogue, compound 27 (Figure 5.4A, compare dark grey to light blue). These results are consistent with Dbl-induced increases in glutamine metabolism, which are sensitive to treatment with 968, but not the inactive analogue 27.

Recently, there has been a greater appreciation for the role imported glutamine plays in the refilling of TCA cycle intermediates, i.e. glutamine-fueled anaplerosis. This anaplerotic process is driven by alterations frequently observed in highly proliferative cells, where the Warburg effect diverts glucose carbon from the TCA cycle to be secreted as lactate. To supplement this shift in glucose metabolism, glutaminolysis is often up-regulated to provide glutamine-derived carbons to refill depleted TCA metabolite pools. To show the increase in glutamine-fueled anaplerosis in Dbl-transformed cells, we used a ^{13}C stable isotope tracing method (Figure 5.5A). Here, Dbl-inducible cells were cultured in glutamine-free DMEM supplemented with uniformly labeled ^{13}C-glutamine ([U-^{13}C]-glutamine). Upon import of [U-^{13}C]-glutamine, downstream metabolite pools resulting from glutamine metabolism are enriched in this ^{13}C isotope, which can be readily extracted from cells and quantified using mass-spectrometry.

Treatment of both Dbl-induced and uninduced cells with [U-^{13}C]-glutamine resulted in a significant increase in glutamine-fueled anaplerosis, detected by the selective enrichment in ^{13}C-containing TCA cycle intermediates (Figure 5.5B, compare black to dark grey). These results are consistent with observations that Dbl-induction causes an increase in GAC expression and in the secreted metabolites,

glutamate and ammonia (Figure 5.4). Importantly, these stable isotope tracing results provide evidence that increased glutaminolysis facilitates the up-regulation of glutamine-fueled anaplerosis. Treatment of Dbl-induced cells with the GAC inhibitor, compound 968, potently inhibited the ^{13}C enrichment below that of un-induced MEFs, showing that 968 inhibits the increase of glutamine-fueled anaplerosis in Dbl transformed cells (Figure 5.5B). Furthermore, treatment with the less effective GAC inhibitor, compound 27, resulted in only a minor inhibition of the ^{13}C enrichment from [U-^{13}C]-glutamine (Figure 5.5B). A modest inhibition of glutaminolysis by 968 was also observed in MEFs not expressing Dbl (see Appendix 4A for the M+5 histograms for Dbl-OFF, +/- 968, and the M+4 histograms in Appendix 4B,C). However, these effects were not accompanied by reductions in cell growth, suggesting that glutamine metabolism is critical for supporting the transformed phenotypes accompanying oncogenic Dbl expression, but not for the proliferative capability of normal MEFs.

FIGURE 5.5 – Glutamine anaplerosis is up-regulated by Dbl induction and potently inhibited by 968. (**A**) Diagram showing ^{13}C enrichment from [U-^{13}C]-glutamine into TCA cycle intermediates, where GAC activation downstream from Dbl is highlighted. ^{13}C-carbons are shown as dark-filled circles and ^{12}C-carbons as light-filled circles. (**B**) Glutamine-derived metabolites (glutamate M+5, fumarate M+4, malate M+4, citrate M+4) were normalized to ^{13}C enrichment observed for MEFs not expressing Dbl. Comparisons were made between treatment with 968, its less potent analog WPK968, and untreated cells. Bars represent the mean (± SD) of triplicate determinations. P-values were determined by the Students t-test (* $p < 0.05$, ** $p < .005$).

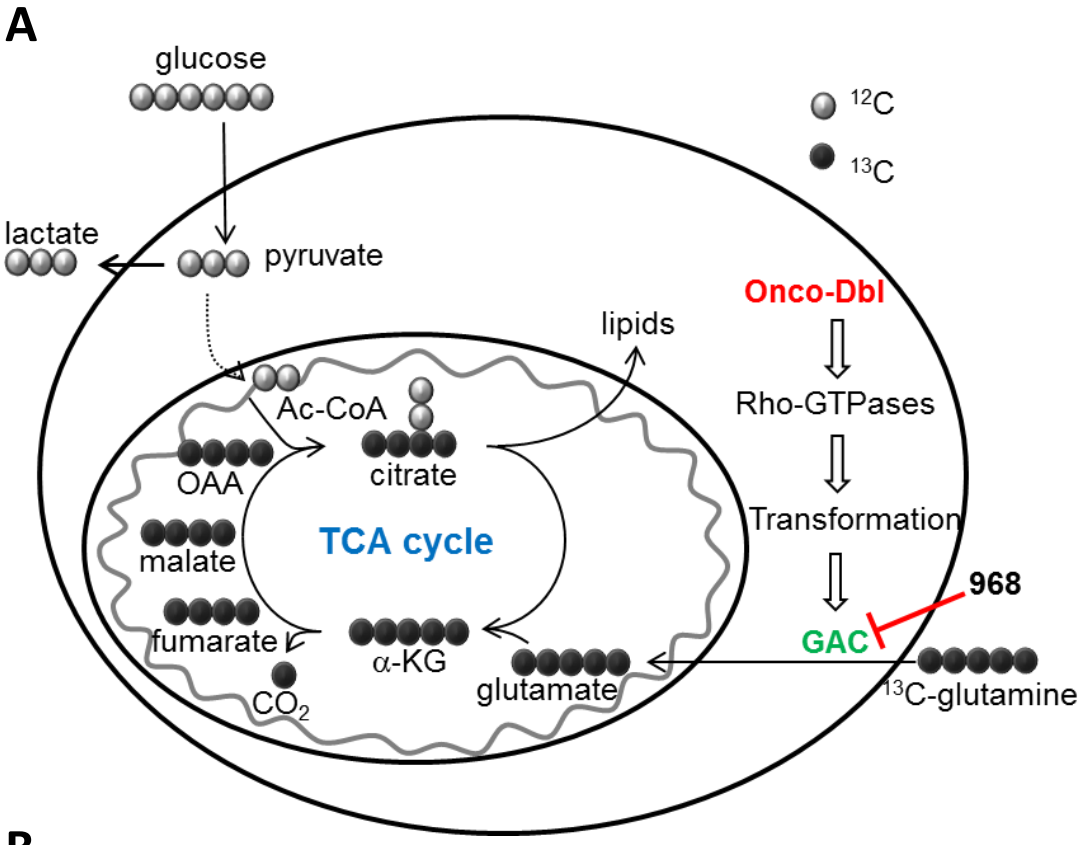
A
glucose
12C
13C
lactate
pyruvate
Onco-Dbl
lipids
Ac-CoA
Rho-GTPases
OAA
citrate
TCA cycle
Transformation
malate
968
GAC
fumarate
α-KG
glutamate
13C-glutamine
CO2

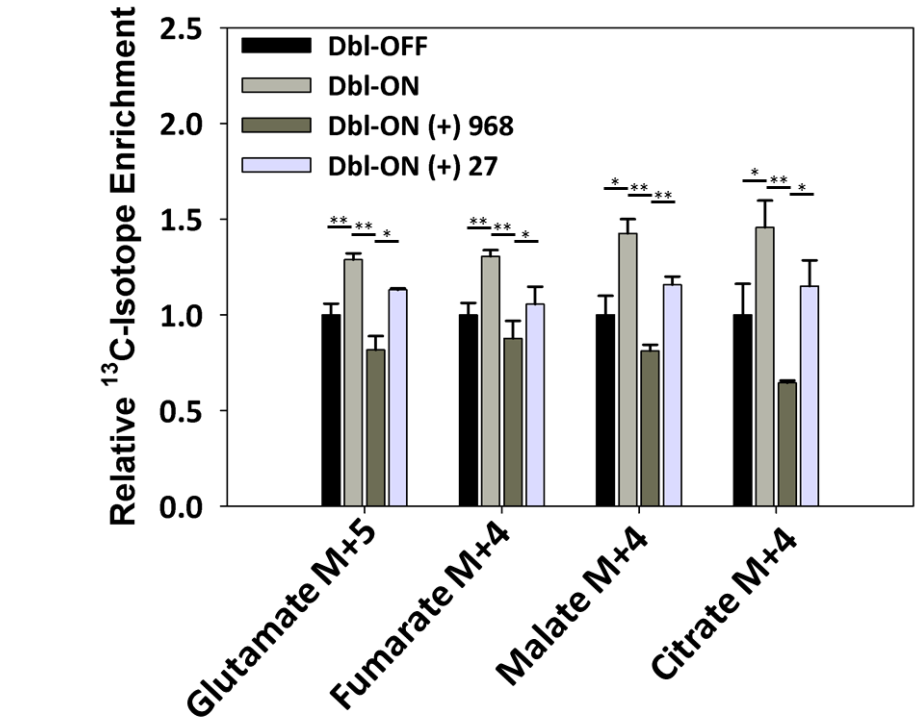
B
Relative 13C-Isotope Enrichment
2.5
2.0
1.5
1.0
0.5
0.0
Dbl-OFF
Dbl-ON
Dbl-ON (+) 968
Dbl-ON (+) 27
Glutamate M+5
Fumarate M+4
Malate M+4
Citrate M+4

5.3.2 Tetrameric GAC is readily observed in Dbl-induced cells and other glutamine dependent cell lines and tissues.

As demonstrated in Chapter 2 above, *in vitro* FRET studies of GAC oligomerization has established the necessity for GAC to form a tetramer in order to become activated. Additional fluorescence studies have shown that the two distinct classes of inhibitors, namely derivatives of benzophenanthridines, where 968 is the prototype, and derivatives of bis-thiadiazoles, where BPTES is the protoype, target discrete oligomeric states of the enzyme by interacting at the monomer-monomer or dimer-dimer interfaces. Therefore, given the importance of this oligomer transition for activity, we were interested in developing a method to screen for the oligomeric species of KGA/GAC enzymes in Dbl-transformed cells. To accomplish this, we developed a workflow where mitochondrial enzymes were first isolated by solubilization in a non-denaturing detergent (dodecylmaltoside, DDM), followed by their separation using 2-dimensional gel electrophoresis (Figure 5.6). In the first dimension, detergent solubilized proteins were separated by their native size using non-denaturing blue-native polyacrylamide gel electrophoresis (BN-PAGE) [26]–[28]. This method was adapted by Wittig *et al.* (2006), where the hydrophobic anionic dye, Coomasie Blue G-250, is added to detergent solubilized proteins to allow for their electrophoretic separation in a gradient polyacrylamide gel (Figure 5.6, (1)) [26]. Then, this single BN-PAGE lane is incubated with the denaturant sodium dodecyl sulfate (SDS) and loaded on top of a denaturing SDS-PAGE gel to separate the native protein complexes into their individual components (Figure 5.6, (2)).

FIGURE 5.6 – 2-Dimensional Blue-Native/SDS PAGE assay for mitochondrial complexes. Mitochondria are isolatedd from cultured cells by differential centrifugation techniques and solubilized with the complex stabilizing detergent, dodecylmaltoside (DDM). DDM solubilized proteins are then incubated with the anionic dye Coomassie Blue G-250 to allow protein complexes bound with the anionic dye to be separated through a gradient polyacrylamide gel by electrophoresis (1^{st} dimension). Once separated, the gel is incubated with the denaturant sodium dodecyl sulfate (SDS) and stacked on a SDS-PAGE gel to separate multi-protein complexes into their individual constituent proteins (2^{nd} dimension). Green spheres represent hypothetical GAC monomers, where dimers and tetramers can readily be separated using this 2D BN/SDS-PAGE assay.

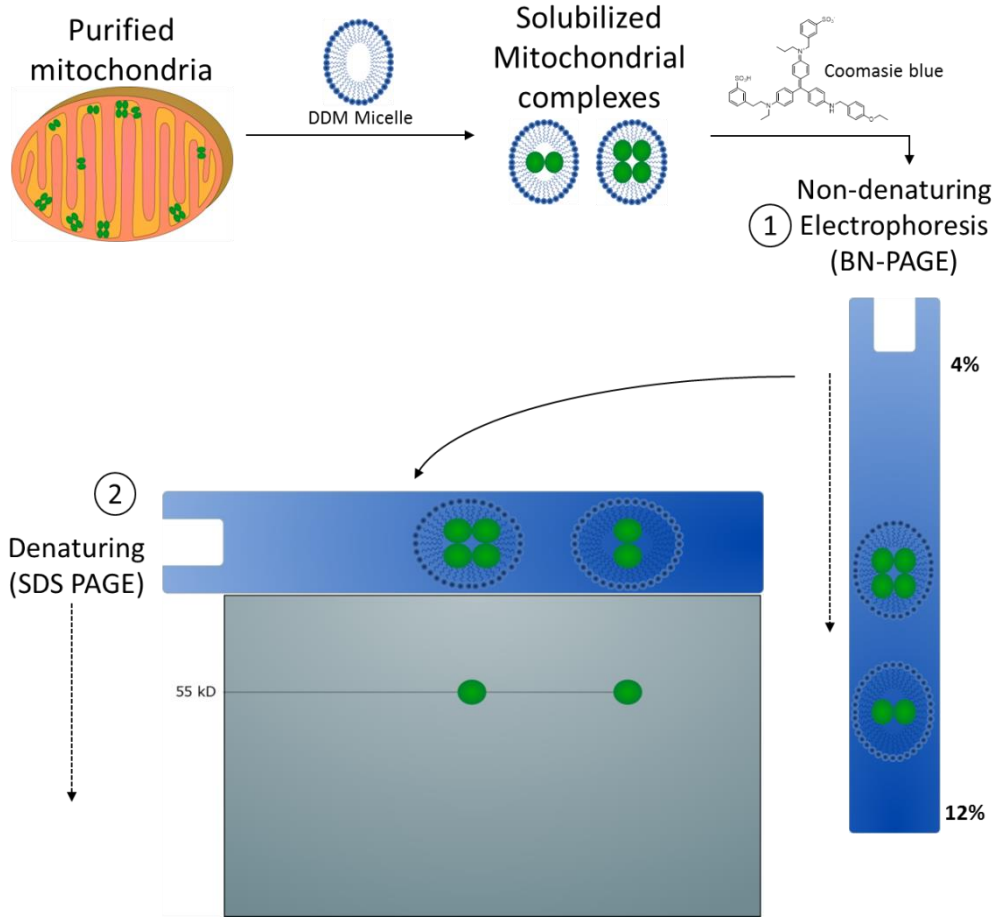
Purified
mitochondria
DDM Micelle
Solubilized
Mitochondrial
complexes
Coomasie blue
Non-denaturing
1 Electrophoresis
(BN-PAGE)
4%
12%
2
Denaturing
(SDS PAGE)
55 kD

Finally, this second gel, where the proteins are first separated by native molecular weight (left to right), and then by their denatured molecular weight (top to bottom), is immunoblotted with an anti-Gls antibody.

The 2-D BN/SDS-PAGE assay was used to determine the oligomeric state of GAC in Dbl-transformed cells. MEFs were either induced to express Dbl or maintained under Dox-controlled repression, and their mitochondria harvested using differential centrifugation methods adapted from Frezza *et al.* (2007) [29]. Analysis of the isolated mitochondrial proteins using 2-D BN/SDS-PAGE and western blotting for KGA/GAC revealed a homogenous population in the un-induced MEFs consistent with a GAC dimer (Figure 5.7A, white circle). However, for MEFs induced to express Dbl, two distinct populations of GAC were observed in the native dimension, but only one population in the denatured dimension, consistent with a GAC dimer and tetramer comprised of GAC monomers (Figure 5.7A, white circles). Additionally, there was an apparent increase in total GAC protein as read out by the intensity of each blot, consistent with previous observations that Dbl induction results in an increased expression of GAC.

To extend these studies, we sought to investigate the oligomeric state of GAC in other transformed cancer cells previously shown to exhibit a significant glutamine dependency [16], [30]. Interestingly, using this 2-D BN/SDS-PAGE assay in both HeLa and TSE cancer cell lines, we observed GAC exclusively as a tetramer (Figure 5.8). Both of these cell lines are known to be highly proliferative and dependent on glutamine metabolism to support their growth phenotype, along with having a robust expression of the GAC enzyme.

FIGURE 5.7 – GAC tetramer formation is induced by onco-Dbl in cells. Western blot of 2D-BN/SDS-PAGE assay of mitochondrial proteins from uninduced (**A**) and Dbl transformed MEFs (**B**) probed with anti-Gls antibody. Uninduced cells have only one population of GAC oligomers consistent with a GAC dimer in the first dimension (112 kD) and monomeric GAC (white circle, 56 kD) in the second dimension. Induced cells have two distinct populations of Gls oligomers in the first dimension (224 kD and 112 kD) that correspond to monomeric GAC (white circles, 56 kD) in the second dimension.

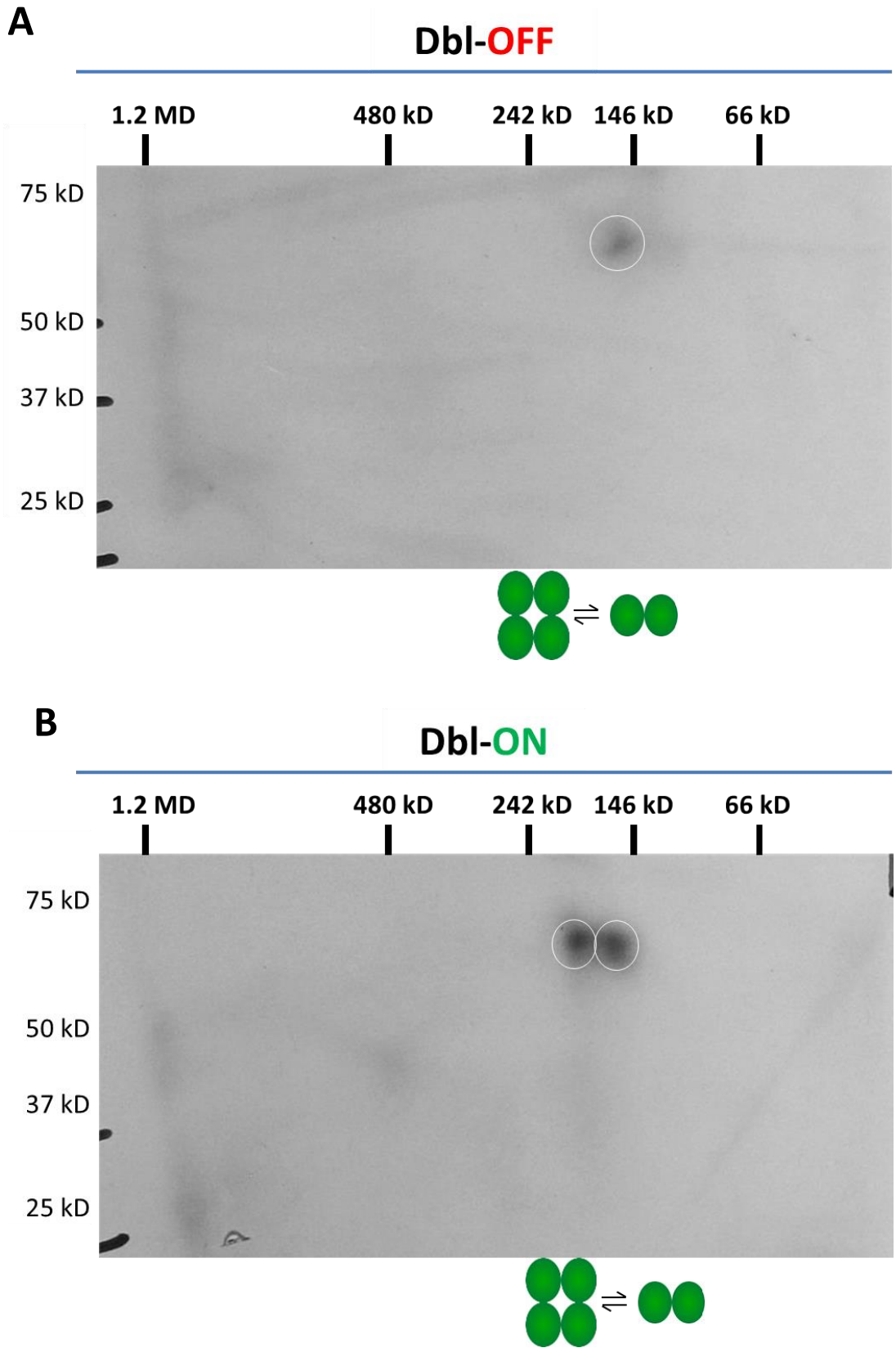
A
Dbl-OFF
1.2 MD
480 kD
242 kD
146 kD
66 kD
75 kD
50 kD
37 kD
25 kD
B
Dbl-ON
1.2 MD
480 kD
242 kD
146 kD
66 kD
75 kD
50 kD
37 kD
25 kD

These results demonstrate the utility of this 2-dimensional assay for profiling the oligomeric state of the GAC enzyme directly in cancer cells.

They also then raised the question whether this assay could be useful for determining the oligomeric state in mitochondrial extracts of tissues. In addition, we wondered whether the metabolic condition of the host organism could impact the distribution of the GAC oligomers. To determine this, we prepared organ tissue from white lab mice that were either fed *ad libitum* or fasted overnight to induce an acute state of famine. Specifically, the kidneys were isolated to perform the 2-D BN/SDS-PAGE analysis due to their high expression of KGA/GAC isoforms and their physiological role in controlling the concentration of glutamine within plasma in response to changes in blood pH (Figure 5.9A) [31], [32]. Interestingly, we found that the KGA/GAC enzymes comprised a heterogeneous population of dimers and tetramers, representing a dynamic equilibrium between oligomeric states (Figure 5.9B,C). The result of fasting significantly increased the total amount of KGA/GAC, and shifted the population towards the tetrameric state, hence representing enzyme activation.

Although the purpose of developing this 2D-BN/SDS-PAGE assay was to investigate the degree of GAC dimers versus tetramers in cells, this assay provided the potential for resolving even higher molecular weight species. To our surprise, we observed a high molecular weight form of GAC in the mitochondrial extracts of mouse kidneys (Figure 5.9B,C, white asterisk). This high molecular weight GAC species (~1.2 MD) was isolated in both the fed and fasted states, with a significant increase observed in the fasted state.

FIGURE 5.8 – GAC is a constitutive tetramer in cancer cells. Western blot of 2D-BN/SDS-PAGE of mitochondrial proteins purified from highly proliferative TSE breast cancer cells (**A**) and HeLa cells (**B**) using anti-Gls antibody. The western blots suggested one population of Gls oligomers in the first dimension consistent with a Gls tetramer (224 kD), and monomeric GAC (56 kD) in the second dimension.

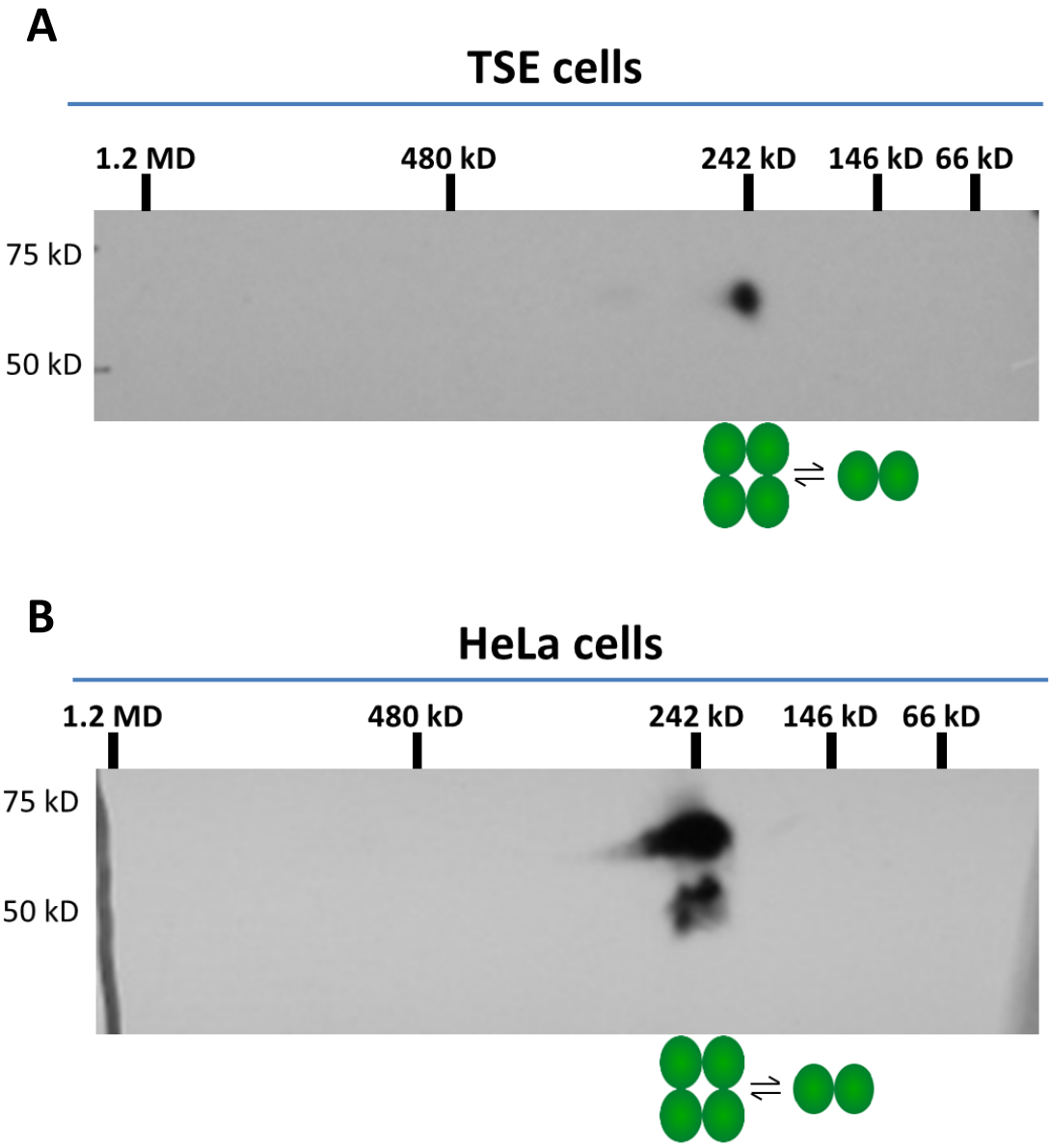
A
TSE cells
1.2 MD
480 kD
242 kD
146 kD
66 kD
75 kD
50 kD
B
HeLa cells
1.2 MD
480 kD
242 kD
146 kD
66 kD
75 kD
50 kD

The detection of a large molecular weight population of GAC suggests that the enzyme is participating in either a multi-protein complex, or it exists as a high molecular weight homo-oligomer. Cassago *et al.* (2013) have characterized an oligomeric form of the GAC enzyme *in vitro*, where GAC tetramers stack end-on-end to form a long linear polymer [33]. They described this GAC polymer formation to be promoted by the allosteric activator, inorganic phosphate, offering the hypothesis that GAC polymer formation is required for activation. However, the results of our native gel assays are not consistent with a polymer form of GAC, but rather suggest that GAC assumes a discrete high molecular weight form. To further demonstrate this, we used purified recombinant GAC to assay its oligomerization, in response to inorganic phosphate, using the native gel assay together with the light scattering technique, SEC-MALS (Figure 5.10A,B). Indeed, we observed a shift in the oligomerization of GAC in response to phosphate using the 1-dimensional BN-PAGE assay; however, the changes in oligomerization represented discrete populations of GAC monomers, dimers, tetramers, and octamers (Figure 5.10A, right most lane). This observation is consistent with the size distribution curve from the analysis of GAC using SEC-MALS in the presence of inorganic phosphate. Here, although a high molecular weight oligomer greater than 1MD is the primary form of GAC, it consists of a polydisperse population of GAC oligomers (Figure 5.10B, compare --- to - -).

FIGURE 5.9 – GAC oligomer distribution in kidney mitochondrial extracts is dependent on metabolic state. (**A**) Diagram of proposed biological function of Gls enzymes in kidney tissues, where glutaminase activity produces ammonia in response to acidotic conditions. Western blot of 2D-BN/SDS-PAGE from purified mitochondrial proteins of kidney tissues from mice either fed *ad libitum* (**B**) or fasted 16 h (**C**) and blotted using an anti-Gls antibody shows a distribution of Gls dimers and tetramers. For mice fasted for 16 h, Gls expression was increased and harbored a significantly greater proportion of Gls tetramers when compared to kidney mitochondria from mice fed *ad libitum*. Both mouse kidney mitochondrial extracts contained a significant population of a large molecular weight species (> 1 MD, marked with a *) that was also increased for mice fasted versus fed.

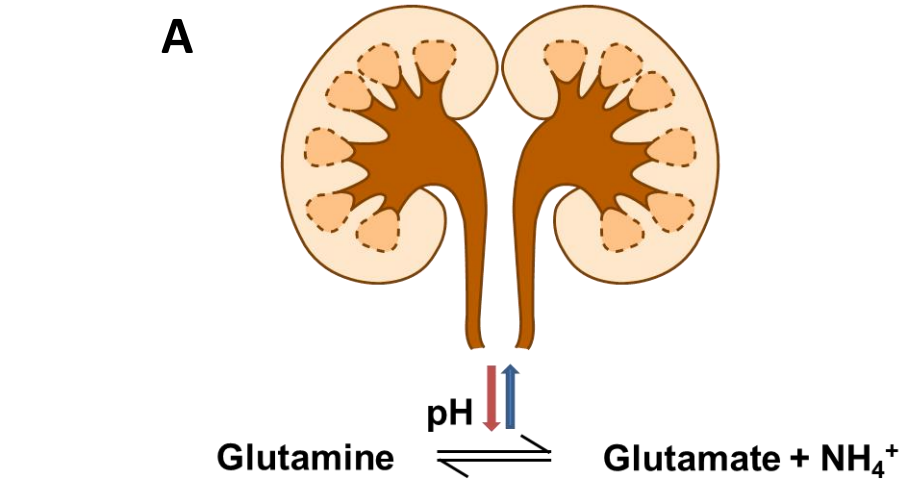
A
pH
Glutamine
Glutamate + NH_4^+

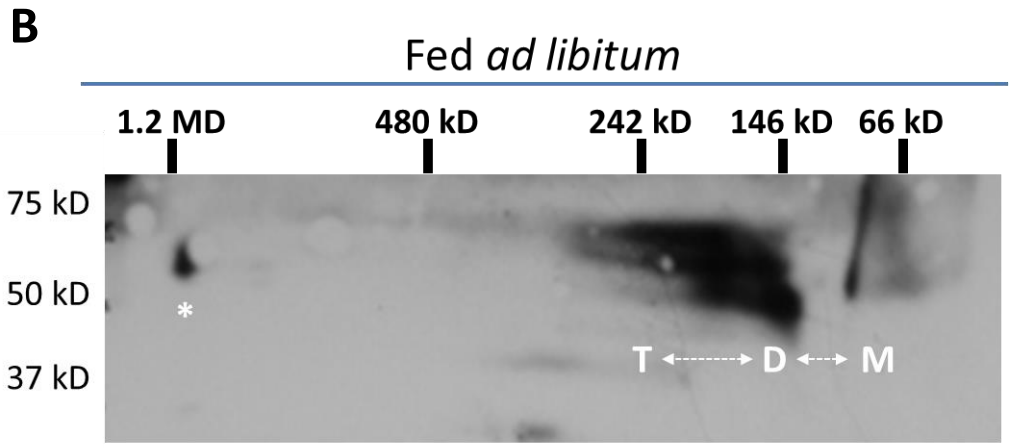
B
Fed *ad libitum*
1.2 MD
480 kD
242 kD
146 kD
66 kD
75 kD
50 kD
37 kD
*
T
D
M

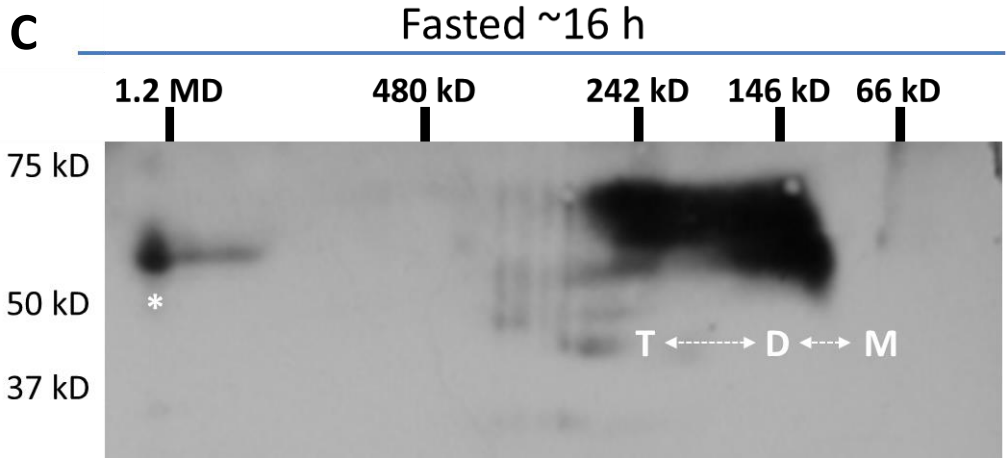
C
Fasted ~16 h
1.2 MD
480 kD
242 kD
146 kD
66 kD
75 kD
50 kD
37 kD
*
T
D
M

FIGURE 5.10 – *In vitro* assays of phosphate induced GAC oligomerization by BN-PAGE and SEC-MALS shows a polydisperse population of oligomers. (**A**) 4-12% BN-PAGE of 5 μg recombinant GAC incubated with increasing concentrations of phosphate and visualized by Coomassie blue protein staining. (**B**) Multi-angle light scattering profiles of 250 μg injection (each) of WT GAC with (—) and without (—) 100 mM phosphate added to the running buffer, where the solid line represents the elution of each species by monitoring refractive index (R.I.), and the broken line designates the calculated molecular weight for the species eluted at that time. Reference lines for the molecular weights of the monomer, dimer, and tetramer forms of the enzyme are included at 58 kD, 116 kD, and 232 kD respectively.

A

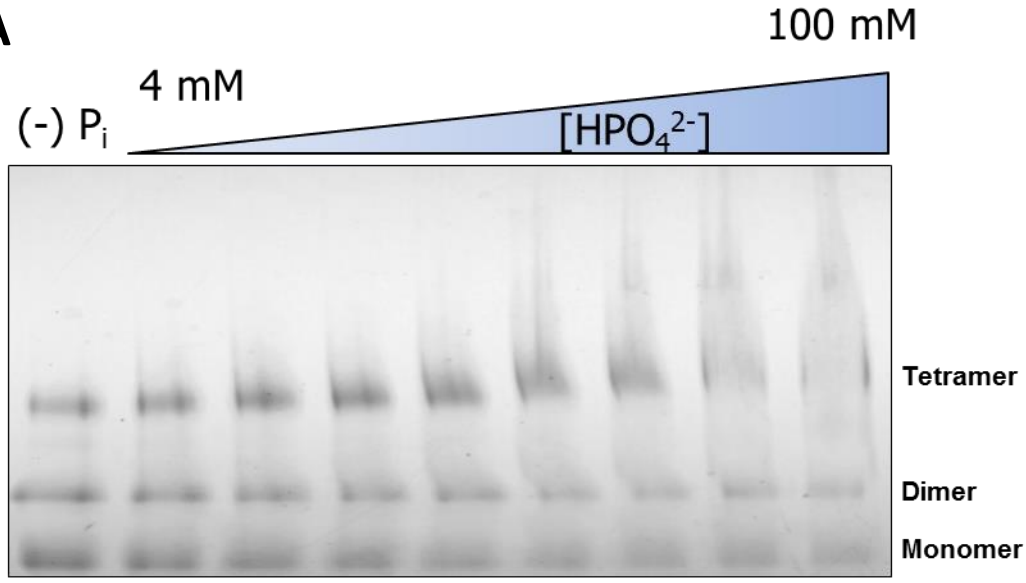
100 mM
4 mM
(-) P_i
$[HPO_4^{2-}]$
Tetramer
Dimer
Monomer

B

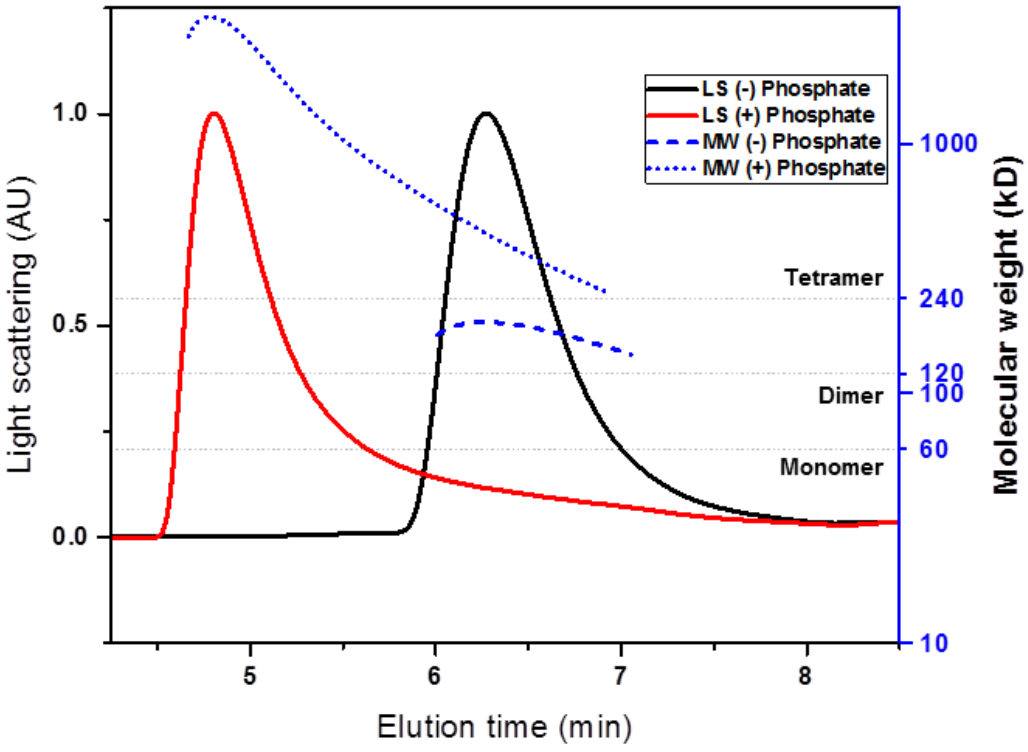
LS (-) Phosphate
LS (+) Phosphate
MW (-) Phosphate
MW (+) Phosphate
Tetramer
Dimer
Monomer
Light scattering (AU)
Molecular weight (kD)
Elution time (min)
1.0
0.5
0.0
1000
240
120
100
60
10
5
6
7
8

5.3.3 Isolation of oligomeric states in mouse tissues correlates with active KGA/GAC tetramers and identifies an active high molecular weight species.

Results from the 2D BN/SDS-PAGE assay of mouse tissues demonstrated a distinct distribution of KGA/GAC within mitochondria. However, while this assay identifies the oligomeric status of KGA/GAC *in vivo*, we were interested in assaying the activity of the isolated enzyme populations. We were particular interested in examining the activity of the high molecular weight enzyme complex. To accomplish this, we developed continuous sucrose density gradient ultracentrifugation techniques to fractionate the detergent solubilized proteins from mouse kidney and liver mitochondria. Here, liver mitochondria were included due to their abundance of KGA/GAC isozymes and physiological role in regulating glutamine levels within plasma. Liver hepatocytes are thought to process the glutamine secreted by muscle tissues to recycle nitrogen, through the coupling of glutamine deamidation to urea production [32]. Therefore, we were interested in comparing the oligomer status of KGA/GAC in both kidney and liver tissues, where they both play vital but distinct roles in glutamine homeostasis.

First, mitochondria were prepared from white lab mice by differential centrifugation as mentioned previously and solubilized in 1% DDM. Solubilized proteins were then added to the top of a continuous sucrose gradient (5%-50%) and centrifuged (>100,000 x g) to separate proteins throughout the density gradient by their molecular size, with larger proteins and protein complexes having the greatest mobility. Equal volume fractions were then analyzed by SDS-PAGE and immunoblotting.

Figures 5.11A,B depicts the results of the sucrose density centrifugation of mouse kidney and liver mitochondria extracts. The distributions of KGA and GAC were dispersed among fractions 2-8 for both tissues, consistent with a dimer to tetramer distribution, when compared to molecular weight markers of control experiments. Additionally, multiple bands of KGA/GAC proteins were identified in the SDS-PAGE gel. The bands were determined to be the previously described high and low molecular weight forms of KGA [34], and the GAC isoform. Each individual band, corresponding to the KGA and GAC proteins, co-purified with its own unique pattern. The high molecular weight band of KGA (Figure 5.11A, top band, inset of lane 3) followed a separate sedimentation pattern (fractions 3-5) when compared to the low molecular weight KGA band, which was distributed through fractions 3-8 (Figure 5.11A, second band, inset of lane 3). Similarly, the GAC protein exhibited a unique sedimentation profile when compared to KGA proteins. These results suggest each form of Gls associates with itself, instead of yielding heterogeneous populations containing both KGA and GAC. This is consistent with previous studies of KGA, where Srinivasan and colleagues (1995) originally described high and low molecular weight KGA forms of this Gls species [34]. Interestingly, *in vitro* FRET assays, as described in Chapter 2.1 above, demonstrate that GAC and KGA are capable of forming heterotetramers when using donor labeled GAC and acceptor labeled KGA (Appendix Figure 7.5A,B).

Similar to the results described in section 5.2.2 above, a discrete population of KGA/GAC was identified in the fraction containing the highest sucrose density, characteristic of a high molecular weight complex (Figures 5.11A,B, white asterisks).

FIGURE 5.11 – Mitochondrial proteins from mouse kidney and liver tissues reveal dimer-to-tetramer distribution and a higher molecular weight species of Gls. 2.5 mg of detergent solubilized proteins from mouse kidney (**A**) and liver (**B**) mitochondria separated by continuous sucrose density gradient. 50 μL of each fraction was separated on a 10% Tricine-SDS PAGE gel and analyzed by immunoblotting against KGA and GAC. Fraction 1 represents the top of the sucrose gradient (i.e. low density) and fraction 13 the bottom (i.e. highest density). Isolated fractions are included to depict the identified proteins, KGA and GAC, using fractions 3 and 5 from mouse kidney and liver.

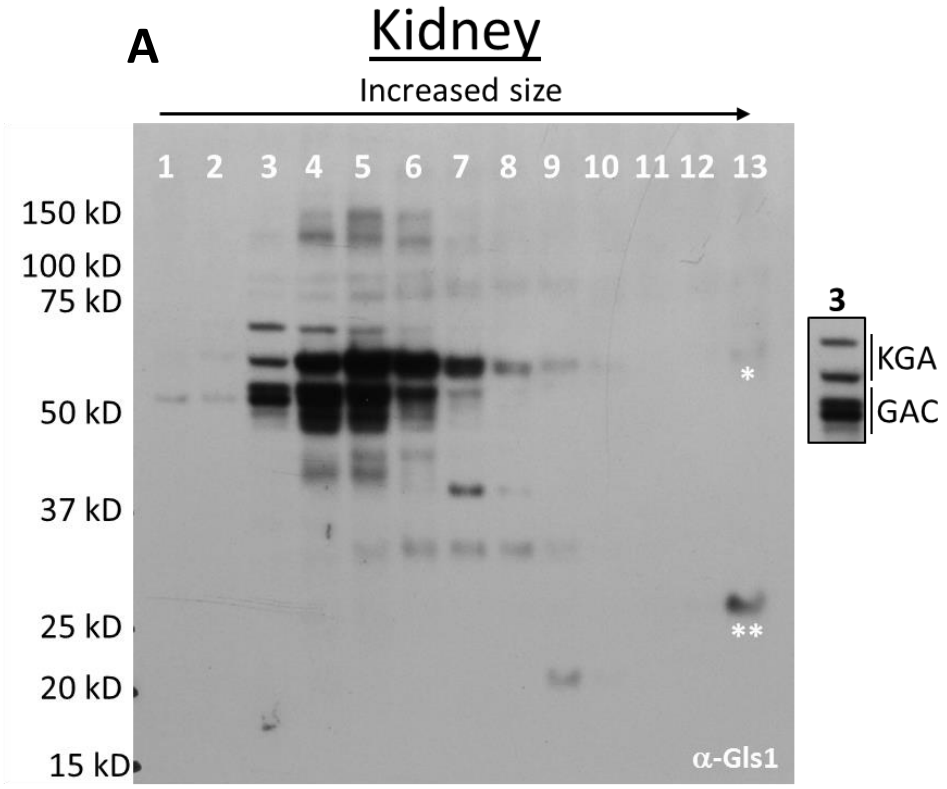
A
Kidney
Increased size
1 2 3 4 5 6 7 8 9 10 11 12 13
150 kD
100 kD
75 kD
50 kD
37 kD
25 kD
20 kD
15 kD
*
**
α-Gls1
3
KGA
GAC

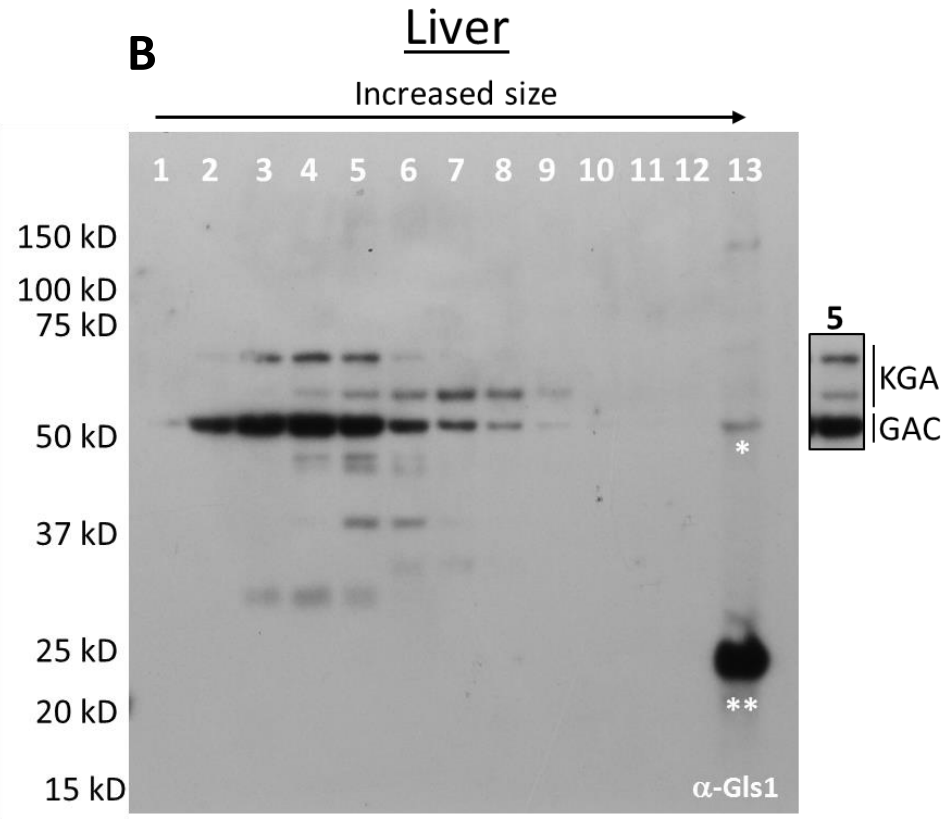
B
Liver
Increased size
1 2 3 4 5 6 7 8 9 10 11 12 13
150 kD
100 kD
75 kD
50 kD
37 kD
25 kD
20 kD
15 kD
*
**
α-Gls1
5
KGA
GAC

When comparing the kidney and liver proteins, we found that this high molecular weight species was enriched in the mitochondria isolated from liver tissue. Additionally, two molecular weight forms were observed in the same fraction, a high molecular weight band (~55 kD) and a low molecular weight band (~25 kD). The 25 kD band is consistently observed in a variety of cancer cell lines when western blotting for KGA/GAC, as well as being present in the inducible Dbl cells. In fact, this 25 kD KGA/GAC fragment was identified in Section 3.2.5 above (Figure 3.9C), where the cross-linking 968 derivative, SU-22, was cross-linked in cells. Moreover, this 25 kD band is exclusively found in the bottom fractions of the continuous sucrose gradient, characteristic of a high molecular weight protein complex.

To determine the KGA/GAC enzyme activities and oligomerization states within these sucrose fractions, each fraction was assayed for glutaminase activity and separated by BN-PAGE (Figure 5.12A-C). Glutaminase activities of each fraction were compared to purified recombinant GAC that was separated using sucrose density gradient sedimentation. As depicted in Figure 5.12A, glutaminase activity was detected within fractions 2-8, agreeing with the distribution from the western blot presented in Figure 5.11A,B. The activities observed in fractions 9-12 for the kidney mitochondria were found to be from the endogenous GDH enzyme, the same enzyme used to read out glutaminase activity through the two-step coupled assay of GAC and GDH. Additionally, this activity profile was in good agreement with fractions for recombinant GAC that were resolved by the same methods. To determine the oligomeric species within each fraction, samples were separated by BN-PAGE and immunoblotted for KGA/GAC. A significantly higher proportion of the KGA/GAC

enzymes were found to be tetramers in the kidney fractions when compared to those of the liver (Figure 5.12B,C). This higher proportion of KGA/GAC tetramers for kidney tissues was in good agreement with the enzymatic activity measured for each fraction, where the kidney fractions had almost twice the glutaminase activity than the fractions from liver (Figure 5.12A, compare (▲) to (■)). However, a significant amount of KGA/GAC was found in a high molecular weight complex in fractions 13 and 14 from liver, and to a much lesser extent in the kidney (Figure 5.12B,C, top insets). Indeed, these fractions contained a measurable glutaminase activity, suggesting this high molecular weight complex (i.e. >1 MD) contains KGA/GAC enzymes that are catalytically active (Figure 5.11A, asterisks). Taken together, these results demonstrate that the KGA/GAC tetramer is the active species in liver and kidney tissues. Additionally, a high molecular weight species of KGA/GAC was identified, that was found to primarily consist of a short 25 kD form, and contained measureable enzyme activity.

FIGURE 5.12 – Glutaminase activity of isolated kidney and liver mitochondrial proteins separated by continuous sucrose gradient centrifugation correlates with tetrameric and high molecular weight oligomeric species of the KGA/GAC proteins. (**A**) Fractions separated by continuous sucrose density centrifugation of 250 mg kidney (▲)and liver (■) detergent solubilized mitochondrial proteins and 5 μg recombinant GAC (●) were assayed for glutaminase activity. (**B**) 50 μg of fractions from (**A**) were separated by 4-12% BN-PAGE and immunoblotted for KGA/GAC proteins. The top of the gel, representing proteins of a greater MW than can be resolved on the gel (i.e. lanes 13 and 14 for kidney and lanes 14 and 15 for liver proteins) are included as insets.

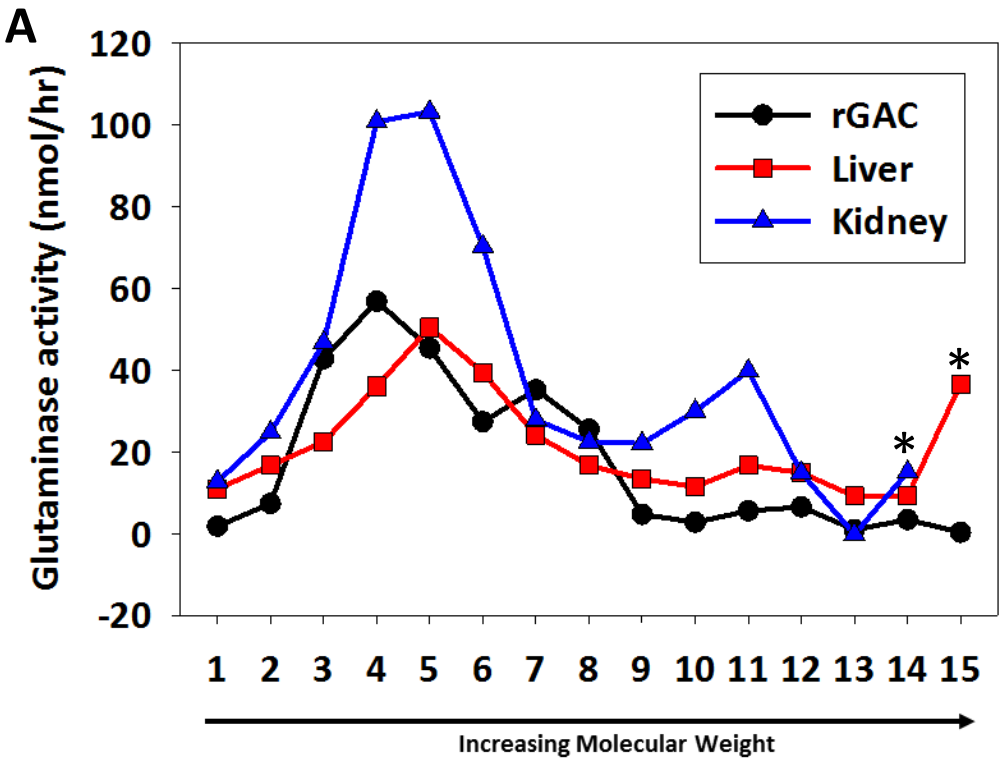
A
Glutaminase activity (nmol/hr)
120
100
80
60
40
20
0
-20
rGAC
Liver
Kidney
*
*
1 2 3 4 5 6 7 8 9 10 11 12 13 14 15
Increasing Molecular Weight

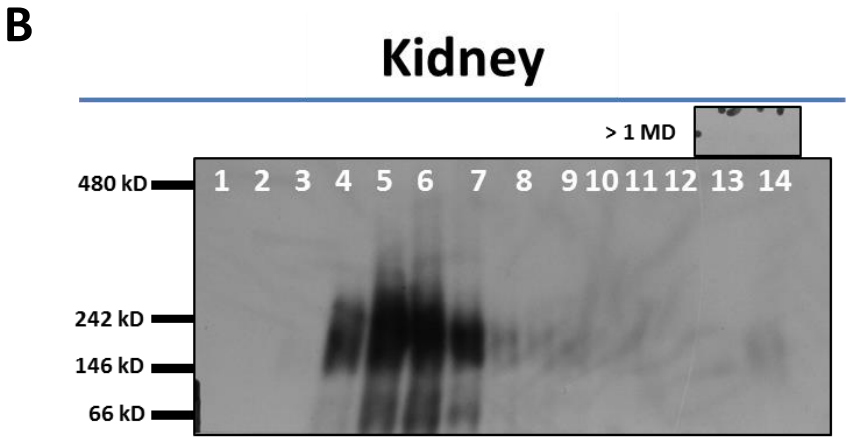
B
Kidney
> 1 MD
480 kD
242 kD
146 kD
66 kD
1 2 3 4 5 6 7 8 9 10 11 12 13 14

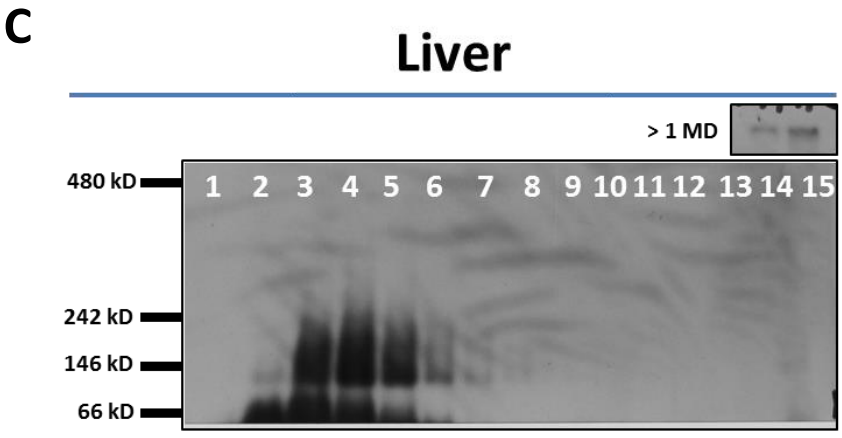
C
Liver
> 1 MD
480 kD
242 kD
146 kD
66 kD
1 2 3 4 5 6 7 8 9 10 11 12 13 14 15

5.4 DISCUSSION

Previous work from our laboratory aimed at identifying inhibitors that specifically block Rho GTPase-dependent transformation, led to the discovery of the benzophenanthridine 968 [35]. Unexpectedly, the protein target for 968 appeared to be a specific splice variant (GAC) of a family of enzymes collectively called glutaminase, that catalyzes the hydrolysis of glutamine to glutamate with the production of ammonia. This highlighted a previously unappreciated connection between the roles of Rho GTPases in driving oncogenic transformation and the regulation of glutamine metabolism. Given the striking specificity that 968 exhibited in its ability to inhibit transformed cells and cancer cells, with little or no effect on their normal cellular counterparts, it was of interest to better understand how 968 functions.

We took advantage of an inducible expression system for oncogenic Dbl that allowed us to temporally control the expression of this upstream activator of Rho GTPases in a well-defined manner. Using this system, we were able to establish a direct correlation between the ability of 968 to prevent a key outcome of Dbl-induced transformation, namely the loss of cell-cell contact inhibition, and to specifically inhibit glutaminolysis. Thus, the inhibitory actions of 968 upon oncogenic transformation appear to be a direct outcome of its ability to interfere with glutamine metabolism. We go on to show that this increased reliance on glutamine metabolism in Dbl-transformed cells results from the direct activation of the GAC enzyme, through the formation of active GAC tetramers within mitochondria. Taken together, we found that the induction of the Dbl oncogene results in an increased expression of GAC within mitochondria, where GAC forms active tetramers, and converts imported

glutamine to glutamate in order to support TCA cycle function. Lastly, this increased glutamine metabolism was directly assayed in cells, where it is indeed potently inhibited by compound 968.

In efforts to extend these investigations of the oligomerization status of KGA/GAC directly in cells, we found the exclusive expression of GAC tetramers in the highly proliferative TSE and HeLa cancer cell lines. These cells have been previously shown to exhibit a high degree of mitochondrial glutaminase expression and glutamine dependency [16], [30], which is consistent with the tetrameric GAC species being the predominant oligomeric form. The exclusive isolation of GAC tetramers in these highly proliferative cells is a surprising finding, and suggests the oligomerization status of GAC is highly regulated within the mitochondria.

The physiological role that mitochondrial glutaminase plays within kidney tissues has been shown to prompt a response to acidotic conditions, through the release of NH_3 as an outcome of the glutaminase reaction [32]. Here, we established a minor acidotic condition through the fasting of mice, thereby inducing a metabolic switch to ketogenesis. Taking advantage of this method, we were able to examine the proportion of KGA/GAC oligomers from isolated mouse tissues and their response to fed and fasted states. Upon fasting, we observed not only an increase in KGA/GAC expression, but a significant shift toward the tetrameric state. Furthermore, we identified a large molecular weight complex (>1 MD) that was up-regulated in the fasted state. Our results show that this high molecular weight complex does not appear to be the same as the supra-oligomeric species of GAC that forms *in vitro*, as

demonstrated previously by Cassago and colleagues (2013) by electron microscopy of phosphate stimulated GAC [33].

As presented in Chapter 2 above, we originally described the dimer-to-tetramer transition to be required for the activation of GAC *in vitro*, and were therefore interested in determining whether this transition is physiologically important *in vivo*. Having identified the oligomeric GAC species from mouse kidneys, we sought to resolve each oligomeric form of the enzyme, so as to assay their activities, and in particular, determine the activity of the high molecular weight complex. The separation of mitochondrial proteins by continuous sucrose gradient centrifugation techniques proved useful for the isolation of native protein oligomers, where the activity of each fraction could be assayed for activity and examined by native BN-PAGE and immunoblotting. The activity profile of isolated fractions from mouse kidney and liver tissues matched the distribution of KGA/GAC within the density gradient, and was directly related to the tetrameric enzyme population within each fraction. These results show directly that the oligomerization status of KGA/GAC is indeed dependent on KGA/GAC tetramer formation within cells, and in good agreement with the biophysical data from *in vitro* experiments presented in Chapters 2, 3 and 4 above.

To our surprise, the high molecular weight form of GAC harbored significant enzymatic activity. Given the data presented here, it is our speculation that KGA/GAC enzymes are in fact participating in a large molecular weight complex, whose principal components have not yet been identified. Interestingly, the known native molecular weight complexes within these fractions are pyruvate dehydrogenase and α-

ketoglutarate dehydrogenase, presenting an attractive hypothesis where glutaminase, the first enzyme responsible for glutamine-fueled anaplerosis, engages in cross-talk with the principal dehydrogenases within the mitochondria that act as gate-keepers for carbon entry to the TCA cycle.

5.5 REFERENCES

[1] S. Y. Lunt and M. G. V. Heiden, "Aerobic Glycolysis: Meeting the Metabolic Requirements of Cell Proliferation," *Annu. Rev. Cell Dev. Biol.*, vol. 27, no. 1, pp. 441–464, 2011.

[2] K. E. Wellen and C. B. Thompson, "A two-way street: reciprocal regulation of metabolism and signalling," *Nat. Rev. Mol. Cell Biol.*, vol. 13, no. 4, pp. 270–276, Apr. 2012.

[3] M. D. Hirschey, R. J. DeBerardinis, A. M. E. Diehl, J. E. Drew, C. Frezza, M. F. Green, L. W. Jones, Y. H. Ko, A. Le, M. A. Lea, J. W. Locasale, V. D. Longo, C. A. Lyssiotis, E. McDonnell, M. Mehrmohamadi, G. Michelotti, V. Muralidhar, M. P. Murphy, P. L. Pedersen, B. Poore, L. Raffaghello, J. C. Rathmell, S. Sivanand, M. G. V. Heiden, K. E. Wellen, and T. V. Team, "Dysregulated metabolism contributes to oncogenesis," *Semin. Cancer Biol.*

[4] R. J. DeBerardinis, J. J. Lum, G. Hatzivassiliou, and C. B. Thompson, "The Biology of Cancer: Metabolic Reprogramming Fuels Cell Growth and Proliferation," *Cell Metab.*, vol. 7, no. 1, pp. 11–20, Jan. 2008.

[5] P. S. Ward and C. B. Thompson, "Metabolic Reprogramming: A Cancer Hallmark Even Warburg Did Not Anticipate," *Cancer Cell*, vol. 21, no. 3, pp. 297–308, Mar. 2012.

[6] A. S. Krall and H. R. Christofk, "Rethinking glutamine addiction," *Nat. Cell Biol.*, vol. 17, no. 12, pp. 1515–1517, Dec. 2015.

[7] D. R. Wise and C. B. Thompson, "Glutamine addiction: a new therapeutic target in cancer," *Trends Biochem. Sci.*, vol. 35, no. 8, pp. 427–433, Aug. 2010.

[8] T. C. Alves, R. L. Pongratz, X. Zhao, O. Yarborough, S. Sereda, O. Shirihai, G. W. Cline, G. Mason, and R. G. Kibbey, "Integrated, Step-Wise, Mass-Isotopomeric Flux Analysis of the TCA Cycle," *Cell Metab.*

[9] "Metabolite concentrations, fluxes and free energies imply efficient enzyme usage," *Nat. Chem. Biol.*

[10] J. Son, C. A. Lyssiotis, H. Ying, X. Wang, S. Hua, M. Ligorio, R. M. Perera, C. R. Ferrone, E. Mullarky, N. Shyh-Chang, Y. Kang, J. B. Fleming, N. Bardeesy, J. M. Asara, M. C. Haigis, R. A. DePinho, L. C. Cantley, and A. C. Kimmelman, "Glutamine supports pancreatic cancer growth through a KRAS-regulated metabolic pathway," *Nature*, vol. 496, no. 7443, pp. 101–105, Apr. 2013.

[11] A. Le, A. N. Lane, M. Hamaker, S. Bose, A. Gouw, J. Barbi, T. Tsukamoto, C. J. Rojas, B. S. Slusher, H. Zhang, L. J. Zimmerman, D. C. Liebler, R. J. C. Slebos, P. K. Lorkiewicz, R. M. Higashi, T. W. M. Fan, and C. V. Dang, "Glucose-Independent Glutamine Metabolism via TCA Cycling for Proliferation and Survival in B Cells," *Cell Metab.*, vol. 15, no. 1, pp. 110–121, Jan. 2012.

[12] P. A. Gameiro, J. Yang, A. M. Metelo, R. Pérez-Carro, R. Baker, Z. Wang, A. Arreola, W. K. Rathmell, A. Olumi, P. López-Larrubia, G. Stephanopoulos, and O. Iliopoulos, "In Vivo HIF-Mediated Reductive Carboxylation Is Regulated by Citrate Levels and Sensitizes VHL-Deficient Cells to Glutamine Deprivation," *Cell Metab.*, vol. 17, no. 3, pp. 372–385, Mar. 2013.

[13] R. C. Sun and N. C. Denko, “Hypoxic Regulation of Glutamine Metabolism through HIF1 and SIAH2 Supports Lipid Synthesis that Is Necessary for Tumor Growth,” *Cell Metab.*, vol. 19, no. 2, pp. 285–292, Feb. 2014.
[14] D. R. Wise, P. S. Ward, J. E. S. Shay, J. R. Cross, J. J. Gruber, U. M. Sachdeva, J. M. Platt, R. G. DeMatteo, M. C. Simon, and C. B. Thompson, “Hypoxia promotes isocitrate dehydrogenase-dependent carboxylation of α-ketoglutarate to citrate to support cell growth and viability,” *Proc. Natl. Acad. Sci.*, vol. 108, no. 49, pp. 19611–19616, Dec. 2011.
[15] D. Herranz, A. Ambesi-Impiombato, J. Sudderth, M. Sánchez-Martín, L. Belver, V. Tosello, L. Xu, A. A. Wendorff, M. Castillo, J. E. Haydu, J. Márquez, J. M. Matés, A. L. Kung, S. Rayport, C. Cordon-Cardo, R. J. DeBerardinis, and A. A. Ferrando, “Metabolic reprogramming induces resistance to anti-NOTCH1 therapies in T cell acute lymphoblastic leukemia,” *Nat. Med.*, vol. 21, no. 10, pp. 1182–1189, Oct. 2015.
[16] M. J. Lukey, K. S. Greene, J. W. Erickson, K. F. Wilson, and R. A. Cerione, “The oncogenic transcription factor c-Jun regulates glutaminase expression and sensitizes cells to glutaminase-targeted therapy,” *Nat. Commun.*, vol. 7, p. 11321, Apr. 2016.
[17] P. Gao, I. Tchernyshyov, T.-C. Chang, Y.-S. Lee, K. Kita, T. Ochi, K. I. Zeller, A. M. De Marzo, J. E. Van Eyk, J. T. Mendell, and C. V. Dang, “c-Myc suppression of miR-23a/b enhances mitochondrial glutaminase expression and glutamine metabolism,” *Nature*, vol. 458, no. 7239, pp. 762–765, Apr. 2009.
[18] M. G. Rathore, A. Saumet, J.-F. Rossi, C. de Bettignies, D. Tempé, C.-H. Lecellier, and M. Villalba, “The NF-κB member p65 controls glutamine metabolism through miR-23a,” *Int. J. Biochem. Cell Biol.*, vol. 44, no. 9, pp. 1448–1456, Sep. 2012.
[19] G. Qing, B. Li, A. Vu, N. Skuli, Z. E. Walton, X. Liu, P. A. Mayes, D. R. Wise, C. B. Thompson, J. M. Maris, M. D. Hogarty, and M. C. Simon, “ATF4 Regulates MYC-Mediated Neuroblastoma Cell Death upon Glutamine Deprivation,” *Cancer Cell*, vol. 22, no. 5, pp. 631–644, Nov. 2012.
[20] C. Yang, J. Sudderth, T. Dang, R. G. Bachoo, J. G. McDonald, and R. J. DeBerardinis, “Glioblastoma Cells Require Glutamate Dehydrogenase to Survive Impairments of Glucose Metabolism or Akt Signaling,” *Cancer Res.*, vol. 69, no. 20, pp. 7986–7993, Oct. 2009.
[21] B. Li and M. C. Simon, “Molecular Pathways: Targeting MYC-induced Metabolic Reprogramming and Oncogenic Stress in Cancer,” *Clin. Cancer Res.*, vol. 19, no. 21, pp. 5835–5841, Nov. 2013.
[22] D. R. Wise, R. J. DeBerardinis, A. Mancuso, N. Sayed, X.-Y. Zhang, H. K. Pfeiffer, I. Nissim, E. Daikhin, M. Yudkoff, S. B. McMahon, and C. B. Thompson, “Myc regulates a transcriptional program that stimulates mitochondrial glutaminolysis and leads to glutamine addiction,” *Proc. Natl. Acad. Sci.*, vol. 105, no. 48, pp. 18782–18787, Dec. 2008.
[23] N. M. Anderson, D. Li, H. L. Peng, F. J. F. Laroche, M. R. Mansour, E. Gjini, M. Aioub, D. J. Helman, J. E. Roderick, T. Cheng, I. Harrold, Y. Samaha, L. Meng, A. Amsterdam, D. S. Neuberg, T. T. Denton, T. Sanda, M. A. Kelliher, A.

Singh, A. T. Look, and H. Feng, “The TCA cycle transferase DLST is important for MYC-mediated leukemogenesis,” *Leukemia*, Feb. 2016.

[24] A. Csibi, G. Lee, S.-O. Yoon, H. Tong, D. Ilter, I. Elia, S.-M. Fendt, T. M. Roberts, and J. Blenis, “The mTORC1/S6K1 Pathway Regulates Glutamine Metabolism through the eIF4B-Dependent Control of c-Myc Translation,” *Curr. Biol.*, vol. 24, no. 19, pp. 2274–2280, Oct. 2014.

[25] A. G. Thomas, C. M. O’Driscoll, J. Bressler, W. E. Kaufmann, C. J. Rojas, and B. S. Slusher, “Small molecule glutaminase inhibitors block glutamate release from stimulated microglia,” *Biochem. Biophys. Res. Commun.*, vol. 443, no. 1, pp. 32–36, Jan. 2014.

[26] “Blue native PAGE : Article : Nature Protocols,” *Nat Protoc.*, vol. 1, no. 1, pp. 418–428, Jun. 2006.

[27] L. G. J. Nijtmans, N. S. Henderson, and I. J. Holt, “Blue Native electrophoresis to study mitochondrial and other protein complexes,” *Methods*, vol. 26, no. 4, pp. 327–334, Apr. 2002.

[28] L.-J. Yan and M. J. Forster, “Resolving mitochondrial protein complexes using non-gradient blue native polyacrylamide gel electrophoresis,” *Anal. Biochem.*, vol. 389, no. 2, pp. 143–149, Jun. 2009.

[29] C. Frezza, S. Cipolat, and L. Scorrano, “Organelle isolation: functional mitochondria from mouse liver, muscle and cultured filroblasts,” *Nat. Protoc.*, vol. 2, no. 2, pp. 287–295, Feb. 2007.

[30] S. L. Colombo, M. Palacios-Callender, N. Frakich, S. Carcamo, I. Kovacs, S. Tudzarova, and S. Moncada, “Molecular basis for the differential use of glucose and glutamine in cell proliferation as revealed by synchronized HeLa cells,” *Proc. Natl. Acad. Sci.*, vol. 108, no. 52, pp. 21069–21074, Dec. 2011.

[31] N. P. Curthoys, T. Kuhlenschmidt, and S. S. Godfrey, “Regulation of renal ammoniagenesis: Purification and characterization of phosphate-dependent glutaminase from rat kidney,” *Arch. Biochem. Biophys.*, vol. 174, no. 1, pp. 82–89, May 1976.

[32] N. P. Curthoys and M. Watford, “Regulation of Glutaminase Activity and Glutamine Metabolism,” *Annu. Rev. Nutr.*, vol. 15, no. 1, pp. 133–159, 1995.

[33] A. P. S. Ferreira, A. Cassago, K. de A. Gonçalves, M. M. Dias, D. Adamoski, C. F. R. Ascenção, R. V. Honorato, J. F. de Oliveira, I. M. Ferreira, C. Fornezari, J. Bettini, P. S. L. Oliveira, A. F. P. Leme, R. V. Portugal, A. L. B. Ambrosio, and S. M. G. Dias, “Active Glutaminase C Self-assembles into a Supratetrameric Oligomer That Can Be Disrupted by an Allosteric Inhibitor,” *J. Biol. Chem.*, vol. 288, no. 39, pp. 28009–28020, Sep. 2013.

[34] M. Srinivasan, F. Kalousek, and N. P. Curthoys, “In Vitro Characterization of the Mitochondrial Processing and the Potential Function of the 68-kDa Subunit of Renal Glutaminase,” *J. Biol. Chem.*, vol. 270, no. 3, pp. 1185–1190, Jan. 1995.

[35] J.-B. Wang, J. W. Erickson, R. Fuji, S. Ramachandran, P. Gao, R. Dinavahi, K. F. Wilson, A. L. B. Ambrosio, S. M. G. Dias, C. V. Dang, and R. A. Cerione, “Targeting Mitochondrial Glutaminase Activity Inhibits Oncogenic Transformation,” *Cancer Cell*, vol. 18, no. 3, pp. 207–219, Sep. 2010.

[36] C. Frezza, S. Cipolat, and L. Scorrano, “Organelle isolation: functional mitochondria from mouse liver, muscle and cultured filroblasts,” *Nat. Protoc.*, vol. 2, no. 2, pp. 287–295, Feb. 2007.
[37] H. Schagger, “Tricine-SDS-PAGE : Abstract : Nature Protocols,” *Nat Protoc.*, vol. 1, no. 1, pp. 16–22, Jun. 2006.

CHAPTER SIX

Conclusions and future directions

Back to the Future: A new paradigm in cancer cell biology

The connection between signal transduction pathways that give rise to cancer and altered cellular metabolism has presented cancer researchers a new context for developing therapeutic approaches. Recent studies focusing on the metabolic requirements of cancer cells have led to new paradigms in cancer biology, revealing some cancers to be bona fide metabolic diseases. Many solid tumors and cancer cell lines exhibit a highly elevated requirement for an exogenous supply of nutrients to support their unregulated proliferation and metabolic demands. Therefore, the direct targeting of metabolic enzymes presents a new strategy that holds great promise for future therapeutics. Of the metabolic enzymes that have been identified as potential drug targets, the mitochondrial enzyme glutaminase represents one of significant interest. This is due to the enzyme's critical role in the first step of glutaminolysis, a process that is upregulated in proliferative cells having aberrant glycolytic flux (i.e. the Warburg effect) to supply the TCA cycle, depleted of glucose-derived carbon, with a glutamine-derived source.

Our interest in mitochondrial glutaminase was driven by the identification of a small molecule that potently inhibited cells transformed by hyperactive Rho-GTPases, but not their non-transformed counterparts. The target of this small molecule, a dibenzophenanthridine designated as compound 968, was determined to be the alternatively spliced isoform of the kidney-type glutaminase, glutaminase C (GAC). Compound 968 was shown to be an allosteric inhibitor, non-competitive with neither

glutamine or allosteric activators like inorganic phosphate. However, there was still much we did not understand regarding how this inhibitor blocks enzyme activity, nor the detailed mechanisms underlying enzyme activation *in vitro* or within transformed cells and cancer cells. Therefore, the motivation for my research was to gain further mechanistic insights into the activation and inhibition of GAC *in vitro*, and to complement this information with studies of glutamine metabolism in transformed/cancer cells.

The glutaminase isoforms KGA and GAC were suggested by early studies to require tetramer formation to become activated, although this had never been definitively demonstrated. In Chapter Two, I describe a fluorescence resonance energy transfer (FRET) assay to study the formation of GAC tetramers and the effects that allosteric activators and inhibitors have on GAC oligomerization. I demonstrate the requirement of tetramer formation for GAC activity, and report a defined dissociation constant that reflects the GAC dimer-to-tetramer transition. Additionally, I demonstrate that allosteric activators, namely inorganic phosphate, further enhance GAC tetramer formation, and propose a model where phosphate binding drives tetramer formation to stimulate enzyme activity. In contrast, two distinct classes of GAC allosteric inhibitors, the bis-thiadiazoles (for which BPTES is the prototype) and the benzophenanthridines (with compound 968 being the prototype), exert distinctly different effects. The BPTES-class of inhibitors induced the rapid formation of a stable BPTES-bound GAC tetrameric complex, whereas 968 neither promoted nor inhibited tetramer formation. Instead, 968 was shown to affect the emission of a fluorescence reporter group, providing a direct read-out for 968 binding to GAC. This

binding assay, together with the development of oligomeric-deficient GAC mutants, trapped in either the dimeric or monomeric states, was used to demonstrate the preferential binding by 968 to the monomeric form of GAC. Therefore, we propose that 968 acts by interfering with oligomer activation through its binding to the GAC monomer.

The real-time 968 binding assay, described in Chapter Two, was then adapted to a high-throughput coupled binding and inhibition assay to screen novel 968-analogues, described in Chapter Four. This simultaneous binding and inhibition assay proved to be a reliable read-out for dibenzophenanthridine derivatives, and lead to the identification of a new lead scaffold (SU-29). Additionally, 968-analogues were generated that harbored useful physical properties, such as intrinsic fluorescence (SU-14), and photo cross-linking abilities (SU-22 and SU-24). These tool compounds were used to covalently modify GAC *in vitro* and in transformed cells and then monitor the incorporated fluorescence. The cross-linking studies *in vitro* provided evidence for a site-specific covalent cross-linking of the 968-derivative that was localized within the monomer-monomer interface of GAC, consistent with 968 binding to the monomeric form of the enzyme. Furthermore, this cross-linked GAC established the ability of a 968-analogue to drive the GAC monomer to form a dimer. This evidence leads to the proposed model in which the binding of 968 to the monomeric form of GAC induces the formation of a very stable complex of 968-bound GAC dimer. Further studies using the SU-22 cross-linker in Dbl-transformed cells not only identified a cross-linked protein, subsequently identified as mitochondrial GAC, but localized the small molecule within mitochondria, consistent with GAC being the cellular target of 968.

In order to examine more closely the mechanism by which the BPTES-class of inhibitors exert their effects on GAC activity, I used tryptophan mutagenesis to install a fluorescence reporter group within a critical loop, referred to as the activation loop, where BPTES binds (Chapter Four). I then took advantage of this novel GAC tryptophan mutant (F327W) to monitor the binding of BPTES, and the best-in-class BPTES analogue, CB-839, and determine their respective dissociation constants. Interestingly, I discovered that allosteric anionic activators (i.e. inorganic phosphate and sulfate) induced the opposite effect on the F327W fluorescence from BPTES-like inhibitors, i.e. a fluorescence enhancement rather than a fluorescence quenching. Taken together, these studies describe direct read-outs for the binding of allosteric activators and inhibitors to the activation loop of GAC, demonstrating how their influence on the conformation of this loop is specific to their abilities to activate or inhibit the enzyme. These results reveal the prerequisite of GAC to form tetramers to enable either activators or BPTES-like inhibitors to bind to the enzyme, and present a strategy for the screening of new activators and inhibitors.

Building upon these studies that highlight the importance of GAC oligomer dynamics *in vitro*, I was interested in how GAC becomes activated in cells. To examine this, I described the stimulation of glutaminolysis and glutamine-fueled anaplerosis in an inducible model cell system, where mouse embryonic fibroblasts (MEFs) were transformed by oncogenic Dbl, which acts to stimulate Rho-GTPase signaling. The increase in glutaminolysis was indeed sensitive to treatment with 968, which potently inhibits Dbl-induced transformation in these cells. To translate the observations of the *in vitro* studies presented in Chapter Two, where the formation of a

GAC tetramer was required for activation, into this inducible-cell system, I developed methods to probe the oligomeric status of GAC in cells. Using native gels to identify protein complexes, I found that the outcome of Dbl-induction both increases GAC expression and induces GAC tetramer formation, whereas only the dimeric form of GAC was isolated from un-induced cells. These studies set the stage for investigations in well-known human cancer cell lines. Using the highly proliferative and glutamine-addicted TSE breast cancer and HeLa cervical carcinoma cells, I isolated the active tetrameric form of GAC, demonstrating the utility of this method for probing the activation status in transformed cells. I extended these studies into whole organ tissues, where GAC plays an essential physiological role for regulating glutamine homeostasis, and readily identified the monomeric, dimeric, tetrameric, and a high molecular weight (>1 MD) complex form.

In summary, this thesis describes the oligomerization of GAC *in vitro* and *in vivo*, and highlights the impact allosteric activators and distinct classes of allosteric inhibitors have on the oligomeric transitions. I present strategies for the screening of both the 968-class and BPTES-class inhibitors, as well as allosteric activators, such as inorganic phosphate. Finally, I demonstrate methods to investigate the oligomeric status of GAC directly in cells and tissues, translating the biophysical studies of purified GAC presented here into the relevant biological context of glutamine dependent cancer cells.

Future Directions

The studies described in this thesis point to multiple areas worthy of further investigation. One aspect warranting further development would build upon the

mechanistic studies described in Chapters Two, Three, and Five concerning 968's mode of action, in order to optimize a 968 analog that could be used in cell culture and tumor models. Efforts made in this direction would further this cancer targeting strategy, with the hope of developing a new therapeutic for clinical trials. A significant challenge for advancing this drug scaffold has been the lack of optimization of the chemical space to develop a stable, bioavailable drug. There is also significant potential for the utility of the chemical tool compounds, described in Chapter Three, to gain insight as to the specific binding interaction of 968 at the monomer-monomer interface of GAC, as well as for a broader picture as to the localization of this small molecule in a variety of cell lines.

Another aspect of this thesis that could be expanded upon would be the utility of the novel tryptophan mutant (F327W GAC), described in Chapter Four, to screen BPTES-analogues, as well as search for new allosteric activators. The physiological role phosphate plays in the activation of GAC *in vivo* remains uncertain, where lines of evidence suggest other anionic ligands (i.e. intracellular metabolites) could potentiate GAC activity in cells. Furthermore, point mutations, included within the F327W background, could be introduced to investigate their impact on the binding of allosteric activators, in the hope of gaining more detailed information regarding phosphate binding and subsequent activation. Lastly, this tryptophan substitution and the readout it provides would be useful for comparing the two glutaminase isozymes, the liver-type (Gls2) and kidney-types (Gls), for their ability to bind allosteric activators and inhibitors. Both Gls2 and Gls are uniquely expressed in different cell types and harbor different activation profiles. Their respective contributions in

supporting the cancer phenotype promises to be an area of active research in the years to come.

Lastly, the methods for investigating the oligomeric forms of KGA/GAC in cells and tissues, described in Chapter Five, present a particularly exciting opportunity for identifying potential binding partners and the constituent subunits in the high molecular weight GAC complex. Metabolic enzymes are known to participate outside their canonical roles as enzymes acting on metabolites, through regulating critical cellular functions through protein-protein interactions. The cellular signaling networks connecting intracellular metabolism, glutamine dependent growth, and cell homeostasis are complex, and represents an area ripe for new important discoveries regarding the nature of cancer cell growth and survival.

APPENDIX ONE

Complementary data

FIGURE A7.1 – Partial trypsin digestion of 488-labeled GAC. WT GAC (800 μg) was incubated with porcine trypsin (37.5 μg) 1 h on ice and quenched with soybean trypsin inhibitor (37.5 μg). (**A**) The reaction mixture was separated by a superdex 75 10/300 GL gel filtration column equilibrated with 20 mM Tris-HCl pH 8.4, 100 mM NaCl, 1 mM NaN_3. Peaks were monitored by UV/vis absorbance at 280 nm (protein) and 490 nm (488-probe). Fractions were collected (1 mL) and pooled to give 5 fractions (depicted by dashed red lines). (**B**) Fractions from (**A**) were concentrated to 100 μL, and 25 μL aliquots were analyzed by SDS-PAGE along with unlabeled and 488-labeled GAC (5 ug) that were not cleaved by trypsin. Bands were visualized using UV-illumination and western blotting (**C**) using an antibody prepared within our laboratory that recognizes the C-terminus of GAC (approx. residues 500-520). A band that was visualized by both UV-illumination (i.e. 488-fluorescence) and immunoblotting was submitted to the Cornell Proteomics Core and analyzed by LC-MS/MS. (**D**) Peptides identified from the submitted bands are highlighted in red, and the structural region that correlates to the observed MW by SDS-PAGE and residues identified is represented in **(E)**, red dashed circle.

A

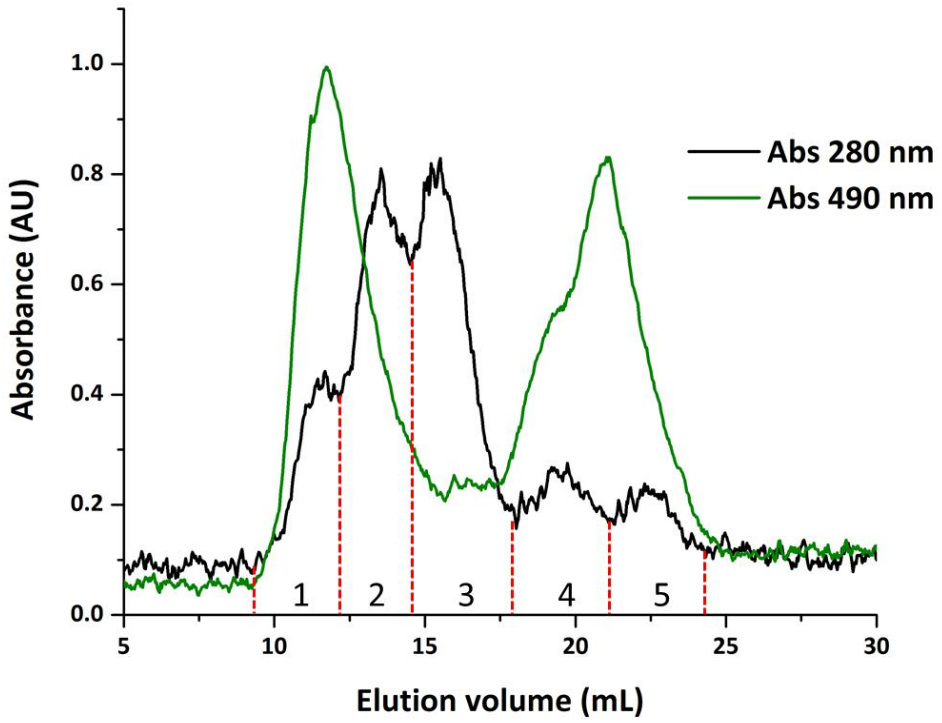
Absorbance (AU)
1.0
0.8
0.6
0.4
0.2
0.0
5
10
15
20
25
30
Elution volume (mL)
Abs 280 nm
Abs 490 nm
1
2
3
4
5

B

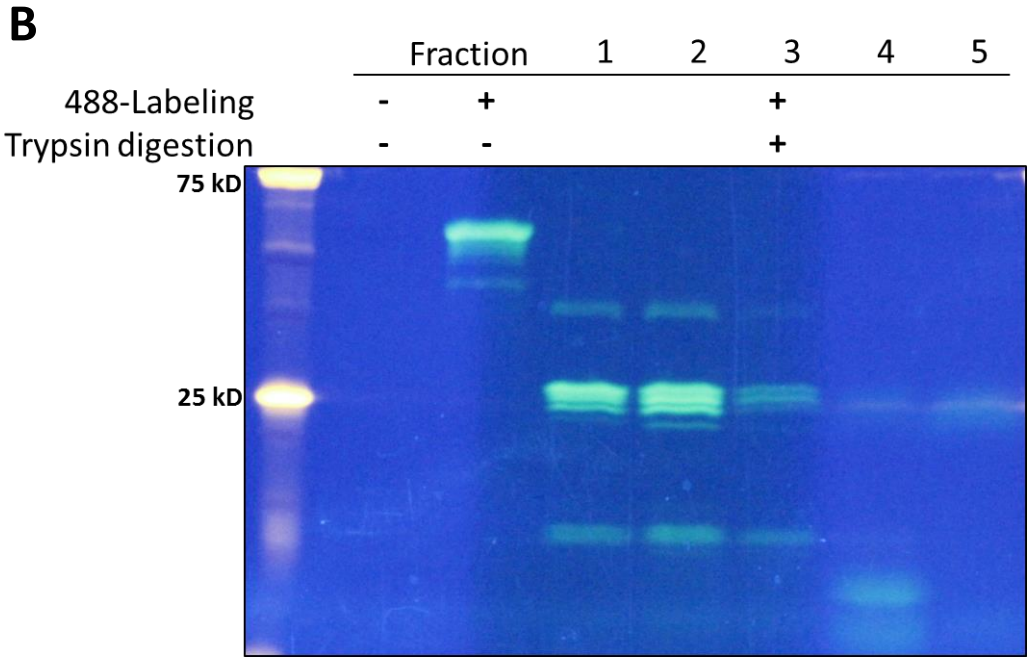
Fraction
1
2
3
4
5
488-Labeling
- + +
Trypsin digestion
- - +
75 kD
25 kD

C

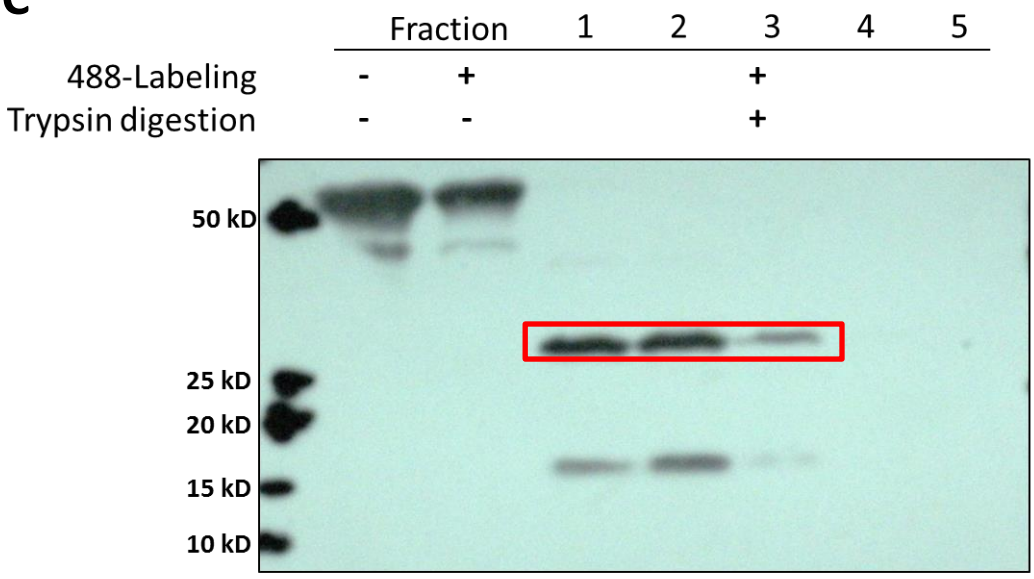

D

Matched peptides shown in **Bold Red**

```
  1 MMRLRGSAML RELLLRPPAA VGAVLRRAQP LGTLCRRPRG GSRPTAGLVA
 51 AARLHPWWGG GGRAKGPGAG GLSSSPSEIL QELGKGGTPP QQQQQQQQQP
101 GASPPAAPGP KDSPGETDAF GNSEGKEMVA AGDNKIKQGL LPSLEDLLFY
151 TIAEGQEKIP VHKFITALKS TGLRTSDPRL KECMDMLRLT LQTTSDGVML
201 DKDLFKKCVQ SNIVLLTQAF RRKFVIPDFM SFTSHIDELY ESAKKQSGGK
251 VADYIPQLAK FSPDLWGVSV CTVDGQRHSI GDTKVPFCLQ SCVKPLKYAI
301 AVNDLGTEYV HRYVGKEPSG LRFNKLFLNE DDKPHNPMVN AGAIVVTSLI
351 KQGVNNAEKF DYVMQFLNKM AGNEYVGFSN ATFQSERESG DRNFAIGYYL
401 KEKKCFPEGT DMVGILDFYF QLCSIEVTCE SASVMAATLA NGGFCPITGE
451 RVLSPEAVRN TLSLMHSCGM YDFSGQFAFH VGLPAKSGVA GGILLVVPNV
501 MGMMCWSPPL DKMGNSVKGI HFCHDLVSLC NFHNYDNLRH FAKKLDPRRE
551 GGDQRVKSVI NLLFAAYTGD VSALRRFALS AMDMEQRDYD SRTALHVAAA
601 EGHVEVVKFL LEACKVNPFP KDRWNNTPMD EALHFGHHDV FKILQEYQVQ
651 YTPQGDSDDG KGNQTVHKNL DGLL
```

E

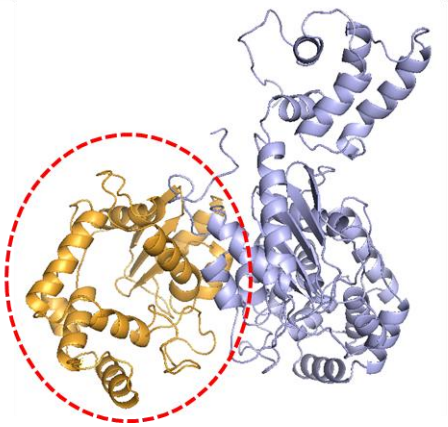

FIGURE A7.2 – UV-vis absorbance of SU-22-conjugated monomer and WT GAC. GAC (WT) and GAC (K316E,D391K,R459E) was reacted with SU-22 and purified as described in Chapter 3 (section 3.2.3). Resulting concentrated SU-22-conjugated monomeric GAC (**A**), WT GAC (**B**), and unreacted SU-22 (10 μM) (**C**) was analyzed by UV-vis spectroscopy. Molar absorptivity and A280 correction factor for unreacted SU-22 was calculated by the spectrum displayed in (**C**), and used to calculate the concentrations of both GAC and SU-22, and the labeling efficiency, depicted in (**D**)

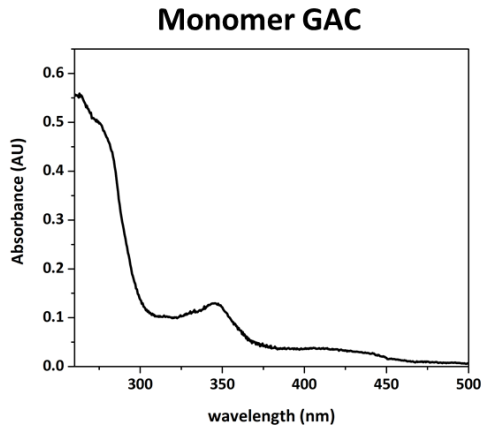

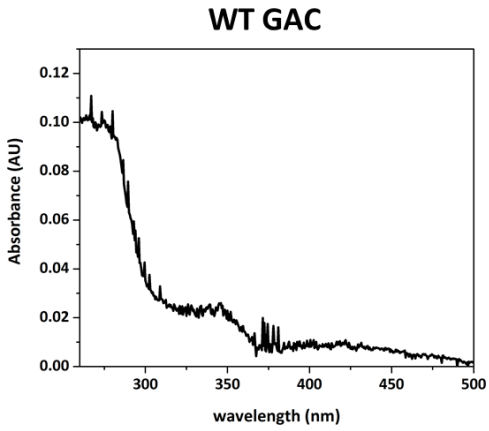

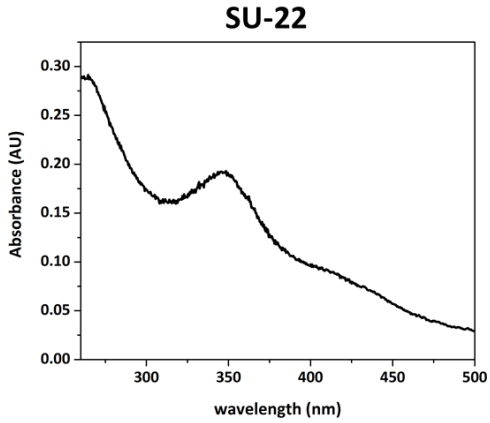

	GAC (WT)	GAC (Monomer)
[GAC] (μM)	9.7	46.0
[SU-22] (μM)	5.3	32.1
Ratio SU-22/GAC	0.54	0.70

FIGURE A7.3 – Partial trypsin digestion of SU-22-labeled and 488-labeled GAC. Trypsin (50 μg) was added to SU-22-labeled and 488-labeled GAC (56 μg each). Aliquots (20 μL) were quenched with soybean trypsin inhibitor (20 μg) at increasing time intervals. Samples were then analyzed by SDS-PAGE and visualized by UV-illumination (i.e. fluorescence of SU-22 or 488 probes).

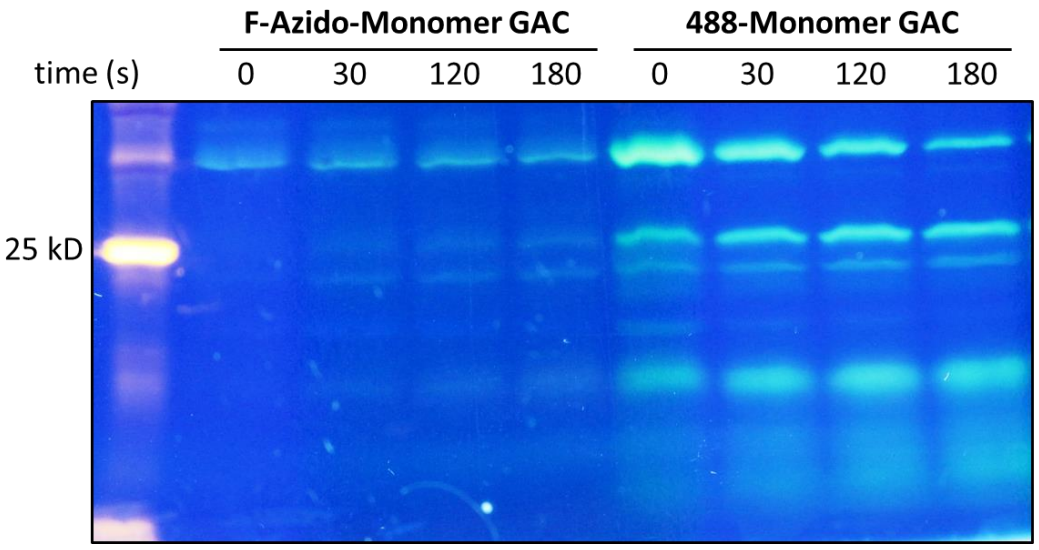
F-Azido-Monomer GAC
488-Monomer GAC
time (s)
0
30
120
180
0
30
120
180
25 kD

FIGURE A7.4 – Isotopologues of TCA cycle intermediates derived from [U-^{13}C]glutamine in non-induced and induced Dbl-MEFs with 968 and compound 27 treatment. (**A**-**D**) Isolated and quantified TCA cycle isotopologues following a 1 h incubation of Dbl-MEFs with U-^{13}C-glutamine in both the induced (- DOX) and non-induced states (+ DOX), with overnight treatment of 8 μM 968, WPK968 or DMSO control to illustrate effects on glutamine metabolism (+)/(-) DOX as well as with drug treatments. [U-^{13}C]glutamine enrichment is noted in the M+5 isotopologue of glutamate (**A**), M+4 of fumarate (**B**), M+4 of malate (**C**), and M+4 of citrate (**D**), where an inhibition of glutamine metabolism by 968 was observed in both induced and non-induced cells as read out by ^{13}C enrichment. (**E**) 968 treatment causes a modest decrease in glutamate pool sizes in non-induced and induced cells while causing no impact on the pool sizes of fumarate, malate, and citrate. Metabolites were quantified by normalizing the integrated peaks for all mass isotopologues with respect to the internal standard (50 nmol of 2-oxobutyrate) and protein content.

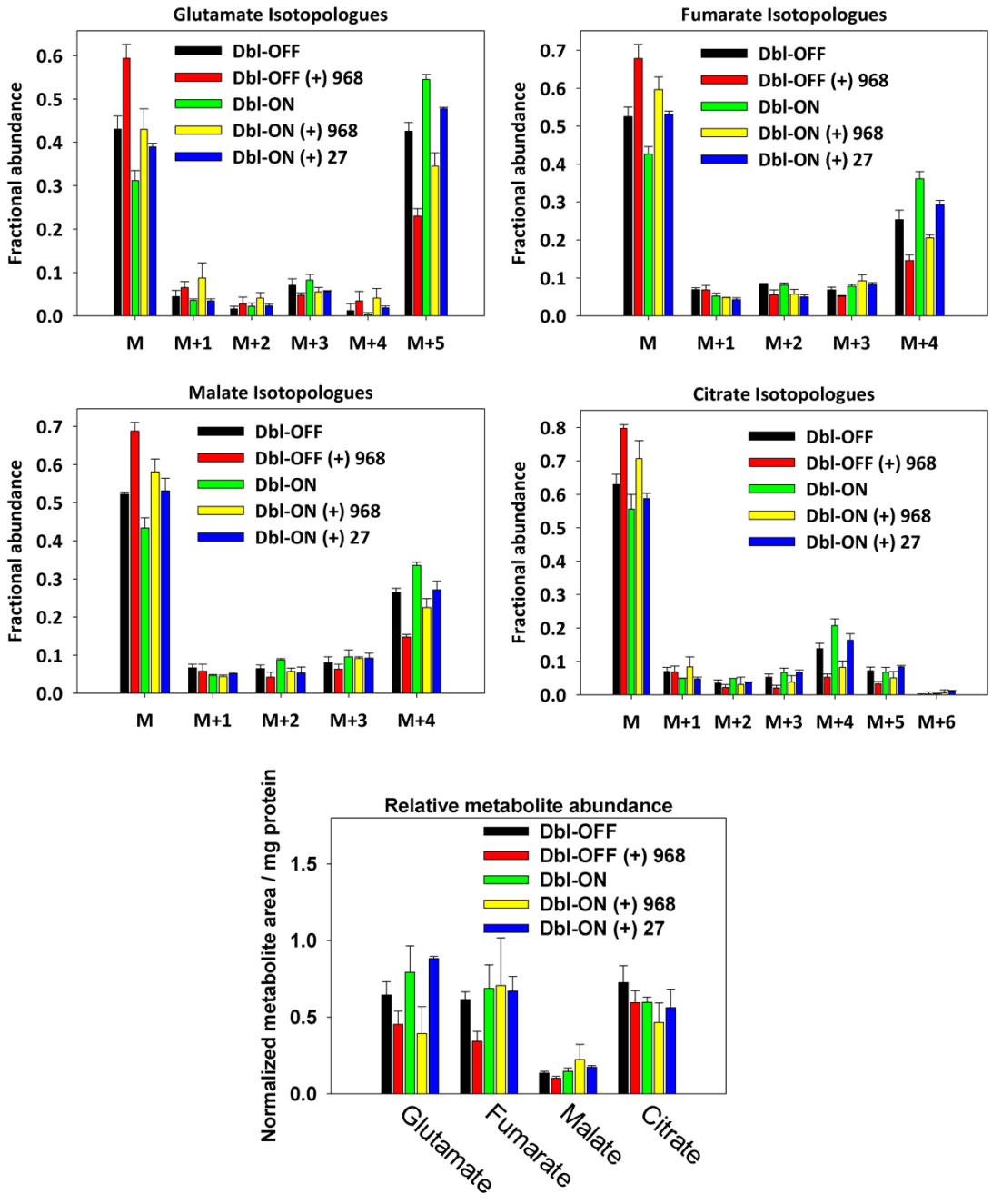
Glutamate Isotopologues
Fumarate Isotopologues
Malate Isotopologues
Citrate Isotopologues
Relative metabolite abundance
Fractional abundance
Normalized metabolite area / mg protein
Dbl-OFF
Dbl-OFF (+) 968
Dbl-ON
Dbl-ON (+) 968
Dbl-ON (+) 27
M
M+1
M+2
M+3
M+4
M+5
M+6
Glutamate
Fumarate
Malate
Citrate

FIGURE A7.5 – KGA forms heterotetramers (KGA:GAC) with the same binding affinity as GAC homotetramers. Increasing concentrations of QSY9-labeled Δ72-GAC were added to 10 nM 488-labeled Δ72-GAC (○) and Δ72-KGA (●), and the fluorescence quenching that results from FRET (see Chapter 2, figure 2.2) was quantified and plotted with respect to the total concentration of KGA/GAC. The curve represents the non-linear fit to a quadratic bimolecular binding isotherm, where the association constants were within good agreement when 488-KGA was used in place of 488-GAC, representing heterotetramers versus homotetramers, respectively.

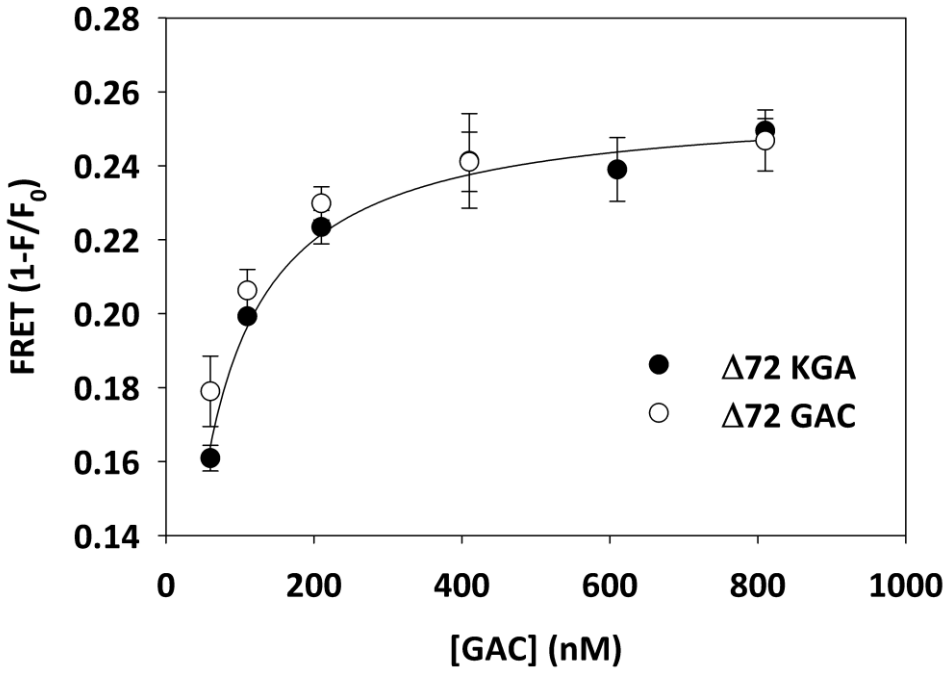
0.28
0.26
0.24
0.22
0.20
0.18
0.16
0.14
FRET (1-F/F0)
0
200
400
600
800
1000
[GAC] (nM)
Δ72 KGA
Δ72 GAC